UNIVERSITAT DE BARCELONA

Depletion of aneuploid cells in epithelial tissues is shaped by cell-to-cell interactions

Elena Fusari

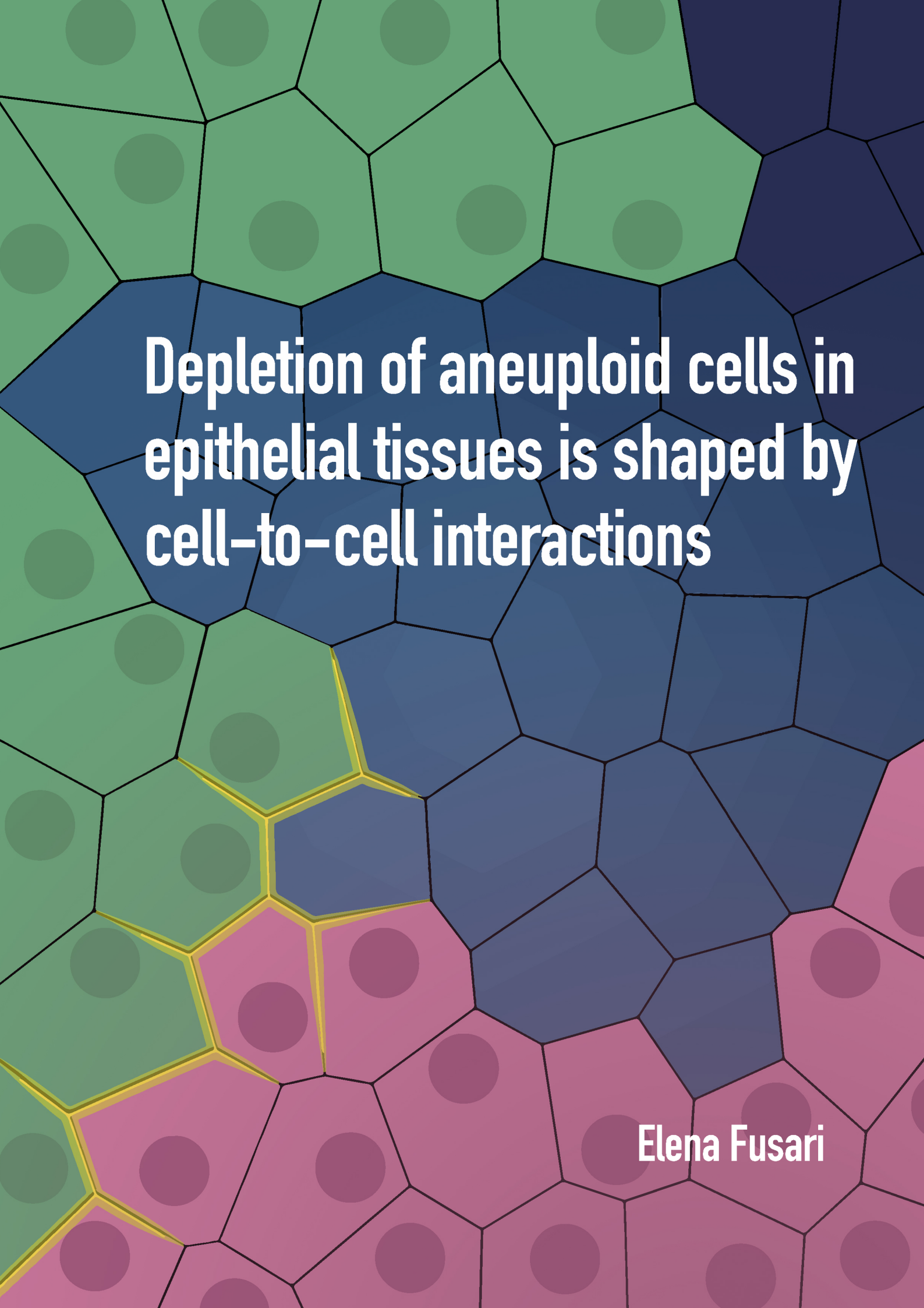

Depletion of aneuploid cells in epithelial tissues is shaped by cell-to-cell interactions

Elena Fusari

Programa de Doctorat del Departament de Biomedicina

Facultat de Medicina

Universitat de Barcelona

Depletion of aneuploid cells in epithelial tissues is shaped by cell-to-cell interactions

L'eliminació de cèl·lules aneuploides en teixits epitelials està determinada per les interaccions entre cèl·lules

Memòria presentada per l'

Elena Fusari

Per a optar al grau de Doctora per la Universitat de Barcelona

Development and Growth Control Laboratory

Institute for Research in Biomedicine (IRB Barcelona) Parc Científic de Barcelona

Barcelona, January 2025

Director:	Estudiant:	Tutor:
Dr. Marco Milán	Elena Fusari	Neus Agell Jané

Table of Contents

Index of Figures and Tables

Abbreviations

(Su(Tpl)) = Suppressor of Triplolethal
AD = Alzheimer's Disease
AEL = After Egg Laying
AT = Ataxia-Telangiectasia
BFB = Breakage-Fusion-Breakage
CNV = Copy Number Variation
CPM = Confined Placental Mosaicism
Crb = Crumbs
DBA = Diamond-Blackfan anemia
DS = Down Syndrome
ecDNA = extrachromosomal circular DNA
en = engrailed
ER = Endoplasmatic Reticulum
ESCs = Embrionic Stem Cells
ey/eye = eyeless
Flp = Flippase
FRTs = Flippase Recombination Targets
fwe = flower
hESCs = human Embrionic Stem Cells
hPSCs = human Pluripotent Stem Cells
hs = heat-shock
ICM = Inner Cell Mass
IVF = In Vitro Fecundation
MDCK = mammalian Madin-Darby Canine kidney
MMCT = Microcell-Mediated Chromosome Transfer
Mn = Minute
MVA = Mosaic Variagated Aneuploidy
NHEJ = Non-homologous End Joining
POF = Painting Of Fourth
RHG = reaper, hid, grim
ROS = Reactive Oxygen Species
Rp = Ribosomal protein
RpG = Ribosomal protein Gene
RS = Recombination Screening
SAC = Spindle Assembly Checkpoint
SCNAs = Somatic Copy Number Alterations
scrib = scribble
SDS = Schwachman–Diamond Syndrome
TAMERE = TArgeted MEiotic REcombination
TE = Trophectoderm
Tpl = Triplolethal
TSG = Twin Spot Generator
UPD =UniParental Disomy
UPR = Unfolded Protein Response

Abstract

Aneuploidy, the major cause of miscarriages, is pervasive in early human embryos, and later in life, it correlates with pathological conditions including cancer and other ageing-related conditions. At the cellular level, both gains and losses of chromosome are deleterious and result in growth defects. At the organismal level, almost all trisomies and monosomies are lethal and those that are compatible with life are associated with severe developmental defects. Surprisingly, 80% of blastocysts are reported to be aneuploid mosaics. In disease, aneuploidy is present in 90% of human solid tumors, it confers selective advantage to cancer cells and significantly contributes to tumorigenesis. Identification of the mechanisms underlying the elimination of aneuploid cells is therefore relevant in development and disease. Since aneuploid cells *in vivo* generally emerge as a consequence of missegregation events during cell division, it is often found in mosaics. One mechanism that has been proposed to participate in the recognition and elimination of aneuploid cells to ensure correct development and tissue homeostasis in cell competition, a process were difference in fitness are sensed and less fit cells are actively eliminated by fitter cells. In order to study aneuploidy it is crucial to dispose of good experimental models. In particular, sequence-specific methods allow to differentiate between general and karyotype-specific effects of gene dosage imbalance. Unfortunately, such strategies have been developed mainly *in vitro* therefore lacking the ability to characterize the impact of the interaction between aneuploid and wild type cells.

Here, we developed a strategy based on the Flp/FRT sequence-specific recombination system to generate labelled segmental aneuploid cells within epithelial tissues of *Drosophila.* We generated cells carrying molecularly defined segmental monosomies and trisomies and characterized their immediate impact on cellular behavior, growth and survival. Our data reveal signs of out-competition of cells carrying monosomies in genomic regions devoid of previously known haploinsufficient genes due to newly identified haploinsufficient genes or to cumulative haploinsufficiency. Notably, these mechanisms of cell competition rely on distinct molecular pathways, namely *Xrp1-mTor*-dependent or -independent cell competition. By simultaneously inducing cells carrying monosomies and trisomies of the same genomic location, we present evidence that segmental trisomies potentiate or alleviate the negative effects of the monosomy on growth. We describe a case of supercompetition of the trisomies, that overgrows respect to control cells at the expenses of the monosomic cells, and a case of growth compensation, where trisomic cells induce compensatory proliferation of otherwise outcompeted monosmies. Furthermore, we describe two triplosensitive regions.

Overall, our results reveal that the genome is full of dosage-sensitive loci and uncover a key role of cell interactions and specifically of cell competition in defining the *in vivo* elimination of aneuploid cells.

Key words: aneuploidy, haploinsufficiency, triplosensitivity, cell competition, cell death

Resum

La aneuploïdia es la principal causa d'avortaments espontanis i és molt present en els embrions humans durant les primeres etapes del desenvolupament. També més endavant s'associa amb condicions patològiques com el càncer i altres malalties relacionades amb l'envelliment com malalties neurodegeneratives. Tant els guanys (trisomía) com les pèrdues (monosomía) de cromosomes són perjudicials i provoquen defectes significatius de creixement o letalitat en la majoria dels casos. Sorprenentment, un 80% dels blastocists són mosaics aneuploides. En el context de les malalties, l'aneuploïdia és present en el 90% dels tumors sòlids humans, contribueix significativament a la tumorogènesi. Identificar els mecanismes que permeten l'eliminació de cèl·lules aneuploides és fonamental tant en el desenvolupament com en el context de la malaltia. *In vivo*, les aneuploïdies sovint apareixen com a conseqüència d'errors en la segregació cromosòmica durant la divisió cel·lular, fet que resulta en mosaicisme. Un dels mecanismes proposats per mantenir l'homeòstasi tissular és la competició cel·lular. Aquest procés implica detectar diferències en la capacitat de supervivència entre cèl·lules, permetent que les menys competitives siguin eliminades activament per les més competitives. Per estudiar l'aneuploïdia, és essencial disposar de models experimentals robustos i adequats. Els mètodes seqüència-específics permeten diferenciar entre efectes generals i efectes específics d'un cariotip concret causats per desequilibris en la dosi gènica. Malauradament, aquestes estratègies s'han desenvolupat principalment in vitro, limitant la capacitat d'investigar l'impacte de les interaccions entre cèl·lules aneuploides i salvatges dins d'un teixit viu. En aquest treball, hem desenvolupat una estratègia basada en el sistema Flp/FRT per generar cèl·lules segmentalment aneuploides marcades dins de teixits epitelials de *Drosophila*. També hem explorat com els desequilibris genòmics impacten en processos específics relacionats amb el desenvolupament tissular. Hem creat cèl·lules amb monosomies i trisomies segmentals molecularment definides, caracteritzant l'impacte d'aquestes anomalies en el comportament cel·lular, el creixement i la supervivència. Els nostres resultats mostren signes clars de competició cel·lular desfavorable per a cèl·lules amb monosomies en regions genòmiques sense gens haploinsuficients prèviament coneguts. Això suggereix l'existència de nous gens haploinsuficients o haploinsuficiència acumulativa. Aquests mecanismes es basen en vies moleculars diferents, incloent mecanismes dependents o independents de Xrp1-mTor. També hem descobert que les trisomies poden potenciar o mitigar els efectes negatius de les monosomies en el creixement. Hem descrit un cas de supercompetència, en què les cèl·lules trisòmiques creixen a costa de les monosòmiques, i un cas de compensació de creixement, on les cèl·lules trisòmiques indueixen proliferació compensatòria de les monosomies que, d'una altra manera, serien eliminades. Finalment, hem identificat dues regions triplosensibles que contribueixen significativament a aquests fenòmens.

En conjunt, els nostres resultats posen de manifest que el genoma conté nombrosos loci sensibles a la dosi gènica i que les interaccions cel·lulars tenen un paper central en la sort de les cèl·lules aneuploides *in vivo*. Això reforça la rellevància de la competició cel·lular com a mecanisme clau per mantenir l'homeòstasi tissular i eliminar cèl·lules anòmales.

Paraules clau: aneuploïdia, haploinsuficiència, triplosensibilitat, competició cel·lular, mort cel·lular

Introduction

1. Aneuploidy: definition and origins

Aneuploidy is a chromosomal abnormality characterized by an imbalanced number of chromosomes, which deviates from the typical diploid set. Unlike euploidy, where cells have complete sets of chromosomes, aneuploidy involves either extra or missing chromosomes, leading to imbalances in gene dosage. Aneuploidy can be classified into several types based on chromosomal composition and mainly we will talk about monosomies, where one chromosome from a pair is missing, and trisomies, where there is an extra chromosome. Additionally, aneuploidy is classified as either whole-chromosome or segmental, depending on whether it involves entire chromosomes or specific segments of them. Segmental aneuploidies can be further defined as segmental monosomies or trisomies. These abnormalities arise from errors in chromosome segregation during cell division, particularly during meiosis in germ cells or mitosis in somatic cells. We will first briefly review the mis-segregation events that can lead to aneuploid cells during cell division and then we will focus on the consequences of aneuploidy in embryonic development and somatic tissues, highlighting its implications for both development and disease in separate sections.

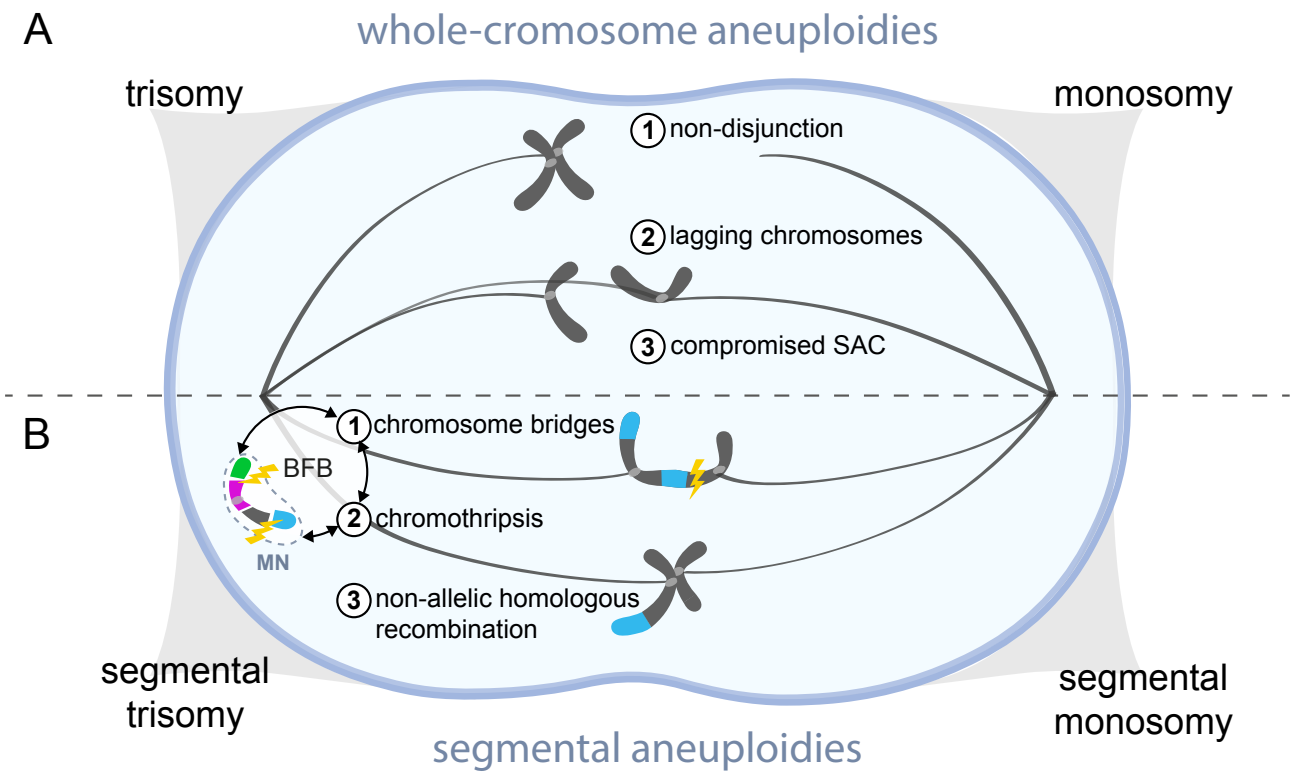

Figure I1. Origins of whole-chromosome and segmental aneuploidies. Schematic representation of errors during chromosome segregation that lead to the formation of aneuploid cells, either of whole-chromosomes, top panel (**A**), or segments of them, bottom panel (**B**). Merotelic kinetochore attachment is shown in correspondence of lagging chromosomes (**A**). Lightning bolt=chromosome breakage and DNA damage. MN=micronuclei. BFB=breakage-fusion-breakage.

Whole-chromosome aneuploidies (Figure I1A) are often the result of meiotic or mitotic nondisjunction, where homologous chromosomes or sister chromatids fail to separate properly during anaphase (Bugge et al., 2007; Hall et al., 2007; Hassold & Hunt, 2001). Another mechanism which leads to whole-chromosome aneuploidies is chromosome lagging, where a chromosome fails to attach to the spindle or moves more slowly than others during anaphase. This can result in the lagging chromosome being excluded from one daughter nucleus, leading to monosomy in one cell and trisomy in the other if the lagging chromosome is eventually incorporated into one of the daughter cells (Thompson & Compton, 2008). Abnormalities in spindle formation such as multipolar spindles can also lead to improper chromosome segregation (Ganem et al., 2009), as well as weakened spindle assembly checkpoint (SAC) (Cahill et al., 1998). The SAC is responsible for delaying progression of the cell cycle into anaphase in case chromosomes are not properly attached. A compromised SAC can allow cells with improperly attached chromosomes to proceed through mitosis, increasing the likelihood of missegregation (Musio et al., 2003). Premature loss of cohesion between sister chromatids can also lead to the formation of lagging chromosome and therefore their improper segregation during anaphase (Chiang et al., 2010). Merotelic attachment of kinetochores of lagging chromosomes to microtubules originating from both spindle poles has been reported to be undetected by the SAC and therefore possibly represents a major mechanism of aneuploidy in mammalian cells (Cimini et al., 2001). Furthermore, Robertsonian translocation, where long arms of two acrocentric chromosomes are fused, can produce aneuploid gametes during meiosis (Manieu et al., 2014; Scriven et al., 2001).

Segmental aneuploidies arise from structural rearrangements, that occur due to DNA breakage and improper repair (Figure I1B). When a chromosome breaks during meiosis or mitosis, for example due to unresolved DNA replication intermediates or telomere loss, the newly broken ends of chromosomes cause the fusion between sister chromatids resulting in a dicentric chromatid. During anaphase, dicentric chromatids can form chromosome bridges where the chromatid is pulled in different directions. Breakage of chromosome bridges often leads to uneven distribution of genetic material, resulting in segmental aneuploidies. Moreover, chromosome bridges can initiate breakage-fusion-bridge (BFB) cycles, a major mechanism for generating focal amplifications and large deletions. Another event that can trigger the formation of chromosome bridges and BFB cycles is chromothripsis, a localized shattering of a chromosome into fragments followed by random reassembly, often through non-homologous end joining (NHEJ). Furthermore, lagging chromosomes, if they are excluded from both daughter nuclei, can produce micronuclei and subsequent DNA damage and chromosome breakage, possibly triggering in turn chromothripsis events and BFB cycles (Crasta et al., 2012; C.-Z. Zhang et al., 2015). Segmental aneuploidies can therefore arise when these chromosome segments are incorporated into the genome. In addition, unequal crossing over during meiosis, or occasionally during mitosis due to misalignment of repetitive DNA sequences, can cause non-allelic homologous recombination. This results in one chromosome gaining extra genetic material while the other loses it (Lupski, 1998). Unlike whole-chromosome aneuploidies, segmental aneuploidies result in a more targeted dosage imbalance, affecting only a subset of genes localized within the altered chromosomal region. Segmental duplications and deletions are

particularly impactful because they can involve critical regulatory or dosage-sensitive genes, which may lead to significant phenotypic consequences even when relatively small regions are affected.

The consequences of aneuploidy can be severe, resulting in a plethora of stresses at the cellular level and in developmental abnormalities, miscarriages, and genetic disorders at the organismal level. Moreover, in the context of human health, aneuploidy is intricately associated with ageing and diseases such as cancer. Significantly, given that chromosome mis-segregation is essentially irreversible, it is critical to understand how cells respond to aneuploidy and how tissue context contributes to the fate of aneuploid cells.

2. Consequences of aneuploidy at the cellular level

Aneuploidy has been demonstrated to be highly detrimental at the cellular level across various models. A common and conserved characteristic of aneuploid cells is reduced fitness, with studies in yeast, mouse, and human cells consistently showing that aneuploidy generally impairs growth rates. We will discuss consequences observed for chromosome gains and losses.

2.1. Chromosome gain

The poor proliferative capacity of trisomic cells was first observed by comparing the growth potential of euploid cells with skin fibroblasts from patients with Down syndrome (Segal & McCoy, 1974). Later, systematic studies with haploid yeast strains bearing an extra copy of all individual yeast chromosomes showed consistent decrease in growth rate (Torres et al., 2007), as well as studies in trisomic mouse embryonic fibroblasts (Williams et al., 2008) and human trisomic and tetrasomic cell lines (Stingele et al., 2012). Transcriptionally, the growth defects observed in yeast disomic strains have been linked to the environmental stress response (ESR), a gene expression signature typically activated under various stress conditions. Consistently, studies in yeast and human cell lines suggest that aneuploidy, while detrimental under normal conditions, can provide a selective advantage under stress, serving as a driver of phenotypic evolution and adaptation (Pavelka et al., 2010; Rutledge et al., 2016). Despite cases of specific aneuploidies giving resistance against specific environmental stresses (Rancati et al., 2008), a common transcriptional response to aneuploidy was also identified in trisomic and tetrasomic human cell lines. This included upregulation of the ER, Golgi and lysosomes related pathways and antigen processing and, consistently with a decreased growth capacity, downregulation of DNA and RNA metabolism and ribosome-related pathways (Dürrbaum et al., 2014). Overall, these findings highlight that a decrease in fitness is a general consequence of gaining an extra chromosome, independently of the karyotype.

Work by many laboratories suggests that the molecular mechanisms underlying the negative impact of aneuploidy on growth stems from altered stoichiometry of protein complexes. In fact, cell physiology relies on correct balance of gene products, which is indeed altered in aneuploid cells. Studies with aneuploid human and yeast cells have shown that extra chromosomes are correlated with a proportional increase in most mRNAs

encoded by the gained chromosome and generally a proportional increase in the corresponding protein translation (Dephoure et al., 2014; Hwang et al., 2021; Pavelka et al., 2010; Stingele et al., 2012). The idea that *Drosophila* cells don't suffer from the same disruption of normal gene stoichiometry upon aneuploidy was presented by some works proposing a compensation mechanism that would buffer the difference in gene copy number at the mRNA and protein level for all autosomes (Stenberg et al., 2009; Y. Zhang et al., 2010), but later works discarded this hypothesis (H. Lee et al., 2016). This will be discussed in more detail in the following chapters.

The non-stoichiometric production of proteins in trisomic cells may affect the functioning of different cellular processes that normally work through balanced protein complexes, therefore causing a variety of cellular stresses, including mitotic, replicative, osmotic, proteotoxic, and metabolic stress [Figure I2A, reviewed in (J. Zhu et al., 2018)]. Aneuploidy disrupts DNA replication complexes by altering stoichiometry of replication proteins, such as helicase subunits. These disruptions stall replication fork progression and cause replication stress, as observed in studies of aneuploid human cells and yeast (Burrell et al., 2013; Passerini et al., 2016). Consistently, aneuploid cells have been shown to lose mitotic fidelity and be chromosomally instable, meaning that they present a high rate of missegregation during mitosis (Passerini et al., 2016; Sheltzer et al., 2011). Interestingly, tracking of karyotype trajectories of aneuploid yeast populations revealed that the degree of chromosomal instability varies with the identity of the aneuploid chromosomes (J. Zhu et al., 2012). The stalling in replication forks could also expose aneuploid cells to increased DNA damage and the emergence of segmental abnormalities as reported for trisomic plants (Papp et al., 1996).

Proteotoxic stress is another hallmark of aneuploidy, caused by the overproduction of unbalanced protein subunits that fail to assemble into proper protein complexes. This overload on the cellular protein homeostasis machinery, or proteostasis, leads to protein aggregation and misfolding, which are prominent in both yeast and human aneuploid cell models (Brennan et al., 2019; Oromendia et al., 2012; Stingele et al., 2012; Torres et al., 2010). Aneuploid yeast strains and mouse embryonic fibroblasts demonstrate protein aggregation and heightened sensitivity to proteasome inhibitors, indicating reliance on the ubiquitin-proteasome system for protein degradation (Oromendia et al., 2012; Tang et al., 2011). Autophagy-related pathways are activated as a compensatory mechanism but are saturated in highly aneuploid cells also in *Drosophila* (Joy et al., 2021). In human cell lines, features such as reduced chaperone activity, altered autophagy, and saturation of lysosomal-mediated degradation have been reported (Ohashi et al., 2015; Santaguida et al., 2015; P. J. Zhu et al., 2019). Consistently, trisomic human cells exhibit reduced expression of heat shock factor 1 (HSF1), a master regulator of the chaperone system, while its overexpression has been shown to mitigate proteotoxic stress in aneuploid human cell lines (Donnelly et al., 2014). Metabolic stress is intricately tied to aneuploidy and it is thought to derive from altered stoichiometry of enzymes and regulators. In yeast and mammalian aneuploid cells, increased glucose uptake, abnormal accumulation of amino acids, and heightened tricarboxylic acid (TCA) cycle activity have been observed (Stingele et al., 2012; Torres et al., 2007; Williams et al., 2008). Trisomy 21 (Down syndrome) cells exhibit reduced mitochondrial biogenesis, increased production of reactive oxygen species (ROS), and oxidative stress (Pogribna et al., 2001; Valenti et al., 2011). Aneuploid mouse embryonic

fibroblasts (M. Li et al., 2010), aneuploid *Drosophila* wing disc cells (Joy et al., 2021), and yeast strains (Dephoure et al., 2014) also show increased ROS levels, highlighting oxidative stress as a common feature of aneuploidy. This oxidative stress results in DNA damage, potentially acting as a feedback loop to exacerbate checkpoint activation and genome instability (Degtyareva et al., 2008).

In summary, the cellular stresses associated with the gain of an extra chromosome arise from the disruption of protein complexes stoichiometry independently from the karyotype and are well-documented in various models, including yeast, *Drosophila*, mammalian cell lines, and trisomic human cells. In addition to this well characterized common behaviors induced by trisomies, specific genes can give rise to a phenotype when present in three copies, in which case they are called triplosensitive. The phenomenon of triplosensitivity and its implication for aneuploidy-induced behaviors will be discussed further in this work.

2.2. Chromosome loss

Chromosome loss, or monosomy, significantly impacts cellular physiology, reducing proliferation and viability, similarly to chromosome gain, across various models, including yeast (Beach et al., 2017) and human cell lines (Chunduri et al., 2021). Investigating the consequences of chromosome loss has been challenging due to its high lethality, probably due to extensive haploinsufficiency in the genome. For instance, the referenced study utilized p53-deficient cell lines to enable the examination of monosomy. Unlike the gain of chromosomes, monosomy does not induce proteotoxic stress or activate major protein-quality control mechanisms, such as autophagy, nor does it result in susceptibility to proteostasis inhibitors or increased genomic instability (Chunduri et al., 2021; Hintzen et al., 2022). Instead, reduced protein translation, linked to haploinsufficiency of ribosomal protein (Rp) genes (Figure I2B), emerges as a central consequence (Chunduri et al., 2021). This is consistent with the fact that almost all human chromosomes with exception of chromosome 7 and 21 bear Rp genes (Uechi et al., 2001). However, work in *Drosophila* highlights how a transcriptional monosomy for the X chromosome induces similar effects in epithelial cells than the gain of chromosomes (Clemente-Ruiz et al., 2016). Therefore, whether gene dosage imbalance contributes to the reduced fitness of monosomic cells and through which molecular pathways, if not by activating responses to proteotoxic stress, remains to be elucidated.

In summary, both chromosome gain- and loss-induced alterations culminate in growth defects. These growth defects likely result from the combined impact of the reviewed cellular stresses and triplosensitivity of particular gene(s) in trisomies, and reduced translation and haploinsufficiency of particular gene(s) in monosomies, which collectively impair the fitness of aneuploid cells in a cell-autonomous manner. In the following chapters, we will explore how the presence of aneuploid cells within predominantly euploid tissues influences their growth through cell-non-autonomous mechanisms *in vivo*.

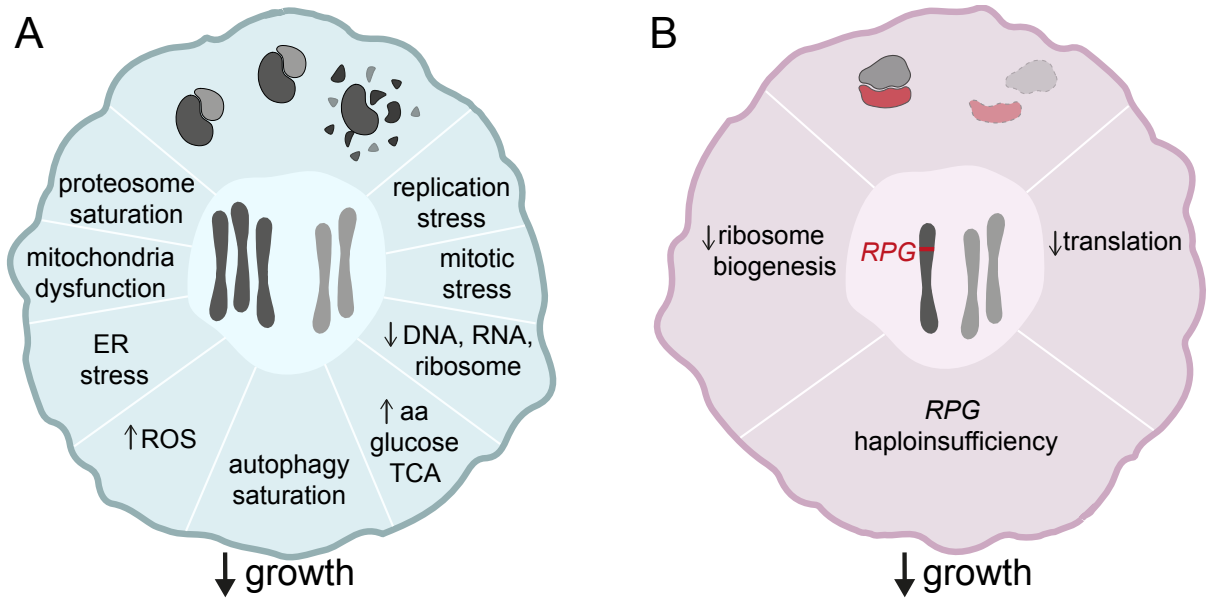

Figure I2. Cellular consequences of chromosome gain and loss. Cellular stresses associated with chromosome gain (**A**), that derive from altered stoichiometry of protein complexes, and loss (**B**). aa=aminoacids, TCA=tricarboxylic acid, ROS=reactive oxygen species, ER=endoplasmatic reticulum, RPG=ribosomal protein gene.

3. Aneuploidy in normal development

In humans, aneuploidy emerges as a highly prevalent feature throughout the lifespan, manifesting during embryonic development, in adult somatic tissues, and with advancing age.

3.1. Aneuploidy in embryonic development

Aneuploidy in embryos can emerge either from meiotic mistakes from maternal or paternal origin, or from mitotic mistakes during post-zygotic divisions. Aneuploidy, both from meiotic and mitotic origin, is highly prevalent in human embryos. Meiotic mistakes will result in organismal aneuploidies, and approximately 20% of human oocytes and 9% of human sperm are thought to be aneuploid (Martin, 2008). This is consistent with a report finding 28,4% of blastocysts being aneuploid of meiotic origin (Scott et al., 2013). On the other side, mitotic mistakes will lead to mosaicism, which has been reported in 73% of embryos resulting from *in vitro* fecundation (IVF) (van Echten-Arends et al., 2011). Not only aneuploidy is extremely prevalent in embryos, but it is the main cause of miscarriages in humans with 50–70% of early miscarriages (Soler et al., 2017) and 25% of perinatal deaths (Zeitlin et al., 2009) being associated with chromosome abnormalities, mostly aneuploidy. A more recent report estimates even higher rates, with 67.8% products of conceptions from early miscarriages reported to bear a chromosomal abnormality (Essers et al., 2023). We will review the main contribution of aneuploidy, both of maternal and paternal origin, and both whole-chromosome and segmental, to miscarriages and lethality of the embryo as well as to developmental defects. In the next two chapters, we will focus on the result of meiotic and mitotic mistakes, respectively, reviewing first organismal aneuploidies and their associated developmental disorders, and then embryo mosaics.

3.1.1. Organismal aneuploidy

Most organismal aneuploidies are whole-chromosome aneuploidies. Whole-chromosome aneuploidies more frequently affect maternally-derived chromosomes with an equal incidence of gains and losses, while whole-chromosome aneuploidies of paternal origins are more rare and principally losses (Konstantinidis et al., 2016; Kubicek et al., 2019; Martin, 2008).

Errors in maternal meiosis, particularly non-disjunction during meiosis I or II, are a primary source of organismal aneuploidies (Rabinowitz et al., 2012). In general, 75% of chromosomal abnormalities found in spontaneously aborted embryos are attributed to errors in the oocyte rather than the sperm (Hassold & Hunt, 2001). In meiosis I, homologous chromosomes fail to separate, while in meiosis II, sister chromatids do not segregate correctly, producing gametes with abnormal chromosome counts (Bugge et al., 2007; Hassold & Hunt, 2001; T. R. Oliver et al., 2008). Upon fertilization, these errors result in zygotes with aneuploid karyotypes, often leading to embryonic lethality or developmental disorders (Figure I3).

Spindle assembly instability and inefficient correction of kinetochore-microtubule attachments are key drivers of aneuploidy in human oocytes. Unlike other organisms, human oocytes assemble spindles slowly without centrosomes, relying on Ran-GTP, which leads to frequent spindle instability, multipolarity, and lagging chromosomes during anaphase (Holubcová et al., 2015). These challenges are unique to human oocyte meiosis, contributing to aneuploidy even in younger women. However, maternal age is indeed a crucial factor that influences the occurrence of non-disjunction events in meiosis, therefore is highly correlated with whole-chromosome organismal aneuploidies. One major cause for mistakes in aged oocytes is the progressive loss of cohesin complexes, which are crucial for maintaining chromatid cohesion during meiosis. Since cohesin is loaded onto oocytes during fetal development and not replenished, its degradation over decades compromises chromosome alignment and segregation (Mihalas, Pieper, et al., 2024). Additionally, microtubule instability and spindle assembly defects in aged oocytes, linked to age-related cytoplasmic changes, further exacerbate missegregation (Patel et al., 2015; Zielinska et al., 2015). These changes are worsened by mitochondrial dysfunction and reduced ATP production, which interfere with the energy-intensive processes of spindle formation and chromosome segregation (Mihalas, Marston, et al., 2024; F.-L. Zhang et al., 2023).

On the contrary, segmental aneuploidies of meiotic origin, are twice as likely to affect paternal chromosomes compared with those derived from the mother, a finding that implicates meiotic processes specific to males and/or sperm DNA damage in the origin of segmental aneuploidy (Konstantinidis et al., 2016). In general, 10.4% of oocytes present segmental aneuploidies that occurred meiotically, of which 6.9% are segmental trisomies and 3.5% segmental monosomies (Babariya et al., 2017). Segmental aneuploidies of paternal origin instead have been reported to be mainly monosomies, and segmental monosomies in 40% of the cases (Konstantinidis et al., 2016). In the same study, of the overall number of aneuploidies detected, 15.7% were segmental with the size of segments gained or lost ranging from 7.8 to 145.6 Mb. Another study reports an occurrence of 5.58% of segmental aneuploidies between chromosomal abnormalities of meiotic origin (53/967), of which 1 gain of maternal origin, 15 losses of maternal origin and 38 of paternal origin (Kubicek et al., 2019). Reinforcing the idea that segmental aneuploidies of meiotic origin are mainly of paternal origin

and mainly monosomies, another report shows that segmental monosomies occur at nonallelic homologous recombination hotspots in the sperm (Turner et al., 2008) (Figure I3). However, segmental aneuploidies arising during the mitotic divisions of the embryo are approximately 2.5 times more common than those of a meiotic origin (Babariya et al., 2017; Konstantinidis et al., 2016), which will be discussed in the next chapter.
When organismal aneuploidies are not lethal, they result in severe developmental defects. We will now discuss viable trisomies and monosomies and their phenotypes in humans, with insights from some model organisms.

Chromosome gain

Viable trisomies differ across species. In humans, the most common autosomal viable trisomies include: trisomy 21 (Down syndrome), with a live birth prevalence estimated between 1/700 and 1/1400 births and a life expectancy of approximately 50 years (Graaf et al., 2017); trisomy 18 (Edwards syndrome), with a live birth prevalence ranging from 1/3600 to 1/10,000 births, a median life expectancy of 14 days and only 5-10% of children surviving beyond the first year (Cereda & Carey, 2012); trisomy 13 (Patau syndrome), estimated in 1/5000 to 1/16000 live births with a median life expectancy of 7 days and only 5-10% of children surviving beyond the first year (Wyllie et al., 1994). Trisomy 21 and 13 can derive from Robertsonian translocation in the gametes, being the translocations 13;14 and 14:21 the most common among the population (Scriven et al., 2001). All these conditions are associated with severe developmental impairments. Individuals affected by Down syndrome present musculoskeletal, neurological and cardiovascular defects, such as intellectual disability and congenital heart defects, and are also more likely to develop certain diseases like hypothyroidism, autoimmune diseases, leukaemia, recurrent infections, anxiety disorders and early-onset Alzheimer disease (Antonarakis et al., 2020). Individuals affected by Edwards and Patau syndromes present more sever intellectual disability and organ malformations, in accordance with their lower life expectancy (Cereda & Carey, 2012; Wyllie et al., 1994). The relative viability of these trisomies is thought to be related to the low gene content of the affected chromosomes. Chromosome 21 is the smallest autosome and contains approximately 235 protein coding genes, which may explain why trisomy 21 is more compatible with life compared to trisomies 18 and 13, which contain 269 and 321 protein coding genes, respectively. The severity of the phenotype of trisomies at the organismal level is clearly associated with the number of genes involved. However, if instead of looking at live births we focus on early pregnancy losses, more trisomies can be observed. In a recent study, 50% of the autosomal trisomies detected in early pregnancy loss involved chromosomes 15, 16, or 22 (Kamar et al., 2021; Soler et al., 2017). This goes accordingly with the chromosomes 15 and 22 being acrocentric, and therefore possibly involved in Robertsonian translocations.
Sexual chromosome aneuploidies are generally better tolerated than autosomal aneuploidies, often resulting in less severe phenotypes and higher survival rates. The most common sex chromosome trisomy is the Klinefelter syndrome (47,XXY), that has an estimated prevalence of between 1:500 to 1:1000 males (Bojesen et al., 2003). Klinefelter syndrome affects males, causing reduced fertility, decreased testosterone production, and mild developmental delays (Bonomi et al., 2017). Triple XXX syndrome (47,XXX), affects 1/1000 females but individuals affected often have mild symptoms or may even be unaware of their condition (Otter et al., 2010).

XXY individuals also present mild symptoms (Berglund et al., 2020). The relative viability of sex chromosome aneuploidies is attributed to two main factors. The first is X-chromosome inactivation, which normally silences one X chromosome through the long non-coding RNA XIST, thus equalizing the gene dosage of XX and XY karyotypes (Fang et al., 2019; Payer & Lee, 2008). The second is the low gene content of the Y chromosome, which includes about 70 genes, of which only 14 are X-Y paired (Bellott et al., 2014).

Regarding segmental trisomies, a study has reported a prevalence of 1/14000 births carrying a duplication, of which 61% liveborn (Wellesley et al., 2012).

In mice, spontaneous occurrence of aneuploidy is quite low. However, breeding schemes with mice bearing Robertsonian translocations were used to generate trisomic strains as animal models for organismal aneuploidy (Gearhart et al., 1986). Mice have 19 pairs of autosomes, from which trisomy 16 and 19 are the only ones reaching birth, and trisomy 18 is the one which reaches the furthest day of gestation (Gearhart et al., 1986). A comparison between chromosome size and the time when embryos die reveals a striking correlation, indicating that in this organism, an inverse correlation also exists between the size of genome present in three copies and organismal fitness. In *Drosophila*, which has 4 pairs of autosomes, autosomal trisomies for the autosomes are detrimental and trisomies of the major chromosome arms (2L, 2R, 3L, 3R) can survive until pupal stages, but never reach adulthood (Bridges, 1921). Again, a correlation between the number of genes included in a trisomy and the severity of its phenotype was found in a study that reported that the fertility of segmentally trisomic flies was inversely proportional to the length of the amplified segment (Patterson et al., 1935). A similar study reported that segmental trisomies result in a set of traits such as lower viability, reduced size, and developmental defects, that are independent of the identity of the triploid segment. Furthermore, the same study reports that viability decreased as the size of the trisomic region increased, with the largest tolerated segment including 66% of chromosome 2 (Lindsley et al., 1972). This reinforces the idea of a correlation between the detrimental effects of the trisomy and its size. Trisomy of chromosome 4 is instead viable, consistently with the small number of genes included in the 4th chromosome (111 genes, compared with the 3500-4000 of the other autosomes arms). Regarding sex chromosomes triploids, XXX flies do not reach adult stages and present developmental delay and other abnormalities (Bridges, 1921). The severity of this phenotype compared to the X trisomy in mammals can be explained with the fact that *Drosophila* has a different mechanism of X-compensation which, instead of silencing the extra X in females, hyper transcribes the one X chromosome in males (Laverty et al., 2010). Therefore, XXX flies cannot inactivate expression on extra X chromosomes to dampen the deleterious effect of gene dosage imbalances.

Chromosome loss

Autosome loss is incompatible with survival in mammals. For instance, monosomy 21 embryos display high rates of developmental arrest in comparison with trisomy 21 embryos (Laverty et al., 2010). This extreme sensitivity to chromosome loss is likely due to haploinsufficiency of essential genes. The only viable monosomy in humans involves the X chromosome, resulting in Turner syndrome (45,X karyotype). Even then, most 45,X conceptuses do not survive to term, with an estimated 99% of 45,X embryos being spontaneously

aborted and the rare survivors with Turner syndrome often displaying mosaicism (Hook & Warburton, 1983). The relative viability of X chromosome monosomy compared to autosomal monosomies is attributed to X-inactivation in females, which shows how expression of only one X chromosome is enough. However, there are about 100 genes reported to escape the XIST-mediated silencing. These genes are therefore differentially expressed in males and females and will be in a condition of hemizygosity in Turner females (Carrel & Willard, 2005). Interestingly, among them, there are 12 paired X-Y genes (Bellott et al., 2014), which highlights their essential role, as maintaining two doses of these genes is crucial for both males and females. This small number of potentially dosage sensitive genes could explain the fact that, even if X chromosome loss does not lead to severe defects compared to an autosome loss, Turner syndrome still results in various developmental abnormalities and reduced fertility.

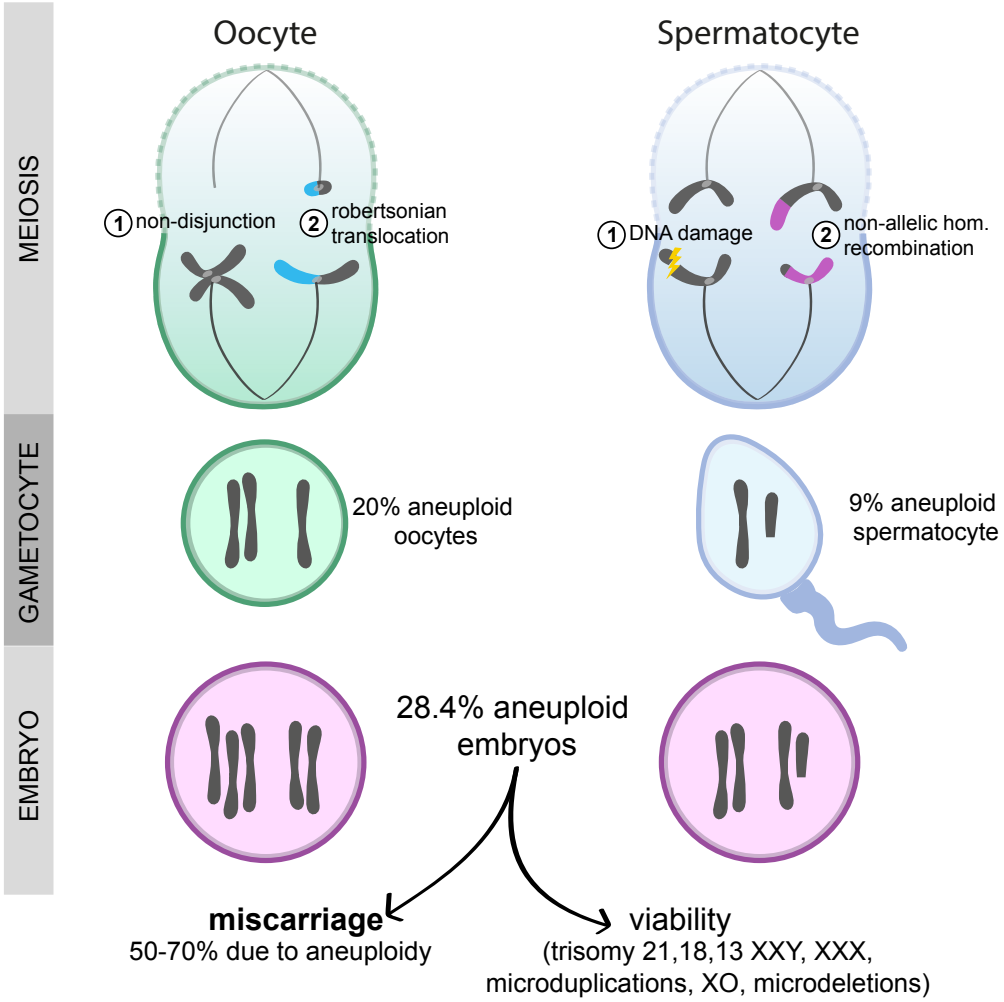

Figure I3. Origin and fate of organismal aneuploidies. Main mechanisms and incidence of formation of aneuploid oocyte and spermatocyte are shown. Fecundation with normal gametocytes generate aneuploid embryos. As a simplification, trisomies of maternal and segmental monosomies of paternal origins are shown.

Regarding segmental monosomies, 1/3200 births were reported to bear a chromosome deletion, of which 72% were liveborn (Wellesley et al., 2012). In particular, 22q11p is the most common microdeletion syndrome in humans, occurring in approximately 1:4000 live births and is associated with cardiac anomalies, hypoparathyroidism, and thymic hypoplasia or aplasia. 211 microdeletion syndromes were known in 2012, while only 79 microduplication syndromes were reported (Weise et al., 2012). The occurrence of a

microdeletion and its reciprocal duplication in meiosis should be similar, therefore the lower amount of reported microduplication syndromes is probably a reflection of their milder or no clinical phenotype compared with their reciprocal microdeletion. For example, 22q11p duplication is much less diagnosed and with a much milder phenotype (Rosa et al., 2009).

In *Drosophila* a study of clones of segmental aneuploidies reports that the survival of segmental monosomic clones decreases linearly as a function of the size of the deleted fragment (Ripoll, 1980). Due to monosomies being highly deleterious both at the organismal and the cellular level, to date this is the only systematic analysis on the relationship between the size of monosomies and their deleterious effect.

In mice, the only monosomy compatible with survival is also monosomy of the X chromosome. The phenotype of monosomy X in mice is less severe: animals are small but viable and have reduced fertility (Burgoyne et al., 1983; Burgoyne & Baker, 1981). This milder phenotype may be due to the fact that the genes on the mouse X chromosome that require two doses are only nine (Bellott et al., 2014), compared to the 100 reported for humans (Carrel & Willard, 2005). In *Drosophila*, flies with a single 4th chromosome are viable and fertile. This viability may be attributed to the dosage compensation mechanism of the 4th chromosome, known as Painting of Fourth (POF) (Johansson et al., 2007, 2012; Larsson et al., 2001). POF is thought to reflect the 4th chromosome's evolutionary origin as a former sex chromosome and operates in a manner similar to X-dosage compensation (Johansson et al., 2012; Vicoso & Bachtrog, 2013). By hyper-transcribing the single copy of the 4th chromosome, POF likely mitigates the harmful effects of monosomy. Additionally, due to the relatively small number of genes on the 4th chromosome, even flies entirely lacking both copies remain viable, though they are sterile and exhibit developmental abnormalities (Bridges, 1921). Curiously, binding of the POF protein is also observed in triploid 4/4/4 flies, were the expression increase observed (139% rather than the expected 150%) suggests a buffering effect (Stenberg et al., 2009). However POF was only essential for survival in monosomic flies 4/0 (Stenberg et al., 2009) suggesting that the buffering effect observed in triploid 4/4/4 flies could be POF-independent and gene-specific. Similarly to humans, XO flies are also viable and healthy, but sterile. The only difference is that in *Drosophila* XO individuals are males, as the determinant for sex is the ratio between X chromosome and autosomes (Bridges, 1925), and not the Y chromosome. This indicates that chromosome Y is critical for male reproduction in *Drosophila*, but not for male sexual characters development nor survival.

The discovery of a dosage compensation mechanism for an autosome, the 4th chromosome, has raised speculation about the existence of general autosomal compensation in *Drosophila*, potentially limiting its suitability as a model for studying aneuploidy. Through genomic approaches, weak buffering was observed in duplications and deletions in heterozygosis opening up the possibility of a general mechanism driving dosage compensation in autosomes (Stenberg et al., 2009; Y. Zhang et al., 2010). However, a more recent systematic examination of deficiencies in heterozygosis covering the left arm of chromosome 2 ruled out a general dosage compensation mechanism for autosomes, proposed the existence of gene-specific regulatory mechanisms driving gene-specific dosage compensation, and concluded that dosage compensation in autosomes had been over-estimated in *Drosophila* because of technical reasons (H. Lee et al., 2016).

3.1.2. Embryo mosaics

After fertilization, the human zygote undergoes eight to nine cleavage divisions before implantation, followed by compaction and the first lineage specification, forming the blastocyst. The blastocyst comprises the trophectoderm (TE), which develops into the placenta, and the inner cell mass (ICM), which later further specifies into epiblast and the hypoblast that give rise to the fetus and yolk sac, respectively.

Mitotic mis-segregation during post-zygotic divisions contributes to the formation of aneuploid mosaics. The timing of the segregation error determines the extent of mosaicism and the specific cell lineages affected. Mitotic errors occur frequently in preimplantation human embryos, particularly during the first three cleavage divisions, with a study reporting that approximately 73% of embryos exhibit mosaic aneuploidy at day three, of which 59% are diploid–aneuploid mosaic and 14% aneuploid mosaic (van Echten-Arends et al., 2011). This makes diploid–aneuploid mosaicism by far the most common chromosomal constitution in spare human preimplantation embryos after IVF. A study using single-cell sequencing of isolated TE and ICM samples, which can detect aneuploidies below the threshold of 20-30% of bulk DNA sequencing, identified mosaic aneuploidy in at least 80% of human blastocyst-stage embryos. Interestingly, in many cases, fewer than 20% of the cells in the blastocyst exhibited defects (Chavli et al., 2024).

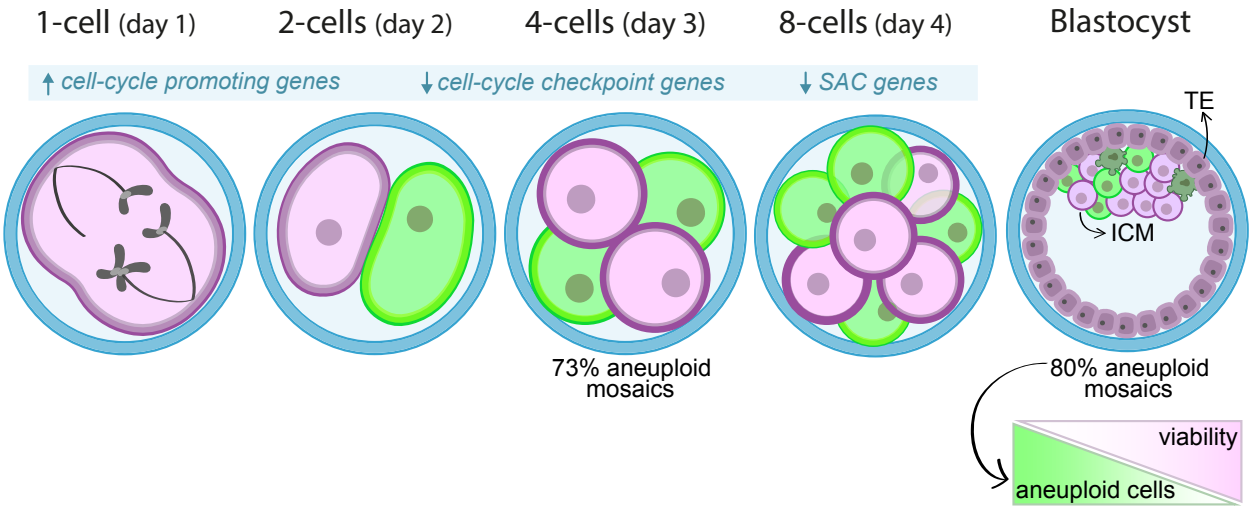

Figure I4. Generation of embryo aneuploid mosaics. Low segregation fidelity in the first embryo mitotic division gives rise to embryos that are aneuploid mosaics. After the 8- 16-cells stage until the blastocyst stage, aneuploid cells decrease indicating mechanisms of specific elimination. Cells with apoptotic blebs are depicted in the blastocyst to represent this phenomenon. The less aneuploid cells are retained in the embryo, the more the viability.

Mitotic aneuploidies involve all chromosomes, with some chromosomes being implicated more frequently. As per whole-chromosome aneuploidies, a study reports as the chromosomes more implicated in mosaic embryos sex chromosomes (24.1%), and particularly 45,X resulting in mosaic Turner syndrome (71.4% of sex chromosome mosaics), chromosomes 8 (12.1%), 2 (8.6%), 16 (8.6%), 7 (5.2%), 13 (5.2%), 18 (5.2%), 20 (5.2%) and 21 (5.2%) (A. Huang et al., 2009). The same study reports a frequency of segmental abnormalities of 8.6%. Regarding segmental aneuploidies, they seem to be much more prevalent in aneuploid mosaics than in organismal aneuploidy. Testing of multiple cells from the same embryos has demonstrated that most segmental abnormalities are mosaic and must therefore arise during the post-zygotic cell divisions (Vanneste et al., 2009; Wells & Delhanty, 2000). Most segmental errors appear to arise during the first few mitoses

following fertilization and seems to be eliminated during embryo development. A study reported that the incidence of segmental abnormalities was 10.4% in oocytes, but this increased dramatically during the first 3 days of embryonic development (24.3%), before starting to decline as embryos reached the final (blastocyst) stage of preimplantation development (15.6%) (Babariya et al., 2017). This is summarized in Figure I4. Interestingly, sites of chromosome breakage associated with segmental aneuploidy were not entirely random but tended to occur within distinct chromosomal regions, some of which correspond to known fragile sites (Babariya et al., 2017). Another study reported that preimplantation embryos rate of segmental aneuploidies is slightly higher than 30% and that the vast majority were segmental aneuploidies in a mosaic state (Picchetta et al., 2023). When looking at what type of aneuploidies are present in mosaic embryo, we must take into account the timings of the analysis, since certain abnormalities could arise early in development but be selectively eliminated. For instance, preliminary data indicate that aneuploidy of chromosomes 1–12 is common in cleavage-stage embryos but rarely persists to the blastocyst stage, whereas aneuploidy of chromosomes 13, 18, or 21 can persist and is even compatible with life (Brezina et al., 2011).

Mosaicism rate in human embryos does not increase with maternal age (Antonarakis et al., 1993; Katz-Jaffe et al., 2005). In particular, this is evident in a study that reports mitotic abnormalities for <34, 35-39 and >40 age groups in 24.5, 26 and 31% of the embryos respectively, versus the 17.5, 42.7 and 75.9% for meiotic abnormalities (Konstantinidis et al., 2016). The high prevalence of aneuploid mosaic embryos is primarily due to the error-prone nature of early mitotic divisions during embryonic development. Evidence for this comes from observation of spindle and nuclear abnormalities in day 3 and 5 of fixed human embryos (Kort et al., 2016) as well as from sequencing data (Vanneste et al., 2009). The first mitotic divisions in human embryos are particularly error-prone (Currie et al., 2022) due to a combination of factors related to the lack of robust cell cycle checkpoints, overexpression of cell-cycle promoting genes, and reliance on maternal and paternal factors (A. Lee & Kiessling, 2017; Mantikou et al., 2012). The first embryonic division in humans occurs approximately 30 hours post-insemination, followed by a second division 16 hours later that produces four cells. By day 3, the embryo divides again to form eight cells, initiating compaction into a morula. At the blastocyst stage (day 5–6), *in vitro* embryos typically consist of 60 cells, while *in vivo* embryos, with faster divisions every 18 hours, reach 120 cells. To facilitate these rapid divisions, there is over-expression of multiple cell cycle-promoting genes, such as cyclin E, Myc, and the Aurora kinases (Kiessling et al., 2010). At the same time, it has been reported that RB, the key protein of the G1 cell cycle checkpoint, and WEE1, the key protein of G2 cell cycle checkpoint, are lacking from normal appearing 8-cell stage human embryos (Harrison et al., 2000). Furthermore, the SAC protein BUB1, which not only ensures correction of misalignments but is also reported to maintain sister chromatid cohesion (Kitajima et al., 2005; Perera et al., 2007), has been found to be lowly expressed after fertilization in human embryos up to the 4-cell stage (Wells et al., 2005). In combination, these results suggest that the absence of proteins critical for proper segregation and chromosome cohesion such as the SAC genes and cell cycle checkpoints during early human preimplantation development likely contributes to mitotic aneuploidy by permitting blastomeres with chromosome segregation errors to progress through mitosis. Notably, human pluripotent stem cells, which share characteristics with early

embryonic cells, exhibit similar vulnerabilities. Reduced kinetochore-microtubule attachment fidelity and weakened spindle assembly checkpoint mechanisms in these cells exacerbate the risk of chromosome mis-segregation (Deng et al., 2023), paralleling the challenges faced by early embryos.

The activation of the zygotic genome in humans occurs at the 4- to 8- cell stage and, before that, maternal and paternal factors could influence proper chromosome segregation. Many of the proteins regulating correct chromosome segregation during the first divisions are provided by the oocyte. However, as previously mentioned, no major correlation has been found between maternal age and mitotic aneuploidies (Antonarakis et al., 1993; Katz-Jaffe et al., 2005). This suggests that the inherently error-prone nature of the first embryonic divisions is such that aged cytoplasm and cohesins in the oocyte do not further exacerbate this condition. About paternal factors, the human egg depends on the fertilizing sperm to be the source of the centrosome. Consistently, there are severe sperm defects, such as those observed in nonobstructive azoospermia (NOA), that can lead to centrosome dysfunction, resulting in increased rates of mitotic abnormalities and mosaicism (Magli et al., 2009). Furthermore, the error-prone nature of the first mitotic divisions seems to be species-specific. Mouse embryos display an extremely low mis-segregation rate in the first mitotic division (2%), compatible with the low level of embryonic aneuploidy observed (Maciejewska et al., 2009), while bovine cleavage stage embryos display levels of aneuploidy comparable with human (74%, of which 88% mosaics). It has been speculated that mosaic aneuploidy in preimplantation embryos in mammals, which produce fewer offspring and invest heavily in gestation and offspring care, could hold biological benefits. The error-prone nature of early mitotic divisions might serve as a selective mechanism that reduce the likelihood of full-term development under unfavorable conditions, such as poor maternal health or low gamete quality, acting as a natural filter for reproductive success (Vázquez-Diez & FitzHarris, 2018). This aligns with the observation that species with a greater reliance on the success of single pregnancies, such as bovines, exhibit higher rates of mosaicism compared to mice, which often have multiple offspring per pregnancy. This mechanism in fact would be particularly advantageous in species where reproductive success hinges on the health of a single offspring, reinforcing the idea that early embryonic error-proneness is an adaptive strategy for selective reproductive success.

Overall, these findings highlight that mosaic aneuploidy is a widespread event in human embryos, which raises questions on its clinical significance and on the developmental potential of mosaic embryos (Robertson & Richards, 2024). Indeed, mosaic aneuploidies have been related with miscarriages and might cause serious fetal complications like intrauterine growth delay, congenital malformations, mental retardation, and uniparental disomy (I. Lebedev, 2011). Mosaic trisomies for example have been reported in 1/16667 births of which only 41% were liveborn (Wellesley et al., 2012). The reported occurrence of mosaic aneuploidies in early miscarriages varies significantly depending on the detection technique employed. Rates range from 94% when using FISH for all chromosomes and 29% with classic cytogenetic analysis (Lebedev et al., 2004), to 48.3% when using FISH for only 11 chromosomes (Vorsanova et al., 2005) and 50.7% with whole-genome SNP genotyping (Essers et al., 2023). However, despite the fact that many miscarriages present mosaic aneuploidies, there is evidence that embryos with mosaicism can also develop into healthy births, indicating

that mosaic aneuploidy is not always incompatible with normal development. For instance, the fact that approximately 8–15% of clinically recognized pregnancies (Regan et al., 1989; X. Wang et al., 2003) and 30% of all pregnancies result in a miscarriage (Wilcox et al., 1988), together with the observation that 70-80% of embryos are aneuploid mosaics (Chavli et al., 2024; van Echten-Arends et al., 2011), suggests that aneuploid mosaics can somehow deal with the presence of aneuploid cells to achieve normal developmental potential. Indeed, several studies support the idea that the degree of aneuploidy compatible with normal development depends on the proportion and allocation of aneuploid cells.

Given that commitment to inner cell mass versus trophoblast begins at approximately the 16-cell stage, when one or two cells become positioned within the ball of blastomeres, during most preimplantation stages around 9-10% of total cells will give rise to the fetus. Even if the ratio between diploid and aneuploid blastomeres needs to be above a certain level to ensure proper development (Evsikov & Verlinsky, 1998), several reports support the idea that even a significant proportion of aneuploid cells may not affect fetal viability. For instance, frozen human embryos that lost nearly half of their blastomeres are still able to result in live births, implying that not all blastomeres of human preimplantation embryos are necessary for proper development into a child (Munné et al., 1995). Furthermore, injection of donor embryonic stem (ES) cells, with only 20% being diploid and the remaining 80% carrying chromosomal abnormalities, into tetraploid blastocysts resulted in fully diploid, normal adult mice. As tetraploid cells are excluded from forming the embryo proper, the resulting offspring must have originated entirely from the injected ES cells (Eggan et al., 2002). Since the deleterious effect of aneuploidy in the entire embryo discussed in the previous chapters, it is a likely possibility that in aneuploid-diploid mosaics aneuploid cells are selected against. Coherently, mosaicism rates in human embryos start declining on day 3 (M. Yang et al., 2021) and continue to decrease as embryos progress from the morula to the blastocyst stage and later post-implantation (van Echten-Arends et al., 2011). Importantly, mosaic aneuploidy can still be compatible with healthy full-term development and live birth (Bolton et al., 2016; Greco et al., 2015), as long as they retain a sufficient amount of euploid cells in the ICM (Capalbo et al., 2021; Munné et al., 2017). In this regard, a study reported that out of 9 mosaic aneuploid blastocysts used for frozen-thawed embryo transfers, the 5 that were successfully delivered presented normal karyotypes in prenatal chromosomal analysis, while 2 out of the 4 miscarried presented the same chromosomal abnormalities as previously detected (M. Yang et al., 2021). Accordingly, persistent aneuploidy in the ICM leads to developmental failure or abnormalities (Essers et al., 2023).

Different mechanisms have been proposed to contribute to the elimination of aneuploid cells from mosaic embryos. For instance, during early embryonic development, mechanisms such as apoptosis play a critical role in maintaining the balance of euploid cells in mosaic embryos. Evidence from mice suggests that apoptosis selectively removes aneuploid cells, especially within the ICM, to support proper development (Bolton et al., 2016). The onset of apoptosis appears to occur after activation of the embryonic genome, as apoptotic markers, such as TUNEL-labeled nuclei, are rarely seen during the cleavage stages but increase significantly by the morula stage (Hardy et al., 2001; Wells et al., 2005). Later, as embryos reach the blastocyst stage, apoptotic markers are upregulated, allowing selective elimination of defective cells (Spanos et al., 2002). Live imaging

in mouse embryos shows that some aneuploid cells in the ICM undergo apoptosis, increasing the proportion of euploid cells (Bolton et al., 2016). Consistently, a study in micropatterned human gastruloids reveals that aneuploid cells are eliminated from embryonic germ layer through bone morphogenetic protein 4 (BMP4)-dependent apoptosis (M. Yang et al., 2021). Overall, these data indicate that viability of aneuploid mosaic embryos depends on the amount of aneuploid cells present. This is coherent with phenotypic variability of individuals affected by Mosaic Variegated Aneuploidy (MVA), caused by mutations in genes of the SAC like *BUB1B* and *CEP57*. Individuals affected by MVA present widespread mosaic aneuploidy, and exhibit microcephaly, growth retardation, developmental delays, and a heightened risk of cancers. Importantly, the severity of the disorder correlates with the degree of aneuploidy, with individuals experiencing less severe phenotypes when aneuploidy levels are lower (Malumbres & Villarroya-Beltri, 2024).

Another proposed mechanism for dealing with aneuploid cells is self-correction. This may operate via cellular fragmentation and blastomere exclusion of abnormal cells (Daughtry et al., 2019; Orvieto et al., 2020) or through additional mis-segregation events that counteract the initial errors, such as trisomy rescue. Trisomy rescue is essentially a reversion event in aneuploid cells, in which one of the three chromosome copies is lost during cell division to restore the diploid genome in at least a portion of the cells of the organism. Uniparental disomy (UPD), where both copies of a certain chromosome in an individual originated from the same parent, has been suggested as proof for the occurrence of trisomy rescue (Balbeur et al., 2016; Katz-Jaffe et al., 2005). Cases of monosomic rescues have been hypothesized in patients with non-mosaic paternal UPD, suggesting a meiotic non-disjunction in maternal meiosis which resulted in a nullisomic egg and subsequent rescue after fertilization through replication of the paternal copy of the missing chromosome (Conlin et al., 2010). The absence of mosaicism compared with trisomic rescues would be explained with the lethality of the monosomic and/or nullisomic cells respect to trisomic cells. Further investigation would be required to determine whether the correction of abnormal blastomeres and embryos occurs as an active mechanism or merely as an accidental event that is later positively selected for.

Different studies report direct evidence of trisomy rescues where zygotes with a meiotic trisomy reverted to disomy during the first cell divisions, resulting in a euploid fetus with uniparental disomy. As a proof of the previous trisomic nature of the embryo, the placenta exhibited a mix of trisomic and disomic lineages (Coorens et al., 2021; Robinson et al., 1997). This suggests that embryos can tolerate some level of mosaicism if aneuploid cells are confined to the TE rather than the ICM. Spatiotemporal allocation of abnormal cells in extraembryonic tissues can lead to a condition called confined placental mosaicism (CPM), defined as a chromosomally abnormal cell line restricted to the placenta, while the chromosomes of the fetus itself are normal (Kalousek & Dill, 1983). CPM is found in about 4% of chorionic villi analyses (Lund et al., 2020) and even if it can be associated with fetal growth restriction (Eggenhuizen et al., 2021; Grati et al., 2020), most CPM pregnancies continue with no complication (Amor et al., 2006). A study that compared DNA of chorionic villi (originating from the TE) and extra-embryonic mesoderm (supposedly originating from the ICM) from miscarriages allowed to determine whether different levels of mosaicisms between the placenta and the fetus affected the fate of early prenatal development and the risk of pregnancy loss. In all samples with autosomal

aberrations, the level of mosaicism was higher in extra-embryonic mesoderm than in chorionic villi (Essers et al., 2023), which contrasts with viable pregnancies where mosaic abnormalities are often restricted to the chorionic villi (Sifakis et al., 2010). All these data further reinforce the idea that aneuploid cells are more tolerated in the placenta. Since the clonal dynamics of human embryos cannot be studied prospectively, no direct evidence supports the idea that aneuploid cells are specifically directed to the trophectoderm. However, Bolton and colleagues have elegantly demonstrated that in mouse embryos aneuploid cells are evenly distributed in the TE and the ICM, but with their depletion occurring through different mechanisms: apoptosis in the ICM and cell cycle arrest and senescence in the TE (Bolton et al., 2016). However, abnormal TE cells, despite decreasing in proportion over time respect to wild type cells, often remained viable. Another insightful study on clonal dynamics in human embryo was performed by Yang and colleagues thanks to mosaic aneuploid gastruloids made of reversine-treated hESCs mixed at various ratios with euploid cells (M. Yang et al., 2021). By exposing these cells to the differentiation factor Bmp4, the gastruloids self-organized into embryonic and extra-embryonic lineages allowing to observe that aneuploid cells died though apoptosis in embryonic lineages and preferentially contributed to extraembryonic tissues like the TE. Interestingly, gastruloids made of up to 75% of aneuploid cells displayed normal self-organization and a higher tendency of accumulating aneuploid cells in the extraembryonic lineage (M. Yang et al., 2021). Overall, these studies strongly suggest that some of these aneuploid cells could persist and contribute to the future placenta, explaining the occurrence of CPM.

That said, it is important to note that a study on aneuploid human blastocyst deriving from meiotic mistakes reports conflicting findings. While the same pathways as mouse embryos seems to be activated in response to aneuploidy such as autophagy, proteotoxic stress and p53, aneuploid human blastocysts show differentiation defects both in the TE and ICM and present more cell death in the TE than the ICM (Regin et al., 2024). This aligns with data on aneuploid mosaics that show lower p53 activation in the ICM than the TE lineage (Martin et al., 2023). A lineage tracing study in human aneuploid-euploid mosaics would unravel whether mosaicism influences clonal dynamics and lineage-specific responses to aneuploidy in embryogenesis, or whether species differences or a reversine-specific effect are responsible for these incongruences.

3.2. Aneuploidy in somatic tissues

In accordance with its prevalence in human embryos and its compatibility with healthy births, aneuploid mosaicism has been also found in adult somatic tissues. Not only the human body is derived from a single zygote through an estimated 10^{16} mitotic divisions, but billions of new cells must divide daily to replace those lost (Iourov et al., 2010). Given this immense scale of cellular processes, it is improbable for every cell in an organism to retain an identical genome. Several studies suggest that somatic mosaicism in adult tissues arises from both embryonic and later mis-segregation events, consistent with the observed increase in aneuploidy levels over lifespan and during aging.

For instance, a study of copy number variations between 19 pairs of monozygotic twins showed that a pattern of different aneuploidies existed between twins, providing an irrefutable example of somatic mosaicism as a result of mitotic errors (Bruder et al., 2008). A study that tested DNA from 11 to 12 tissues such as brain, skin,

heart, muscle, kidney, liver and mucosa from three deceased males, observed at least six segmental aneuploidies ranging from 82 to 176 kb affecting a single organ or one or more tissues of the same subject (Piotrowski et al., 2008). This supports a scenario in which mitotic abnormalities could arise both earlier during embryo development and later in life. Accordingly, new technologies allowed detection of widespread somatic mosaicism in the human body, the grade of which varies from tissue to tissue. For example, it spanned from 14% in fibroblasts and amniocytes (K. Jacobs et al., 2014) to 30% (Abyzov et al., 2012) in fibroblasts. Interestingly, most of the detected abnormalities were segmental aneuploidies with a reported average size spanning from hundreds of kb (Abyzov et al., 2012) to around 20.0 Mb (K. Jacobs et al., 2014; McConnell et al., 2013), most of which included the telomeres (K. Jacobs et al., 2014).

There are certain tissues which have shown to be physiologically aneuploid. For instance, hepatocytes in both mice and humans exhibit significant levels of aneuploidy while maintaining normal functionality. In both human (Duncan et al., 2012) and mice (Duncan et al., 2010), hepatocytes undergo a process known as the "ploidy conveyor," where polyploid cells transition through multipolar divisions, generating aneuploid daughter cells. This process results in 25% of hepatocytes being aneuploid at three weeks of age, increasing to 60–70% in older mice (Duncan et al., 2010). Similarly, human hepatocytes also demonstrated high rates of aneuploidy, with 25–50% of cells showing chromosomal imbalances with sets of probes for discrete chromosome combinations (20-25% autosomal gain and 65-80% loss) (Duncan et al., 2012). Interestingly, aneuploidy appears to be independent of patient age in humans. Aneuploidy may enhance the genetic diversity of hepatocytes, providing adaptive advantages under conditions such as chronic liver injury. This aligns with various studies suggesting that aneuploidy and karyotype variability serve as adaptive mechanisms for responding to stress in diverse contexts, including cancer evolution (Laughney et al., 2015; Rutledge et al., 2016).

Another organ where it has been reported high presence of aneuploid mosaicism is the brain. In mice, 33% of the neural stem cells during development have been reported to be aneuploid by spectral karyotype analysis (Rehen et al., 2001) due to chromosome segregation defect such as lagging chromosomes (A. H. Yang et al., 2003). In the embryonic cerebral cortex in mice, metaphase chromosome analyses revealed that 15.3% and 20.8% of cerebellar neural stem cells are aneuploid at postnatal day 0 and 7, respectively (Westra et al., 2008). Human fetal brains display similar levels of aneuploidies around 30-35%, determined by FISH (Yurov et al., 2007). In the adult human and mouse brain, aneuploidy frequencies are much lower than those observed in the developing brain, suggesting that most aneuploid cells may be removed during development. Whole-chromosome aneuploidies for chromosome 21 were observed by FISH in approximately 4% of human brain cells, suggesting that nondisjunction is a recurrent feature of somatic variation in the brain (Rehen et al., 2005). This is coherent with trisomies being found in the mouse brain especially for chromosome 16, which is syntenic with human chromosome 21 (Mukamel et al., 2023). Using set of probes for sets of specific chromosomes, 0.1-0.8% of aneuploid cells were observed in human adult brain (Iourov et al., 2009; Yurov et al., 2005) and especially chromosome loss was found in the adult cerebellum at a rate of approximately 1% per chromosome in both neuronal and nonneuronal populations (Westra et al., 2008). Studying aneuploidy through FISH has

the limitation of allowing observation of only certain chromosome combinations at the same time and of underestimating segmental aneuploidies. With more recent single-cell sequencing approaches, at least one segmental aneuploidy of 1Mb was found in 13-41% of human neurons, with deletions twice as common as duplications (McConnell et al., 2013). Whole-chromosome aneuploidies have been reported in <1% of cells of the adult mouse brain, with rates up to 1.8% in non-neuronal cell types (Mukamel et al., 2023). Despite aneuploidy being correlated with dysfunction and pathological conditions in the brain such as microcephaly, neurodegeneration, and cancer predisposition (Iourov et al., 2009; Malumbres & Villarroya-Beltri, 2024; Mirzaa et al., 2014; Yurov et al., 2019), a certain percentage of aneuploid neurons could be compatible with normal function. Consistently, immediate early gene expression confirmed that aneuploid neurons can be functionally active (Kingsbury et al., 2005). This evidence altogether supports the idea that a certain degree of aneuploidy is a physiological aspect of mammalian nervous system development and function, with evolutionary origins tracing back to bony fishes (Rajendran et al., 2007). On one side, aneuploidy could contribute to neuronal diversification in the developing brain (Muotri & Gage, 2006). On the other side, the resulting mosaic neural circuits, including functioning aneuploid neurons intermixed with euploid populations, may contribute to physiological and behavioral variation in the adult mammalian brain by altering neuronal signaling properties through ploidy-dependent gene dosage mechanisms like chromosomal loss (Kaushal et al., 2003) and duplication (Singleton et al., 2003).

Even if these studies suggest widespread ploidy changes in somatic tissues, other studies argue that due to technical challenges somatic aneuploidy has been overestimated (Knouse et al., 2014). Knouse and colleagues in this study analyze liver and brain samples from healthy individuals and found no aneuploid nuclei among 66 mouse liver cells, while in human hepatocytes (100 cells from two males), aneuploidy was found in only 4% of cells, compared to the 25-50% observed by FISH in 200 hepatocytes per sample from 21 different individuals (Duncan et al., 2012). Regarding the adult brain, the prevalence of aneuploid cells was reported as 1% in mouse (from 43 cells) and 2.2% in humans (89 cells from four individuals), coherently with single-cell-sequencing-based reports for whole-chromosome aneuploidies (McConnell et al., 2013; Mukamel et al., 2023). The information about the brain appears more contradictory when looking at segmental aneuploidies in adult neurons, detected up to 41% by McConnel and colleagues compared to none in this study, and when looking at the developing brain, detected up to 35% by previous studies (Rehen et al., 2001; Yurov et al., 2007) compared to none in this study (0/36 mouse embryo cells analyzed). Differences in methodologies, sample size, and sample sources likely contribute to the inconsistencies observed in reports on somatic aneuploidy levels. For the liver, aneuploid cells have indeed been observed, but their prevalence appears much lower in single-cell sequencing studies compared to earlier FISH analyses. Despite the higher precision of single-cell sequencing, the limited number of samples analyzed in this study must be acknowledged. In contrast, FISH, while involving larger sample sizes, may overestimate aneuploidy due to its technical limitations. Thus, the evidence supports the presence of aneuploid hepatocytes, but the extent remains uncertain. Regarding the brain, the discrepancies are particularly pronounced when comparing studies on the developing brain that suggest aneuploidy levels of up to 35% in embryonic brain cells in earlier studies, while single-cell sequencing

studies detected none. Regardless of these variations, the data, summarized in Figure I5, consistently indicate that the majority of aneuploid brain cells are eliminated before adulthood, leaving the role of aneuploid cells in the adult brain largely unresolved.

Overall, while the notion of a functional role for aneuploid cells in somatic tissues remains intriguing, current evidence suggests that such cells are less prevalent than previously thought, and their significance in normal tissue function remains to be conclusively demonstrated.

3.2.1. Aneuploidy and ageing

We have discussed the prevalence and significance of mosaic aneuploidy during development and in adult somatic tissues. Somatic aneuploidy has been also linked to aging and age-associated diseases (Figure I5). A correlation between ageing and aneuploidy has been established already many years ago in oocytes (Stone & Sandberg, 1995; Guttenbach et al., 1994; Mukherjee et al., 1996; Mukherjee & Thomas, 1997). In the examples of somatic cells discussed previously, the percentage of aneuploid cells increases with age. For instance, 60–70% of aneuploid hepatocytes are observed in older mice compared to 25% at three weeks of age (Duncan et al., 2010), and aneuploid cells for blood and buccal samples increased with age from 0.23% under 50 years to 1.91% between 75 and 79 years (K. B. Jacobs et al., 2012). In the mice brain, aneuploidy was found to accumulate with age in a chromosome-specific manner especially in non-neuronal cells (Faggioli et al., 2012). Consistently, aneuploidy levels are notably higher in brain disorders associated with accelerated aging, such as Alzheimer's disease (AD), ataxia-telangiectasia (AT), and Down syndrome, with 20-50% of neurons estimated to be aneuploid in AT versus 10% in controls, and 6-18% of AD neurons displaying trisomy 21 versus 0.8-1.8% in controls, supporting its role in these conditions (Dierssen et al., 2009; Iourov et al., 2009; Yurov et al., 2009).

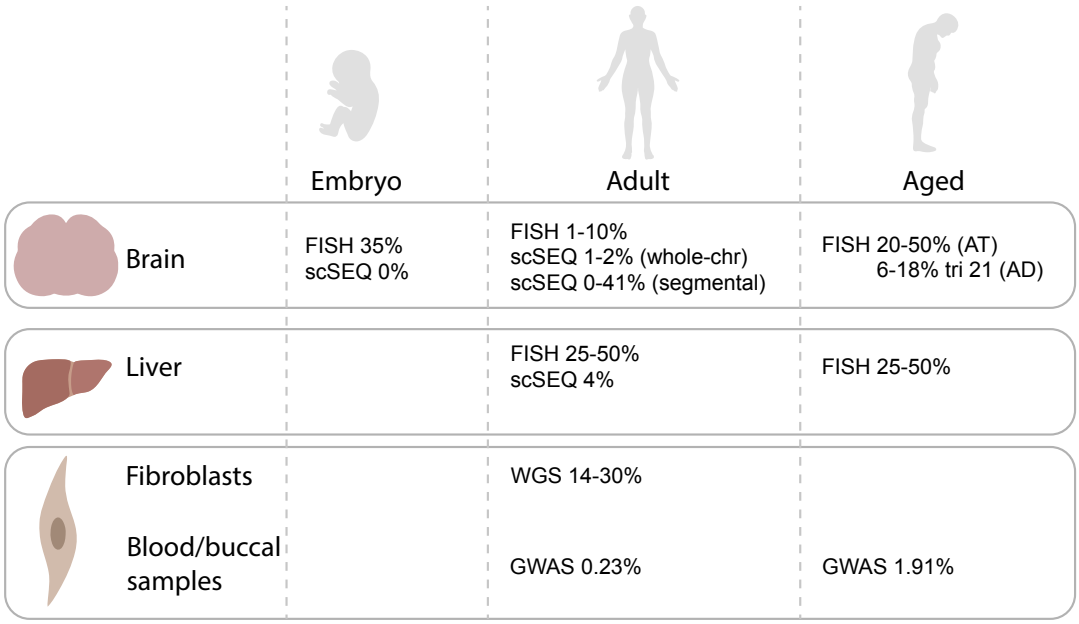

Figure I5. Detected aneuploidy in somatic tissues. Detected aneuploidy varying according to age, tissue and technique employed. scSEQ=single cell sequencing. WGS=whole genome sequencing (including array-based methods). GWAS=genome wide association study. AT= ataxia-telangiectasia. AD= Alzheimer's disease. Tri 21=trisomy 21.

Increasing evidence suggests that the accumulation of senescent cells plays a significant role in the aging process (Hernandez-Segura et al., 2018; López-Otín et al., 2023). Senescent cells are characterized by a permanent cell cycle arrest and the secretion of inflammatory cytokines, chemokines, growth factors, and proteases, collectively known as the senescence-associated secretory phenotype (SASP). Interestingly, it has been observed a senescent-like phenotype and up-regulation of the SASP components in non-neuronal cells in normal brain aging, age-related neurodegeneration and Alzheimer's disease (Chinta et al., 2015). In this context, the emergence of senescence in the brain may serve as a unifying mechanism linking age-related inflammation and neurodegeneration (Andriani et al., 2017), potentially contributing to the increased incidence of brain tumors with aging (Flowers, 2000). The relationship between aneuploid cells and the senescence phenotype has been widely investigated both in ageing and cancer (see more in next chapter). A study of young, middle-aged and old-aged human dermal fibroblasts revealed that elderly fibroblast display higher mitotic duration and segregation mistakes due to a transcriptional repression of mitotic genes in pre-senescent dividing cells, and exhibit SASP (Macedo et al., 2018). A causative relationship between the emergence of aneuploidy, ageing and senescence has been established by a study on mutant mice with low levels of the spindle assembly checkpoint protein BubR1 (D. J. Baker et al., 2004). Reduced BubR1 expression led to progressive aneuploidy and the development of progeroid features, such as a shortened lifespan, cachectic dwarfism, cataracts, and impaired wound healing, as well as increased cellular senescence and defects in meiotic chromosome segregation, resulting in infertility. Interestingly, natural aging in wild-type mice was marked by decreased expression of BubR1 in multiple tissues (D. J. Baker et al., 2004). Conversely, sustained high-level BubR1 expression corrects age-dependent mitotic checkpoint impairments, prevents microtubule-kinetochore attachment defects, extends lifespan and delays age-related tissue deterioration (D. J. Baker et al., 2013). Consistently, another study reported a decrease in the gene expression level of genes involved in centromere and kinetochore function and in the microtubule and spindle assembly apparatus in aged fibroblasts and lymphocytes (Geigl et al., 2004). Furthermore, the majority of MVA patients, which present progeroid features, have mutations in the SAC genes (Matsuura et al., 2006). Overall, these data suggest a mutual causality between ageing and aneuploidy.

One interesting proposed mechanism for the loss of segregation fidelity with age is that the shortening of telomeres, a renown hallmark of ageing (López-Otín et al., 2023), makes chromosomes more prone to mitotic missegregation. In this context, a study with lymphocytes and buccal mucosa cells revealed a significant negative correlation between chromosomal aneuploidy and telomere length, indicating that chromosomes with higher loss rates had shorter telomeres (Leach et al., 2004). This is an interesting scenario considering the previously discussed studies that reported a higher rate of chromosome loss respect to chromosome gain in adult somatic tissues (Duncan et al., 2012; McConnell et al., 2013; Westra et al., 2008).

4. Aneuploidy in disease: the case of cancer

Aneuploidy has been found in most malignant cancers with great heterogeneity within tumors and between different tumor types. 90% of solid tumors and 75% of hematopoietic cancers were reported to be aneuploid

(Weaver & Cleveland, 2006; Taylor et al., 2018). With a median of 5 gains and 3 losses of chromosome arms per cancer cell, it is fair to say that no other genetic alterations affect cancer genomes to this extent. In the previous chapters we have thoroughly discussed the deleterious effects of aneuploidy on fitness both at the cellular and organismal level, therefore it might seem contradictory to find such a high prevalence of aneuploid cells in tumors that are generally made by highly proliferative cells. However, there are several works that explain the role of aneuploidy in promoting tumorigenesis.

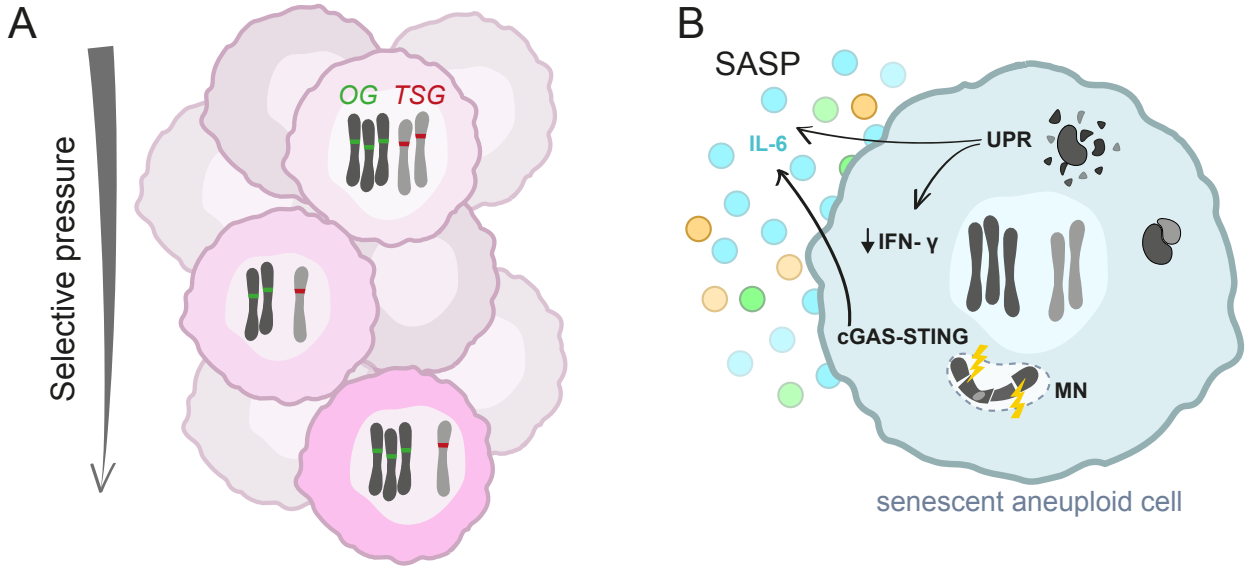

Figure I6. Karyotype-dependent and independent contribution of aneuploid to tumorigenesis. (**A**) Karyotype-dependent contribution of aneuploid to tumorigenesis has been explained in terms of gaining oncogenes (OG) and loosing tumor suppressor genes (TSG) through copy number variations. (**B**) Karyotype-independent contribution of aneuploidy to tumor relies on the senescent phenotype of aneuploid cells that through SASP modulate systemic effects, metastatic behavior, and that alongside the UPR and cGAS-STING pathway create an immunodepressive microenvironment.

In tumor tissues, aneuploidy is the consequence of ongoing chromosomal instability (CIN), a high rate of missegregation events during mitosis. CIN's role in cancer progression has been explained in terms of source of adaptability (Jaarsveld and Kops, 2016). The existence of characteristic aneuploidy patterns within some cancer types [e.g. loss of Y, which encodes for several immunogenic genes, in bladder cancer (Abdel-Hafiz et al., 2023)] suggests that specific deletions or duplications, positively selected between the different karyotypes induced by CIN (Laughney et al., 2015), can drive tumorigenesis (Figure I6A). Furthermore, as already mentioned, aneuploid cells are in turn inherently more chromosomally instable and can therefore exponentially increase intratumor heterogeneity. *In vivo* models of random aneuploidies in mice have demonstrated that specific karyotypes bearing gain of oncogenes are preferentially acquired over time (Shoshani et al., 2021; Trakala et al., 2021). Conversely, cancer cells can depend on specific aneuploidies for survival (Girish et al., 2023). Consistently with the proposal that CIN-induced intratumor heterogeneity in the form of gene-dosage alterations increases adaptability, tumors with a higher level of CIN have been correlated with a higher resistance to anti-cancer therapy (Crowley et al., 2022; Ippolito et al., 2021; Lukow et al., 2021; Replogle et al., 2020) and with relapse (Kusumbe & Bapat, 2009).

At the same time, tumors often lack specific aneuploidy signatures suggesting that aneuploidy might have a general positive effect on tumor progression independently on the karyotype. In this regard, it has been

proposed that aneuploid cells otherwise eliminated from a healthy tissue can remain in the tissue in the presence of aneuploidy-tolerating mutations, such as mutations in the apoptotic pathway. In this direction, models in both mice and *Drosophila* propose a direct causal relationship between aneuploidy and tumorigenesis by showing that pathways activated in aneuploid cells as a stress-response contribute to tumor development if aneuploid cells are not correctly depleted from the tissue (Thompson and Compton, 2010, Li et al., 2010, Dekanty et al., 2012, Clemente et al., 2016). The role of aneuploid cells in eliciting a tumorigenic response has been connected to senescence. In fact, aneuploid cells have been shown to enter into senescence and exhibit SASP in human cells *in vitro* (Santaguida et al., 2017) and in *Drosophila in vivo* (Joy et al., 2021). We have previously commented the implication of senescence in the context of ageing-induced aneuploidization. In the context of cancer, in a *Drosophila* model of tumorigenesis the SASP of aneuploid cells is reported to modulate local tumor proliferation, invasive behavior of aneuploid cells, systemic delay of the organism, and ultimately, lethality (Joy et al., 2024). In mammals, the senescent nature of aneuploid cells has huge implications on the recruitment and modulation of the immune system (Figure I6B). In fact, aneuploid cells *in vitro* have been shown to be eliminated by NK cells through NF-κB signaling (Santaguida et al., 2017; R. W. Wang et al., 2021). Interestingly, in cancer cells, NF-κB upregulation correlates with the degree of aneuploidy but this upregulation alone is not sufficient to trigger NK cell-mediated clearance (R. W. Wang et al., 2021). This suggests that, during cancer evolution, additional mechanisms may arise to counteract NF-κB-mediated immunogenicity, allowing aneuploid cancer cells to evade immune detection. Consistently, aneuploidy has been shown to correlate with immune evasion (Davoli et al., 2017). Several works have investigated the mechanisms underlying immune evasion by aneuploid cells. For instance, the UPR response has been linked to upregulation of the immune-suppressive cytokine IL-6 and the downregulation of the immunogenic IFN- γ (Xian et al., 2021). This is especially relevant in the case of gain of chromosomes that have been shown to activate the UPR response. Furthermore, the cGAS-STING pathway, activated as an intracellular response to cytosolic DNA triggered by the presence of micronuclei in aneuploid cells subjected to CIN (K. J. Mackenzie et al., 2017), has been correlated both with immunosuppression through IL-6 upregulation (Hong et al., 2022) and metastatic behavior (Bakhoum et al., 2018).
However, in exploring the relationship between aneuploidy and cancer, this work will focus on the first, karyotype-dependent, contribution of aneuploidy to tumorigenesis.

4.1. Cancer as an aneuploid mosaic

Cancer can be thought of as a genetic mosaic, encompassing somatic single nucleotide variants, structural chromosomal changes, and chromosomal copy number alterations. As a matter of facts, tumors represent mosaics of genetic imbalances harbored by aneuploid cells. In the cases of monosomies or segmental monosomies, these cells harbor heterozygous losses, while trisomies or segmental trisomies result in amplifications of multiple genes. Each gene within the aneuploid region that exhibits a dosage-sensitive phenotype—whether through haploinsufficiency or triplosensitivity (where losing or gaining a single copy of a gene produces a phenotype, respectively)—contributes collectively to the behavior and fate of the aneuploid

cell. In essence, aneuploid mosaics can be regarded as mosaics of functional mutations, with gene dosage imbalances acting equivalently to classical mutations in altering cellular function. This framework is particularly compelling in the context of cancer, a genomic disease characterized by pervasive mutations and chromosomal instability (CIN) (Taylor et al., 2018), where CIN and the resulting karyotypic and mutational heterogeneity in daughter cells are closely linked to poor prognosis (Ippolito et al., 2021).

We have thoroughly discussed the prevalence of aneuploid mosaicism in adult tissues as a result of missegregation events throughout development. Whether aneuploid mosaicism can predispose to cancer remains an intriguing question. In a study of 1,991 individuals with bladder cancer, genomic abnormalities were found in 1.7% of the samples but were present in both the blood and bladder tissues, suggesting an early developmental origin rather than emergence in the bladder tissue itself as a tumor-initiating event (Rodríguez-Santiago et al., 2010). In this regard, another study investigated whether detectable clonal mosaicism predisposes to hematological and non-hematological cancer. Although only 3% of subjects with detectable clonal mosaicism had records of hematological cancer, the study estimated that the risk of hematological cancer was tenfold higher for mosaic than for non-mosaic individuals (Laurie et al., 2012). Regarding non hematological cancer, the evidence pointed at a positive relationship between mosaic status and cancer but lacked statistical significance (Laurie et al., 2012). Another studied reported that mosaic abnormalities in gene copy number were more frequent in individuals with solid tumors than cancer-free individuals (0.97% versus 0.74%, K. B. Jacobs et al., 2012). These findings suggest a correlation between aneuploid mosaicism and cancer. However, it looks like the emergence of cancer-predisposing mutations in somatic cells could occur both early and late in development and, for technical reasons, it is challenging to distinguish between these two scenarios.

It is known that cancer is a complex genetic disorder driven by alterations in both coding and non-coding regions of the genome, with two major classes of high-penetrance genes identified: oncogenes and tumor suppressor genes (Weinberg, 1994). Oncogenes, such as *c-Myc*, promote tumor development when activated by dominant mutations or overexpression, while tumor suppressor genes, like *p53* or *RB*, inhibit cancer progression but are inactivated through diverse mechanisms (Weinberg, 1994). Traditionally, tumor suppressor genes inactivation was thought to require the complete loss of function (Knudson, 1971), where both gene copies must be inactivated to drive cancer. However, recent findings highlight the role of haploinsufficiency, where the loss or mutation of a single allele reduces gene activity below a critical threshold necessary for suppressing tumorigenesis. This incomplete inactivation of tumor suppressor genes underscores their ability to contribute to cancer development and progression even when one functional allele remains, challenging the traditional view of tumor suppressor gene inactivation as a fully recessive process. The first gene that was identified as haploinsufficient for tumor progression was the Cdk inhibitor $p27^{kip1}$, through the observation that heterozygous mice presented accelerated tumor progression (Fero et al., 1998). After that, many genes such as *p53* (Venkatachalam et al., 1998) and *PTEN*, among others (reviewed in Berger & Pandolfi, 2011; Inoue & Fry, 2017) were reported to be haploinsufficient for tumor progression. Other recently described examples of potential haploinsufficient tumor suppressor genes are *BRCA1/2* and *MIIP*, proteins involved in ensuring

genomic stability, in mammary and colorectal cancer, respectively (Minello & Carreira, 2024; Sun et al., 2017). The mechanisms of haploinsufficiency can be diverse. P53 for example works in homotetramers, therefore a reduction in its concentration drastically affects its binding affinity and in fact it results in 25% expression of mRNA and protein in heterozygous mutants respect to wild types (Lynch & Milner, 2006). The case of *PTEN* is particularly intriguing as it introduces the concept of "obligate haploinsufficiency", where partial loss of gene function can be more tumorigenic than its complete loss. While heterozygous loss of *PTEN* enhances cell proliferation, complete loss paradoxically triggers a p53-dependent cellular senescence program that acts as a barrier to tumor development (Chen et al., 2005). Therefore, in a wild-type *p53* context, partial loss of *PTEN* is more advantageous for tumorigenesis. However, in cells with mutated or dysfunctional *p53*, where the senescence mechanism cannot be activated, complete loss of *PTEN* becomes more tumorigenic than its heterozygous loss (Alimonti et al., 2010). Other works propose that heterozygous mutation of certain genes could predispose pre-cancerous lesions to become cancerous, such as the genes *VHL* or *TSC1*/2 in renal cell carcinoma (Peri et al., 2016).

Overall, these findings highlight how partial loss of certain genes can synergize with either partial or complete loss of others, underscoring the cooperative interactions between tumor suppressor pathways. In this direction, it is highly relevant in the case of aneuploidy a phenomenon called cumulative haploinsufficiency, when multiple tumor suppressor genes that are located on specific chromosomal arms collectively contribute to tumor suppression, and their partial loss leads to synergistic effects on cancer progression. Examples are the chromosome arms 3p (L. Ji et al., 2005), 8p (Wistuba et al., 1999), 5q (Ebert, 2009) and 7q (Honda et al., 2015), which are frequently deleted in various cancers. Murine models allowed through RNAi screening to identify the different genes involved in those arms that cooperatively inhibit tumorigenesis, for example *Dlc1, Vps37a* and *Fgl1* on human 8p22 (Xue et al., 2012). Consistently with this idea, tumors present recurrent deletions and amplifications. A study that systematically analyzed somatic copy-number alterations (SCNAs) across 3,131 cancer samples, identified 158 recurrent focal SCNAs: 82 deletions and 76 amplifications. Deletions had a median of seven genes per peak region (range: 1–173), with 11% involving validated tumor suppressor genes such as *PTEN*, *RB1*, and *CDKN2A/B*. Amplifications had a median of 6.5 genes per peak region (range: 0–143), with 33% containing functionally validated oncogenes like *MYC*, *CCND1*, *ERBB2*, and *KRAS* (Beroukhim et al., 2010). To address the possibility that recurrent deletions are enriched for recessive tumor suppressor genes, a later work analyzed these regions for the presence of known or putative recessive tumor suppressor genes. The study found that the deleted regions are enriched for genes which negatively regulate cell proliferation (*STOP* genes) while tend to avoid essential genes that positively regulate cell proliferation (*GO* genes) (Solimini et al., 2012). The cumulative effect of haploinsufficiency of multiple *STOP* genes within these deletions likely optimizes tumor cell fitness by reducing their proliferative restraints. Concordantly, a later study also showed that recurrent amplifications in cancer genome are enriched for oncogenes while recurrent deletions on chromosome arms, such as 3p, 5q, and 8p, are enriched for *STOP* genes and avoid *GO* genes, suggesting selective pressure to avoid loss of genes critical for survival (Davoli et al., 2013). These findings underscore the non-random nature of SCNAs in tumors, where hemizygous deletions

maximize the advantage of reducing tumor-suppressive restraints while avoiding deleterious fitness costs. Importantly, this study presents evidence that the cumulative imbalance between *STOP* and *GO* gene dosage within specific chromosome arms is able to predict the selective patterns of chromosomal gains and losses seen in cancer, proposing that aneuploidy patterns in cancer genomes are shaped through a process of cumulative haploinsufficiency and triplosensitivity (Davoli et al., 2013).

5. Aneuploidy and cell competition

In the past chapters we have highlighted how aneuploidy *in vivo*, both in development and disease, is often found in the form of mosaic. It is therefore highly relevant to determine whether the interaction between aneuploid and euploid cells plays any role in the identification and elimination of aneuploid cells. In this regard, it has been proposed that cell competition might contribute to the elimination of aneuploid cells in certain contexts.

5.1. Cell competition in development and tumorigenesis

Cell competition is a homeostatic process conserved from *Drosophila* to mammals that compares the fitness of a cell with that of its neighbors and eliminates cells that, although viable, are less fit. During competition the cells that are eliminated become ‘‘losers’’, and the fitter cells, the ‘‘winners’’, repopulate the tissue through compensatory proliferation, maintaining tissue homeostasis. This mechanism was described in *Drosophila* for the first time many years ago for *Minute* (*Mn*) genes, genes encoding ribosomal proteins. Homozygous mutation for the *Mn* genes is lethal, while heterozygous $Mn^{+/-}$ animals are viable but display reduced body size (hence the name ‘minute’) and developmental delay due to slower proliferation of their cells (Morata & Ripoll, 1975). Surprisingly, clones of $Mn^{+/-}$ cells in the wing disc epithelium undergo apoptosis when surrounded by $Mn^{+/+}$ cells and specifically in the outer border of the loser clone, adjacent to wild type cells (Morata & Ripoll, 1975; Moreno et al., 2002). A similar phenomenon has been described in mice for the RP gene *Rpl24*, where $Rpl24^{+/-}$ cells have decreased rates of proliferation and are outcompeted by wild-type cells in chimeras (E. R. Oliver et al., 2004).

Another group of mutations that are eliminated by cell competition is the one including cell polarity genes such as *scribble*, *lethal giant larvae* (*lgl*), *discs large* (*dlg*) or overexpression of *Crumbs*, that induce tumors in whole-animals mutant but are eliminated by apoptosis when surrounded by wild type cells (Igaki et al., 2006; Tamori et al., 2010; Norman et al., 2012; Hafezi et al., 2012).

A complementary example of cell competition, where wild type cells are eliminated by fitter cells, is supercompetition induced by Myc, which has been extensively studied in both *Drosophila* and mammals. In *Drosophila* imaginal wing discs, cells overexpressing *dMyc*, the homolog of mammalian *c-Myc*, proliferate at higher rates and act as supercompetitors by inducing the elimination of neighboring wild-type cells that instead divide at slower rates (Figure I7A) (de la Cova et al., 2004; Moreno & Basler, 2004). Similar findings have

been observed in mammals, where mosaic overexpression of *c-Myc* during early mouse development or in differentiating embryonic stem cells leads to the elimination of adjacent wild-type cells through apoptosis (Clavería et al., 2013; Sancho et al., 2013). Conversely, establishing differential levels of *c-Myc* between wild type cells and loser cells in other types of cell competition is critical for elimination of the loser cells (Sancho et al., 2013). Interestingly, in the epiblast, *c-Myc* levels are normally heterogeneous and it has been shown that endogenous cell competition eliminates cells with low relative *c-Myc* levels, findings that were supported also by data in ES cells (Figure I7B) (Clavería et al., 2013). This was later explained by the fact that low *c-Myc* cells eliminated by cell competition were found to be less pluripotent than their high *c-Myc* counterparts, so that *c-Myc*-induced competition would be a mechanism to safeguard pluripotency (Díaz-Díaz, Fernandez de Manuel, et al., 2017). Other triggers for cell competition in the mouse embryo have been reported to be the Hippo pathway transcription factor TEAD (Hashimoto & Sasaki, 2019) and different levels of p53 (G. Zhang et al., 2017). Furthermore, p53 is responsible for elimination of less fit cells in other models of cell competition such as in BMP signaling defective cells (*Bmpr1a*$^{-/-}$, responsible for proper patterning) (Bowling et al., 2018). These results suggest that natural cell competition in early mammalian embryo could be a mechanism designed to remove viable cells that are unfit and that may compromise the general fitness or the viability of the organism. Furthermore, cell competition during development ensures correct organ formation. For instance, in the mammalian epidermis, cell competition operates as a crucial mechanism for correct tissue morphogenesis, in a first stage of development through apoptosis and engulfment and later through induction of early differentiation of loser cells (Figure I7C). Disruptions to this process compromise epidermal integrity and permeability during development (Ellis et al., 2019).

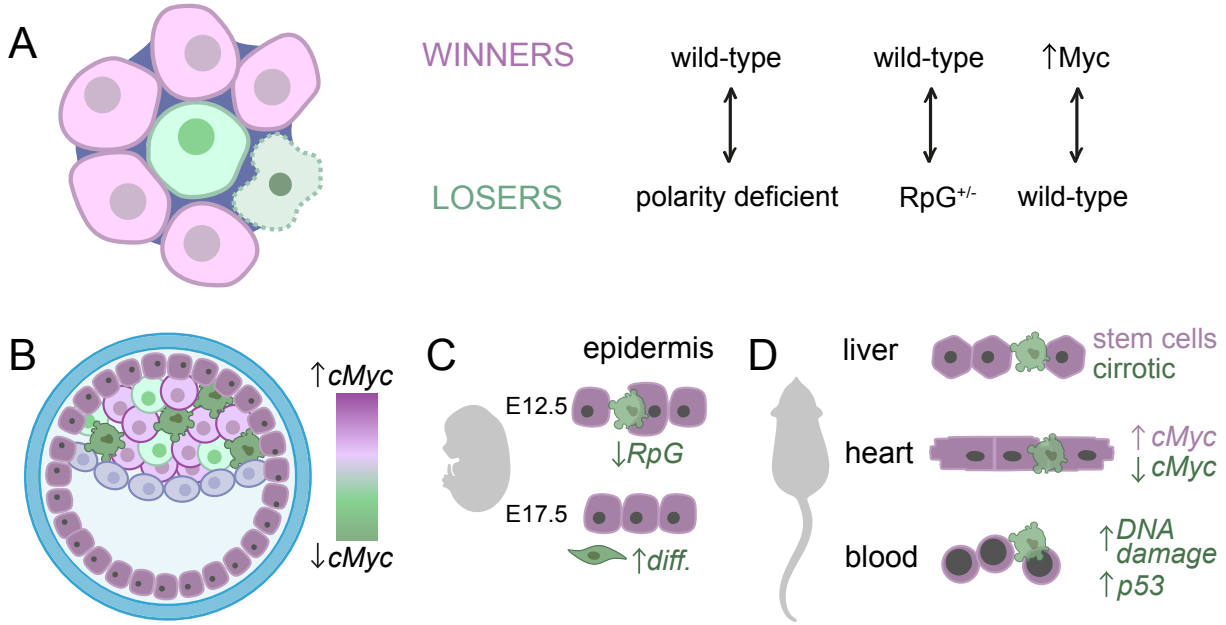

Figure I7. Cell competition during development. (**A**) Set of mutations that establish competitive interactions. Examples of cell competition processes during mice early (**B**) and later development (**C**), as well as in adult somatic tissues that maintain tissue homeostasis (**D**).

Cell competition has been reported to not only shape organ morphogenesis during development, but also maintain its homeostasis through damage and ageing (Figure I7D). For example, liver stem cells transplanted

into a diseased liver in mice induced apoptosis of host hepatocytes immediately adjacent to transplanted cells in a very similar manner as in *Mn*-induced cell competition in *Drosophila*, and repopulated the liver while maintaining overall organ size (Ding et al., 2011; Oertel et al., 2006). Furthermore, liver repopulation with liver stem cells occurs four to five times more rapidly and extensively in older hosts, where cells are less fit (Menthena et al., 2011). Interestingly, the *Azot* gene in *Drosophila*, which is essential for elimination of unfit cells during certain types of cell competition (e.g. *Mn*-induced cell competition and *dMyc*-induced supercompetition), decreases lifespan and accelerates organ degeneration when mutated while it increases lifespan when duplicated (Merino et al., 2015). This has interesting implications for the connection between cell competition and ageing and suggests that aged cells can be replaced by fitter cells through cell competition. Importantly, the capacity for cell competition in mammals is not restricted to stem cell populations as shown by the replacement of wild-type cardiomyocytes with *c-Myc*-overexpressing cardiomyocytes (Villa del Campo et al., 2014).

Cell competition has been also observed in the mammalian hematopoietic system, where DNA-damaged cells are outcompeted through non-cell autonomous growth arrest in a p53-dependent fashion and depending on the relative levels of p53 (Bondar & Medzhitov, 2010). A peculiar case of cell competition found in hematopoietic stem cells relates to revertant mosaicism (also known as somatic genetic rescue). Revertant mosaicism occurs when all cells in the embryo initially carry a deleterious variant, but a later mutational event either restores the variant allele to its wild-type form or compensates for it indirectly, such as by inactivating a gain-of-function variant. This phenomenon seems to be particularly common in the hematopoietic system (Revy et al., 2019; Wada & Candotti, 2008). If the reversion happens early enough in embryogenesis, it may be subjected to the same forces of competition as any other mosaic variant thus resulting in reverted variants of blood cells accumulating over time respect to the original mutation (Kuijpers et al., 2013).

If cell competition acts to maintain tissue homeostasis, it is not surprising that it has been reported to have tumor suppression effects in some cases (Figure I8A) (Kajita & Fujita, 2015). Examples in mammals have been described in the thymus, oesophagus and the skin epithelia. In mice, a constant turnover between young bone-marrow-derived and old thymus-resident progenitors is regulated by natural cell competition and disruption of this competition leads to T-cell acute lymphoblastic leukaemia (Martins et al., 2014). In the oesophagus, which suffers high rates of mutations over time, tissue homeostasis is maintained through clonal competition of mutations that confers a proliferative advantage (Colom et al., 2020). It has been shown that microscopic tumors that emerge in the mice oesophagus as a consequence of mutagenic treatment are outcompeted by fitter clones that expand in the surrounding normal tissue, leading to tumor loss (Colom et al., 2021). In the mice skin it has been shown how wild type cells are able to eliminate aberrancies generated from activated Wnt/β-catenin stem cells and oncogenic *Hras* (Brown et al., 2017). An example in *Drosophila* are the polarity genes such as *scrib*, that cause imaginal disc epithelia to overgrow into disorganized cell masses when generally mutated or knocked-down (Bilder et al., 2000), but lead to elimination through cell competition when mutated in clones in wild-type tissues (Brumby & Richardson, 2003).

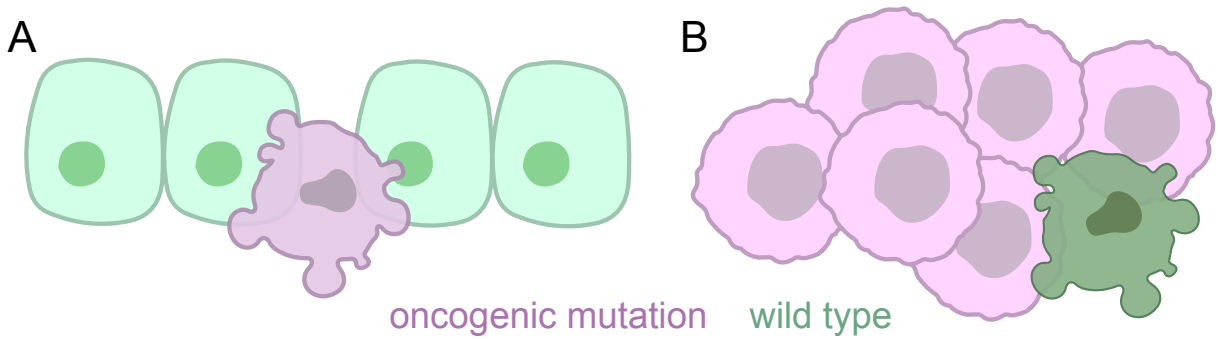

Figure I8. Tumor suppressive and promoting role of cell competition. Schematic representation of cases in which cells bearing potentially oncogenic mutations are eliminated through cell competition **(A)**, and cases in which oncogenic mutations make cells supercompetitors that kill wild type cells **(B)**.

Cell competition has also been proposed to play a role in tumor promotion (Figure I8B). Given the phenomenon of *Myc*-induced super competition, one might think that this could be an example. However, neither in mammals nor in *Drosophila Myc*-induced super competition has a phenotype or give rise to tumors (de la Cova et al., 2004; Moreno & Basler, 2004). However, works in *Drosophila* report mechanisms of supercompetition that are indeed responsible for neoplastic transformation. In particular, cells expressing EGFR and the microRNA miR-8 in the wing disc (Eichenlaub et al., 2016) or $APC^{-/-}$ cells in the intestine (Suijkerbuijk et al., 2016) compete with and kill surrounding cells. An interesting work in *Drosophila* shows that small mutant clones of *Rab5*, a gene involved in endocytosis, while outcompeted by wild type cells, if comprising more than 400 cells form an overgrowing tumor (Ballesteros-Arias et al., 2014). Importantly, in all the cases discussed, tumorigenic potential depends on the ability of these cells to induce apoptosis of nearby wild type cells.

5.2. Mechanisms of cell competition

The process of cell competition comprises two phases, the first of recognition of a difference fitness levels and the second of elimination of the less fit cell (Figure I9). Molecular mechanisms underlying cell competition have been investigated and still many questions remain unsolved.

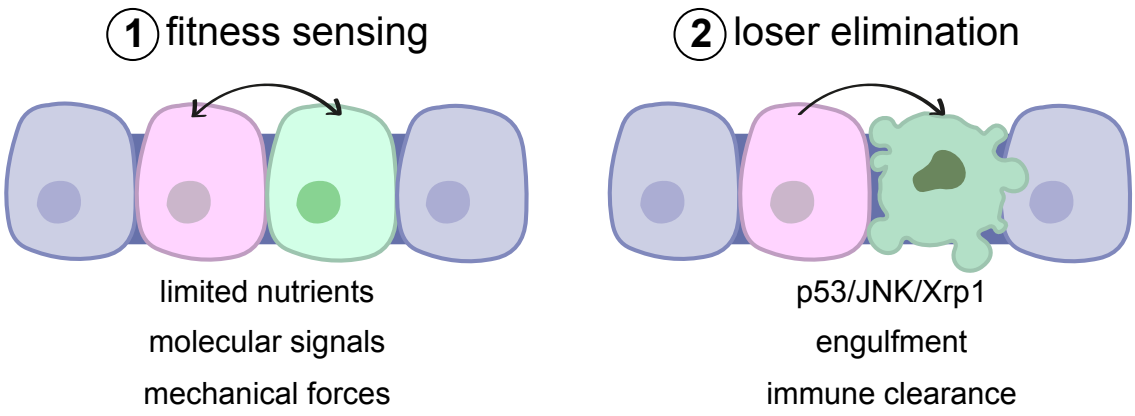

Figure I9. Mechanisms of cell competition. Sum up of the principal proposed mechanisms for fitness difference sensing and loser elimination in cell competition.

Regarding fitness-sensing mechanisms, it has been proposed that cells compete for limited extracellular factors such as growth factors or nutrients. For example, in *Drosophila*, loser cells exhibit reduced BMP/Dpp signaling, which leads to their elimination (Moreno et al., 2002). However, contradictory results regarding Dpp levels have raised doubts about this model's universality (Martín et al., 2009). Alternatively, cells can directly compare their fitness levels via molecular signals. A key example is the Flower code, where specific isoforms of the Flower transmembrane protein mark loser cells for elimination while winners express a ubiquitous isoform (Rhiner et al., 2010). Additionally, in *Drosophila*, fitness differences activate an innate immune-like response involving Toll-related receptors (TRRs) and NF-κB, which trigger pro-apoptotic pathways in loser cells (Meyer et al., 2014). Fitness can also be sensed through mechanical stress caused by differences in growth rates or crowding. It is clear that a difference in growth rate characterizes cell competition (Morata & Ripoll, 1975), even if increased rates of cell proliferation alone it is not sufficient to trigger the winner status (de la Cova et al., 2004). Interestingly, in a model of skin regeneration, wild type cells, that are normally outcompeted by $Hras^{G12V/+}$ and $Kras^{G12D/+}$ cells, are able to counteract the expansion of these protumorigenic cells when their proliferation rate is increased either upon injury or loss of cell-cycle inhibitors (Gallini et al., 2023). Faster-growing cells can compress neighboring slower-growing cells, leading to mechanical stress-induced apoptosis. For example, in *Drosophila*, Ras activation in clones led to crowding-induced cell death that was independent of known pathways (Levayer et al., 2016). Also, in cultured MDCK cells, differential mechanical forces were shown to activate p53, which mediate cell elimination under mechanical compression (Wagstaff et al., 2016). We have presented several evidence that the main regulator of loser cell clearance is p53 in mammals. In *Drosophila*, the role of JNK in inducing apoptosis in the outcompeted cell has been investigated, and while its role is clear in eliminating polarity-deficient cells (Igaki et al., 2006), contradictory evidence has been presented in *Mn*- and *Myc*-induced cell competition where certain works present evidence of JNK-dependent outcompetition (Moreno et al., 2002; Moreno & Basler, 2004) and others fail to observe the same (de la Cova et al., 2004).

The molecular mechanisms underlying *Mn*-induced cell competition in *Drosophila* have been identified and rely on the activation of the transcription factor Xrp1 that initiates the cascade that extrudes loser cells from the epithelium and activates apoptosis (Baillon et al., 2018). It has been proposed that Rps12, a component of the 40S ribosomal subunit, acts as a sensor of *RpG* imbalances and activates Xrp1 translation in response to defective ribosome assembly, thereby activating JNK signaling and promoting cell elimination (Z. Ji et al., 2019). Other works propose that proteotoxic and oxidative stress in the loser cells initiate a feedback loop that activates Xrp1 and is responsible for outcompetition (Baumgartner et al., 2021; Langton et al., 2021). In prospect looser cells autophagy is impaired in a Xrp1-dependent manner (Kiparaki et al., 2022; Langton et al., 2021) but knockdown of autophagy elements do not ameliorate outcompetition of loser cells (Baumgartner et al., 2021), indicating that this is not the mechanism through which loser cells are eliminated. However, upregulation of UPR genes was observed in loser cells (Kiparaki et al., 2022) as well as proteotoxic stress, and proteotoxic stress was sufficient to trigger outcompetition (Baumgartner et al., 2021; Langton et al., 2021). Furthermore, ameliorating proteotoxic stress by overexpression of FOXO, which is inhibited by Tor signaling

and promotes autophagy and proteosome function (Webb & Brunet, 2014), rescues cell competition. There is however ambiguous evidence on whether proteotoxic stress is activated upstream or downstream Xrp1. On one side, proteotoxic stress-triggered cell competition was rescued by Xrp1 depletion and Xrp1 overexpression can activate proteotoxic stress (Langton et al., 2021). On the other side, Xrp1 was shown to be activated downstream of proteotoxic stress by the oxidative stress sensor Nrf2 (Langton et al., 2021). One proposal is that Xrp1 and proteotoxic stress act in a feedback loop. However, it was demonstrated that the GstD1-GFP sensor for proteotoxic and oxidative stress that was used in these works not only has a Nrf2-responding element, but also an Xrp1-responding element, and that GstD1-GFP activity in *Mn*-induced cell competition is suppressed when the Xrp1-responding element in the construct is mutated (Kiparaki et al., 2022). Overall, these data suggest that proteotoxic stress is a key element in driving the loser cell status in *Mn*-induced cell competition, downstream of Xrp1. However, what non-autonomous signal or mechanism underlies Xrp1 activation, which is activated in loser cells only when juxtaposed to wild type cells, remains unclear.

5.3. The link with aneuploidy

We have previously discussed how aneuploid cells are progressively eliminated in embryo mosaics. Given that aneuploid cells in embryo mosaic are eliminated through apoptosis and that euploid cells are able to repopulate the embryo to ensure correct size, it has been proposed that this elimination happens through cell competition (Bolton et al., 2016). Recently, in a mouse model of chromosome mosaicism, it was shown that aneuploid cells upregulate p53 and that p53 is responsible for increased autophagy. Aneuploid cells are therefore preferentially eliminated from the embryonic lineage through p53- and autophagy-dependent apoptosis. Moreover, diploid cells undertake compensatory proliferation during the implantation stages to confer embryonic viability and restore normal size (Singla et al., 2020). Overall, it seems that different features of cell competition are recapitulated (Figure I10A). Interestingly, a model of cell competition with embryo mosaics of tetraploid and diploid cells shows that tetraploid cells in mice embryos suffer a p53-dependent downregulation of mTor that leads to apoptosis (Bowling et al., 2018). This is consistent with the role of mTor in inhibiting autophagy (Y. C. Kim & Guan, 2015) and reinforces the idea of increased autophagy in the loser cell as a key element in its elimination. However, treatment with rapamycin, an inhibitor of mTor which increases autophagy, increased cell death in tetraploid-diploid mosaics (Bowling et al., 2018) but not in the aneuploid-diploid mosaics, which have been later shown to be depleted through autophagy-dependent apoptosis (Singla et al., 2020). Due to differences in the nature of tetraploidy, a balanced chromosome gain, and CIN-induced aneuploidy, an imbalance in the number of chromosomes including both gains and losses, it could be that the activation of autophagy in aneuploid-diploid mosaics is not dependent on the mTor axis, or that in diploid-tetraploid mosaics mTor reduction leads to elimination of less fit cells through different mechanisms than autophagy.

Relevant findings have been made in human pluripotent stem cells (hPSCs), which can serve as a model of aneuploid mosaics due to their high genomic instability and segregation mistakes (D. Baker et al., 2016). hPSCs with recurrent culture-acquired aneuploidies display growth advantages over wild-type diploid cells that are outcompeted through a mechanism where redistribution of F-actin and sequestration of yes-associated

proteins (YAPs) in the cytoplasm induces apoptosis by mechanical stress (Price et al., 2021). This might be counterintuitive with the reported deleterious effects of aneuploidy and the proposal that aneuploid cells are eliminated by wild type cells through cell competition. However, since these aneuploidies are acquired through multiple rounds of selection in proliferation in culture, it could be that specific set of advantageous genes are selected (D. E. C. Baker et al., 2007; Draper et al., 2004). Importantly, these findings highlight that some aneuploid cells might acquire a proliferative advantage through behaviors akin to supercompetition. Conversely, a very recent report showed that aneuploid hPSCs, probably bearing disadvantageous aneuploidies, are outcompeted by wild type cells in culture and present lower c-Myc and higher p53, similarly to what is observed in other types of cell competition in mice embryogenesis (Sancho et al., 2013; G. Zhang et al., 2017).

Furthermore, we have discussed in the previous chapter how different heterozygous mutations can lead to cell competition, and monosomies harbor heterozygous mutations for several genes. In this direction it has been proposed that *Mn* genes in *Drosophila*, which are in total 66 and spread across the genome (Marygold et al., 2007), act as guardians of the ploidy status of the cell. Coherently with this proposal, Rp genes in humans are also spread across all chromosomes, with exception of chromosome 7 and 21 (Uechi et al., 2001). As a result, monosomic cells in *Drosophila* epithelia would be eliminated through *Mn*-dependent cell competition (Figure I10B). A recent analysis of 17 segmental monosomies derived from targeted chromosome excision including 11 different *Mn* genes and up to 8.5 Mb in the eye epithelia of *Drosophila* showed that segmental monosomies are eliminated through the RpS12-Xrp1 cell competition pathway (Ji et al., 2021). However, this work fails to characterize the impact of cell competition, if any, on monosomies not including *Mn* genes.

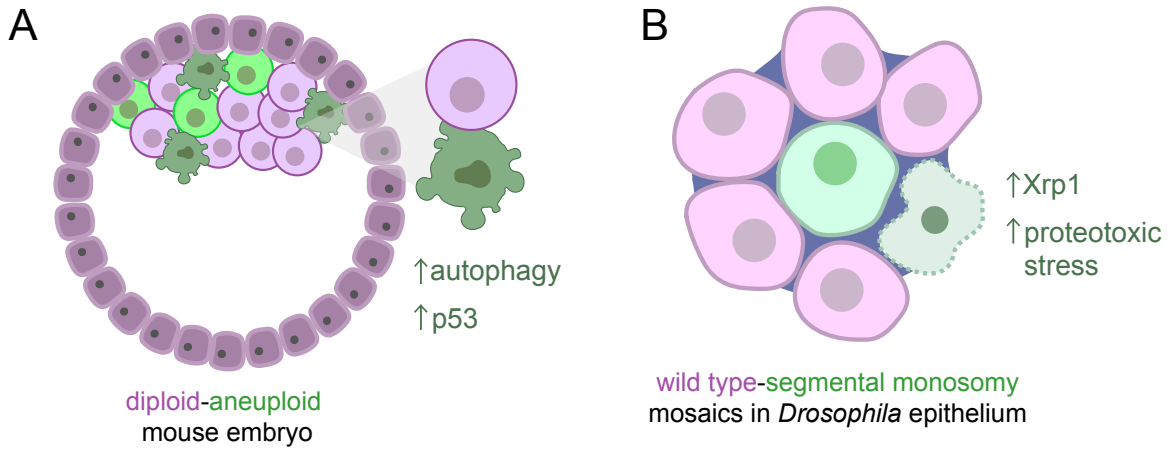

Figure I10. **Aneuploid cells in vivo are eliminated through cell competition.** Examples of aneuploid cells eliminated through cell competition in mouse embryo (random aneuploid cells) **(A)** and in Drosophila epithelia (segmental monosomies including *Mn* genes) **(B)**.

6. Experimental models of aneuploidy

Addressing key questions about the role and impact of aneuploid cell emergence *in vivo* in humans requires the use of suitable experimental models. In this study, we developed a conditional, sequence-specific model of aneuploidy in *Drosophila* epithelial tissues. Here, we will first review the conserved features between

mammalian and *Drosophila* epithelia that establish *Drosophila* as an effective model for studying aneuploidy emergence *in vivo*. Secondly, we will highlight the significance of sequence-specific aneuploidy models, and the advancements made in the field to refine these approaches.

6.1. Conserved behaviors and pathways in *Drosophila* and mammals' epithelia

To tackle key questions about the role and consequences of aneuploid cell emergence *in vivo* in humans, we developed a conditional model of aneuploidy in the epithelial tissues of *Drosophila*. While it is important to acknowledge that *Drosophila* is not a mammal, and therefore certain mammalian-specific behaviors or molecular interactions may not be fully recapitulated, the model provides significant insights into the complex phenomenon of interaction between aneuploid and euploid cells. *Drosophila* not only offers several advantages as a model for studying mosaic aneuploidy in epithelial tissues thanks to its genetic tractability, but also recapitulates key cellular behaviors observed in human epithelial aneuploidy, such as competition between aneuploid and euploid cells, altered proliferation, extrusion and cell death. These parallels validate the relevance of the model and highlight its utility in dissecting the mechanisms underlying aneuploidy, which are majorly conserved across species.

For instance, cell competition, whose interconnection with aneuploidy we have highlighted in the previous chapters, was first discovered in *Drosophila* (Morata & Ripoll, 1975). Importantly, despite higher redundancy observed in mammals, certain features and molecular players that ensure the correct development of epithelial tissues and that are also relevant in the context of cell competition, are highly conserved. For instance, mechanisms that ensure epithelial apical-basal polarity exhibit remarkable conservation between *Drosophila* and mammals (reviewed in Shiel & Caplan, 1995; Buckley & St Johnston, 2022). Thus, the apical domain is regulated in flies and mammals by the Crumbs complex - comprising Crumbs (CRB in mammals), Stardust (PALS1), and PATJ proteins - as well as by the PAR complex - including PAR-6, aPKC, and PAR-3 (Bazooka in *Drosophila*). At the basolateral domain, the Scribble complex - consisting of Scribble (Scribble, Erbin, Lano and Densin in mammals), Discs large (DLGL1–5), and Lethal giant larvae (LLGL1 and LLGL2) - ensures the exclusion of apical polarity factors and maintains lateral integrity. Junctional proteins like E-cadherin and its associated β-catenin (Armadillo in *Drosophila*) stabilize adherens junctions in both systems. Moreover, key cytoskeletal components, such as spectrin and actin, provide structural support, further reinforcing polarity. Another relevant key element of epithelial tissues that are highly conserved are cell cycle regulators, including CDK1 and 2, cyclin A, B and E, APC/C, Tribbles (TRIB1-3 in mammals) and String (cdc25), among others (Sakaue-Sawano et al., 2008; Zielke et al., 2014). Importantly, the role of mTor in responding to nutrients availability and insulin signaling to promote growth is also conserved (Oldham et al., 2000; Soucek et al., 2001). As we will discuss in greater detail in the Discussion, mTor exerts its function in flies and mammals by promoting translation (Ma & Blenis, 2009; Miron & Sonenberg, 2001), and inhibiting autophagy (Chang & Neufeld, 2009; J. Kim et al., 2011).

Furthermore, key cellular behaviors observed more specifically in the process of cell competition such as cell death in the periphery of the loser cells (Moreno et al., 2002; E. R. Oliver et al., 2004), compensatory proliferation of the winner cells at the expense of the loser cells (Oertel et al., 2006), extrusion, either basally in *Drosophila* epithelia or apically in mammalian cell culture (Tamori et al., 2010), engulfment by wild type cells (W. Li & Baker, 2007; Clavería et al., 2013), were found to be conserved between *Drosophila* and mammals.

Regarding molecular pathways activated during cell competition, the JNK pathway has been identified as a key player across multiple model systems, though its specific role remains a subject of debate and seems to depend on the trigger of cell competition. In *Drosophila,* there are contradictory data on the role of JNK in the elimination of loser cells in *Mn*-dependent cell competition, where apoptosis of $Mn^{+/-}$ cells was found to be completely rescued upon JNK blockage in certain studies (Moreno et al., 2002), while it remained unaffected in others (Tyler et al., 2007) . It is true that the means of inducing clones and blocking JNK were different and relied in heat-shock-induced clones and overexpression of a JNK inhibitor in the first study (*puckered*), and an eye-specific recombinase and different JNK pathway mutants (msn^{102}, a kinase required for JNK activation, bsk^{2} and bsk^{170B}, the *Drosophila* JNK, $RhoA^{BH}$, and jun^{2}) in the second. Also in the context of *dMyc* -induced supercompetition, while certain studies could completely rescue cell death in loser cells by blocking JNK (Moreno & Basler, 2004), others failed to observe the same and were able to reduce cell death in the loser cells only by 30% (de la Cova et al., 2004). In the first study, JNK was blocked by overexpression of *puckered* and *dMyc* upregulation was induced in clones, while in the second study JNK was blocked by a *hep* (JNKK) mutant and *dMyc* was upregulated in an entire compartment. Overall, these discrepancies suggest that the role of JNK in *Mn*-dependent cell competition and *dMyc*-induced supercompetition may vary depending on the experimental tools used, as differences in JNK levels and the number of cells involved in competition can influence the outcome. Consistent with this idea, JNK is generally proposed to function as an enhancer of cell competition in these contexts. By contrast, the role of JNK in triggering apoptosis of loser cells is clear in the case of cell competition driven by mutations in polarity genes. In *Drosophila*, mutations in the polarity genes *scribble* or *disc large* cause tumor-suppressive outcompetition of mutant cells by JNK-dependent apoptosis triggered by TNF (Brumby & Richardson, 2003; Igaki et al., 2006, 2009). Mutations or knockdown of Lgl, a tumor suppressor protein involved in maintaining epithelial polarity in both *Drosophila* (Agrawal et al., 1995) and mammals (Yamanaka et al., 2003), or its binding partner Mahjong (Mahj)/viral protein R-binding protein (VprBP) lead to the elimination of mutant cells surrounded by wild-type cells both in the wing disc epithelium of *Drosophila* and in mammalian Madin-Darby canine kidney (MDCK) epithelial cells. JNK inhibition suppresses cell death in both systems, underscoring the pathway's conserved role in mediating cell competition (Tamori et al., 2010).

Another key player in the elimination of loser cells is p53, though its role varies slightly between *Drosophila* and mammals. In mammals, p53 is involved in cell competition triggered by DNA-damage in the immune system (Bondar & Medzhitov, 2010; Marusyk et al., 2010), by karyotypic abnormalities (Sancho et al., 2013; Horii et al., 2015; Bowling et al., 2018) and mis-patterning in mice embryos (Sancho et al., 2013; Bowling et

al., 2018), by *c-Myc* overexpression in ESCs (Díaz-Díaz, Manuel, et al., 2017), by loss of polarity by making loser cells hypersensitive to mechanical stress (Wagstaff et al., 2016), and by mutations in the Rp genes (Oliver et al., 2004; Deisenroth et al., 2016). In contrast, in *Drosophila,* p53 is not reported to have a role in the elimination of loser cells during cell competition. However, in the context of dMyc-induced supercompetition, it was shown that p53 was responsible of shifting metabolism of the winner cells and therefore promoting their survival and ability to eliminate nearby wild type cells (de la Cova et al., 2014). In *Drosophila*, the role of p53 in elimination of loser cells appears to be supplanted either by JNK, as discussed above, or Xrp1 in the context of *Mn*-dependent cell competition (Figure I9,10). While p53 does not eliminate $Rp^{+/-}$ cells in *Drosophila* (Kale et al., 2015), Xrp1 is a transcriptional target of p53 (Akdemir et al., 2007) and may functionally substitute for the mammalian role of p53 during cell competition (Baker et al., 2019; Baker, 2020). Multiple genes previously identified as p53 targets are upregulated in $Rp^{+/-}$ cells in an Xrp1-dependent manner [e.g. Nrf2 (Kucinski et al., 2017; Lee et al., 2018)], suggesting that Xrp1 may directly regulate these genes, bypassing the need for p53.

Regarding aneuploidy-induced cellular behavior and underlying molecular pathways, as reviewed throughout this Introduction, there is also high conservation between *Drosophila* and mammals' models. An example is the response to CIN-induced aneuploidy, with extrusion of aneuploid cells from the epithelium and cell death by p53- and JNK-dependent apoptosis in mammals and *Drosophila,* respectively (Li et al., 2010; Dekanty et al., 2012). Also, human monosomic cells show impairment in ribosome biogenesis (Chunduri et al., 2021), similarly to segmental monosomic cells in *Drosophila* heterozygous for Ribosomal Protein Genes (Ji et al., 2021), while cells bearing extra chromosomes show UPR, proteotoxic stress and increased autophagy in both models (Brennan et al., 2019; Joy et al., 2021).

6.2. Models of sequence-specific aneuploidy

Aneuploidy, defined as the deviation from the normal chromosomal number, has been extensively studied using a variety of experimental techniques. Over time, these methods have evolved from generating random chromosomal instability (CIN) to achieving more targeted manipulations of individual chromosomes or chromosomal segments.

Historically, early approaches relied on inducing CIN by disrupting the mitotic machinery, often through the depletion of spindle assembly checkpoint (SAC) proteins either through reversine, an inhibitor of the monopolar spindle 1 (Mps1) kinase (Santaguida et al., 2017), or through mutation of SAC genes such as BUB3, ROD, MAD2 or BUBR1 (Andriani et al., 2016; Dekanty et al., 2012; Musio et al., 2003), which led to mis-segregation events during cell division. These methods typically produced both whole-chromosome and segmental aneuploidies, offering insights into the general consequences of chromosomal imbalances but lacking the precision to study specific aneuploid karyotypes and relying on sequencing techniques to monitor the aneuploidies that are being induced (Figure I11A).

Experimental models to study chromosome-specific aneuploidy were first developed in model organisms like *Drosophila* and mice. In *Drosophila*, X-ray irradiation was used to induce chromosomal breaks, generating

segmental aneuploidies due to errors in meiotic or mitotic repair (Lindsley et al., 1972; Patterson et al., 1935; Stern, 1936). This method led to gains or losses of specific chromosomal regions but required extensive screening to isolate desired karyotypes (Figure I11B). Similarly, in mice, trisomies were generated using Robertsonian translocations, where the fusion of two acrocentric chromosomes enabled the production of offspring trisomic for specific chromosomes through meiotic non-disjunction events (Figure I11C) (Gropp et al., 1983; Williams et al., 2008). These approaches were groundbreaking but limited by their reliance on random events and inability to systematically manipulate chromosomal content.

The advent of microcell-mediated chromosome transfer (MMCT) marked a significant advance in the study of aneuploidy. MMCT involves generating microcells containing specific chromosomes from donor cells, which are subsequently fused into recipient cell lines (Figure I11D) (Fournier & Ruddle, 1977). This technique allows for precise control over the introduction of extra chromosomes and has been widely applied to model human trisomies *in vitro*, such as trisomy 21 (Shinohara et al., 2001). Despite its precision, MMCT remains labor-intensive and is restricted to cultured cells, limiting its applicability to complex tissue environments.

More recent advancements include CRISPR/Cas9-based approaches, which allow for the targeted deletion or truncation of specific chromosomes or chromosomal arms (Figure I11E). Either by inducing double-strand breaks along a chromosome of interest (Leibowitz et al., 2021; Papathanasiou et al., 2021), or by introducing double-strand breaks near centromeres (Adikusuma et al., 2017), CRISPR/Cas9 can lead to chromosome elimination .

Recently, it has been developed the use of a nuclease-dead Cas9 (dCas9) and a sgRNA to tether proteins that interfere with faithful segregation to a repetitive sequence in a chromosome of interest (Figure I11F). These proteins are for instance KNL1 mutant, a protein that normally modulates kinetochore-microtubule attachments (Bosco et al., 2023), the kinetochore-nucleating domain of centromere protein CENP-T to assemble ectopic kinetochores (Tovini et al., 2023), and a minus-end-directed kinesin (Truong, Cané-Gasull, de Vries, et al., 2023).

Another way of inducing specific chromosome aneuploidy is the Cre/loxP system, which uses recombination between inverted loxP sites on the same chromosome to create acentric or dicentric fragments (Figure I11G). Acentric fragments are lost during cell division (Ly et al., 2017), while dicentric fragments undergo breakage-fusion-bridge cycles before elimination (Thomas et al., 2018). This method has been applied *in vitro* (Matsumura et al., 2007) and *in vivo* in mice lymphocytes (Y. Zhu et al., 2010). Strikingly, this is the only technique which has been implemented *in vivo*. However, it must be taken into account that variability in Cre recombination efficiency across the tissue results in mosaicism in chromosomal loss that cannot be monitored therefore leaving unaddressed whether the observed behavior are in fact due to chromosome loss (Hérault et al., 2010).

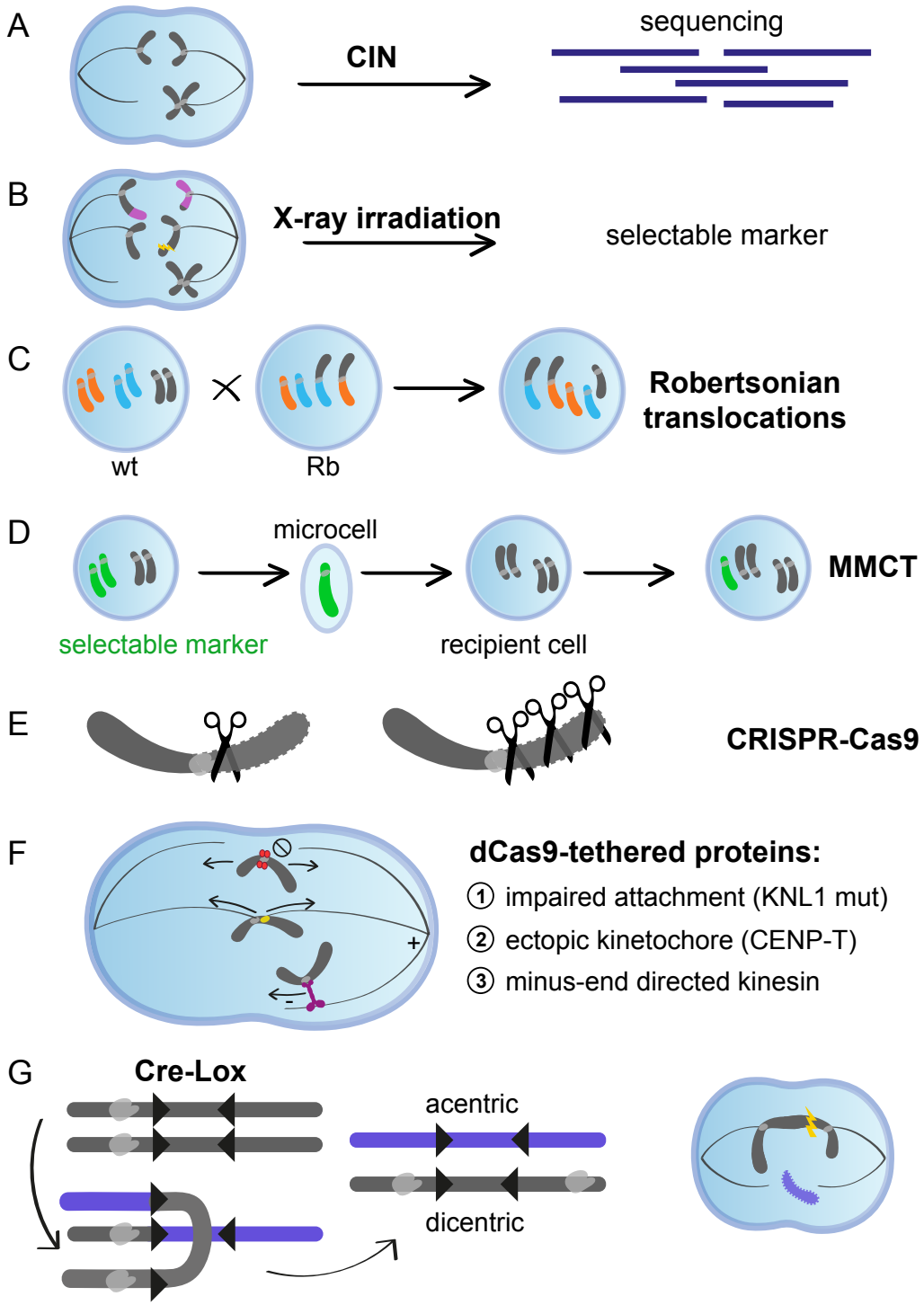

Figure I11. Techniques to introduce chromosome-specific aneuploidies.

Despite the advancements achieved with the cited *in vitro* models, they fall short of capturing the complexities of living tissues. The high rates of aneuploidy observed in both normal and abnormal tissues underscore the importance of understanding how tissue context shapes the fate of aneuploid cells. Therefore, to thoroughly dissect the impact of aneuploid cells in development and disease, there is a need for *in vivo* models capable of generating sequence-specific aneuploid mosaics within an euploid tissue. Such models would not only provide critical insights into how aneuploid cells interact with their environment and their contributions to developmental processes and pathogenesis, but also allow for the discrimination of effects driven by

haploinsufficiency or triplosensitivity of particular regions versus general effects of aneuploidy. This is particularly relevant in the perspective in which aneuploid cells could be eliminated *in vivo* through non-autonomous effects given by interactions with neighboring cells or the broader tissue environment, such as cell competition. A sequence-specific *in vivo* approach would therefore represent a transformative tool to unravel the different mechanisms underlying aneuploidy-related phenotypes.

To address this gap, in this work, we developed a novel sequence-specific recombination-based approach to generate molecularly defined segmental aneuploidies *in vivo* within *Drosophila* epithelial tissues. In particular, we employed the Flp/FRT recombination system, similar to Cre/Lox in mammals, which is composed by the enzyme Flippase, a recombinase, which recognizes and recombines two oriented DNA sequences, the Flippase Recognition Targets (FRTs) (Golic&Lindquist, 1989). By engineering the FRTs either *in cis* on the same chromosome (Figure I12A) or *in trans* on homologous chromosomes (Figure I12B) we will generate precise segmental monosomies or complementary pairs of segmental monosomies and trisomies, respectively. By conditionally expressing Flp, we will induce aneuploid cells within an otherwise euploid tissue, allowing us to analyze their interaction with wild type cells (Figure I12C). By combining precise genetic engineering with targeted labeling of aneuploid cells, this approach will provide a robust *in vivo* platform to dissect the fate and interactions of aneuploid cells within their tissue context.

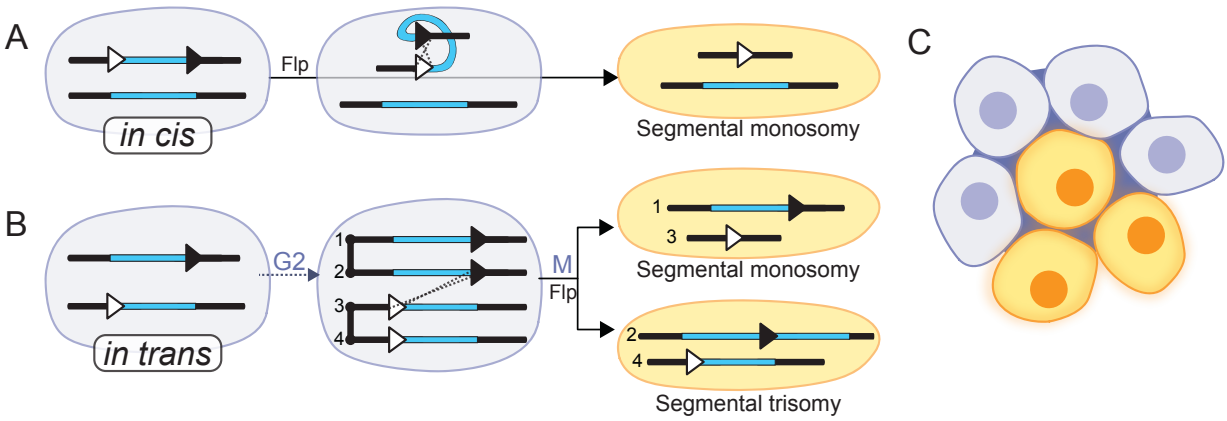

Figure I12. The Flp/FRT recombination system to generate aneuploid mosaics in *Drosophila* tissues. Application of the Flp/FRT system *in cis* (**A**) and *in trans* (**B**) to generate mosaics of segmentally trisomic and monosomic cells (**C**). Flp=Flippase. G2=G2 phase of the cell cycle. M=mitosis.

Objectives

1. Test if the Flp/FRT system can be efficiently used *in trans* to generate and mark segmental monosomies and trisomies in an euploid tissue.

1.1. Test with the RS FRTs screening method if the Flp/FRT system can be used *in trans* at a considerable distance.

1.2. Test if it is possible to differentially mark segmental monosomies and trisomies through the Twin Spot Generator technique.

2. Test if the Flp/FRT system can be efficiently use *in cis* to generate and mark segmental monosomies in an euploid tissue.

3. Describe the behavior of segmental monosomies induced through the Flp/FRT system *in cis* in a region devoid of previously reported haploinsufficient genes.

3.1. Observe if segmental monosomies present a growth effect that correlates with size.

3.2. Determine if segmental monosomies are eliminated through *Mn*-dependent cell competition or other molecular mechanisms.

4. Describe the behavior of segmental aneuploidies induced through the Flp/FRT system *in trans* in a region devoid of previously reported haploinsufficient and triplosensitive genes.

4.1. Observe if segmental monosomies and trisomies present a growth effect that correlates with size.

4.2. Determine the molecular mechanisms underlying the behavior of segmental monosomies.

4.3. Determine the molecular mechanisms underlying the behavior of segmental trisomies.

Materials and Methods

Table M1. Key Resource Table.

REAGENT or RESOURCE	SOURCE	IDENTIFIER
Antibodies		
rabbit anti-DsRed (632496)	Takara Bio	RRID:AB_10013483
goat anti-GFP (ab6673)	Abcam	RRID:AB_305643
rat anti-Ci (2A1)	DSHB	RRID:AB_2109711
Cy2-AffiniPure Donkey Anti-Goat IgG (H+L)	Jackson ImmunoResearch	RRID:AB_2307341
Cy3 AffiniPure Donkey Anti-Rabbit IgG (H+L)	Jackson ImmunoResearch	RRID:AB_2307443
Cy5 AffiniPure Donkey Anti-Rat IgG (H+L)	Jackson ImmunoResearch	RRID:AB_2340671
Chemicals, Peptides and Recombinant Proteins		
DAPI	Sigma Aldrich	Code: 28718-90-3
Experimental Models. Organisms/Strains		
w[1118], P{w=RS3}CB-0072-3	Kyoto Drosophila Stock Center	RRID:DGGR_123026
w[1118], P{w=RS3}CB-0142-3	Kyoto Drosophila Stock Center	RRID:DGGR_123052
w[1118], Dp(y+), P{=RS3}CB-0257-3	Kyoto Drosophila Stock Center	RRID:DGGR_123095
w[1118], P{=RS3}CB-0321-3	Kyoto Drosophila Stock Center	RRID:DGGR_123126
w[1118], P{w=RS3}CB-5025-3	Kyoto Drosophila Stock Center	RRID:DGGR_123418
w[1118], Dp(y+), P{=RS3}CB-5232-3	Kyoto Drosophila Stock Center	RRID:DGGR_123520
w[1118], P{w=RS3}CB-5607-3	Kyoto Drosophila Stock Center	RRID:DGGR_123708
w[1118], P{w=RS3}CB-6325-3	Kyoto Drosophila Stock Center	RRID:DGGR_124049
w[1118], P{=RS3}CB-6332-3	Kyoto Drosophila Stock Center	RRID:DGGR_124054
w[1118], P{w=RS3}CB-6633-3	Kyoto Drosophila Stock Center	RRID:DGGR_124151
w[1118], P{w=RS3}CB-6668-3 , TM6C, Sb[1]	Kyoto Drosophila Stock Center	RRID:DGGR_124172
w[1118], Dp(y+), P{w=RS3}CB-6769-3	Kyoto Drosophila Stock Center	RRID:DGGR_124213
w[1118], P{w=RS5}5-HA-1949	Kyoto Drosophila Stock Center	RRID:DGGR_125491
w[1118], P{w=RS5}5-HA-2386	Kyoto Drosophila Stock Center	RRID:DGGR_125605
w[1118], P{w=RS5}5-HA-3035	Kyoto Drosophila Stock Center	RRID:DGGR_125780
w[1118], P{w[+mW.Scer\FRT.hs]=RS5}5 SZ-3018	Kyoto Drosophila Stock Center	RRID:DGGR_125839
w[1118], Dp(y+), P{w=RS5}5-SZ-3099	Kyoto Drosophila Stock Center	RRID:DGGR_125886
w[1118], P{w=RS5}5-SZ-3126	Kyoto Drosophila Stock Center	RRID:DGGR_125905
w[1118], P{w=RS5}5-SZ-3272	Kyoto Drosophila Stock Center	RRID:DGGR_125972
w[1118], Dp(y+), P{w=RS5}5-SZ-3273	Kyoto Drosophila Stock Center	RRID:DGGR_125973
w[1118], Dp(y+), P{w=RS5}5-SZ-3486	Kyoto Drosophila Stock Center	RRID:DGGR_126092
w[1118], P{w=RS5}5-SZ-3499	Kyoto Drosophila Stock Center	RRID:DGGR_126103
w[1118], Dp(y+), P{w=RS5}5-SZ-3713	Kyoto Drosophila Stock Center	RRID:DGGR_126198

w[1118], Dp(y+), P{w=RS5}5-SZ-3717	Kyoto Drosophila Stock Center	RRID:DGGR_126201
w[1118], P{w=RS5}5-SZ-3903	Kyoto Drosophila Stock Center	RRID:DGGR_126206
w[1118], P{w=RS5}5-SZ-3954	Kyoto Drosophila Stock Center	RRID:DGGR_126251
y[1] w[*]; Mi{y[+mDint2]=MIC}MI07218	Bloomington Drosophila Stock Center	RRID:BDSC_43615
y[1] w[*]; Mi{y[+mDint2]=MIC}MI04015	Bloomington Drosophila Stock Center	RRID:BDSC_36936
y[1] w[*]; Mi{y[+mDint2]=MIC}MI00750	Bloomington Drosophila Stock Center	RRID:BDSC_40163
y[1] w[*]; Mi{y[+mDint2]=MIC}MI03514/TM3, Sb[1] Ser[1]	Bloomington Drosophila Stock Center	RRID:BDSC_36406
y[1] w[*]; Mi{y[+mDint2]=MIC}MI09966	Bloomington Drosophila Stock Center	RRID:BDSC_56571
y[1] w[*]; Mi{y[+mDint2]=MIC}MI06148	Bloomington Drosophila Stock Center	RRID:BDSC_43044
y[1] w[*]; Mi{y[+mDint2]=MIC}MI01095	Bloomington Drosophila Stock Center	RRID:BDSC_35938
y[1] w[*]; Mi{y[+mDint2]=MIC}MI00089	Bloomington Drosophila Stock Center	RRID:BDSC_31404
y[1] w[*]; Mi{y[+mDint2]=MIC}MI13177/TM3, Sb[1] Ser[1]	Bloomington Drosophila Stock Center	RRID:BDSC_58655
y[1] w[*]; Mi{y[+mDint2]=MIC}MI10238	Bloomington Drosophila Stock Center	RRID:BDSC_53833
y[1] w[*]; Mi{y[+mDint2]=MIC}MI08121	Bloomington Drosophila Stock Center	RRID:BDSC_44927
y[1] w[*]; Mi{y[+mDint2]=MIC}MI06382	Bloomington Drosophila Stock Center	RRID:BDSC_44869
Df(1) y ac, w 1118 Flp22 ; Act5C-N-CD8 dGFP[>] C-RFP	Griffin et al. 2009	N/A
Df(1) y ac, w 1118 Flp22 ; Act5C-N-CD8 dRFP[>]CGFP	Griffin et al. 2009	N/A
hsflp y[1] w[1118] P{ry[+t7.2]=70FLP}3F Dp(1;Y)y[+]; TM2 / TM6C, Sb[1]	Kyoto Drosophila Stock Center	RRID:DGGR_150540
eyflp	Bloomington Drosophila Stock Center	RRID:BDSC_5621
Df(3L)H99, kni[ri-1] p[p] (ΔRHG in the text)	Bloomington Drosophila Stock Center	RRID:BDSC_1576
xrp1^{M2-73}	Bloomington Drosophila Stock Center	RRID:BDSC_81270
mTor$^{\Delta P}$	Bloomington Drosophila Stock Center	RRID:BDSC_7014
en-Gal4	Bloomington Drosophila Stock Center	RRID:BDSC_1973
UAS-Xrp1-i (107860)	VDRC Stock Center	RRID:VDRC ID_107860
eye-gal4, UAS-Flp	Bloomington Drosophila Stock Center	RRID:BDSC_6343
UAS-Rpl26-HA	FlyORF	N/A
fwe^{DB56}*FRT80B*	Bloomington Drosophila Stock Center	RRID:BDSC_51610
hsflp;; arm-LacZ, FRT80B	Bloomington Drosophila Stock Center	RRID:BDSC_6341
hsflp;; ubi-GFP, FRT80B	Bloomington Drosophila Stock Center	N/A
UAS-fwe-A	Bloomington Drosophila Stock Center	RRID:BDSC_51611
UAS-fwe-ubi	Rhiner et al 2010	N/A
Software and Algorithms		
Fiji	https://fiji.sc	RRID:SCR_002285
Excel	Microsoft Excel 2016	N/A
GraphPad Prism 7 Project	GraphPad	RRID:SCR_002798

1. Fly maintenance, husbandry, transgene expression and clones' induction

Strains of *Drosophila melanogaster* were maintained on standard medium (4% glucose, 55 g/L yeast, 0.65% agar, 28 g/L wheat flour, 4 ml/L propionic acid and 1.1 g/L nipagin) at 25°C in light/dark cycles of 12 hours. The sex of experimental larvae was not considered relevant to this study and was not determined. The strains used in this study are summarized in the Key Resources Table (Table M1). Details of egg layings and clone induction are reported below for each set of experiment.

1.1. Recombination between RS-FRTs *in trans* and recombination efficiency

From the DrosDel collection (Ryder et al., 2004, 2007), we selected RS (Rearrangement Screening) FRTs inserted in intergenic regions that were either RS3(-) or RS5(+) (Table M2). Each RS element carries a functional *mini-white* gene (possessing the same ORF as the *white+*) with an FRT cassette placed within the first intron of the gene (Figure M1). In addition, they carry a second FRT in the same orientation as the first one either upstream (RS3) or downstream (RS5) of the *mini-white* exons. As a result, should they undergo a Flip-out, the remaining RS5 construct (RS5r) will carry the 5'-exon of the *mini-white* gene, while the RS3 the six 3'-exons (RS3r). In addition, each remaining element will be flanked on one side by a single FRT site. Each *yw;;RS FRT* (red-eyed) line was crossed with *yw hsflp/Dp(1;Y)y+;;TM2/TM6C* flies (white-eyed) and kept at 25°C. These crosses were allowed to lay eggs for 24 h and the larvae were heat-shocked at 72 h after egg laying (AEL) at 37°C for 1 h. *yw,hsflp;;RS FRT/TM6C* males were then selected. These flies are mosaics and will display either white eyes, if the flip-out was very efficient, or white clones in the eyes. They will carry either the RS (bringing the whole *white+* gene) or the RSr (bringing a truncated *white+* gene) FRT in the germline. Since each flip-out event that occurred in the germline is independent, single white-eyed *y,w,hsflp;;RSr FRT/TM6C* males were crossed again with *y,w,hsflp;;TM2/TM6C* flies. *y,w,hsflp;;RSr FRT/TM6C* white-eyed males and females were finally selected and crossed to establish the stock. Two independent stocks for each position were therefore established. By crossing flies bearing RS3r(-) and RS5r(+)FRTs (where RS3r is more proximal and RS5r more distal respect to the centromere on the 3L), the *white* gene will be reconstituted upon FLP induction on the chromosome bearing the segmental trisomy (Figure R2B). As controls, we crossed flies bearing RS3r(-) and RS5r(+)FRTs in the same location (78F3, Figure R3A). We set up the screening this way because monosomies are notoriously more deleterious than trisomies, and we wanted to recover the maximum number of clones possible in order not to underestimate efficiency. It is important to point out that this setup does not allow differential marking of G1 from G2 products of recombination, therefore both euploid and aneuploid cells will be marked in red. This allows the detection of recombination events even if aneuploidy is deleterious for the cell. For the acute induction, 19 combinations of *y,w,hsflp;;RS3r/TM6C* and *y,w,hsflp;RS5r/TM6C* were kept at 25°C, allowed to lay eggs for 24 h and heat-shocked at 38°C for 1 h either at 72 h or 96 h AEL (Figure M2A). Each cross was performed in at least two independent replicates. *y,w,hsflp;;RS3r/RS5r* adults were screened for clones in the eye. Population

Coverage (number of eyes with clones with respect to the total number of eyes examined) and Eye Coverage (percentage of the eye area covered by clones) were measured. For the chronic induction, *yw,eyflp;;RS3r/TM6B* females were crossed with *yw;RS5r/TM6C* males, allowed to lay eggs for 24 h, and the eggs were kept at 25°C until adults emerged. Population and Eye Coverage in *yw,eyflp;;RS3r/RS5r* adults was measured. A minimum of 28 eyes and a maximum of 186 were screened for each genotype and condition.

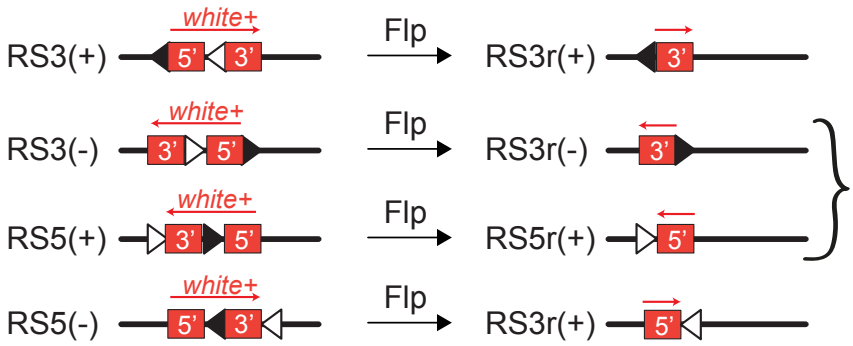

Figure M1. RS FRTs lines. The different orientation of FRTs and nomenclature is indicated. In this work we have combines RS3(-) and RS5(+) lines.

Table M2. RS5 and RS3 lines

FRT type	Line ID	Origin	insertion	orientation respect to chr
Rs5(+)	126198	DGRC	70E1	+
Rs5(+)	126092	DGRC	72B2	+
Rs5(+)	125905	DGRC	73B1	+
Rs5(+)	126251	DGRC	73E5	+
Rs5(+)	126206	DGRC	75A4	+
Rs5(+)	125973	DGRC	77C1	+
Rs5(+)	125605	DGRC	78F3	+
Rs5(+)	125886	DGRC	78D5	+
Rs5(+)	126103	DGRC	79A2	+
Rs5(+)	126201	DGRC	79A4	+
Rs5(+)	123975	DGRC	80C2	+
Rs3(-)	124054	DGRC	70C6	+
Rs3(-)	123520	DGRC	70E5	+
Rs3(-)	123418	DGRC	71B1	+
Rs3(-)	123026	DGRC	71E1	+
Rs3(-)	123095	DGRC	73D1	+
Rs3(-)	124049	DGRC	75F7	+
Rs3(-)	124213	DGRC	77E4	+
Rs3(-)	123708	DGRC	78C9	+
Rs3(-)	124172	DGRC	78F3	+
Rs3(-)	124151	DGRC	79A4	+

1.2. Recombination between RS-FRTs *in cis* and generation of segmental monosomies

We generated a collection of recombinant fly lines bearing 21 different combinations of RS5r and RS3r-FRTs located in the same chromosome (*in cis*), where RS5r is more proximal to the centromere and RS3r more distal on the 3L (*RS3r RS5r*, Table M3). To generate flies bearing RS5r and RS3r-FRTs *in cis* we let females heterozygous for the two RSr-FRTs egg laying with *y,w,eyflp;; FRT82B/TM6B* males for 24 h. From this cross, we selected *y,w,eyflp;;RS5r RS3r/TM6B* males, recognized by the fact that they presented red clones in the eyes, sign that they had inherited from the female a chromosome resulting from meiotic recombination where both FRTs were present. These males where then crossed separately with *y,w,hsflp;;TM2/TM6C* flies and *y,w,eyflp;; FRT82B/TM6B* females to establish *y,w,hsflp;; RS3r RS5r/TM6C* and *y,w,eyflp;; RS3r RS5r/TMB* stocks respectively. Then, we used these lines to generate segmental monosomies.

Table M3. Recombinant *RSr3 RSr5* lines

Genotype		Label	Pos RS3	Pos RS5	RS3 DGRC ID	RS5 DGRC ID	RS3 nt	RS5 nt	Diff(bp)	Mb	N genes
eyflp; 73-75	*hsflp; 73-75*	**73-75**	73D1	75A4	123095	126206	16800857	17850544	1049687	1,049687	166
eyflp; 70-72B2	*hsflp; 70-72B2*	**70-72B2**	70E5	72B2	123520	126092	14625700	15948261	1322561	1,322561	204
eyflp; 71-73B1	*hsflp; 71-73B1*	**71-73B1**	71E1	73B1	123026	125905	15525670	16605347	1079677	1,079677	247
eyflp; 77-78	*hsflp; 77-78*	**77-78**	77E4	78F3	124213	125605	20723348	21815069	1091721	1,091721	247
eyflp; 70E5-72D9	*hsflp; 70E5-72D9*	**70E5-72D9**	70E5	72D9	123520	125972	14625700	16157381	1531681	1,531681	256
eyflp; 77-79	*hsflp; 77-79*	**77-79**	77E4	79A4	124213	126201	20723348	21935345	1211997	1,211997	266
eyflp; 75-77	*hsflp; 75-77*	**75-77**	75F7	77C1	124049	125973	19094051	20394712	1300661	1,300661	272
eyflp; 70C6-72B2	*hsflp; 70C6-72B2*	**70C6-72B2**	70C6	72B2	124054	126092	13932268	15948261	2015993	2,015993	282
eyflp; 71-73E5	*hsflp; 71-73E5*	**71-73E5**	71E1	73E5	123026	126251	15525670	17042518	1516848	1,516848	324
eyflp; 75A4-77	*hsflp; 75A4-77*	**75A4-77**	75A4	77C1	124168	125973	17850477	20394712	2544235	2,544235	468
eyflp; 70-73	*hsflp; 70-73*	**70-73**	70C6	73E5	124054	126251	13932268	17042518	3110250	3,11025	537
eyflp; 75-79	*hsflp; 75-79*	**75-79**	75F7	79A4	124049	126201	19094051	21935345	2841294	2,841294	608
eyflp; 66-70	*hsflp; 66-70*	**66-70**	66E1	70E1	123215	126198	8820579	14530694	5710115	5,710115	619
eyflp; 70-75	*hsflp; 70-75*	**70-75**	70C6	75A4	124054	126206	13932268	17850544	3918276	3,918276	663
eyflp; 75A4-78D5	*hsflp; 75A4-78D5*	**75A4-78D5**	75A4	78D5	124168	125886	17850477	21526856	3676379	3,676379	708
eyflp; 75A4-78F3	*hsflp; 75A4-78F3*	**75A4-78F3**	75A4	78F3	124168	125605	17850477	21815069	3964592	3,964592	785
eyflp; 73-79	*hsflp; 73-79*	**73-79**	73D1	79A4	123095	126201	16800857	21935345	5134488	5,134488	970
eyflp; 71-77	*hsflp; 71-77*	**71-77**	71B1	77C1	123418	125973	15007510	20394712	5387202	5,387202	999
eyflp; 70-77	*hsflp; 70-77*	**70-77**	70C6	77C1	124054	125973	13932268	20394712	6462444	6,462444	1131
eyflp; 70-78	*hsflp; 70-78*	**70-78**	70C6	78D5	124054	125886	13932268	21526856	7594588	7,594588	1371
eyflp; 70-79	*hsflp; 70-79*	**70-79**	70C6	79A4	124054	126201	13932268	21935345	8003077	8,003077	1467
eyflp; 70-80	*hsflp; 70-80*	**70-80**	70C6	80C2	124054	123975	13932268	22991401	9059133	9,059133	1725

Upon FLP-induced recombination, the *white* gene will be reconstituted on the chromosome bearing the segmental monosomy (Figure R4A). For the acute induction, *y,w,hsflp;; RS5r RS3r/TM6C* flies were kept at 25°C, allowed to lay eggs for 6 h, and eggs were heat-shocked at 38°C for 1 h at 48 h AEL. For the chronic

induction, *y,w,eyflp;; RS5r RS3r/TM6B* flies were allowed to lay eggs for 24 h and the eggs were kept at 25°C until adults emerged (Figure M2B). Each cross was performed in a minimum of two until a maximum of 22 independent replicates. *y,w,hsflp;; RS3r RS5r/TM6C* and *w,eyflp;; RS3r RS5r/TM6C* adults were screened for clones in the eye. Population Coverage (number of eyes with clones with respect to the total number of eyes examined), Eye Coverage (percentage of the eye area covered by clones), and clone size (in number of ommatidia) were measured. To avoid quantifying fused clones, and therefore overestimating growth capacity, we took into consideration the reduced number of clones per eye as a strong argument that each clone originated from a single recombination event, and we measured clones that were clearly isolated from other red cells and followed a clear direction of growth in the tissue. A minimum of 7 eyes (for control intronic deletions that presented many clones per eye due to high recombination efficiency) to a maximum of 1086 were screened for each genotype and condition. Not all crosses were performed in parallel but the control 73-75 was always analyzed in parallel with all batches. A minimum of 28 clones and a maximum of 186 were quantified for each genotype and condition.

As control clones, we used 8 different RS-FRTs (RS5 and RS3-FRTs with a functional *mini-white* gene) located in the 3L region. These flies present red eyes, and a FLP-mediated recombination event will disrupt the *white* gene and produce clones of *white* mutant cells (Figure R4B, R6A,C,D, grey boxes). Due to the close proximity of the pair of FRTs, recombination is expected to be highly efficient. Thus, two different regimes were implemented in order to produce either a low number of recombination events and white clones in a red background (short heat-shock: 2-3 minutes at 36°C) or a large number of recombination events, thus labeling clones of cells where recombination did not occur in red (long heat-shock: 45 min-1 h at 38°C). Average size of euploid clones (independently of the regime) was roughly constant in the 8 original single RS-FRT-containing lines (Figure R6D). We noticed that the long heat-shock regime was more efficient in detecting small clones (labeled in dark grey in Figure R6D) than the short heat-shock regime (labeled in gray in Figure R6D), most probably because red clones in a *white* background are more visible and easier to detect. To check whether cell death and the Xrp1-mTor axis were involved in the out-competition of cells bearing segmental monosomies of the whole Region 1 (70C6-75A4), the whole Region 2 (75F7-79A4), or the Region 3 where *RpL26* is located (70C6-77C1, 73D1-79A4, 75A4-77C1), the corresponding *y,w,hsflp;; RS5r RS3r/TM6C* flies (for the acute induction) or y*,w,eyflp;; RS5r RS3r/TM6B* flies (for chronic induction) were crossed with *Df(H99)/TM3, Xrp1*$^{M2-73}$*/TM6B* and *mTor*$^{\Delta P}$*/CyO* flies, allowed to lay eggs for 6 h and eggs were kept at 25°C until adults emerged. For the acute induction, larvae were heat-shocked at 38°C for 1 h at 48 h AEL. Clones of cells bearing a segmental monosomy of the genomic regions 73D1-75A4, which do not present any growth defect, and 66E1-70D1, which includes the three *Minute* genes *RpS17*, *RpS9* and *RpS4* were used as controls in these experiments. Genes included in each segmental monosomies are listed in Annex I.

1.3. Recombination between TSG-FRTs *in trans*: segmental monosomies, trisomies and translocations in imaginal tissues

The collection of RG-FRT and GR-FRT lines for Twin Spot Generator (TSG) was made by BestGene Inc (https://www.thebestgene.com/, California, USAA) by PhiC31 Recombinase Mediated Cassette Exchange (RMCE). AWM-2attB-(N-GFP/FRT/C-RFP, GR) and/or AWM-2attB-(N-RFP/FRT/C-GFP, RG) hybrid constructs (Griffin et al, 2009) were injected into MiMIC lines (Table M4) selected at different intergenic positions on the 3L (69F1, 70A8, 72A1, 73A5, 75A1, 75F1, 76A3, 79A4, 80B1) and 3R (87A4, 89A1, 92F6) chromosome arms. For each position, 8 positive transgenic flies were isolated by loss of y+ marker and crossed with *TM3, Sb, Ser* to generate a balanced stock. For each individual line, the presence and orientation of the GR/RG cassette was confirmed by reverse PCR and sequence analysis with specific primers for each position. One stock with "plus" orientation of each position was selected for experiments. Flies bearing the *hsflp* construct and either one GR or RG construct were crossed with flies bearing the RG or GR construct (Table M4) to induce segmental aneuploidies in the region of choice. Flies were allowed to lay eggs for 6 h and larvae were heat-shocked at 48 h or 64 h AEL at 38°C for 1 h to produce aneuploidy and 5-10' for controls. As controls we used lines bearing GR and RG construct at the same genomic location (Figure R12A) which recombine at a much higher efficiency, therefore need weaker induction to produce separate clones. Wing discs and eye discs were dissected at 120 h AEL (Figure M2C). We quantified Clone Area (in μm^2) with ImageJ for non-fused clones in the epithelia from whole-z-stacks of the tissues. At least three independent replicates for each genotype were analyzed. Clone area from each genotype was normalized with respect to the average size of G1-derived euploid clone of the same genotype. This reduced variability caused by the site of the insertion that might affect the growth of the euploid controls and allowed us to visualize effects specifically due to aneuploidy.

Table M4. TSG-FRT bearing lines

FRT type	Line ID	Origin	insertion	orientation respect to chr
TSG GR	43615 (MiMIC)	BSDC	69F1	+
TSG RG	36936 (MiMIC)	BSDC	70A8	+
TSG GR	36936 (MiMIC)	BSDC	70A8	+
TSG RG	40163 (MiMIC)	BSDC	72A1	+
TSG RG	36406 (MiMIC)	BSDC	73A5	+
TSG GR	36406 (MiMIC)	BSDC	73A5	+
TSG RG	56571 (MiMIC)	BSDC	75A1	+
TSG GR	56571 (MiMIC)	BSDC	75A1	+
TSG GR	43044 (MiMIC)	BSDC	75F1	+
TSG RG	35938 (MiMIC)	BSDC	76A3	+
TSG RG	Griffin et al 2009	Perrimon lab	77C4	+
TSG GR	Griffin et al 2009	Perrimon lab	77C4	+
TSG GR	31404 (MiMIC)	BSDC	79A4	+
TSG GR	58655 (MiMIC)	BSDC	80B1	+

TSG GR	53833 (MiMIC)	BSDC	87A4	+
TSG RG	53833 (MiMIC)	BSDC	87A4	+
TSG GR	44927 (MiMIC)	BSDC	89A1	+
TSG GR	44869 (MiMIC)	BSDC	92F6	+

Genetic rescues with *Xrp1-i* to measure clone size were performed by generating recombinant *engrailed-gal4-UAS-Xrp1-i* flies and combining them with the *hsflp,* GR and RG constructs. We generated these flies by crossing females heterozygous for the *engrailed-gal4(w+),* in which the mini-white rescue gives an orange eye color, and the *UAS-Xrp1-i(y+)* transgenes with *y,w; If/CyO-GFP* flies. We isolated *y,w; engrailed-gal4-UAS-Xrp1-i/CyO-GFP* recombinant males by selecting males with orange eyes and normal body color and used them to construct *y,w; engrailed-gal4-UAS-Xrp1-i/CyO-GFP; TSG-FRT/TM6B* stocks, with GR or RG constructs on the third chromosome. Rescues with *UAS-Xrp1-i* and clones induced acutely were performed by crossing these recombinant flies with *hsflp;;TSG-FRTs/TM6B* flies with the GR or RG construct of interest. Rescues with *UAS-Xrp1-i* and clones induced chronically were performed by crossing *y,w; engrailed-gal4-UAS-Xrp1-i/CyO-GFP; TSG-FRT/TM6B* with *UAS-flp/CyO-GFP;TSG-FRT/TM6B* flies. Rescues with *UAS-miRHG(w+)* were performed by recombining this construct with the *UAS-flp(w+)* construct, which both give the fly an orange eye color. Heterozygous females for *UAS-miRHG(w+)* and *UAS-flp(w+)* were crossed with *w; If/Cyo-GFP* males. We isolated *y,w; UAS-miRHG,UAS-flp/CyO-GFP* recombinant males by selecting males with red eyes, since color of the mini-white construct often gives an additive phenotype where two copies of the gene result in darker color than one single copy. *Engrailed-Gal4/CyO-GFP;TSG-FRT/TM6B* flies were then crossed by *UAS-miRHG,UAS-flp/CyO-GFP;TSG-FRT/TM6B* flies. Rescues with *UAS-Rpl26* and *UAS-fwe* were performed in the eye primordium by combining these constructs with *eyeless-gal4-UAS-flp* flies, and the GR and RG constructs.

UAS-Rpl26 flies were generated by phiC31-mediated integration, in the FlyORF Drosophila Injection Service (https://www.flyorf-injection.ch/, Zurich, Switzerland). The pGW-Rpl26-3xHA.attB plasmid (F002737, FlyORF) was injected into the *phiC31; attP40* strain (position 25C-2L). Transgenic flies were identified by the gain of *y+*, crossed with the *y,w* strain to establish the stock, and balanced with *y,w, Gla/SM6a.*

Genes included in each segmental monosomies and trisomies are listed in Annex I.

1.4. Generation of *fwe* mutant clones

Control and mutant clones were generated by heat-shocking *hsflp;; arm-LacZ, FRT80B, / ubi-GFP, FRT80B,* flies and *hsflp;; arm-LacZ, FRT80B / fwe^{DB56}, FRT80B,* larvae, respectively, at 70h AEL for 45 minutes and at 38°C. Larvae were collected from egg layings of 6-12h. Wing discs were dissected at 120h AEL.

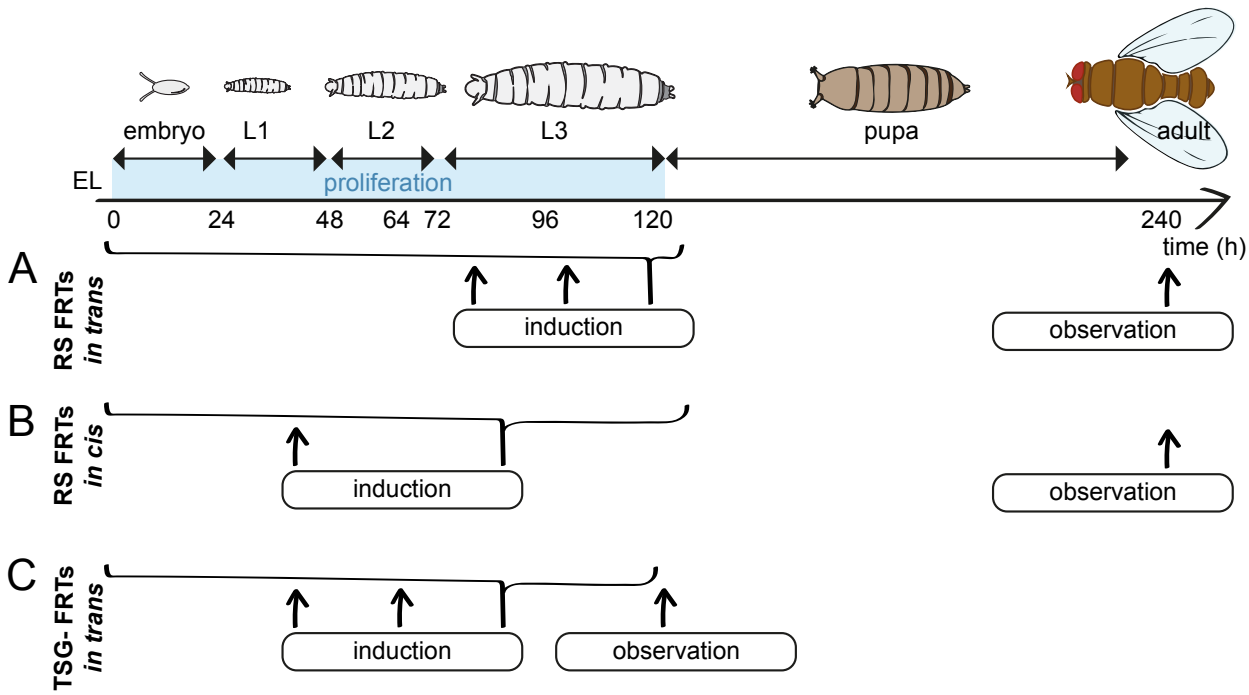

Figure M2. Protocol of clones' induction according to the experiment. Life cycle of Drosophila according to time (hours) after egg laying (EL) is shown on top. The blue bar indicates the phases where tissues grow and cells proliferate. After pupariation cell proliferation stops. Arrows indicate acute induction while the bracket indicates chronic induction.

2. Immunohistochemistry and microscopy

2.1. Immunohistochemistry

Late third instar larvae (120 h after egg laying) were selected, and wing and eye imaginal discs were dissected in phosphate-buffered saline (PBS), fixed for 20 min in 4% formaldehyde in PBS, washed in PBS with 0.2% Triton X-100, blocked in PBS with 0.3% BSA, 0.2% Triton X-100 and stained with antibodies diluted in PBS with 0.3% BSA, 0.2% Triton X-100. Primary and secondary antibodies are summarized in the Key Resources Table (Table M1).

2.2. Microscopy

A Zeiss LSM780 Spectral Confocal Microscope was used to obtain high-resolution images of larval imaginal discs bearing clones. Z-stacks were acquired using a 40x oil immersion objective. The most representative image(s) is shown in all experiments. At least 20 imaginal discs per genotype were imaged. An Olympus MVX10 Macroscope was used to take images of adult eyes bearing clones. Image acquisition was done at 6.2X magnification. The EFI (Extended Focus Image) technology in the Cell program allowed us to take 8-10 photos of different planes in a width of 0.20-0.30 mm for each eye and merge them into one image. The most representative image is shown in all experiments. At least 15 eyes per genotype were imaged.

3. Quantification and Statistical Analysis

3.1. Clones in the adult eye

Fiji [National Institute of Health (NIH) Bethesda, MD] was used to process images and manually count the Eye Coverage or number of ommatidia for each clone. For Eye Coverage, for each eye, red area and total eye area was measured. The ratio is represented as percentage in Figure R3C R5D. For number of ommatidia, due to the non-normal distribution of the Clonal Area (probably due to the biology of the tissue and the differentiation wave, which stops proliferation starting from 72 h AEL), we performed ANOVA on logarithmically transformed data. To analyze the impact on growth (Figure 6-11), batches of different crosses were performed where the 73-75 monosomy was always used in parallel as a control. Log-transformed values were used to determine statistical significance of differences between Monosomies and Control groups using Mixed Linear Models with ID as random effect. Dunnet multiple contrasts for statistical significance of each ID vs Control were done using the glht function, and pvalues were adjusted using Benjamini-Hochberg. In the genetic interaction experiments (Figure R9, 11) all crosses for each interaction were performed in parallel. Differences were considered significant when p values were less than 0.001 (***), 0.01 (**), or 0.05 (*). Mean values and standard deviations were calculated and the corresponding statistical analysis and graphical representations were carried out with GraphPad Prism 7.0 statistical software.

3.2. Wing disc clones

Fiji [National Institute of Health (NIH) Bethesda, MD] was used for image processing and measuring the size of single clones. Image stacks for a given number of wing discs were obtained using a 40X oil immersion objective with 1.5 µm per optical section to cover the entire thickness of each disc. Statistical analysis was generally performed by ANOVA either on Area (in μm^2) or Area normalized by average Area of euploid clones (absolute value). Differences were considered significant when p values were less than 0.001 (***), 0.01 (**), or 0.05 (*). All genotypes included in each histogram were analyzed in parallel. Mean values and standard deviations were calculated and the corresponding statistical analysis and graphical representations were carried out with GraphPad Prism 7.0 statistical software.

Results

1. The FLP/FRT system can be employed to generate segmental aneuploidies in epithelial tissues in *Drosophila*

1.1. The FLP/FRT system can be used efficiently *in trans* until at least 7.5 Mb

In order to generate molecularly-defined segmental aneuploidies we employed the FLP/FRT system, a sequence-specific recombination system very similar to the Cre/Lox technique used in mice. The FLP/FRT recombination system was commutated from yeast for the use in *Drosophila* many years ago (Golic & Lindquist, 1989) and is composed by two specific DNA sequences with orientation (Flippase Recognition Targets, FRTs) that are recognized and recombined by the Flp recombinase (Figure R1).

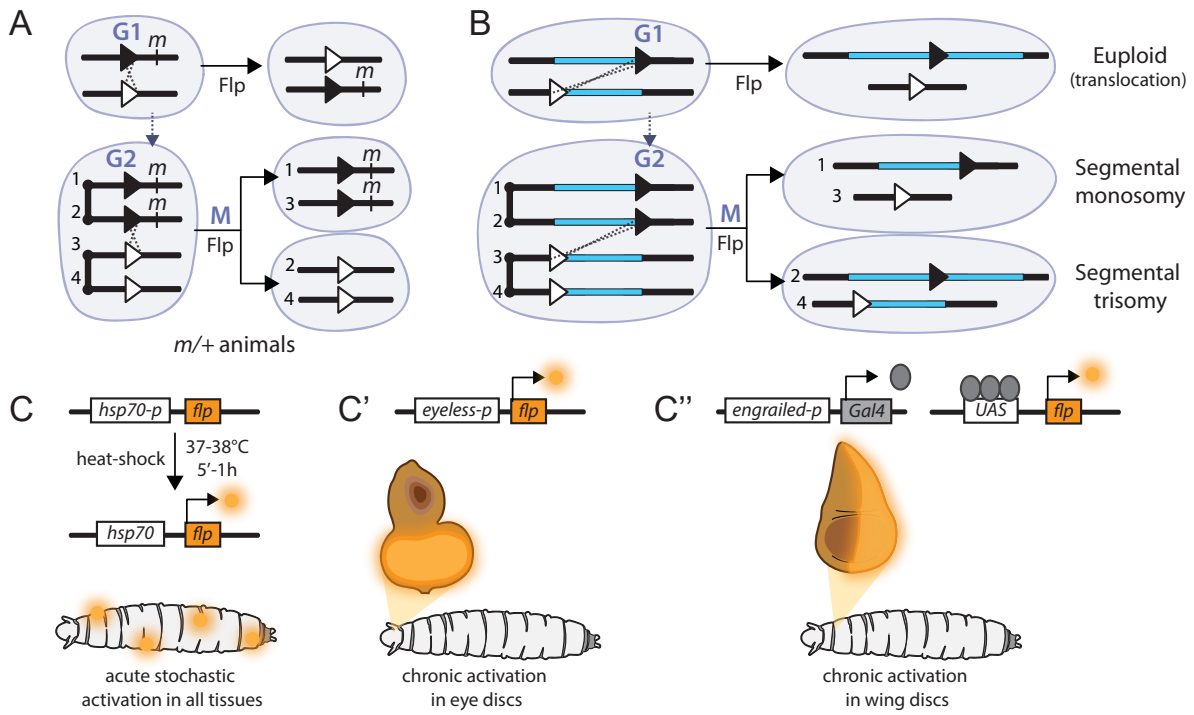

Figure R1. The FLP/FRT system can be used *in trans* to generate segmental aneuploidies *in vivo* in larval tissues of *Drosophila*. (A) FRTs in trans to generate homozygous mutant cells (*m/m*) in heterozygous mutant animals (*m/+*) upon G2-recombination events. FRTs are represented as triangles and recombination between FRTs is represented as two crossed dotted lines. Sister chromatids in G2 are represented as connected through a line. Upon mitosis (M) sister chromatids will segregate apart from each other. **(B)** FRTs in trans at a certain distance to generate segmental aneuploid cells upon G2- and euploid translocation upon G1-recombination events. The region comprehended between the FRTs is highlighted in blue and is going to be present in one and three copies respectively in the two daughter cells resulting from G2-recombination events. **(C)** Induction of the Flp enzyme (represented in orange) through a heat-shock dependent promoter (*hsp70-p*) in larval stages will result in stochastic expression of the Flp in all the larval tissue for the time of the heat shock (from 5' to 1h). **(C')** Chronic induction of the Flp in the eye disc though an eye-specific promoter (*eyeless-p*). **(C")** Induction of the Flp through the binary system GAL4/UAS, in this case shown with a promoter specific for the posterior side of the larval wing disc epithelium (*engrailed-p*). Later on indicated as *en>flp*.

This system has been widely used to engineer *Drosophila*'s genome in multiple ways and in particular to induce mitotic recombination and generate genetic mosaics. Recombination in somatic tissues is possible in *Drosophila* thanks to the fact that, unlike in mammals, homologous chromosomes experience pairing in somatic cells (Metz, 1916; Csink & Henikoff, 1998). The outcomes of recombination vary depending on the phase of the cell cycle in which it occurs. Mitotic recombination in the G2 phase of the cell cycle between FRTs placed in the same location and orientation in homologous chromosomes (*in trans*) that carry constructs in heterozygosis can give rise to clones of genetically distinct cells (Figure R1A). Specifically, twin clones, each homozygous for one of the two constructs that were originally in heterozygosis, will arise. Instead, recombination in the G1 phase of the cell cycle will give rise to cells that are genetically identic to their progenitors (Figure R1A). Recombination between FRTs *in trans* has been widely used in cell lineage experiments or analysis of gene function at the cellular level (Griffin et al., 2014). What makes this system extremely modular is that the induction of the clones can be thoroughly controlled both in a time- and tissue-specific manner by regulating the expression of the Flp. In this work, we will induce expression of the Flp in larval tissues either acutely or chronically through development. For acute induction, we will use the Flp enzyme under the control of the heat-shock-dependent promoter *hsp70* (*hsflp* construct) (Figure R1C). In this case, clones of recombinant cell will form stochastically across all body tissues, with their frequency determined by recombination efficiency, which depends on the duration of the heat shock and the developmental stage. In fact, inducing recombination earlier in development leads to a lower likelihood of successful recombination events because fewer cells are present at that stage. For chronic induction, we will use the Flp under the control of an eye specific promoter (*eyflp,* Figure R1C'*)* and under the control of the Gal4-UAS system (Figure R1C''). The Gal4-UAS system is a binary genetic system (Brand & Perrimon, 1993) composed by the activator of transcription Gal4 under the control of a tissue-specific promoter and its responder sequence UAS, followed by the gene of interest (*UAS-Flp*). The combination of the two elements will result in overexpression of the Flp in the tissue of choice, in this work eye or wing discs (Figure R1C'').

In order to produce clones of cells bearing segmental aneuploidies, we thought to engineer the two FRTs in the same orientation but in different locations along the two homologous chromosomes (Figure R1B). When such FRTs recombine, two chromosomes will be generated: one bearing a duplication and the other bearing a deletion between the FRTs. Segregation of these chromosomes during mitosis will give rise to either aneuploid or euploid daughter cells depending on the phase of the cell cycle when the recombination happened (Figure R1B). After a recombination event in G2, the two recombinant chromosomes (2 and 3 in Figure R1B) will segregate apart from each other together with a normal chromosome (1 and 4 in Figure R1B), therefore producing two daughter cells that are aneuploid, one with the chromosome bearing the deletion (segmental monosomy) and the other one with the chromosome bearing the same region duplicated (segmental trisomy). After recombination in G1, the two recombinant chromosomes will segregate together therefore producing two daughters that remain euploid but carry a translocation of the region between the two FRTs from one homologous chromosome to the other (Figure R1B). All the recombination events described are not the only ones that can happen, but the only ones that modify the genotype of the daughter cells. Furthermore, and

especially in the case of chronic induction, it is possible that recombination events happen again in the daughter cells. It is important to take into account that products of G2-recombination events are stable and will keep the same genotype even if they recombine again. To the contrary, G1-recombination products can recombine again in G2 and therefore produce genetically distinct daughter cells.

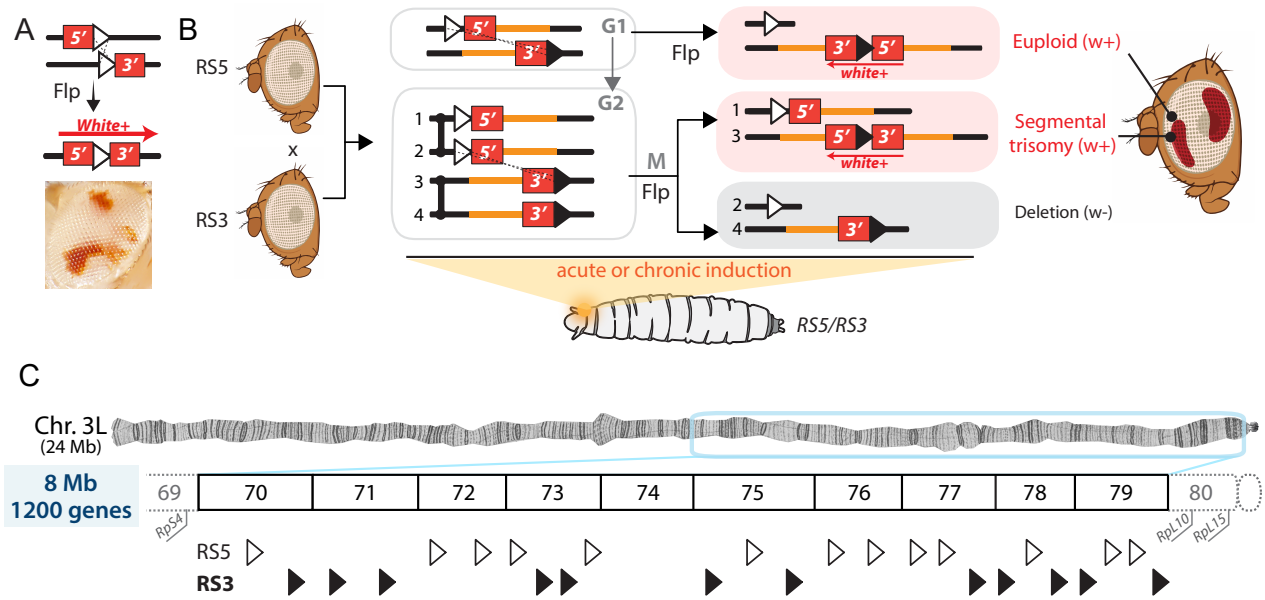

Figure R2. The RS FRTs collection as a way to monitor recombination efficiency between distant FRTs. (A) The RS5 bearing the 5' and the RS3 bearing the 3' segment of the *white+* gene coding sequence flanking the FRT sequence reconstitute the *white+* sequence upon recombination. The cells where recombination is induced will be red colored. **(B)** Protocol of clones induction for screening until what distance two FRTs can recombine. White-eyed RS5 and RS3-bearing flies were crossed and the clones were induced in the resulting RS5/RS3 larvae either acutely with *hsflp* or chronically with *eyflp*. The pairs of FRTs chosen are oriented in such a fashion that the *white+* gene is reconstructed on the chromosome bearing the duplication of the segment between the FRTs (highlighted in orange). For clarity, FRTs included in the RS5 construct are represented as white triangles while FRTs in the RS3 construct in black, even if the sequence is identical. **(C)** The FRTs used for the screening are located in a region of the left arm of the 3rd chromosome (3L) which is 8 Mb long and includes around 1200 genes. Genomic locations are identified through the cytological position that for the region selected range from 69 (more distal to the centromere) to 80 (more proximal). Previously reported haploinsufficient genes outside of this region are represented in gray (*RpS4* in 69F6, *RpL10* in 80D1 and *RpL15* in 80F9).

FRTs *in trans* at a different genomic location have been used to generate small deletions or duplications (Ryder et al., 2007) but never to induce larger imbalances, which is the first objective of this thesis. In order to monitor how effective is the Flp to mediate recombination of distant FRTs *in trans*, we used the *Drosophila* eye primordium and pairs of a special type of FRTs (RS-FRTs). The eye primordium is a monolayered epithelial tissue that grows exponentially during larval development to give rise to the adult eye, and RS-FRTs are pairs of FRTs that are flanked by either the 5'- or 3'- sequence of the *white* gene, which is responsible for the red pigmentation of the eye. When RS-FRTs recombine with each other, they reconstitute the *white* sequence (Golic & Golic, 1996; Ryder et al., 2004) thus labeling daughter cells in red in an otherwise *white* mutant background (Figure R2A). We used 25 different RS-FRTs lines in 19 different combinations *in trans* (Figure R2C-F) placed at a distance spanning from 0 to 7.5 Mb, and located in the region 70-79 of chromosome 3L, which is the biggest region in *Drosophila* genome devoid of previously reported haploinsufficient and triplosensitive loci (Lindsley et al., 1972; Marygold et al., 2007). In this thesis we will mainly work with this region to avoid interference from previously described dosage-sensitive genes in the phenotypes analyzed. For

this screening, we engineered the RS-FRTs in such a way that the *white* gene will be reconstituted on the chromosome bearing the segmental trisomy. It is important to point out that in this set up both euploid and aneuploid products of recombination will be marked in red (Figure R2B) so that, even if aneuploidy is deleterious for the cell, we would still be able to detect recombination events. Recombination between RS-FRTs was induced acutely with the *hsflp* construct by heat-shocking at 38°C for 1h third instar larvae at various developmental points (48, 72 and 96h after egg laying, AEL), or chronically with the *eyflp* construct which drives FLP expression throughout the development of the growing eye primordium (Figure M2A). As a proxy for recombination frequency, we quantified the percentage of eyes with clones (Population Coverage) and, in those eyes presenting clones, the percentage of eye area covered by red clones (Eye Coverage).

As expected, frequency of recombination between two RS-FRTs *in trans* was highest when recombination was induced chronically with *eyflp* with a 100% of eyes presenting clones in most of the cases (Figure R3 A,B). Recombination frequency increased with the developmental time of acute induction, being lower when clones were induced at 72h AEL (with a 100% of eyes presenting clones for the closest pairs of FRTs and 22.8% for the furthest) and higher when clones were induced at 96h AEL (with a 100% of eyes presenting clones for the closest pairs of FRTs and 32.5% for the furthest). As previously mentioned, this is a consequence of the increase in the size of the eye primordium which means an increased number of cells and results in an increased probability of some of them to undergo a recombination event. Furthermore, recombination efficiency decreased with the distance between the two RS-FRTs (Figure R3 A-C). We can notice that Eye Coverage decreases at lower distances respect to Population Coverage. This is particularly evident when looking at clones induced with *eyflp.* This makes sense considering that, when efficiency decreases, we may observe less fused clones which would be reflected in a smaller Eye Coverage but still the same Population Coverage. Furthermore, this could also be due to a decreased fitness of the recombination products. However, considering that in this set up we cannot distinguish triploid from euploid cells (Figure R2B), and that with *eyflp* we don't know at which time point each clone has been induced, we cannot draw any conclusions on a possible effect of increasing distance between FRTs on cell fitness.

The observed distance-independent subtle variations in frequency might be a consequence of differences in the efficiency of the corresponding FRTs (effect of the insertion), gene or region-specific effects. We noted, for example, that the FRT insertion located in 75F7 was not working as efficiently as others as in all combinations tested presented a much lower Population Coverage and Eye Coverage than other combinations comparable in size. For instance, Population Coverage with chronic induction was 100% for all combinations tested (Figure R3B) except for combinations including the FRT inserted in 75F7 such as 75A4-75F7 (1.2Mb), 73B1-75F7 (2.5Mb) and 70E1-75F7 (4.5Mb) for which it was 94.4%, 75.3% and 77% respectively. Moreover, we can also notice that these three combinations have lower Eye Coverage than combinations of similar or bigger size (1.6%, 0.6% and 0.5% respectively, Figure R3C).

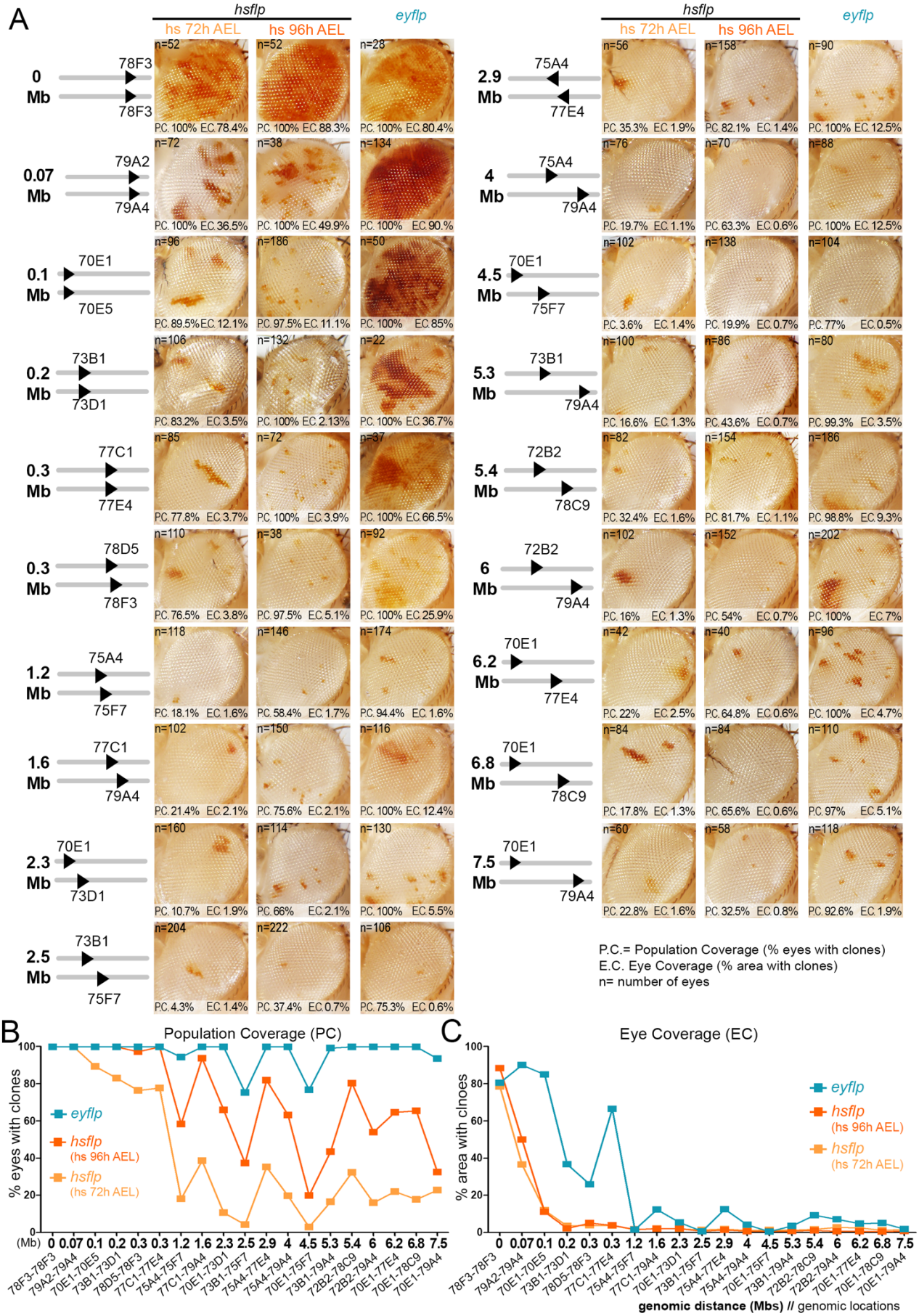
A
hsflp
hs 72h AEL
hs 96h AEL
eyflp
0 Mb 78F3 78F3 n=52 n=52 n=28 P.C. 100% E.C. 78.4% P.C. 100% E.C. 88.3% P.C. 100% E.C. 80.4%
0.07 Mb 79A2 79A4 n=72 n=38 n=134 P.C. 100% E.C. 36.5% P.C. 100% E.C. 49.9% P.C. 100% E.C. 90.%
0.1 Mb 70E1 70E5 n=96 n=186 n=50 P.C. 89.5% E.C. 12.1% P.C. 97.5% E.C. 11.1% P.C. 100% E.C. 85%
0.2 Mb 73B1 73D1 n=106 n=132 n=22 P.C. 83.2% E.C. 3.5% P.C. 100% E.C. 2.13% P.C. 100% E.C. 36.7%
0.3 Mb 77C1 77E4 n=85 n=72 n=37 P.C. 77.8% E.C. 3.7% P.C. 100% E.C. 3.9% P.C. 100% E.C. 66.5%
0.3 Mb 78D5 78F3 n=110 n=38 n=92 P.C. 76.5% E.C. 3.8% P.C. 97.5% E.C. 5.1% P.C. 100% E.C. 25.9%
1.2 Mb 75A4 75F7 n=118 n=146 n=174 P.C. 18.1% E.C. 1.6% P.C. 58.4% E.C. 1.7% P.C. 94.4% E.C. 1.6%
1.6 Mb 77C1 79A4 n=102 n=150 n=116 P.C. 21.4% E.C. 2.1% P.C. 75.6% E.C. 2.1% P.C. 100% E.C. 12.4%
2.3 Mb 70E1 73D1 n=160 n=114 n=130 P.C. 10.7% E.C. 1.9% P.C. 66% E.C. 2.1% P.C. 100% E.C. 5.5%
2.5 Mb 73B1 75F7 n=204 n=222 n=106 P.C. 4.3% E.C. 1.4% P.C. 37.4% E.C. 0.7% P.C. 75.3% E.C. 0.6%
2.9 Mb 75A4 77E4 n=56 n=158 n=90 P.C. 35.3% E.C. 1.9% P.C. 82.1% E.C. 1.4% P.C. 100% E.C. 12.5%
4 Mb 75A4 79A4 n=76 n=70 n=88 P.C. 19.7% E.C. 1.1% P.C. 63.3% E.C. 0.6% P.C. 100% E.C. 12.5%
4.5 Mb 70E1 75F7 n=102 n=138 n=104 P.C. 3.6% E.C. 1.4% P.C. 19.9% E.C. 0.7% P.C. 77% E.C. 0.5%
5.3 Mb 73B1 79A4 n=100 n=86 n=80 P.C. 16.6% E.C. 1.3% P.C. 43.6% E.C. 0.7% P.C. 99.3% E.C. 3.5%
5.4 Mb 72B2 78C9 n=82 n=154 n=186 P.C. 32.4% E.C. 1.6% P.C. 81.7% E.C. 1.1% P.C. 98.8% E.C. 9.3%
6 Mb 72B2 79A4 n=102 n=152 n=202 P.C. 16% E.C. 1.3% P.C. 54% E.C. 0.7% P.C. 100% E.C. 7%
6.2 Mb 70E1 77E4 n=42 n=40 n=96 P.C. 22% E.C. 2.5% P.C. 64.8% E.C. 0.6% P.C. 100% E.C. 4.7%
6.8 Mb 70E1 78C9 n=84 n=84 n=110 P.C. 17.8% E.C. 1.3% P.C. 65.6% E.C. 0.6% P.C. 97% E.C. 5.1%
7.5 Mb 70E1 79A4 n=60 n=58 n=118 P.C. 22.8% E.C. 1.6% P.C. 32.5% E.C. 0.8% P.C. 92.6% E.C. 1.9%
P.C.= Population Coverage (% eyes with clones)
E.C. Eye Coverage (% area with clones)
n= number of eyes
B
Population Coverage (PC)
% eyes with clones
eyflp
hsflp (hs 96h AEL)
hsflp (hs 72h AEL)
(Mb) 0 0.07 0.1 0.2 0.3 0.3 1.2 1.6 2.3 2.5 2.9 4 4.5 5.3 5.4 6 6.2 6.8 7.5
78F3-78F3 79A2-79A4 70E1-70E5 73B1-73D1 78D5-78F3 77C1-77E4 75A4-75F7 77C1-79A4 70E1-73D1 73B1-75F7 75A4-77E4 75A4-79A4 70E1-75F7 73B1-79A4 72B2-78C9 72B2-79A4 70E1-77E4 70E1-78C9 70E1-79A4
C
Eye Coverage (EC)
% area with clnoes
eyflp
hsflp (hs 96h AEL)
hsflp (hs 72h AEL)
0 0.07 0.1 0.2 0.3 0.3 1.2 1.6 2.3 2.5 2.9 4 4.5 5.3 5.4 6 6.2 6.8 7.5
78F3-78F3 79A2-79A4 70E1-70E5 73B1-73D1 78D5-78F3 77C1-77E4 75A4-75F7 77C1-79A4 70E1-73D1 73B1-75F7 75A4-77E4 75A4-79A4 70E1-75F7 73B1-79A4 72B2-78C9 72B2-79A4 70E1-77E4 70E1-78C9 70E1-79A4
genomic distance (Mbs) // genomic locations

Figure R3. Recombination efficiency between FRTs in trans decreases with distance but happens until 7.5 Mb. (**A**) Macroscope images of adult eyes where clones were induced between the 19 pairs of FRTs at a distance spanning from 0 to 7.5 Mb either acutely with *hsflp* at 72h after egg laying (AEL, in light orange), 96h AEL (dark orange) or *eyflp* (blue). For each genotype and condition, the number of eyes screened is reported, as well as Population Coverage (P.C.), the % of eyes with clones, and Eye Coverage (E.C.), the % of area with clones, that are plotted in **B** and **C** respectively. (**B-C**) The distance in Mb and the cytological locations of the two FRTs are indicated for each combination. Average is shown.

Most importantly, recombination still occurred between RS-FRTs located 7.5 Mb apart and comprehending up to 1200 genes, which corresponds to roughly 12% of the *Drosophila* genome and an average human chromosome. In other words, aneuploidies of at least 7.5 Mb and 1200 genes can be generated with the FLP-FRT system. These results indicate that the FLP/FRT system is a highly efficient tool to be used *in trans* to generate segmental aneuploidies of different sizes in a growing epithelium.

1.2. The FLP/FRT system can be used efficiently *in cis* until at least 9.1 Mb

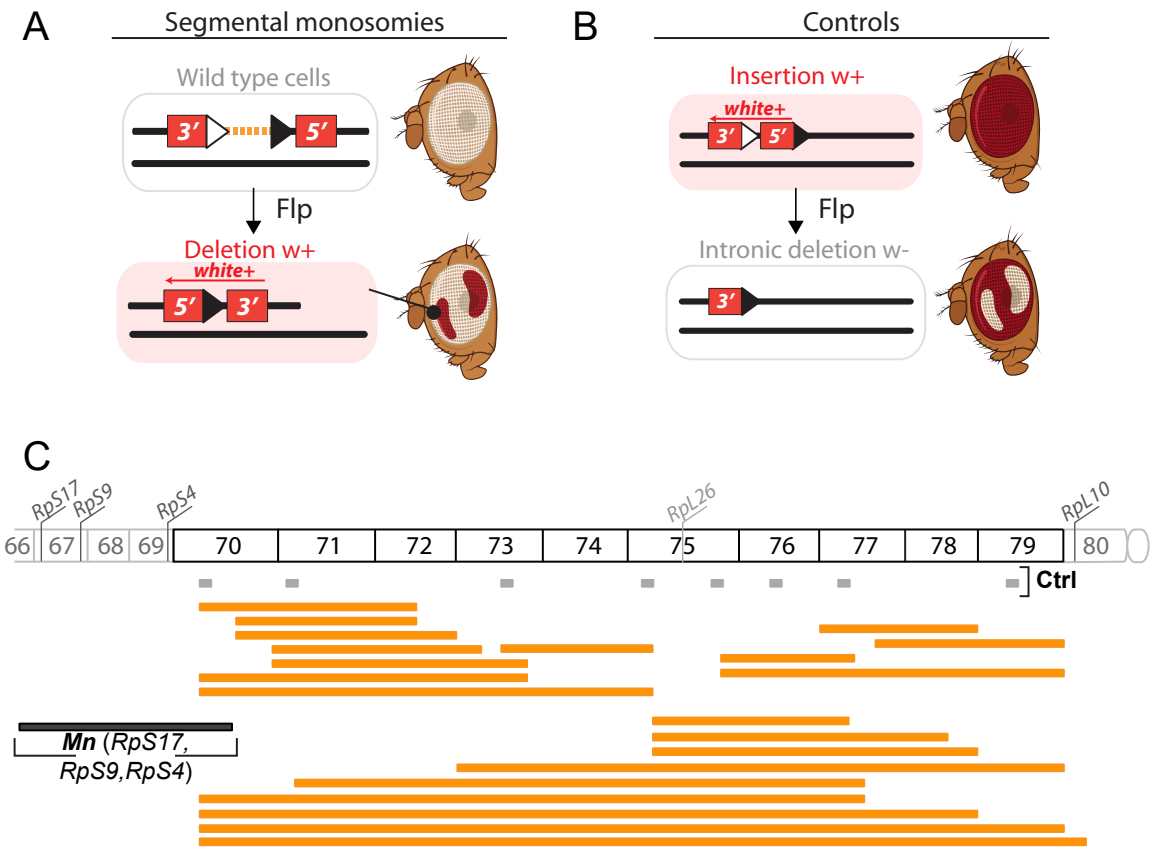

Figure R4. The FLP/FRT system with RS FRTs in cis to generate a collection of monosomies positively marked in the adult eye of *Drosophila*. (**A**) RS5 and RS3 are engineered *in cis* along the same chromosome to give rise to *white+* marked cells bearing a deletion (segmental monosomies) of the segment comprehended between the FRTs (dotted orange line) in a wild type tissue. (**B**) White clones bearing a deletion of a segment of the *white* gene were used as controls. The lines used to generate these clones are the original RS-FRT lines from which we derived the RS5 and RS3 constructs represented in **A** and in Figure R3 (more details in Materials and Methods). (**C**) Map of the collection of 27 lines bearing the FRTs *in cis* at the location indicated. Segmental monosomies to characterize are represented in orange. Control lines bearing the construct represented in **B** are shown in light grey. A line were the FRTs are flanking known haploinsufficient genes (*RpS17, RpS9* and *RpS4*) is used as negative control and is represented in dark grey. The *Rpl26* gene in 75E4 is shown in light grey as possible unreported haploinsufficient gene.

We then used the RS-FRTs to generate a collection of segmental monosomies that could be labeled in red and monitored in the eye epithelia. The FLP/FRT system has been previously reported to be a highly efficient tool to generate segmental monosomies when located in the same chromosome (*in cis*) at a distance of up to 8.5 Mb apart (Ji et al., 2021). Differently from what happens with FRTs *in trans*, recombination between two FRTs *in cis* always generates a segmental monosomy, independently of the phase of the cell cycle in which the recombination happens (Figure R4A). We generated 21 recombinant lines (Figure R4C) bearing different combinations of FRTs at a distance spanning from 1 to 9.1 Mb and 166 to 1725 genes, respectively.

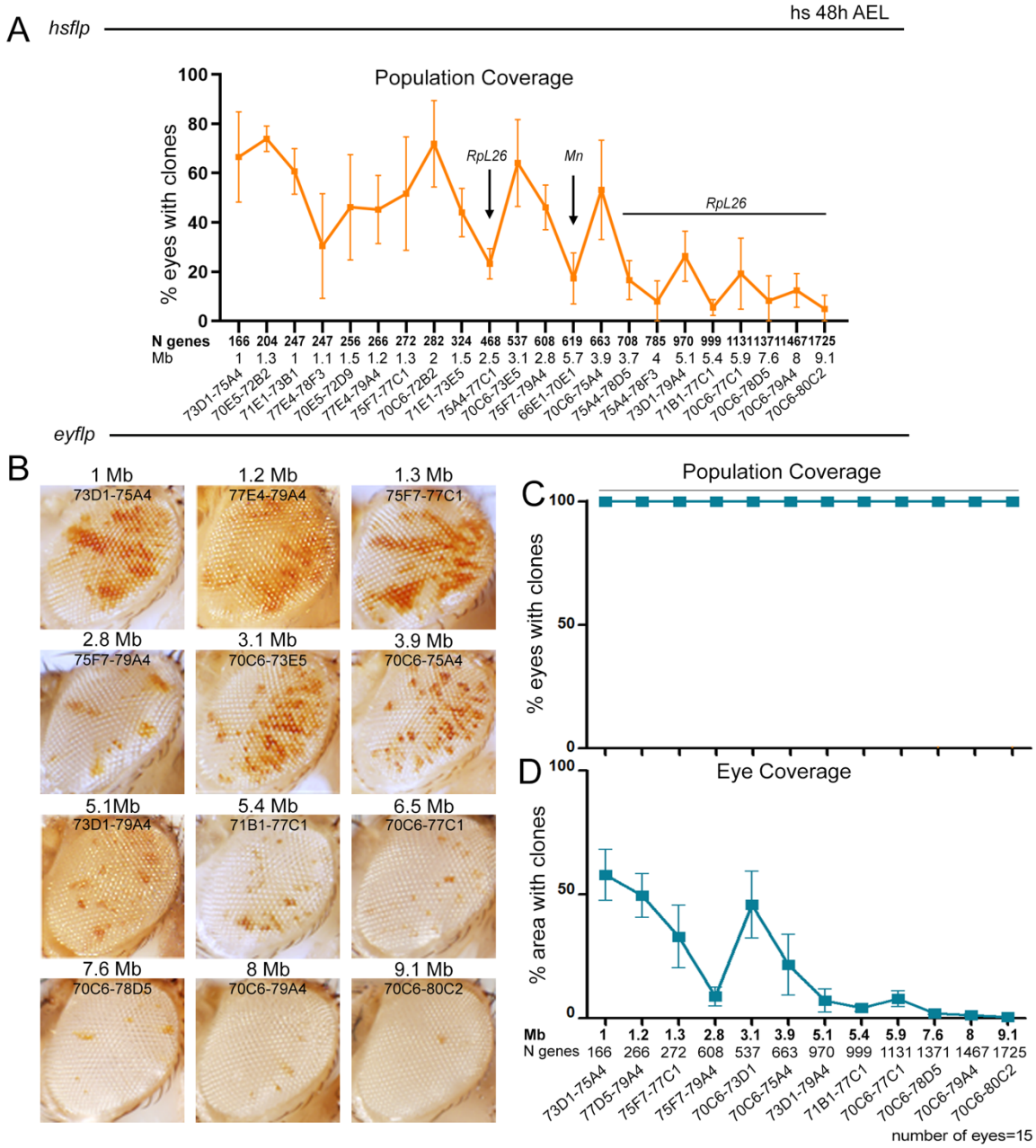

Figure R5. Recombination efficiency between FRTs in cis decreases with distance but happens until 9.1 Mb. (**A**) Population Coverage (% eyes with clones) for each combination *in cis* with clones induced through the *hsflp* construct with a heat-shock at 38°C for 1h at 48h AEL. The number of genes included, the distance in Mb and the cytological location of the two FRTs are indicated for each combination. The number of eyes screened varies from 68 to 1086 (n for each combination is shown on the microscopy images in Figures R8 and R10). Presence of *Mn* or *Rpl26* is indicated. (**B**) Macroscope images of eyes with clones induced through the *eyflp* construct with the respective quantification of Population Coverage (**C**) and Eye Coverage (**D**). 15 eyes per genotype were quantified. Average and SD are shown.

As an indicator of efficiency, we measured % of eyes with clones (Population Coverage) in *hsflp*-induced clones and % of eyes with clones and Clonal Area (Eye coverage) in *eyflp*-induced clones (Figure R5). Clones induced with *hsflp* were also analyzed to assess growth capacity of monosomies respect to positive controls of euploid cells (see next chapters), for which we used 8 original single RS-FRT containing lines [Figure R4B (Golic & Golic, 1996), see also Materials and Methods]. Instead, *eyflp*-induced clones were used just to assess efficiency of recombination. For this reason, only 12 out of the 21 monosomies were analyzed with the *eyflp* induction.

In terms of Population Coverage, chronic induction of Flp expression with the *eyflp* construct gave a higher frequency of recombination (100% for all pairs tested, Figure R5C) than acute induction at 48h AEL with the *hsflp* construct (from 77,87% for the closest to 4,89% for the furthest pair of FRTs, Figure R5A). When looking at Clonal Area of *eyflp*-induced clones, the highest efficiency was 57,85% for the closest pair of FRTs and the lowest was 0,47% for the furthest. Again, as it happened for *in trans* FRTs (Figure R3B,C), Eye Coverage in clones induced with *eyflp* decreases with the distance while Population Coverage stays constant at 100%. This indicates that chronic induction is indeed highly efficient in inducing at least one recombination event per eye. Both Population Coverage of clones induced with *hsflp* and Eye Coverage of clones induced with *eyfl*p decreased with the distance between the two RS-FRTs (Figure R5A,D). However, as already commented for recombination between *in trans* FRTs, there are oscillations in frequency that might be a consequence of gene- or region-specific effects of the insertion of the correspondent FRT. Overall, with these lines we were able to generate segmental monosomies of different sizes and we extended the possible distance at which two FRTs *in cis* can recombine up to 9.1 Mb (Figure R5).

2. Impact of segmental monosomies on growth in an otherwise wild type epithelium

2.1. Size of segmental monosomies does not exactly correlate with a negative impact on growth

Monosomies including haploinsufficient genes that affect growth rates such as Ribosomal protein encoding genes (*RpGs*), *Minute* genes (*Mn*) in *Drosophila*, or genes involved in ribosome function and translation, are eliminated from the tissue by cell competition-driven cell death (Ji et al., 2021; Kiparaki et al., 2022). In order to address whether segmental monosomies not including this type of genes have also an effect on clonal growth or survival, we used our collection of 21 different recombinant lines bearing *in cis* FRTs intentionally located in the region 70-80 of chromosome 3L, which as mentioned previously is the biggest region devoid of previously reported haploinsufficient loci [Figure R2C, 4C (Marygold et al., 2007)]. This collection allowed us to generate overlapping segmental monosomies of increasing sizes (Figure R4C) and therefore address the size-dependent versus the gene-specific effects on clonal growth. Previous methods to induce molecularly-defined aneuploidy have been limited to *in vitro* models (Truong, Cané-Gasull, & Lens, 2023) therefore not allowing to address gene-specific effects of monosomies in a growing tissue.

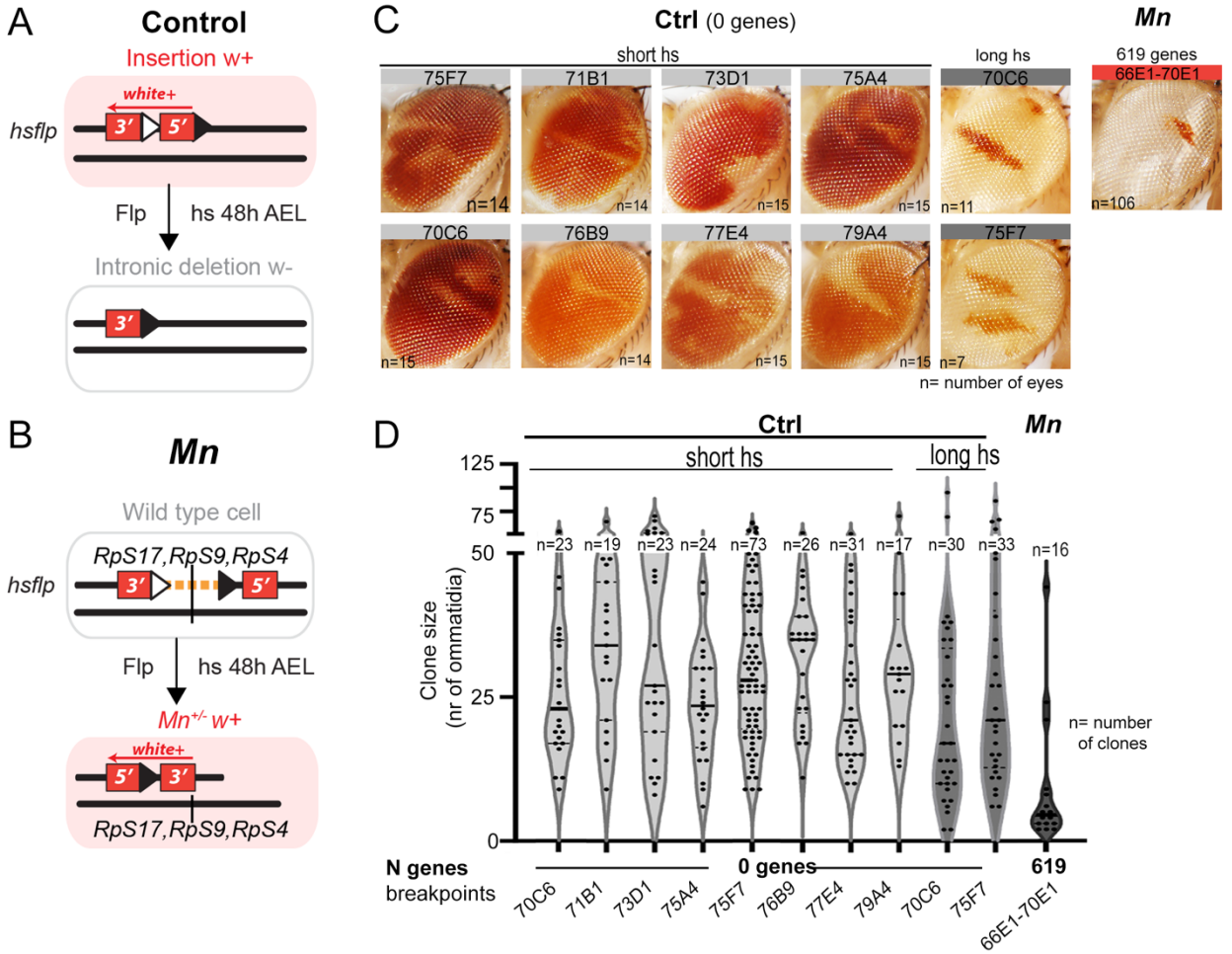

Figure R6. RS FRTs in cis can recapitulate cell-competition and growth defect of monosomies including Mn genes compared to euploid controls. (**A**) Cartoon of the construct used to generate control clones, clones bearing a deletion of a segment of the *white* gene. The lines used to generate these clones are the original RS-FRT lines from which we derived the constructs represented in **B** and in Figure R2 (more details in Materials and Methods). Given the close proximity of the FRTs, recombination is highly efficient and a weaker induction protocol was used. Clones were induced with a heat-shock at 48h AEL at 36.5°C either for 2 minutes (short hs) or 5 minutes (long hs). (**B**) Cartoon of the line used to produce *white+* clones of cells bearing a deletion of the *Mn* genes *RpS17, RpS9* and *RpS4.* Clones were induced with a 1h heat-shock at 48h AEL at 38°C. (**C**) Macroscope images of the control clones and *Mn+/-* clones where the cytological location of the construct insertion is indicated as well as the number of genes included and number of eyes screened. (**D**) Quantification of size in number of ommatidia of clones of each genotype. The cytological location of the construct insertion is indicated as well as the number of genes included and number of clones quantified. Median is shown as a black line. Controls induced with short hs are shown in light grey while clones induced with long hs in darker grey. The monosomy including the *Mn* gene is shown in black

As positive controls to monitor the growth of euploid cells, we used 8 original single RS-FRT containing lines, where one of the fragments of the *white* gene is flanked by two FRTs placed in an intronic elements [Figure R4B, 6A,C,D, (Golic & Golic, 1996), see also Materials and Methods]. These flies bring an intact *white* sequence and therefore present red eyes. A Flp-mediated recombination event will disrupt the *white* gene and produce clones of *white* mutant cells in a wild type background (Figure R4B, 6A). Due to the close proximity of the pair of FRTs, recombination is expected to be highly efficient. Thus, two different regimes were implemented in order to produce either a low number of recombination events and white clones in a red background (with a short heat-shock, see Materials and Methods for details) or a big number of recombination events thus labeling clones of cells where recombination did not occur in red (with a long heat-shock, see

Materials and Methods for details). Average size of euploid clones (independently of the regime) was roughly constant in the 8 original single RS-FRT containing lines (Figure R6C,D). We noticed that the long heat-shock regime was more efficient in spotting small clones (labeled in dark grey in Figure R6D) than the short heat-shock regime (labeled in grey in Figure R6D), most probably because red clones in a white background are more visible and easier to detect. In fact, the labeling method for segmental monosomies based on the reconstruction of the *white* gene in a *white* mutant background facilitated the identification of even very small clones. This allowed to finely monitor compromised proliferative growth as a consequence of aneuploidy. For the sake of simplicity, in the next chapters we will represent just two of the 8 controls, and in particular the ones with the FRTs inserted in 70C6 and 75F7 induced with both the short and long heat-shock regimes. However, in all cases, statistical analysis was performed comparing each monosomy with all controls.

As negative control, we used a monosomy ranging from positions 66E1-70D1 affecting 619 genes and including the haploinsufficient *Mn* genes *RpS17*, *RpS9* and *RpS4* (Figure R6B). Recombination was induced acutely by heat-shocking early second instar larvae (48 h AEL) and clone size was quantified in the adult eye as number of ommatidia, a proxy for number of cells and the functional unit of the fly compound eye. We can notice that size of the monosomy including the *RpGs* is significantly smaller than the euploid control, proving that our method of clone induction and size quantification is reliable (Figure R6D). We have considered that the *hsflp* construct, being on the X chromosome, could be differentially expressed in males and females and could therefore result in a different efficiency (Laverty et al., 2010). However, since we took care of analyzing non-fused clones, a difference in efficiency will not result in a difference in growth and for this reason we didn't separate males from females for this analysis.

By monitoring growth rates of 21 segmental monosomies of different sizes and ranges of overlap (Figure R4C, 7A), we noticed that, despite a significant negative correlation between number of genes included in the monosomy and clone size (Figure R7B), the negative impact of the size of the monosomy on clonal growth was not exactly linear (Figure R7A). While the impact of small monosomies of up to 400 genes was very heterogenous (in Figure R7A, compare size of monosomies of 247, 256, 266, 288 genes, being on average 20.1, 28.9, 12, 24.8 ommatidia big respectively) the drastic effect of monosomies of more than 400 genes on clonal growth was not further affected by the increase in the number of genes. On one side, we concluded that there is a minimal growth capacity that every segmental monosomy, once it survives, is able to reach, at least when growing in the eye epithelium. On the other side, we considered that specific genomic region could influence clonal growth independently on their size.

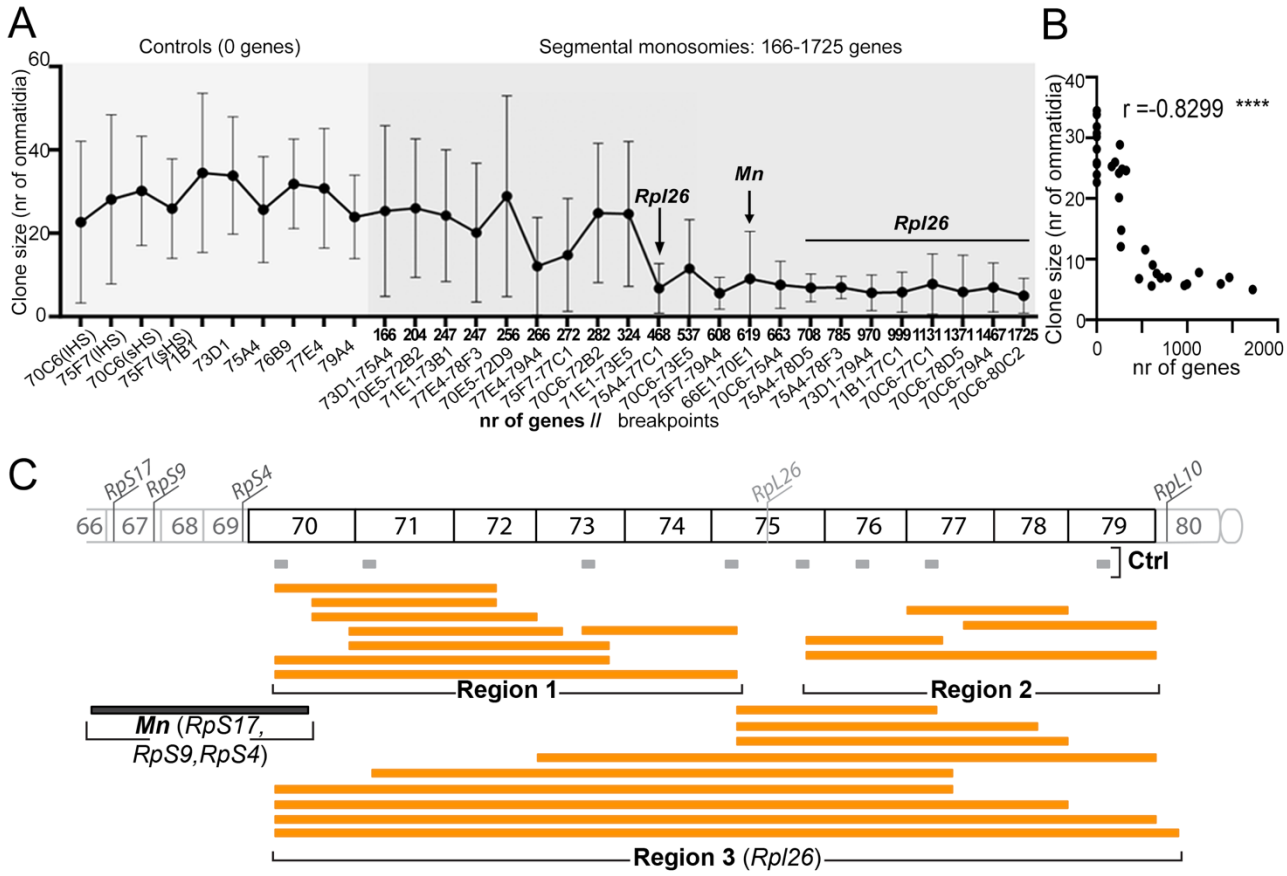

Figure R7. Size of the segmental monosomies induced with RS-FRTs in cis negatively correlated with growth, but it appears that there are region-specific effects. (**A**) Size in number of ommatidia of all the controls and 27 monosomies. The cytological location of the FRTs insertion is indicated as well as the number of genes included is indicated. Average and SD are shown. (**B**) Correlation analysis of clone size and number of genes included in the monosomies. Correlation test performed with r indicating negative correlation (ns p>0.05; * p ≤ 0.05; ** p ≤ 0.01; *** p≤ 0.001; **** p ≤ 0.0001). (**C**) Monosomies divided in three regions, upstream of *Rpl26 (*Region 1*),* downstream (Region 2) or including *Rpl26* (Region 3).

We took into consideration the presence of *RpL26*, a gene encoding for a ribosomal protein of the large ribosomal subunit, located in 75E4 in this region, which was previously discarded as a potential *Minute*-like haploinsufficient gene (Cook et al., 2012; Marygold et al., 2007). However, we noticed that the *RpL26* gene lies in a genomic gap in deletion coverage (Flybase). This led us to hypothesize that *RpL26* might indeed act as a haploinsufficient gene. For these reasons, and to better address region-specific effects, we analyzed clonal growth by dividing the segmental monosomies in three subregions (Figure R7C): Region 1, upstream of *RpL26* from location 70 to 75A; Region 2, downstream of *Rpl26* from 75F to 79; Region 3, all the segments including *Rpl26*. Clones in each region were classified into three qualitative categories according to their growth defect (Figure R8,10): growing normally, when they didn't present a significative difference with controls (light orange); with an intermediate growth defect, when their average was significantly smaller than control clones but still some clones could grow at control levels (dark orange); with a strong growth defect, when all clones were smaller than the controls and similar in size as the negative control (red).

2.2. Segmental monosomies in a region devoid of haploinsufficient genes present growth defect due to cumulative haploinsufficiency

When analyzing the impact on clone size of segmental monosomies not including the *RpL26* gene (Regions 1 and 2 in Figure R7C,8A), we noticed that clones bearing large segmental monosomies covering any of these two regions were reduced in size, but that this reduction was not observed in clones bearing smaller monosomies included within (Figure R8B,C).

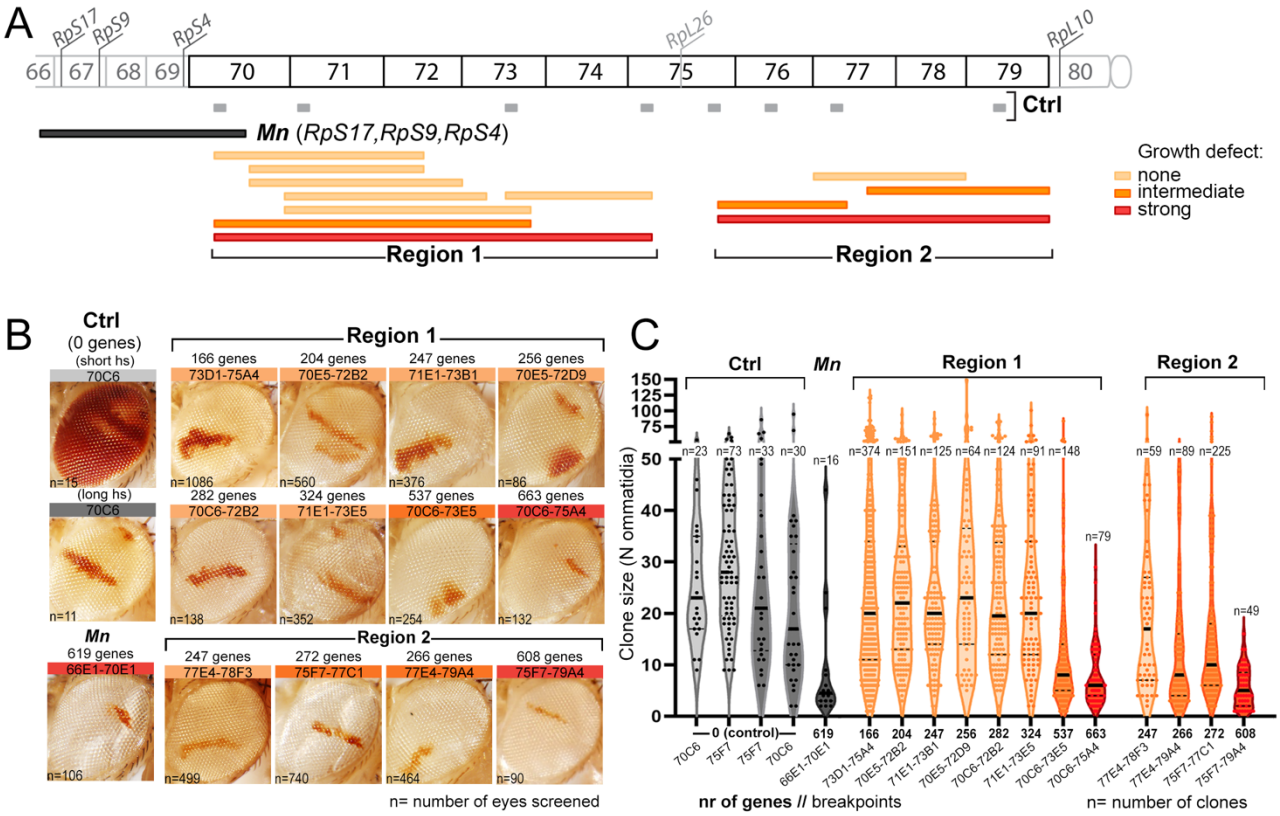

Figure R8. Segmental monosomies not including haploinsufficient genes present growth defect due to cumulative haploinsufficiency. (**A**) Map of the monosomies of Region 1 and 2 color-coded according to their growth defect. Light orange=no difference with control. Dark orange=intermediate defect (statistically significant difference with control but still presents bigger clones). Red=strong defect (statistically significant difference with control and no clone grows as controls). (**B**) Macroscope images of the adult eyes presenting the clones. Number of genes included, cytological location of the FRT insertions and the number of eyes screened are indicated for each monosomy. Clones were induced at 48h AEL with a 1h heat-shock at 38°C for monosomies and as indicated in Figure R6 for controls. (**C**) Quantification of clone size in number of ommatidia. Median is show as a black line. Number of genes included, the cytological location of the FRT insertions and the number of clones quantified for each monosomy are indicated. Log-transformed values were used to determine statistical significance of differences between Monosomies and Control groups using Mixed Linear Models with ID as random effect. Dunnet multiple contrasts for statistical significance of each ID vs Control were done using the glht function, and p values were adjusted using Benjamini-Hochberg.

In particular, in the case of Region 1, none of the six smaller overlapping monosomies spanning from 166 to 324 genes each and covering a total number of 663 genes presented a growth defect compared with controls (Figure R8B,C). This proves that none of those 663 genes is haploinsufficient by itself, neither in combination with up to 324 genes. However, the monosomy including 537 genes presents an intermediate growth defect, which becomes strong when all the 663 genes are depleted together (Figure R8B,C). Similarly, in the case of Region 2, three overlapping monosomies including 247, 266 and 272 genes present respectively none and

milder growth defects, while the bigger monosomy which includes all those 608 genes together presents a strong growth defect (Figure R8B,C). The two regions located in 77E4-79A4 and 75F7-77C1 and including respectively 266 and 272 genes, must include one or more mildly haploinsufficient genes whose impact on growth is significant but not drastic. However, when combined, the impact on growth gets stronger suggesting that the effect of haploinsufficient genes is additive. It is interesting to point out that the bigger monosomies of Region 1 and Region 2, located in 70C6-75A4 and 75F7-79A4 respectively, despite including different set of genes are similarly affected in their growth capacity.

All these observations support the proposal that growth impairment caused by segmental monosomies in the absence of haploinsufficient genes is due to cumulative haploinsufficiency of a discrete number of genes in Regions 1 and 2 rather than a gradual effect of all the genes included in the monosomies.

2.3. Cumulative haploinsufficiency-induced growth defect relies on distinct molecular mechanisms than *Mn*-induced cell competition

Once having described two independent monosomies that present a growth defect due to cumulative haploinsufficiency, we investigated if this growth defect was due to a common molecular mechanism.

During growth and differentiation of the eye primordium, there are no major cellular rearrangements. Consequently, the neighborhood relationships of the cells are maintained, and clones normally stay in a coherent group (Figure R9A). We noticed that clones of cells bearing segmental monosomies with impaired growth were frequently broken, which is a sign of out-competition by neighboring euploid cells (Figure R9A). As reviewed in the Introduction, cell competition is a fitness-sensing mechanism where cells with lower fitness ("loser" cells) are killed, by apoptosis, when surrounded by fitter ("winner") cells (Morata, 2021). In particular, heterozygous mutant cells for *Mn* genes in *Drosophila* (Ribosomial Protein genes) are eliminated from a wild type tissue by Xrp1-induced apoptosis, and proteotoxic stress contribute to the "loser" status of heterozygous *Mn* cells through a feed-forward-loop (Baillon et al., 2018; Kiparaki et al., 2022; Langton et al., 2021; C.-H. Lee et al., 2018; Recasens-Alvarez et al., 2021).

We selected the two biggest monosomies from Region 1 and 2 for genetic interaction analysis to check if, despite not including any *Mn* gene, they were outcompeted through the same molecular players involved in *Mn*-induced cell competition. Therefore, we monitored the contribution of apoptosis, Xrp1 and proteotoxic stress to the observed growth defect. We used the 73D1-75A4 monosomy, which doesn't present any growth defect, as a control. Furthermore, we used the 66E1-70D1 monosomy including the *Mn* genes *RpS17*, *RpS9* and *RpS4* as control that our tools were working properly, since its growth defect should be rescued by apoptosis, Xrp1 and proteotoxic stress downregulation. For the purpose of this experiment, we monitored clones induced both acutely, with the *hsflp* construct and a heat-shock at 48h AEL, and chronically, with the *eyflp* construct. With the acute induction, since all clones are induced in a synchronized manner, we can finely monitor and compare clonal growth between the different conditions. With the chronic induction, we can more easily detect effects on survival. In fact, chronic induction allows the generation of clones until later moments

in development and also increases efficiency of the system. We would therefore be able to detect cases in which survival but not growth is rescued. However, quantification of *eyflp*-induced clones' size as Clonal Area is a much less accurate measure than number of ommatidia due to the 3D surface of the eye. In fact, while an ommatidium will be always counted as one independently from where is located in the eye surface, when measuring Area (μm^2) in ImageJ, size of lateral clones will be underestimated compared to clones in the center of the eye. Furthermore, the shape of fused clones and the presence of small single-ommatidium clones makes it hard to carefully determine the Area of the clones. For this reason, we did not consider this a reliable measure to monitor subtle differences that may emerge as a consequence of partial rescues and we used this set up in a qualitative fashion.

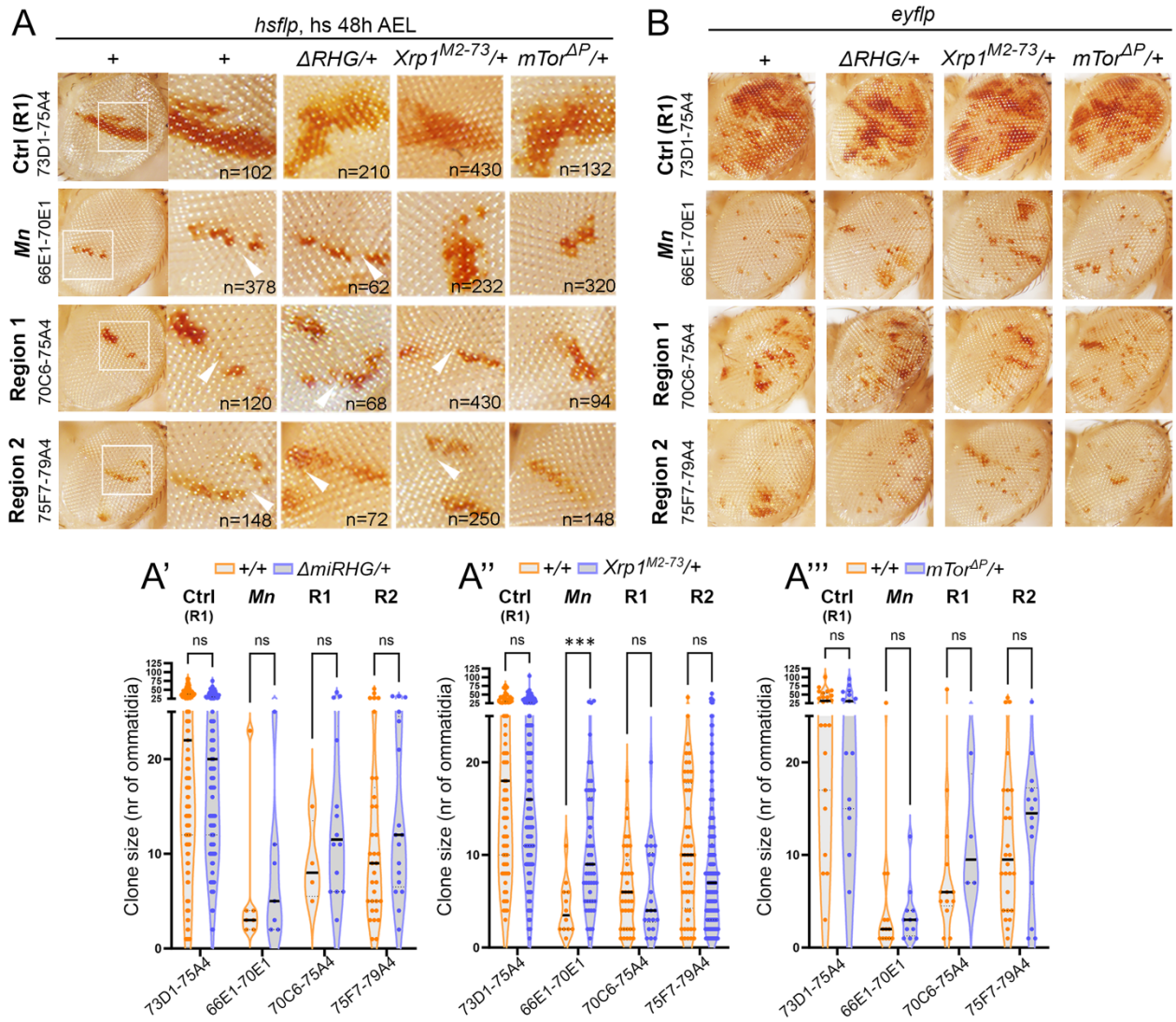

Figure R9. Cumulative haploinsufficiency relies on an *Xrp1*-independent mechanism different than *Mn*-induced cell competition. (A-B) Macroscope images of adult eyes and magnifications of clones induced either at 48h AEL with a 1h heat-shock at 38°C (A) or with *eyflp* **(B)**. Each monosomy (Control, including *Mn,* Region 1 and Region 2) is combined with a deletion of the proapoptotic genes (*ΔRHG*), a mutant of Xrp1 ($Xrp1^{M2-73}$) or of mTor ($mTor^{\Delta P}$). Quantification of clone size of the monosomies induced with *hsflp* and combined with *ΔRHG*, $Xrp1^{M2-73}$ and $mTor^{\Delta P}$ is shown in **(A')**, **(A'')**, **(A''')**, respectively. The monosomy is represented in orange and the monosomy combined with the mutants in purple. Median is shown as a black line. 2way ANOVA with Šidák correction for multiple comparisons test was performed on logarithmically transformed data.

To assess the role of apoptosis, we used a deficiency of the pro-apoptotic genes. The pro-apoptotic genes *reaper hid* and *grim* (*RHG* genes) are clustered in the genomic location 75C6 and their deficiency [*Df(H99)*] in heterozygosis is well known to cause a general reduction in the activity of the apoptotic machinery. Surprisingly, combining this deficiency with segmental monosomies from Region 1 and 2 did not rescue growth impairment (Figure R9A,B,A') and out-competition (as in broken clones indicated by white triangles in Figure R9A) neither when clones were induced with the *hsflp* construct (Figure R9A,A') nor with the *eyflp* (Figure R9B). It is to note that the growth defect of the 66E1-70D1 monosomy including the *Mn* genes was not rescued with [*Df(H99)*] in heterozygosis with the acute induction with *hsflp* but it appears to be partially rescued with the chronic induction with *eyflp*.

To assess the role of Xrp1, we used an Xrp1 mutant in heterozygosity with the monosomies. Halving the dose of Xrp1, which partially rescued the 66E1-70D1 monosomy including the *Mn* genes both with *hsflp* (Figure R9A, A'') and *eyflp* (Figure R9B), did not rescue the outcompetition of segmental monosomies of Region 1 and Region 2.

As a way of increasing autophagy to counteract the role of proteotoxic stress in cell competition, we targeted mTor, as previously done (Recasens-Alvarez et al., 2021). Considering that variations in the developmental time of clones induction drastically influence clone size (the earlier, the bigger), it is important to take into account that *mTorM/+* flies present a developmental delay (Layalle et al., 2008). However, considering that this delay only affects larvae from the L3 stage and that clone induction was performed at L2 stage, this will not affect clone size. This is supported by the fact that no difference in size is observed between +/+ and *mTorM/+* clones of the control 73D1-75A4 (Figure R9A'), while if *mTorM* flies were already delayed at the time of the induction they would have presented bigger clones. Heterozygosity for the *mTor* gene did not rescue neither the monosomies of Region 1 and 2 nor the 66E1-70D1 monosomy including the *Mn* genes (Figure R9A, A''', B).

2.4. The segmental monosomies including the region between 75A and 77C present a growth defect due to a newly identified *Mn*-like gene

When analyzing the impact on clone size of segmental monosomies including the *RpL26* gene (Region 3 in in Figure R7C,8A), we noticed that all clones of cells bearing segmental monosomies including the *RpL26* gene were much smaller than control ones and that this reduction in clone size was independent of the number of genes included in the monosomy (from 468 to 1725 genes, Figure R10 A,B,C). Interestingly, the impact on growth of these monosomies was identical to the one caused by the 66E1-70D1 monosomy affecting 619 genes and including the *Mn* genes (Figure R10C). These observations challenge the previous characterization of *RpL26* as a non-haploinsufficient ribosomal encoding gene (Cook et al., 2012; Marygold et al., 2007).

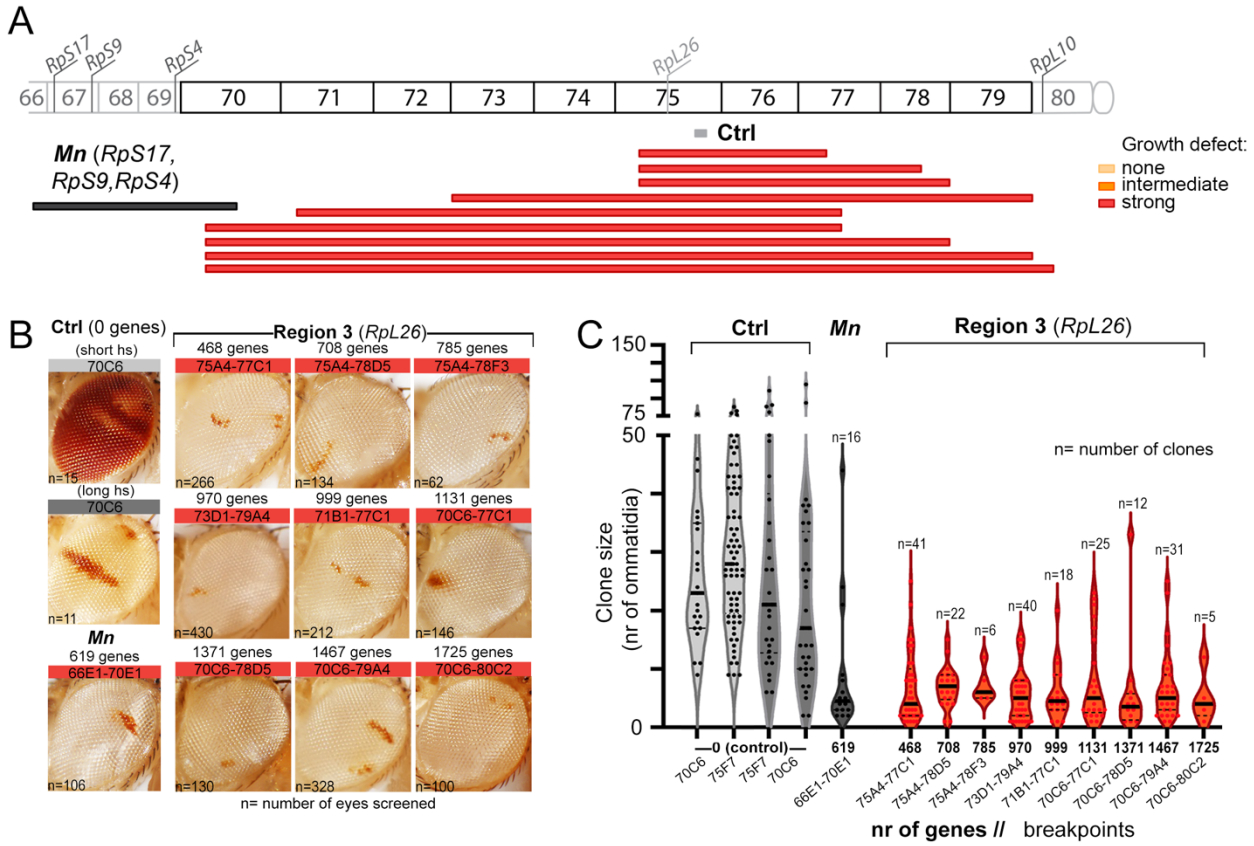

Figure R10. A newly identified haploinsufficient gene lies between 75A4 and 77C1. (A) Map of the monosomies of Region 3 color coded according to their growth defect. Light orange=no difference with control. Dark orange=intermediate defect (statistically significant difference with control but still presents bigger clones). Red=strong defect (statistically significant difference with control and no clone grows as controls). **(B)** Macroscope images of the adult eyes presenting the clones. Number of genes included, cytological location of the FRT insertions and the number of eyes screened are indicated for each monosomy. Clones were induced at 48h AEL with a 1h heat-shock at 38°C for monosomies and as indicated in Figure R6 for controls. **(C)** Quantification of clone size in number of ommatidia. Median is show as a black line. Number of genes included, the cytological location of the FRT insertions and the number of clones quantified for each monosomy are indicated. Log-transformed values were used to determine statistical significance of differences between Monosomies and Control groups using Mixed Linear Models with ID as random effect. Dunnet multiple contrasts for statistical significance of each ID vs Control were done using the glht function, and p values were adjusted using Benjamini-Hochberg.

Luckily, the pro-apoptotic genes *reaper*, *hid* and *grim* (*RHG* genes) - whose deficiency [*Df(H99)*] in heterozygosis causes a reduction in the activity of the apoptotic machinery - are clustered in the genomic location 75C6 and included in all segmental monosomies affecting the *RpL26* gene. Surprisingly, though, growth impairment (Figure R10) and out-competition (Figure R11A) were still observed. However, we must consider the possibility that by rescuing a copy of the *RHG* genes we might observe an even more drastic reduction in clone size.

We have chosen three segmental monosomies that include *Rpl26* to test whether apoptosis, Xrp1 or proteotoxic stress contributed to their growth defect, and therefore whether *Rpl26* acted as a *Mn* gene: 75A4-77C1 including 468 genes; 73D1-79A4 including 970 genes; 70C6-77C1 including 1131 genes. We choose the first because it is the shortest monosomy to include *Rpl26*, in order to limit interference from other genes as much as possible. We choose the second and the third because they were the biggest monosomies with a good recombination efficiency and to assess the role of cumulative haploinsufficiency of other genes.

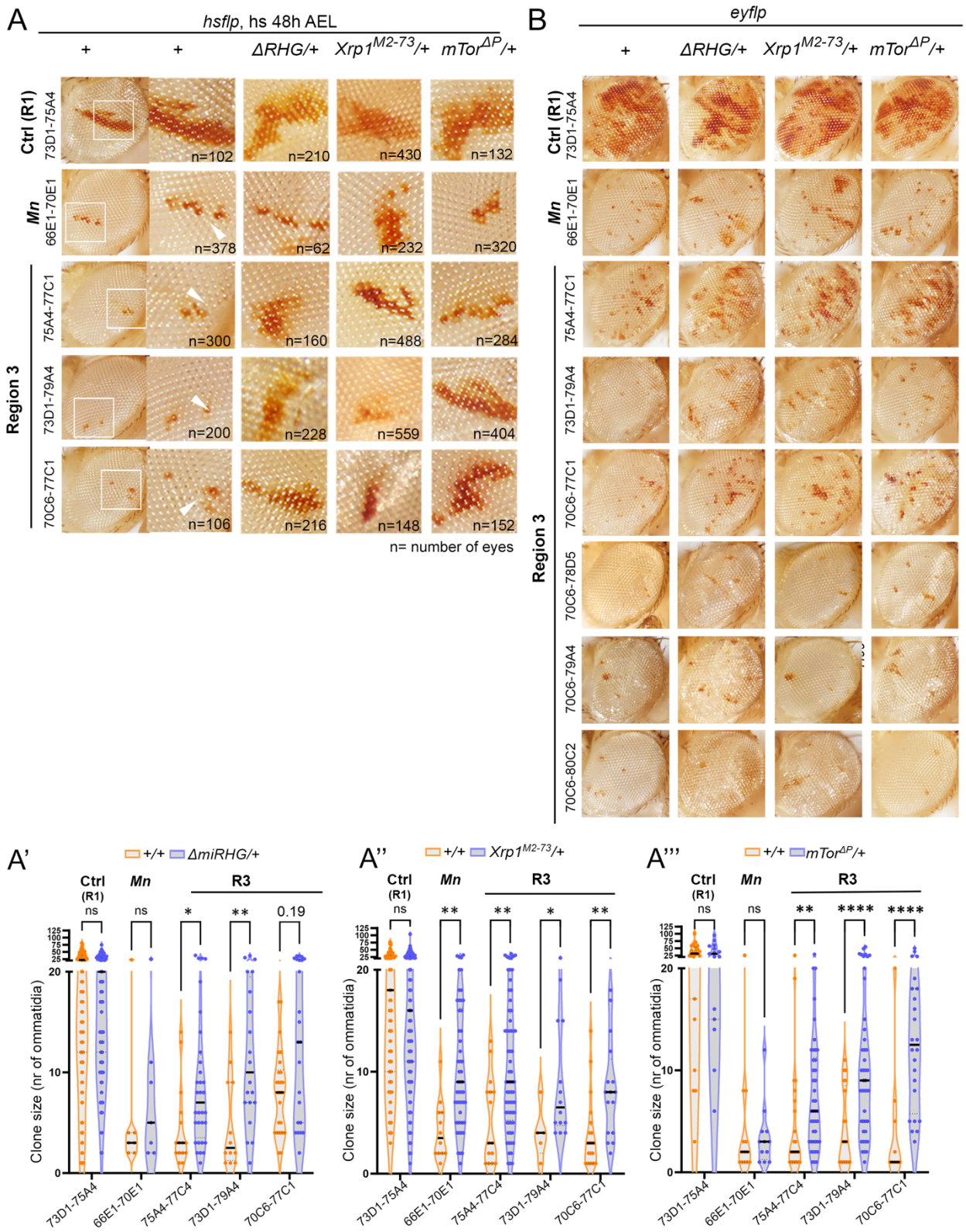

Figure R11. Segmental monosomies including a newly identified Mn-like gene present growth defects due to Xrp1-dependent Mn-induced cell competition and cumulative haploinsufficiency. (**A**) Macroscope images of adult eyes and magnifications of clones induced either at 48h AEL with a 1h heat-shock at 38°C (**A**) or with *eyflp*. Each monosomy (Control, including *Mn* and Region 3) is combined with a deletion of the proapoptotic genes (*ΔRHG*), a mutant of Xrp1 ($Xrp1^{M2-73}$) or of mTor ($mTor^{\Delta P}$). Quantification of clone size of the monosomies induced with *hsflp* and combined with *ΔRHG*, $Xrp1^{M2-73}$ and $mTor^{\Delta P}$ is shown in (**A'**), (**A''**), (**A'''**) respectively. The monosomy is represented in orange and the monosomy combined with the mutants in purple. Median is shown as a black line. 2way ANOVA with Šidák correction for multiple comparisons test was performed on logarithmically transformed data.

By comparing the effect of these genetic interactions on growth between the short and the bigger monosomies including *Rpl26,* we wanted to assess if including a bigger number of genes changed how Xrp1-dependent cell competition contributed to the growth defect (Figure R11). As commented previously, increasing distance between the FRTs decreases significantly the efficiency making it harder to have a sufficient number of clones for a solid statistical analysis. To test the biggest monosomies in our possession (70C6-78D5, 70C6-79A4, 70C6-80C2, including respectively 1371, 1467 and 1725 genes) we used only induction with the *eyflp* construct which, by inducing chronic expression of the Flp, increases recombination efficiency (Figure R11B). Homozygosity for the *RHG* genes (when these segmental monosomies were combined with a chromosome containing a deletion of the *RHG* gene complex), halving the dose of Xrp1 (when they were combined with a chromosome bringing a mutant for of the *Xrp1* gene, *Xrp1M*), and reducing proteotoxic stress (when they were combined with *mTorM*), rescued clone size (*hsflp*, Figure R11A,A',A'',A''') and survival (*eyflp*, Fig11B) of all the three monosomies analyzed, except the 70C6-77C1 monosomy which did not show a significant difference in size when the proapoptotic genes were deleted (p value=0.19). This was in accordance with the behavior of the monosomy including the *Mn* genes *RpS17*, *RpS9* and *RpS4* that was clearly rescued by halving the dose of Xrp1 (Figure R11A,A'',B), and in contrast with cumulative haploinsufficient monosomies from Region 1 and Region 2 that were not rescued by any of these interactions (Figure R10). The reason why the growth of the monosomies including *Rpl26* are rescued by downregulating apoptosis and proteotoxic stress, while the growth of the monosomy including the *Mn* genes *RpS17*, *RpS9* and *RpS4* is not (Figure R11A, A', A'', A'''), could be a matter of number of *Mn* genes and strength of the different tools to inhibit *Mn*-induced cell competition (see more in the Discussion). Altogether these results indicate that the region 75A-77C includes a *Mn*-like gene, which we have shown to be outcompeted through *Mn*- and *Xrp1*-dependent cell competition. It is important to highlight that we have not yet demonstrated with these experiments that this *Mn-like* gene is *Rpl26*. Indeed, it is technically challenging to perform genetic interactions with this set up since all most used transgenics in *Drosophila* bear a *mini-white* rescue inside the construct which will make the entire eye red and therefore make it impossible to monitor red clones of monosomic cells. For instance, we could not overexpress any gene through the Gal4/UAS system. For this reason, we have performed all the genetic interactions (Figure R9, 11) with mutants that have a *white* mutant background. To demonstrate that is *Rpl26* acting as a *Mn* in this region we have tried to make transgenic animals bringing an extra copy of this gene in another chromosome to see if by restoring two copies of *Rpl26* we were able to rescue the growth defect of the 75A4-77C1 monosomy. Unfortunately, we failed in generating these animals. However, later in this work and by using another technique, we will demonstrate that this *Mn*-like gene is indeed *Rpl26*.

It is interesting to note that with the *hsflp* induction the growth capacity of the shorter monosomy (75A4-77C1) is much better rescued by downregulating Xrp1 than the bigger ones (Figure R11A''). Furthermore, when looking at *eyflp*-induced clones, it is clear how downregulating all the tested pathways (apoptosis, Xrp1, and proteotoxic stress) rescues better the shorter (75A4-77C1) than the bigger monosomies (Fig11B). In this case, the rescue will be a consequence of both improved growth and survival rate. When looking at the 70C6-78D5, 70C6-79A4 and 70C6-80C2 monosomies (including respectively 1371, 1467 and 1725 genes) it is especially

clear that inhibiting the *Mn*-driven cell competition machinery does not rescue neither clone size nor survival to the same level that it does for the 75A4-77C1 monosomy (including only 468 genes) (Figure R11B). This reinforces the idea that cumulative haploinsufficiency plays a role in inducing a *Mn*- and *Xrp1*-indipendent growth defects and out competition in bigger monosomies.

3. Impact of segmental trisomies and monosomies on growth and survival

3.1. The Twin-Spot Generator technique can be used to generate and differentially label segmental monosomies and trisomies

In order to study segmental monosomies as well as trisomies and their interaction both with each other and wild type cells, we had to implement the *in trans* technique with appropriate markers. In fact, when we used *in trans* RS-FRTs (Figure R2B), only the chromosome bearing the segmental duplication was carrying the reconstructed marker, therefore not allowing to mark both the trisomy and the monosomy. For this reason, we employed the Twin Spot Generator technique (TSG, Griffin et al., 2009), which uses FRT elements bringing upstream and downstream the FRT cassette either the N-terminus or C-terminus sequence of either GFP or RFP (Figure R12A,B). In this thesis, we will refer to the construct bearing the N-terminus of the GFP sequence upstream and the C-terminus of the RFP sequence downstream the FRT cassette as “GR” while we will call “RG” the construct that presents the N-terminus of the RFP sequence upstream and the C-terminus of the GFP downstream the FRT. By using two different fluorescent markers, we can follow both chromosomes resulting from recombination between *in trans* FRTs. In fact, when the FRTs recombine, the GFP sequence will be reconstructed on one recombinant chromosome and the RFP on the other (Figure R12A). After G1-recombination events, the two recombinant chromosomes will stay together into the same cell which will therefore be marked in yellow, as well as its progeny (Figure R12A,D). This means that differently than other recombination-based methods for lineage tracing, the TSG technique can label in yellow cells that are not mitotically active. After G2-recombination events instead, the two recombinant chromosomes during mitosis will segregate apart from each other and together with non-recombinant chromosomes thus generating a twin clone of GFP marked cells close to RFP marked cells (Figure R12A,D). Depending on the experiment, we used the highly proliferative epithelia either of the *Drosophila* wing or eye primordia, that grow exponentially in size and number of cells during the 5 days of larval development. We induced clones either acutely or chronically. For the acute induction method we used the *hsflp* construct, let flies egg laying during 6h, heat-shocked them at 64h AEL and dissected wing discs at 120h AEL. We chose this time of induction since it precedes the 72h AEL which is the developmental time at which the L2/L3 transition happens and the D/V boundary, a region of non-proliferation, gets specified. To uncover differences in size, we needed to leave enough times for the clones to grow. However, earlier time points induction significantly decreases efficiency. For the chronic induction method we either used the *eyflp* or *eye-Gal4,UAS-Flp (eye>flp)* constructs and

dissected eye discs, or the *enG4,UAS-Flp (en>flp)* construct and dissected wing discs. We used chronic induction for some experiments of genetic interactions. On the other hand, for thorough analysis of clone size and growth capacity, we analyzed wing discs where clones were induced acutely at the same developmental timing.

For growth analysis, as control clones, we used clones deriving from recombination between FRTs inserted in the same genomic location in the two homologous chromosomes. In this case, G1- and G2-derived clones will be genetically identical (Figure R12A). Considering that the wing disc is a proliferative tissue, we expect G1-derived clones (yellow) to be double in size than single twin clones (either green or red), since a mitotic event will generate one green and one red cell after G2 recombination and two yellow cells (the double) after G1 recombination. Furthermore, since the length of G1 and G2 cell cycle phases in the wing disc is approximately the same (Neufeld et al., 1998), by chance we would expect to observe 50% of G1-derived clones and 50% of G2-derived twin clones. As shown in Figure R12F, we observe that this is the case, with 53% of the control clones that are G1-derived while 47% are G2-derived. By quantifying the Area of the clones (see Materials and Methods for details) we observe that in control clones single GFP+ and RFP+ clones are equal in size between each other and 0,64 the size of G1-derived yellow clones (Figure R12 G). The fact that twin clones are slightly bigger in size than the exact half of the G1-derived clones could be a consequence of variability depending on the location of the clones in the tissue. In fact, not every cell in the wing disc proliferates at the same rate but there are areas where, according to the developmental time, proliferation rate is lower or higher. For instance, if a clone touches the D/V boundary, the previously mentioned region of non-proliferation in the middle of the wing disc epithelium, its proliferation will be arrested from late L3 onwards.

In order to induce segmental aneuploidies, we used TSG FRTs located at a certain distance between each other (Figure R12B). If the GR construct is located downstream the RG construct, the recombinant chromosome carrying the segmental monosomy will bear the RFP and the recombinant chromosome carrying the segmental trisomy the GFP marker. Instead, if the GR construct is located upstream, the chromosome carrying the segmental monosomy will bear the GFP and the one carrying the segmental trisomy the RFP. For simplicity, in this work we will always represent the monosomy in red and the trisomy in green, independently if they were marked with GFP or RFP. Genotypes for each experiment will be specified in the Figure legends. G1-derived yellow clones will carry a chromosome with a segmental monosomy and a chromosome with the complementary segmental trisomy and therefore will be euploid (Figure R12B). As such, these clones will serve as internal controls of the effects of the recombination between distal FRTs elements. In order to reduce variability due to differential rates of development between samples or effects of genomic rearrangements, clone size was normalized to the size of euploid clones of each combination (see next chapter and Materials and Methods for details).

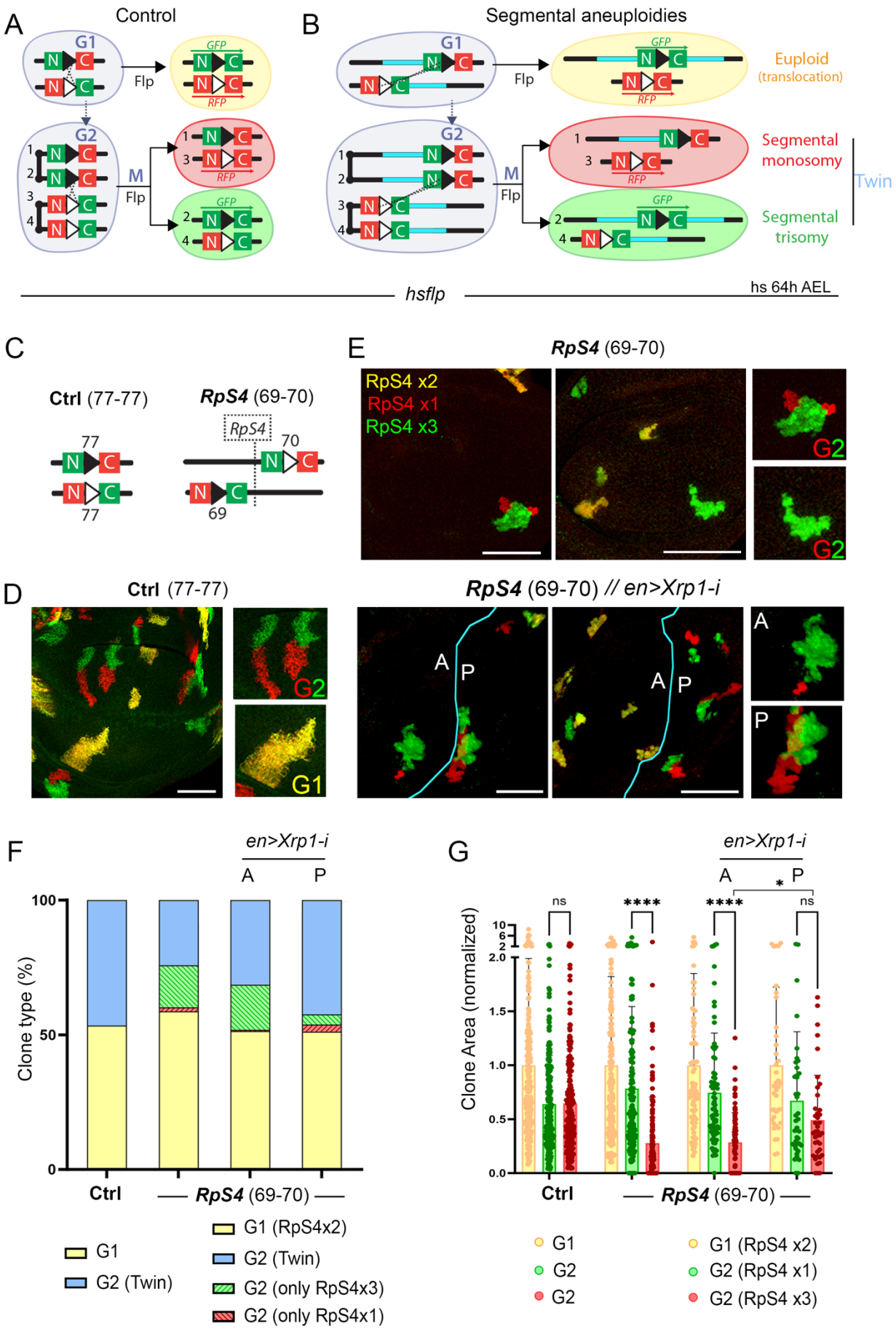
A
Control
G1
Flp
GFP
RFP
G2
M
Flp
B
Segmental aneuploidies
Euploid
(translocation)
Segmental
monosomy
Segmental
trisomy
Twin
hsflp
hs 64h AEL
C
Ctrl (77-77)
RpS4 (69-70)
RpS4
77
70
69
E
RpS4 (69-70)
RpS4 x2
RpS4 x1
RpS4 x3
G2
D
Ctrl (77-77)
G1
RpS4 (69-70) // en>Xrp1-i
A
P
F
en>Xrp1-i
Clone type (%)
100
50
0
Ctrl
RpS4 (69-70)
G1
G2 (Twin)
G1 (RpS4x2)
G2 (Twin)
G2 (only RpS4x3)
G2 (only RpS4x1)
G
Clone Area (normalized)
ns
****
*
G1
G2
G2
G1 (RpS4 x2)
G2 (RpS4 x1)
G2 (RpS4 x3)

Figure R12. The Twin Spot Generator technique can be used to acutely generate segmental monosomies and trisomies and spot differences in cell fitness. **(A, B)** Drawing of recombination events between two TSG-FRTs that reconstitute the GFP and RFP genes. Recombination events in G1 label the two daughter cells in yellow, those in G2 label one daughter cell in red and the other one in green. When the two FRTs are located at a distance **(B)**, yellow cells carry a segmental translocation, and red and green cells carry segmental monosomies or trisomies, respectively. **(C)** Genomic location and orientation of control TSG-FRTs located *in trans* in the same orientation to produce two euploid cells (left) and TSG-FRTs flanking the *RpS4* gene to produce cells with 1, 2 and 3 doses of the *RpS4* gene (right). (**D, E**) Wing primordia epithelia with control clones resulting from recombination in G1 (yellow) or in G2 (twin clones, one in red and the other in green) **(D)**, and with clones with one (red), two (yellow) and three (green) doses of the *RpS4* gene **(E)**. When Xrp1 is depleted in the posterior (P) compartment, the size and recovery of red RpS4x1 clones is rescued. Scale bars, 50 µm. **(F, G)** Plots representing clone type distribution **(F)** and clone area **(G)** (normalized to the one of euploid cells) of control clones and clones with the indicated doses of *RpS4*. Average **(F)** and mean and SD **(G)** are shown. 2way ANOVA with Šidák correction for multiple comparisons test was performed in **G**. Clones were induced at 64h AEL with a heat-shock at 38°C of 5-7 minutes for the control and of 1h for the other combinations. ns, not significant ($p>0.05$); * $p \leq 0.05$; ** $p \leq 0.01$; *** $p \leq 0.001$; **** $p \leq 0.0001$.

As a proof of principle that the TSG technique with *in trans* FRTs would allow us to spot differences in size between segmental monosomies and trisomies and their euploid control, we placed a pair of TSG-FRTs *in trans* at both sides of the *Minute*-like gene *RpS4* (Marygold et al., 2007) located at 69F6, respectively at 69F1 and 70A8, to generate segmental aneuploidies of relatively small size (89 genes) with different doses of *RpS4* (Figure R12C). Whereas the ratio between G1 (yellow clones) and G2 recombination events (twin clones) was, as expected, roughly maintained with 58.2% of G1-derived clones (Figure R12F), those clones of cells bearing a monosomy for the *RpS4* gene (labeled in red) were lost from the epithelium in 37.5% of the twin clones (Figure R12F). The size of monosomic clones was markedly reduced when compared to the size of euploid clones (Figure R12G) and in many cases, monosomic clones were broken and lost contact with the clone bearing the trisomy (Figure R12E). It is important to note the cases when only the trisomic clone was observed and the monosomic twin was lost were taken into account in the size quantification by plotting the area of the monosomic clone as zero. We can notice how the GFP and RFP proteins are localized in the cellular membrane in the control while the cytoplasm for the 69-70 clones. This is because the GR and RG constructs inserted in the position 77C4 bear a membrane localization sequence while all other TSG-FRT constructs do not (See Materials and Methods for details). For this reason, whenever one line bringing the TSG-FRT construct in the position 77 is used in combination with another line, either the GFP or the RFP will be localized in the membrane.

We then depleted Xrp1 by driving an RNAi form in the posterior (P) compartment of the wing through the *enG4,UAS-Xrp1-i* construct (Figure R12E). The anterior (A) compartment of these discs is genetically identical to discs without RNA-i and serves as internal control. Xrp1 depletion in the posterior compartment rescued the size from 0.28 to 0.49 and the loss of clones bearing only one copy of *RpS4* from 37.5% to only 1.82% of the twin clones (Figure R12E,F,G). Interestingly, the size of the trisomy was significantly increased up to 0,78 of the euploid clones in the clones bearing three copies of *RpS4* respect to the 0,64 observed in the control (Figure R12G). An increase to 0,74 was also observed in the case of the anterior compartment of the *enG4,UAS-Xrp1-i* discs but was not significant. The size of *Rps4(*x3) clones was restored to 0,67 in the posterior compartment upon Xrp1 depletion. This points to a potential case of Xrp1-dependent overproliferation caused either cell autonomously by the three copies of *RpS4* or by compensatory proliferation induced by the outcompeted clone.

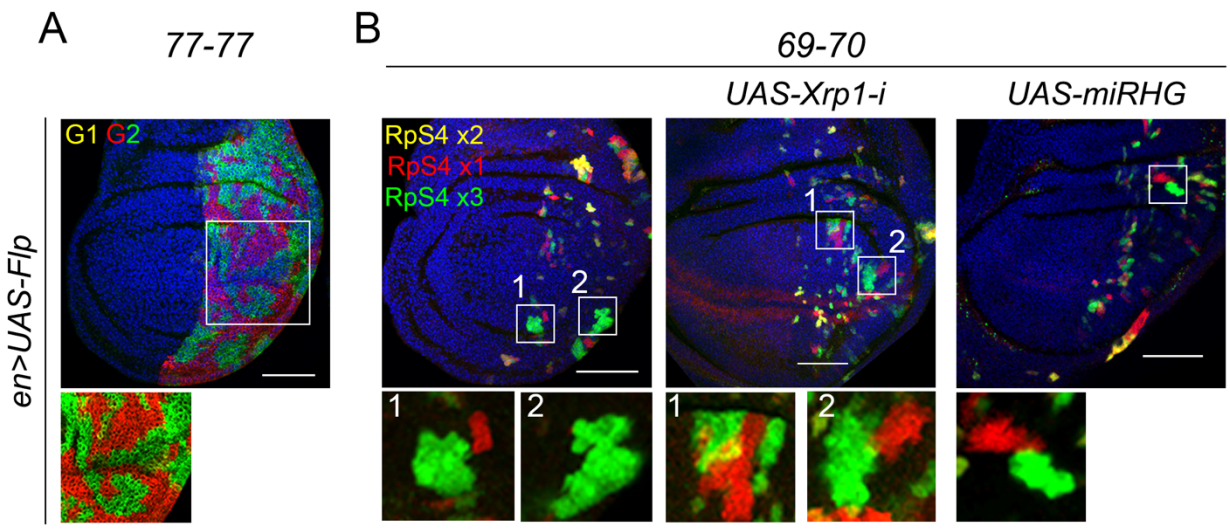

Figure R13. The Twin Spot Generator technique can be used to chronically generate segmental monosomies and trisomies and spot differences in cell fitness. (A,B) Wing primordia where clones were induced through the *en>flp* construct either to produce control clones **(A)** or clones with different doses of *RpS4* (yellow *RpS4*x2, green *RpS4*x3 and red *RpS4*x1) **(B)**. Loss of the *RpS4*x1 clone is rescued by downregulating Xrp1 or apoptosis (by overexpressing the *miRHG* miRNA against proapoptotic genes). Scale bars, 50 µm.

We could observe similar effects when clones were induced chronically with the *enG4,UAS-Flp* construct. As it can be noticed, in the control there are no yellow G1-derived clones (Figure R13A). This happens because if G1-derived yellow clones recombine in G2, red and green twin will arise. Once established, green and red twin clones cannot lose their marker nor change their genotype, even upon further recombination events. Therefore, since the wing disc epithelium proliferates throughout the expression of the *engrailed* promoter, and recombination between FRTs in the same genomic location is highly efficient, it is almost impossible that a cell in the *engrailed* compartment will not undergo a G2-recombination event. This results in the presence of only twin clones in the posterior compartment of control discs. On the other side, clones induced chronically between FRTs in 69F1 and 70A8 and bearing different copies of the *RpS4* gene, are visibly different in size concordant with the fact that they are induced at different developmental timings. We can observe that bigger clones are not as many as smaller clones, which can be explained thinking that recombination at later developmental times is more efficient. We can also see how clones near the D/V boundary are much smaller, consistent with the non-proliferative nature of this region after L3. Due to this difference in size between clones in the same tissue, it is not so straightforward to observe a difference in growth between *RpS4*(x1) and *RpS4*(x3) clones. However, if we focus on bigger clones (induced before) we can clearly recapitulate the difference in size as well as the rescue with Xrp1 downregulation (Figure R13B) and apoptosis inhibition, through overexpression of the micro-RNA *miRHG* against the proapoptotic genes *reaper*, *hid* and *grim* (Figure R13B).

All this taken together confirms that our method of acute clones' induction and size quantification is highly reliable and consistent in spotting differences in cell fitness that result in loss of less fitted cells due to cell competition.

We generated a collection of 14 different TSG-FRT-bearing transgenic lines located in the region 69-80 of chromosome 3L (see Materials and Methods for details) that we used in 27 different combinations (Figure

R14), at a distance spanning from 0 to 9 Mb and including from 89 to 1517 genes, to characterize the impact of monosomies and trisomies to the growth and survival of cells. We will see in the next chapters how generating a segmental monosomy alongside its complementary trisomy can influence the behavior of the monosomy and change what we have observed in the previous chapters, when we induced just the monosomy in a wild type tissue.

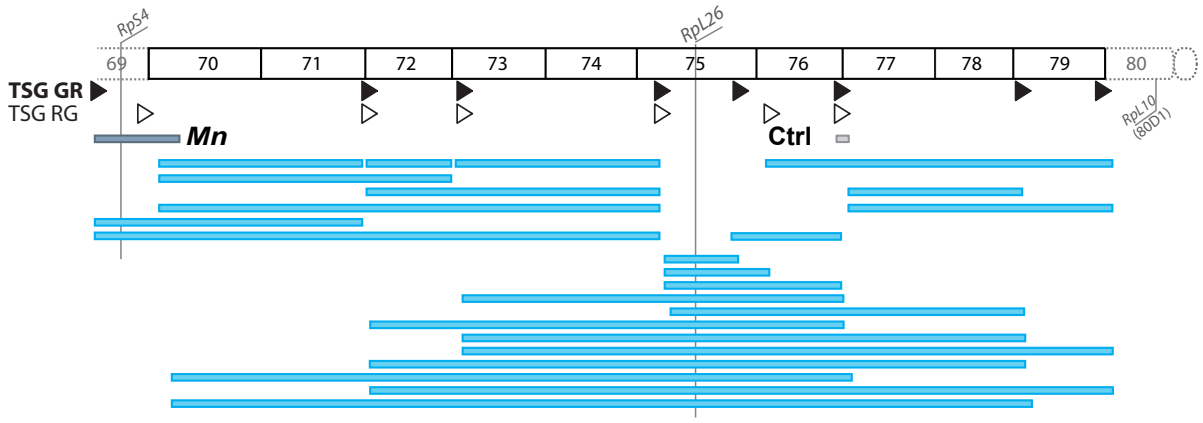

Figure R14. A collection of 14 TSG-FRT bearing lines used in trans to generate 27 different segmental trisomies and monosomies from the positions 69 to 80 in the chromosome 3L. Map of the collection of TSG-FRTs. Black triangles represent TSG GR (bearing the N terminal segment of the GFP sequence upstream the FRT and the C terminal of the RFP downstream) and white triangles RG (bearing the N terminal segment of the RFP sequence upstream the FRT and the C terminal of the GFP downstream). The 27 aneuploidies that will be generated by combining TSG-FRTs *in trans* are represented in blue with respect to the location on the chromosome. For each region euploid controls, monosomies and trisomies will be induced in the same tissue.

3.2. Rearrangements between distal FRTs cause growth defects

When looking at the euploid rearrangements for the 27 combinations of FRTs tested, in 22 out of 27 the G1-derived clones were smaller in size than the control, the only exceptions being the combinations 75A-F (201 genes), 72-75A (379 genes), 77-80 (485 genes), 73-77 (717 genes), 72-77 (896 genes) (Figure R15A,B). It looks like there is not any commonalities between the combinations that do not present a growth defect in the euploid clone size, neither in terms of number of genes nor location where the FRTs are inserted. This is consistent with what speculated about variations in frequency both for RS-FRTs *in trans* (Figure R3) and *in cis* (Figure R5A). Effects of the site of the insertion of the couple of FRTs in terms of flanking genes or chromatin structures could influence both the fitness and the survival of the resulting cell and therefore the frequency of recombination. For this reason, and to address the impact of the monosomies and trisomies on cellular fitness without being biased by the impact of recombination per se, we have normalized the size of the G1-derived clones and of each twin clone to the size of the correspondent G1-derived clones. Therefore, all the G1-derived clones will have an average area of 1 and the twin clones an average area that is a fraction of 1 (see Figure R4G). For simplicity purposes, in the following Figures where the impact of segmental monosomies and trisomies on cellular fitness is analyzed, we will plot the normalized area of monosomies and trisomies but not of euploid controls, whose area is plotted, not normalized, in Figure R15B to show variability.

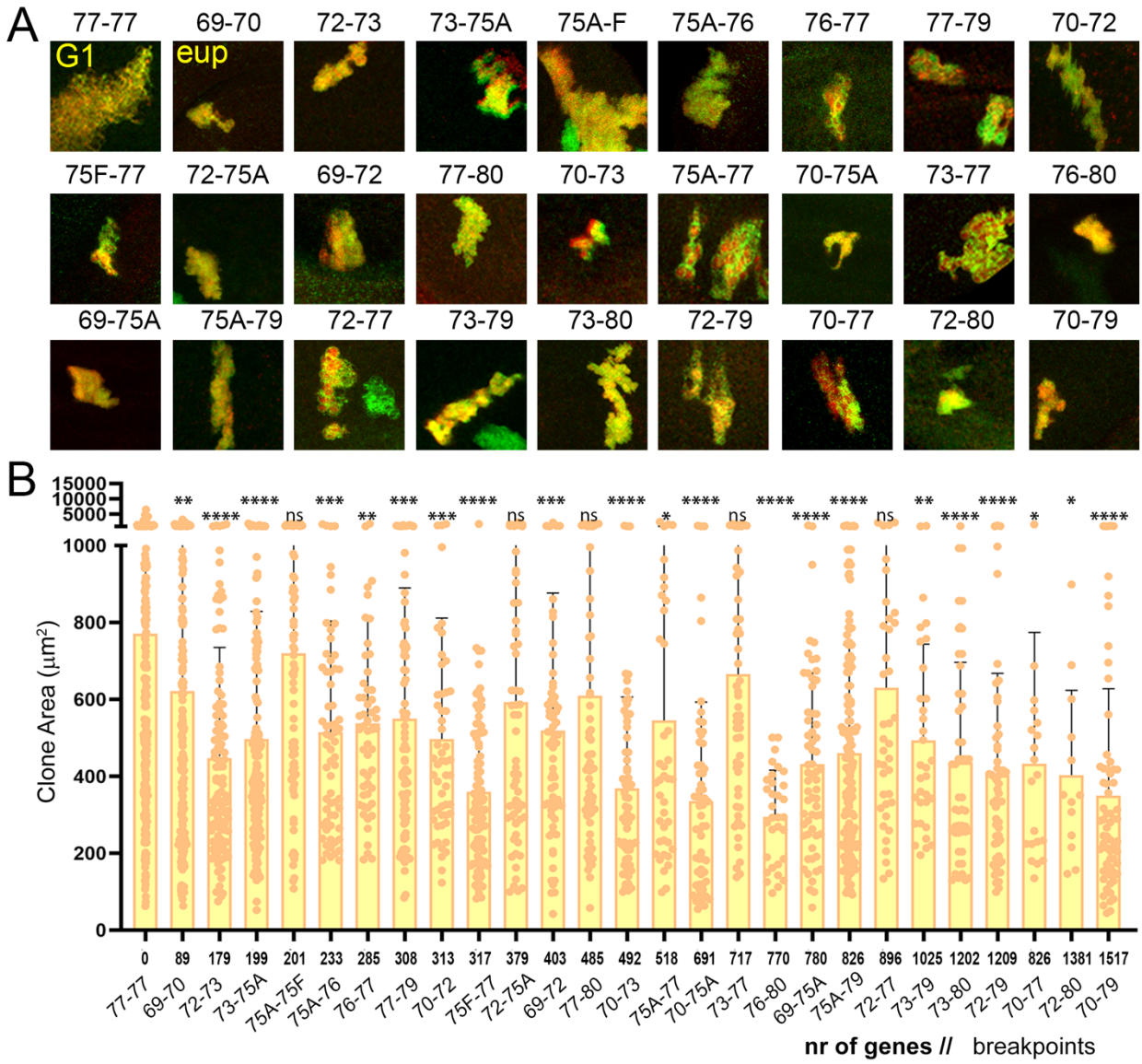

Figure R15. Recombination between distal FRTs induces growth defects in euploid controls. (**A**) Magnification of euploid clones in wing primordia. Clones were induced at 64h AEL with a heat-shock at 38°C of 5-7 minutes for the control and of 1h for the other combinations. Each image is 50x50 µm. (**B**) Plot representing the impact on clone size (in μm^2) of the size (in number of protein-encoding genes) of the euploid translocation. Genomic breakpoints of these translocations are indicated. Mean and SD are shown. 2way ANOVA with Šidák correction for multiple comparisons test was performed. ns, not significant (p>0.05); * $p \leq 0.05$; ** $p \leq 0.01$; *** $p \leq 0.001$; **** $p \leq 0.0001$.

3.3. Size of segmental monosomies causes a non-linear impact on growth

We analyzed the size of each type of clone (euploid, monosomy, trisomy) for the 27 different combinations (Figure R14) with respect to the number of genes included between the two TSG-FRTs.

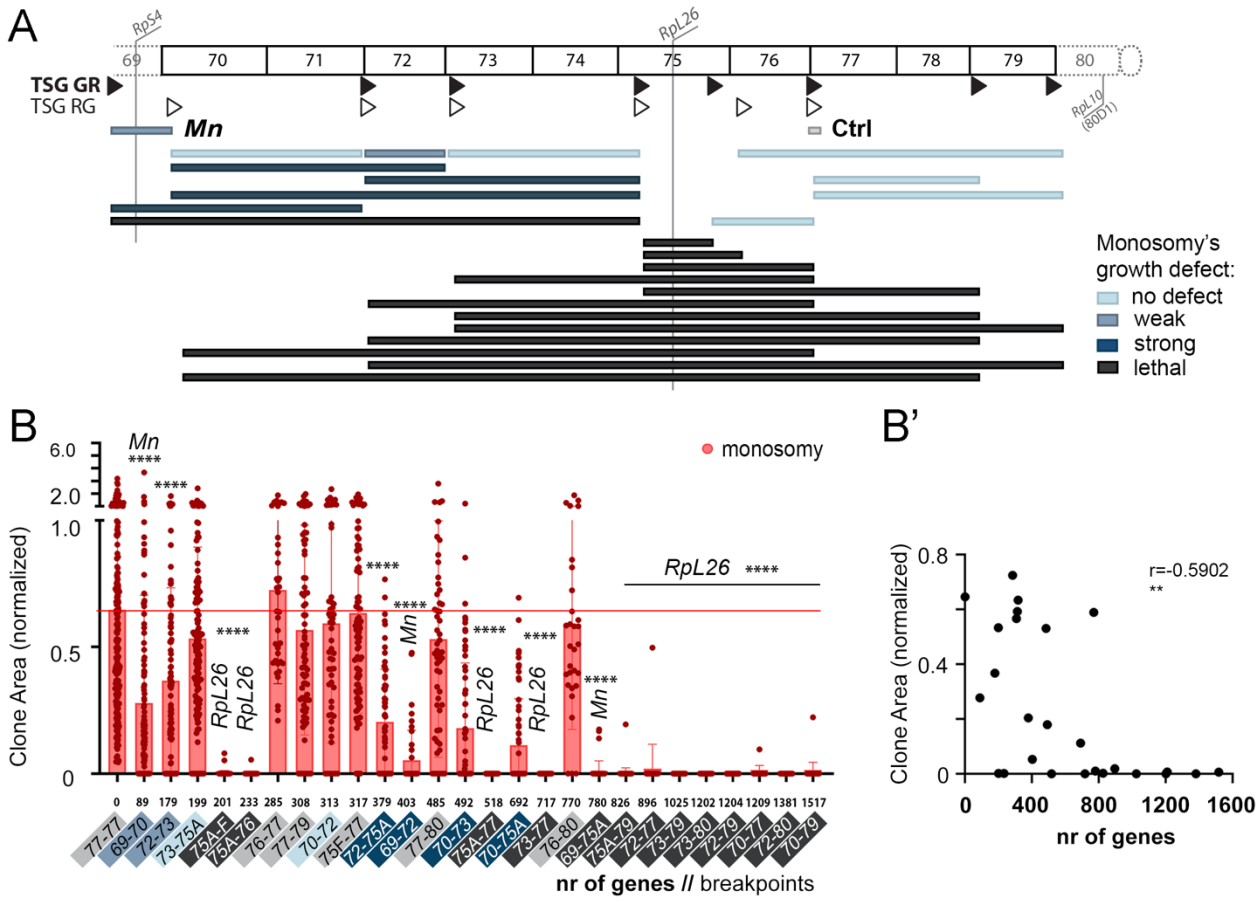

Figure R16. **Growth of the segmental monosomies induced with TSG-FRTs in trans is impacted by region-specific effects more than the size of the monosomy. (A)** Map of the monosomies analyzed color coded according to their growth defect compared to the control. Light blue=no difference with control. Blue=weak growth defect, comparable to the 60-70 (including the *Mn* gene *RpS4*). Dark blue=strong, stronger than the 69-70. Dark grey=lethal, when almost no monosomies were recovered. Clones were induced at 64h AEL with a heat-shock at 38°C of 5-7 minutes for the control and of 1h for the other combinations. **(B)** Plots representing the impact on clone size (normalized to the size of euploid clones) of the size (in number of protein-encoding genes) of the segmental monosomy. Mean and SD are shown. 2way ANOVA with Šidák correction for multiple comparisons test was performed. ns, not significant (p>0.05); * p ≤ 0.05; ** p ≤ 0.01; *** p≤ 0.001; **** p ≤ 0.0001. **(B')** Correlation analysis of clone size and number of genes included in the monosomies. Correlation test performed with r indicating negative correlation (ns p>0.05; * p ≤ 0.05; ** p ≤ 0.01; *** p≤ 0.001; **** p ≤ 0.0001).

Regarding segmental monosomies, as observed with clones bearing segmental monosomies in the adult eye (Figure R7A,B), the negative impact of the size (in number of genes) of the monosomy on clonal growth was very strong but not linear (Figure R16 B,B'). In fact, despite presenting a significant negative correlation of -0.5902, it is clear how specific regions present growth defects that do not correlate with the number of genes. Examples are the monosomy 72-73, including only 89 genes, that grows much worse than the bigger 73-75A, including 199 genes, or the monosomies 75A-F and 75A-76, including respectively 201 and 203 genes, that are clearly eliminated from the tissue despite including a relatively small number of genes. Other examples are the monosomies 72-75A and 69-72 including respectively 379 and 403 genes that grow much worse than the bigger monosomy 77-80 (485 genes), or the 76-80 monosomy which despite including a fairly big number of genes (770) does not show any difference in size with respect to the control. It is interesting to note that, despite presenting few oscillations, the correlation between size of the segmental monosomy and its impact on growth is much higher (r=-0.8299, Figure R7B) when segmental monosomies are growing surrounded by wild type

cells, and not side by side with segmental trisomies. This is in accordance with what we will describe later about how the presence of the trisomy can influence the behavior of the monosomy.

Furthermore, as a general observation, it is striking how all the monosomies including the region 75A-75F, where the *Rpl26* gene is located are lethal and cannot be recovered in the tissue.

3.4. Segmental trisomies up to 1500 genes in the region analyzed do not show growth defects

When analyzing the correspondent 27 segmental trisomies with respect to the number of genes included between the two TSG-FRTs, it resulted that they did not have a statistically significant negative impact on the size of the clones up until 1517 genes, with a correlation coefficient of -0.1438 (Figure R17 B,B').

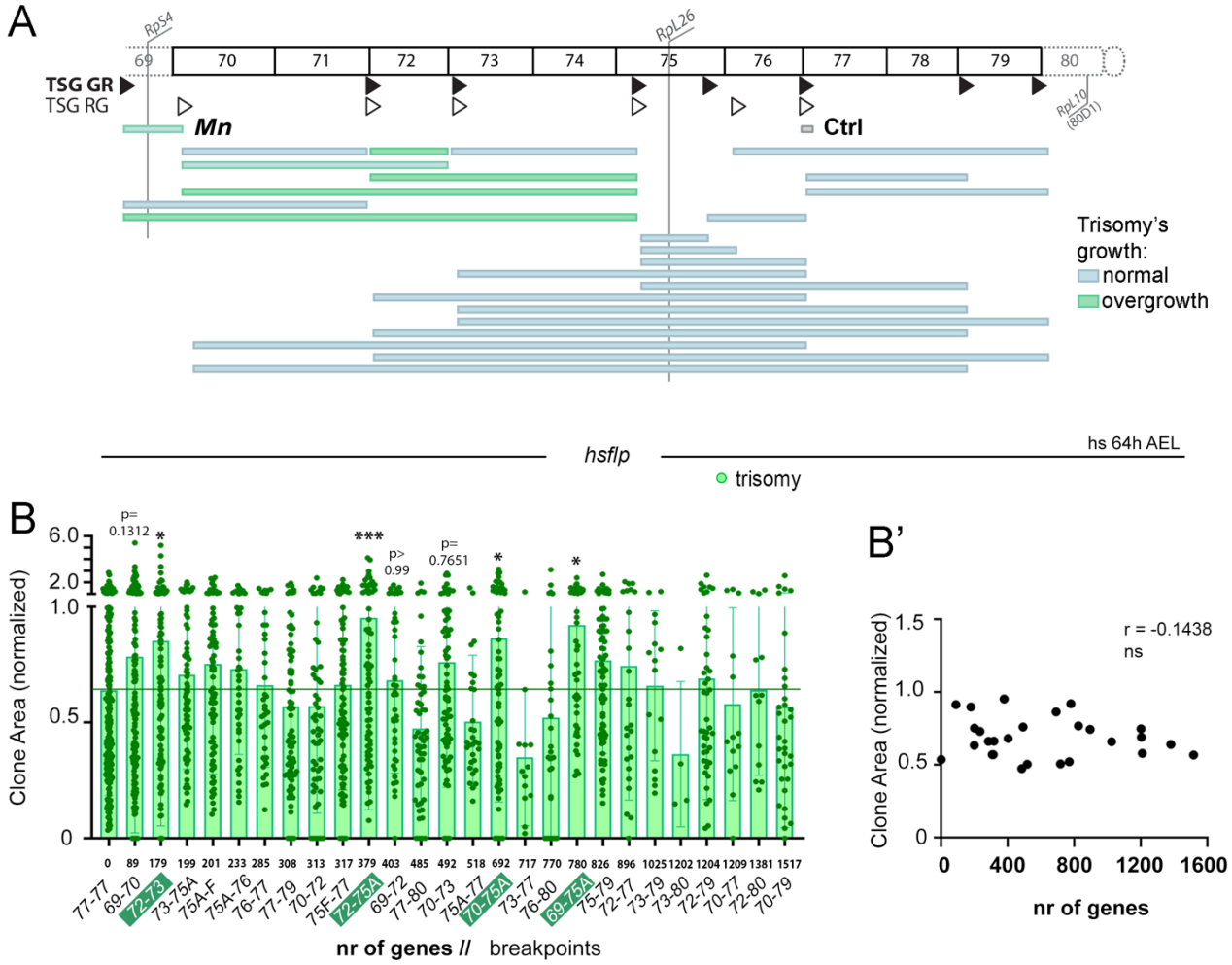

Figure R17. Growth of the segmental trisomies induced with TSG-FRTs in trans is not compromised according to the size of the trisomy. (**A**) Map of the trisomies analyzed color coded according to their growth capacity compared to the control. Light blue=no difference with control. Green=bigger than control. Clones were induced at 64h AEL with a heat-shock at 38°C of 5-7 minutes for the control and of 1h for the other combinations. (**B**) Plots representing the impact on clone size (normalized to the size of euploid clones) of the size (in number of protein-encoding genes) of the segmental trisomies. Trisomies significantly bigger than control are highlighted in green. Mean and SD are shown. 2way ANOVA with Šidák correction for multiple comparisons test was performed. ns, not significant (p>0.05); * p ≤ 0.05; ** p ≤ 0.01; *** p≤ 0.001; **** p ≤ 0.0001. (**B'**) Correlation analysis of clone size and number of genes included in the monosomies. Correlation test performed with r indicating no correlation (ns p>0.05; * p ≤ 0.05; ** p ≤ 0.01; *** p≤ 0.001; **** p ≤ 0.0001).

Indeed, some segmental trisomies (labeled in dark green) had a positive impact on the size of the resulting clones. In particular, the 72-73, 72-75, 70-75 and 69-75 were significantly bigger than the control. All these trisomies include the region between 72-73. The only trisomy which includes the 72-73 region and doesn't show a significant increase in size respect to the control is the 70-73, which could be due to variability. Despite this, four out of five trisomies including the 72-73 region were significantly bigger than the control pointing to a phenomenon of super-competition due to some gene or group of genes included in the 72-73 region. The 69-70 trisomy including the *Mn* gene *RpS4*, which was significantly bigger than the control when comparing *RpS4x1* with *RpS4x3* and *Rps4x2* clones (Figure R12G), doesn't show a significant increase in size in this data set although it shows a clear tendency (Figure R17B, p=0.1312). Instead, the 69-72 trisomy, which also includes *RpS4* but a bigger number of genes (403 versus 89 genes), doesn't show an increase in size with respect to the control (Figure R17B, p>0.99). Trisomies which didn't show a difference in size with respect to control are shown in light blue in Figure R17A, while trisomies which overgrow are depicted in green. For the reasons discussed above, trisomies 70-73 and 69-70 are represented in light blue with a green stroke to indicate that they probably overgrow despite not presenting a significant difference in this dataset.

As commented in the previous chapter, it is clear for both segmental monosomies and trisomies that the genomic region and the genes that are included in the aneuploidy deeply influence their growth and survival. For this reason and following the observation that all monosomies that include *Rpl26* are eliminated from the tissue, we will analyze growth by dividing the segmental aneuploidies that we induced in the wing disc with the TSG technique into approximately the same three subregions in which we divided the segmental monosomies that we induced in the adult eye (Figure R7C): Region 1, upstream of *RpL26* from location 69 to 75A (Figure R18A); Region 2, downstream of *Rpl26* from 75F to 80 (Figure R20A); Region 3, all the aneuploidies including *Rpl26* (Figure R22A). As previously discussed, as controls we used clones where G1-derived yellow clones and RFP+ and GFP+ twin clones are genetically identical. Furthermore, we will use the previously described clones bearing different copies of *RpS4* as an example of cell competition and therefore a control of outcompetition and haploinsufficiency. In the next chapters we will analyze how the segmental monosomies and trisomies of Regions 1, 2 and 3 grow, if monosomies and their respective trisomies display a difference in size and survival between each other and with respect to controls, and, in case any growth defect is observed, if it is similar in entity and molecular mechanism to the *Mn- Xrp1*-dependent cell competition described for *Rps4*. Since the majority of trisomies do not present an impact on size respect to control, the aneuploidies of each genomic region will be represented in a color code that describes the impact of the monosomy on clone size: similar in size as control ones (light blue), weak (blue) or strong (dark blue) growth impairment, and lethality (black).

3.5. A case of supercompetition in Region 1

Comparing the effects of monosomies in Region 1 induced by RS-FRTs in the adult eye (monosomies 73D1-75A4, 70E5-72B2, 71E1-73B1, 70E5-72D9, 70C6-72B2, 71E1-73E5, 70C6-73E5, 70C6-75A4 in Figure R8)

with those induced by TSG-FRTs in the wing disc that cover the same genomic regions (70-72, 72-73, 73-75, 70-73, 72-75, 70-75 in Figure R18), we observe that some monosomies exhibit growth defects when induced by TSG-FRTs, which were not present with RS-FRTs. In particular, while the monosomies including the regions 70-72 and 73-75 did not display any growth defect with neither the TSG- nor the RS-FRTs set ups, the monosomy including the region 72-73 displayed a clear growth defect when compared to its complementary trisomy and to the control when induced with the TSG technique that monosomies including the same region did not present when induced with RS-FRTs (70E5-72B2, 71E1-73B1, 70E5-72D9, 70C6-72B2, 71E1-73E5 in light orange in Figure R8). This proves that none of the genes included in this region is haploinsufficient by itself. Most interestingly, as pointed above when analyzing the impact of the size of the trisomy on clonal growth (Figure R17 A,B), almost all clones of cells bearing trisomies for the region 72-73 of Region 1 were significantly larger than controls (Figure R17B, 18C). The regions in which the trisomy presents an overgrowth are represented with a green stroke in Figure R18A. Coherent results are observed when looking at the survival of monosomic clones, measured as presence of both twin clones (blue) versus presence of only the trisomic clone (green, Figure R18). In fact, while for regions 70-72 and 73-75 we observe a small percentage of twin clones that lost the monosomic cells (5.1 and 5.6% respectively), 13.1% of twin clones including the 72-73 region lost the monosomic twin. We can observe in almost all cases a small percentage of twin clones (from 1 to 5.9%) that lost the trisomic clones (represented in red). This is coherent with the fact that recombination events between distal FRTs are per se generally deleterious for the cells (Figure R15), which could result in stochastic loss of either one of the two twin clones. When the frequency of these events stays approximately below 5% and does not correlate with a decrease in clones' size, we can speculate that loss of those clones is something that happens due to recombination and not to an effect of the aneuploidy on cell fitness.

These results taken together point towards a potential case of super-competition caused by the presence of trisomic cells acting as competitive winners towards the monosomic cells. We identified a small genomic region of 179 genes located in 72-73 that is able to reproduce the growth impairment of monosomic clones in all five monosomies analyzed that include this region (72-73, 70-73, 72-75, 70-75, 69-75) and the increase in the size of trisomic clones in four out of five trisomies analyzed (72-73, 72-75, 70-75, 69-75) (Figure R18C). The fact that the same genes when included in monosomies generated with RS-FRTs *in cis* in a wild type context do not show haploinsufficiency, is coherent with a scenario where segmental monosomies including these genes are outcompeted by cells bearing a trisomy for the same genes and not by wild type cells. Similar observations were found in the eye primordium as well by inducing the clones through the *eyflp* construct, ruling out any tissue-dependent effects (Figure R18E).

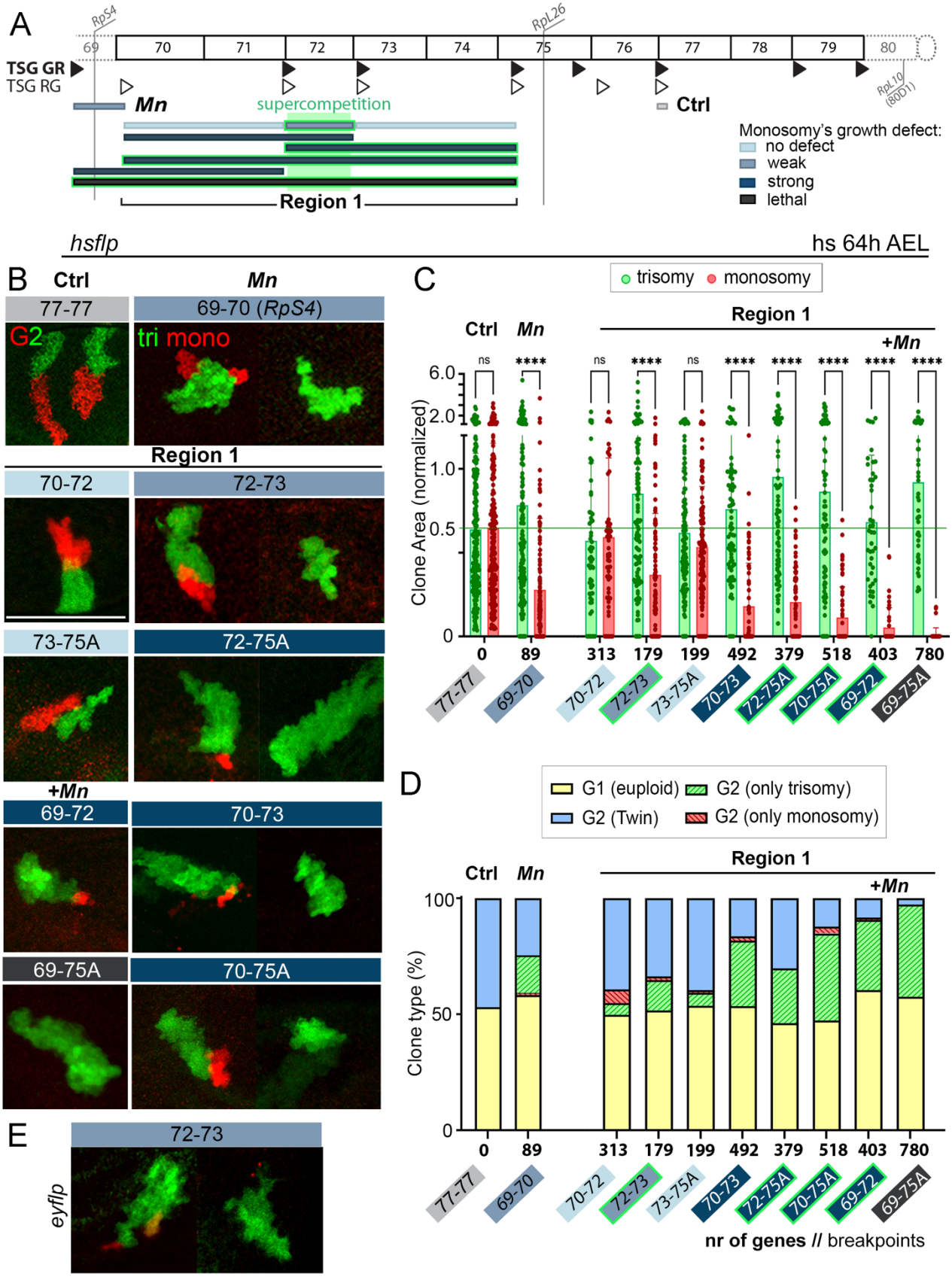

Figure R18. Growth of the segmental monosomies in Region 1 is compromised due to super-competition and cumulative haploinsufficiency. (A) Map of the trisomies and monosomies analyzed color coded according to the growth defect of the monosomy compared to the control. Light blue=no difference with control. Blue=weak growth defect. Dark blue=strong growth defect. Dark grey=lethal. The trisomies that are significantly bigger than the control are highlighted with a green stroke. **(B)** Magnification of twin clones in the wing primordia. The cytological location of each FRT

insertion is indicated in the same color code used in A. Each image is 50x50 µm. **(C, D)** Plots representing clone area of monosomies and trisomies of the same region (normalized to the one of euploid cells) (**C**) and clone type distribution **(D)**. Average **(D)** and mean and SD **(C)** are shown. 2way ANOVA with Šidák correction for multiple comparisons test was performed in **C**. Clones were induced at 64h AEL with a heat-shock at 38°C of 5-7 minutes for the control and of 1h for the other combinations. ns, not significant (p>0.05); * p ≤ 0.05; ** p ≤ 0.01; *** p≤ 0.001; **** p ≤ 0.0001.

3.6. Cumulative haploinsufficiency enhances super-competition and *Mn*-induced cell competition in Region 1

Furthermore, we noticed that the effects on the size of monosomic clones was stronger when more genes were included in the monosomy, pointing again to a contribution of cumulative haploinsufficiency of neighboring genomic regions on growth. One example is that decrease in clone size and loss of segmental monosomies of region 69-70 including the haploinsufficient genomic region bearing *RpS4* was clearly enhanced when this monosomy was also including the region 70-72 (Figure R18C,D). If we compare the 69-70 and 70-72 monosomies with the 69-72, we see that the size of the monosomy is 0.28, 0.6 and 0.05 respectively and that 15.66%, 5.06% and 30.22% of the clones respectively are twin that lost the monosomic clone. Therefore, by adding to the 69-70 monosomy the 70-72 region, that per se did not present neither decrease in size nor loss of the monosomic clone compared to the control (Figure R18C,D), we are able to enhance 5.6 times the effect on size (from 0.28 to 0.05) and by the double the effect on survival (from 15.66% to 30.22%). A similar example is that decrease in clone size and loss of segmental monosomies observed in the 70-73 region due to super-competition is much higher respect to the 72-73 region alone. The monosomy of the 70-72 region, again, despite not presenting any growth defect, enhances by two times the super-competition of the 72-73 monosomy and reduces clone size from 0.37 to 0.18 and the occurrence of loss of the monosomic twin from 13.1% to 28.2% (Figure R18C,D, compare 70-72 and 72-73 with 70-73). The same happens with the 70-75 monosomy: despite including the region 73-75 which does not present any growth defect, it displays a worse phenotype than the 70-73 monosomy with a clone size of 0.11 and 37.5% of clones that are twin that lost the monosomy (Figure R18C,D, compare 70-73 with 70-75). Furthermore, we can also see how different phenomena of cell competition and cumulative haploinsufficiency have an additive effect in compromising cell fitness of monosomic cells. In fact, the worse effects were observed for the 69-75 monosomy where super-competition of the 72-73 trisomy is added to the *RpS4*-induced cell competition of region 69-70 and cumulative haploinsufficiency of regions 70-72 and 73-75 (Figure R18C,D, compare 69-70 and 70-75 with 69-75). Indeed, this turned to induce cell lethality as almost no clone bearing monosomic cells was recovered, with the average size of the 69-75 monosomy being reduced to only 0.01 and 93,7% of twin clones (39.8% out of a total of 42,48% of twin clones) losing the monosomy.

3.7. Super-competition in Region 1 is Xrp1-independent

The previous results unravel a super-competitive behavior of trisomic over monosomic clones and reinforce the effect of cumulative haploinsufficiency in enhancing these behaviors. The observed super-competitive behavior was largely independent of Xrp1, as the size of the two types of clones was unaffected by Xrp1

depletion (Figure R19 A,B). We can notice how the negative effect on the monosomy and the overgrowth of the trisomy are enhanced in this experiment comparing to previously analyzed clones (0.9 for the trisomy and 0.1 for the monosomy in Figure R19B versus 0.75 and 0.5 in Figure R18C). These experiments were not performed in parallel and even if the protocol of egg laying and clone induction was always maintained unaltered, even slight and unpredictable differences in developmental timing (e.g. due to differences in temperature, humidity, fly food ingredients) will result in a different moment of clones' induction. In this case in the Xrp1 rescue experiment (Figure R19) the clones were clearly induced earlier therefore giving more time to the trisomic clone to overgrow and to the monosomic clone to be outcompeted. We next searched for the responsible gene or genes.

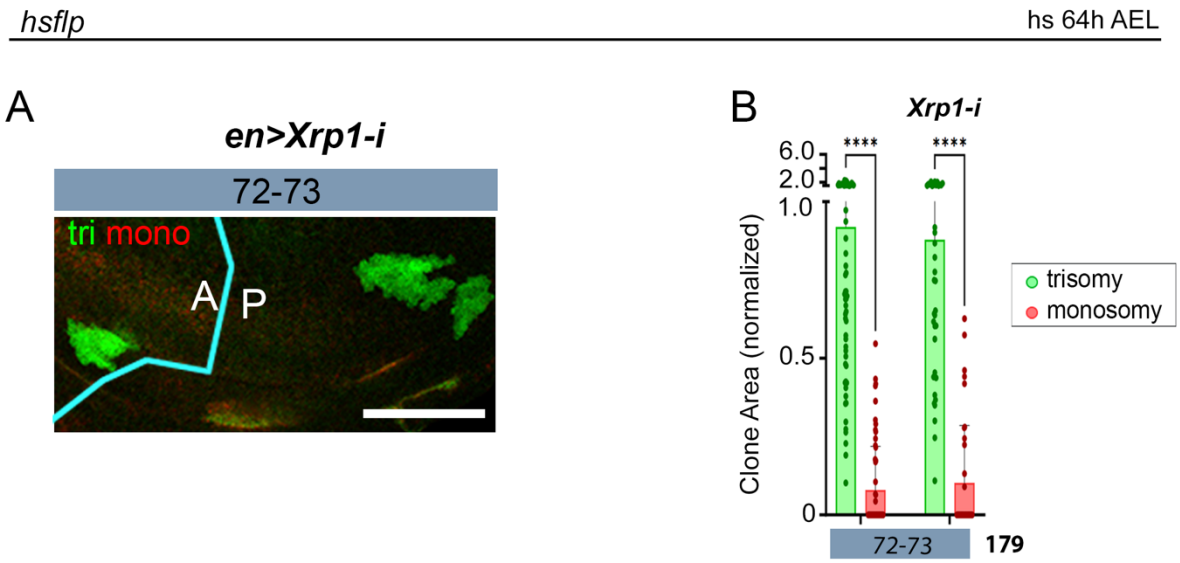

Figure R19. Supercompetition in Region 1 is Xrp1-independent. (A) Magnification of clones in wing primordia in tissues that expressed an RNAi form of Xrp1 in the posterior (P) compartment. Scale bars, 50 µm. **(B)** Plot representing clone area (normalized to the one of euploid cells) of monosomies and trisomies in absence (anterior compartment, A), or presence of *Xrp1-i*. Clones were induced at 64h AEL with a heat-shock at 38°C of 1h. 2way ANOVA with Šidák correction for multiple comparisons test was performed in B. ns, not significant (p>0.05); * $p \leq 0.05$; ** $p \leq 0.01$; *** $p \leq 0.001$; **** $p \leq 0.0001$.

3.8. Super-competition in Region 1 is mediated by *flower* and other genes

When looking at the genes comprised between the positions 72A1-73A5 that could have a role in cell-competition, one that caught our attention was *flower.* The gene *flower* (*fwe*, located in 72A1), encodes for a transmembrane protein conserved in multicellular animals and proposed to be a Ca^{2+} channel in neurons (Yao et al., 2009). Interestingly, *flower* has been reported to be upregulated in winner cells in the context of *dMyc*-induced super-competition (Rhiner et al., 2010). In particular, this study proposes a model in which the fwe^{Lose} and fwe^{ubi} isoforms of the *fwe* gene are differentially expressed in the loser and winner cells respectively, and that cell-to-cell comparison of relative fwe^{Lose} and fwe^{ubi} levels ultimately determines which cell undergoes apoptosis. Since what we observed is that cells bearing three copies of the region including *fwe,* along with other 178 genes, are capable of overgrowing in the epithelium while inducing outcompetition of the cells including only one copy of the same region (Figure R18), we wondered if differences in copies of *fwe* alone could recapitulate this phenotype. To assess this, we generated twin clones of cells bearing either zero or two

copies of *fwe* in the wing disc epithelia of *fwe*+/- animals by employing the Flp/FRT system as represented in Figure R1A. Induction was performed at 70h AEL. When comparing these clones with control clones bearing either zero or two copies of the *Lac-Z* construct, clones bearing two copies of *fwe* were twice the size while the clones bearing zero copies of *fwe* presented cell death markers and were drastically reduced in size (Figure R20 A,B). Therefore, by generating twin clones bearing two and zero copies of *fwe* in a tissue bearing one copy of *fwe* we could recapitulate the phenotype we observed when we generated twin clones bearing three and one copy of Region 1 (including *fwe*) in a tissue bearing two copies of the same region. This suggests that a difference of one dose respect to the surrounding tissue and two doses respect to the loser twin is enough to trigger super competition.

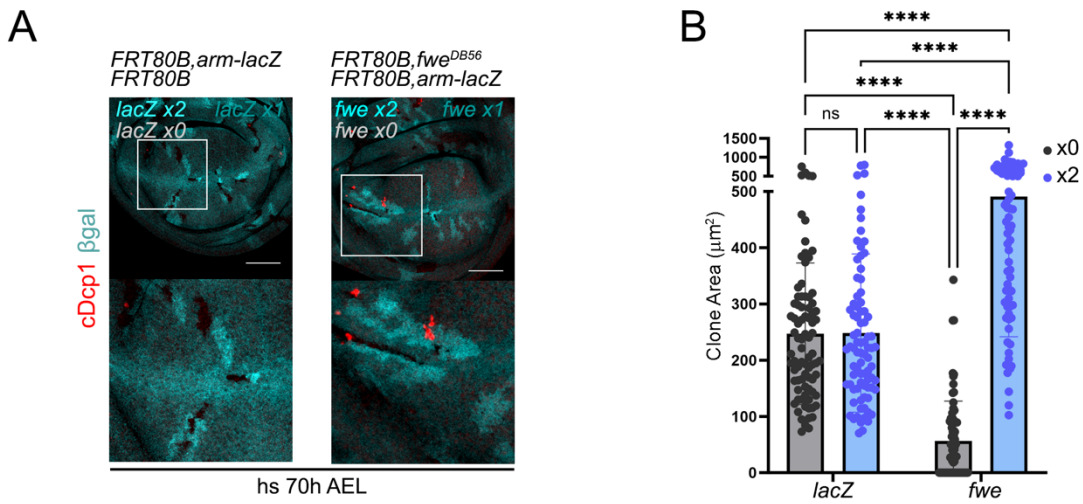

Figure R20. Differences in copies of *fwe* is sufficient to induce super-competition. (A) Magnification of clones in wing primordia where clones of cells bearing one or two copies of either *lacZ* (left) or *fwe* (right) were induced through FRT-mitotic recombination in heterozygous animals. Correspondent genotypes are indicated. βgal staining is in cyan and Dcp1 in red. Scale bars, 50 μm. **(B)** Plot representing clone area of the indicated genotype. Clones were induced at 70h AEL with a heat-shock at 38°C of 45'. 2way ANOVA with Šidák correction for multiple comparisons test was performed in B. ns, not significant (p>0.05); * p ≤ 0.05; ** p ≤ 0.01; *** p≤ 0.001; **** p ≤ 0.0001.

After seeing that we were able to phenocopy the observed effect of super-competition of Region 1 by confronting cells with two and zero copies of the *fwe* gene (Figure R20 A,B), we tried to rescue super-competition of Region 1 by overexpressing *fwe.* For this purpose, we used the eye primordia and induction through the *eye-Gal4,UAS-Flp* construct (*eye>flp).* We speculate that the huge amplification of gene expression achieved through the Gal4-UAS system will equal the one copy difference in *fwe* levels between the twin clones. The outcompetition of the monosomic clone for Region 1 was not rescued by *fwe* overexpression, neither with the ubi isoform used by Rhiner and colleagues (Rhiner et al., 2010) nor with the A isoform (Yao et al., 2009) (Figure R21). These results suggest that the super-competitive behavior of Region 1 relies on the cumulative effect of two or more genes located in this region. The fact that *fwe* overexpression does not rescue the presence of the monosomic clone, but that juxtaposed cells with different *fwe* copies recapitulate Region 1 supercompetition, suggest that it is still possible that increased *fwe* levels are responsible for the overgrowth of the trisomic clone of Region 1. However, more genes must contribute to the elimination of the monosomic clone of Region 1. Consistent with this proposal, we identified two other genes in this region previously reported to be involved in processes of cell competition, namely Death-associated inhibitor of

apoptosis 1 (Diap1, located in 72D1), and the secreted Wnt inhibitor Notum (located in 72C3, (Vincent et al., 2011)). Whether these two genes or any other located in this region contribute to the supercompetitive behavior of Region 1 remains to be elucidated. Furthermore, it must be taken into account that overexpression of *fwe* through the Gal4-UAS system is not the best technical set up to perform the rescue experiment and that such a huge overexpression of *fwe* could interfere with the expected results by for example exacerbating supercompetition. However, providing just the monosomic clone of Region 1 with an extra copy of *fwe* isn't technically feasible.

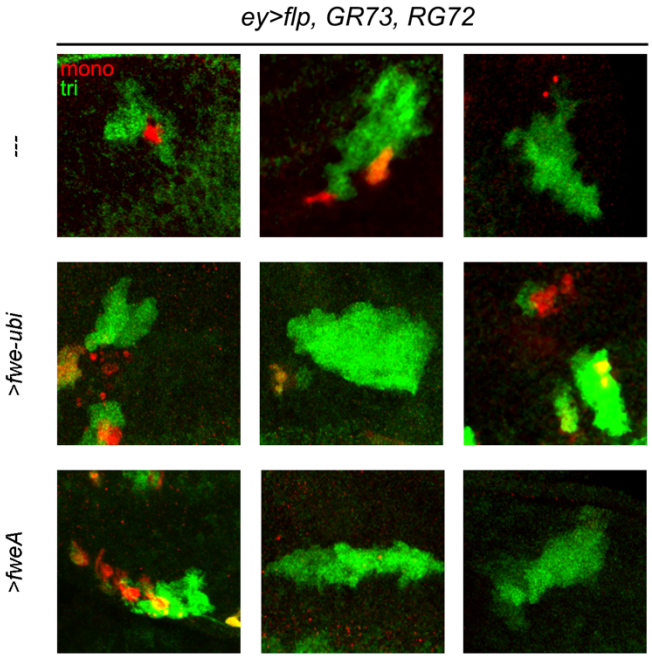

Figure R21. Increasing levels of *fwe* does not rescue super-competition of Region 1. Magnification of clones in eye primordia where clones are induced chronically through the construct *eye>flp*. Correspondent genotypes are indicated. Scale bars, 50 µm. Each image is 50x50 µm.

3.9. A case of growth compensation in Region 2

When analyzing clones carrying segmental aneuploidies in the Region 2 (75F7-80), we realized, to our surprise, that clones of monosomic cells did not show any growth defect or sign of out-competition (Figure R22B,C,D). This appears in disagreement with what observed in the same region with segmental monosomies induced with RS-FRTs *in cis* (77E4-79A4, 75F7-77C1, Figure R8) in wild type eye epithelia, where the monosomies including the region 75F7-79A4 already presented a growth defect respect to the control, indicating presence of two or more haploinsufficient genes. The fact that the monosomies in the same region generated through the TSG technique does not present the same growth defect indicates that somehow the presence of the complementary trisomy rescues the growth defect of the monosomy. Similar observations were found in the eye primordium as well (Figure R22G), ruling out any tissue-dependent effects.

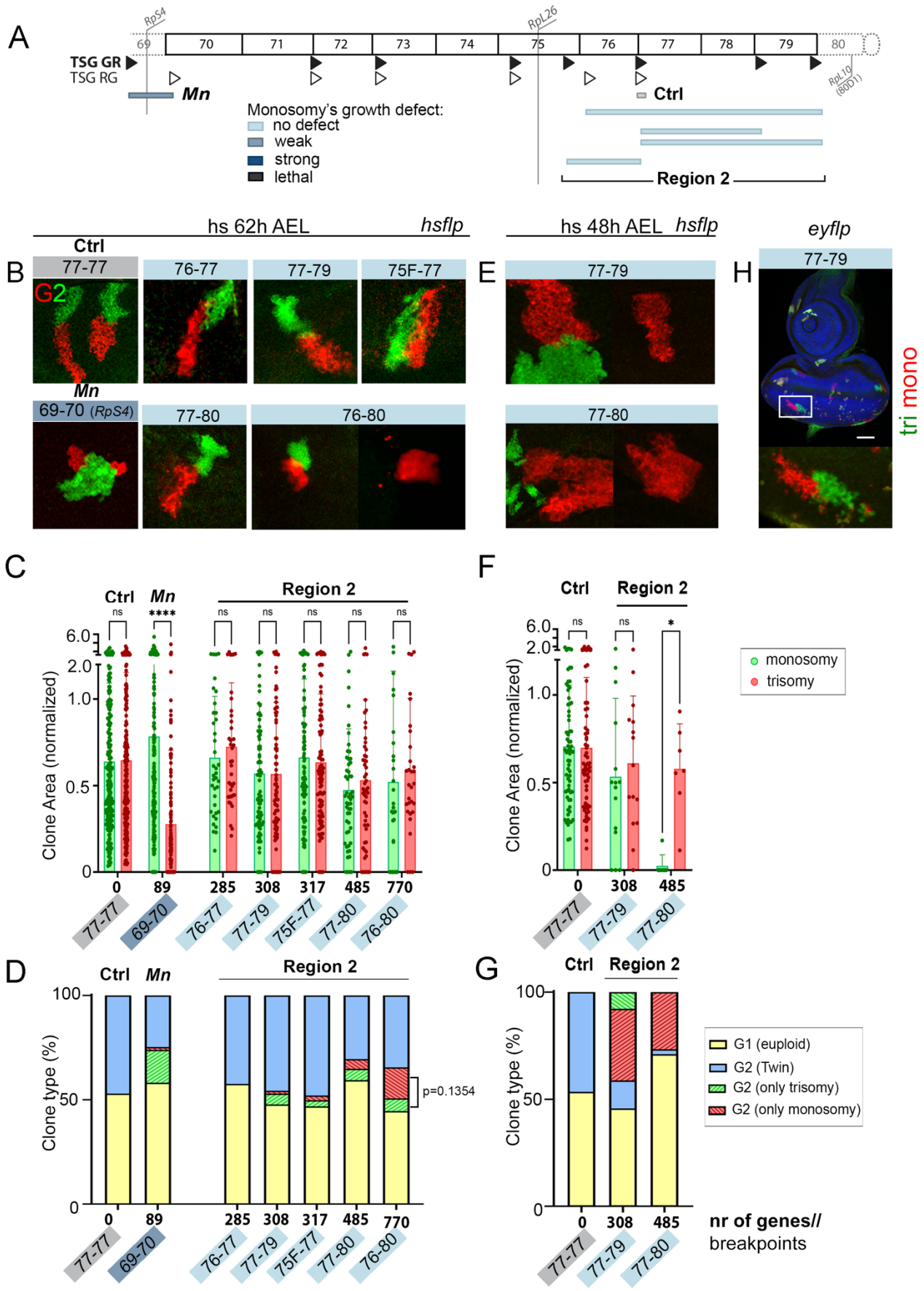

Figure R22. Growth of the monosomies in Region 2 is rescued by the presence of their complementary trisomies. (**A**) Map of the trisomies and monosomies analyzed color coded according to the growth defect of the monosomy

compared to the control. Light blue=no difference with control. Blue=weak growth defect. Dark blue=strong growth defect. Dark grey=lethal. Magnification of twin clones in the wing (**B, E**) and eye (**H**) primordia. The cytological locations of the FRTs is indicated in the same color code used in **A**. Each image is 50x50 µm. Clones were induced at 64h AEL (**B, C, D**) or at 48h AEL (**E, F, G**) with a heat-shock at 38°C of 5-10 minutes for the control and of 1h for the other combinations. (**C, F**) Plots representing clone area of monosomies and trisomies of the same region (normalized to the one of euploid cells) induced at 64h AEL (**C**) and 48h AEL (**F**). Mean and SD are shown. 2way ANOVA with Šidák correction for multiple comparisons test was performed. ns, not significant ($p>0.05$); * $p \leq 0.05$; ** $p \leq 0.01$; *** $p \leq 0.001$; **** $p \leq 0.0001$. (**D, G**) Plots representing clone type distribution of clones induced at 64h AEL (**D**) and 48h AEL (**G**). Averages are shown. (**G**) Eye primordia where clones are induced chronically through the *eyflp* construct. Scale bar 50µm.

We noticed that differently to what observed for Region 1, twin clones of regions 77-79, 75F-77 and 77-80 lose in similar grades both the trisomy and the monosomy (5.18% and 1.41%, 2.94% and 2.25%, 5.43% and 4.66% respectively). Interestingly, 14.77% of the clones of region 76-80 are twin that lost the trisomic clone while only 6.14% lost the monosomy (Figure R22D). Although the difference is not statistically significant ($p=0.1354$) the percentage of twin clones that lost the trisomy it is much higher than what observed for other combinations and may indicate that trisomic clones are being lost from the epithelium.

We have already observed how appropriate timing of the induction is crucial in order to uncover differences in cell fitness. For this reason and in order to investigate if trisomic clones were in fact being lost, we induced clones in Region 2 at earlier developmental stages through a heat shock at 48h AEL. We noticed that trisomic clones tended to be lost from the epithelium (Figure R22D,E,F). This is especially clear when looking at clone size of trisomic clones of region 77-80 (0.02 when induced at 48h versus 0.52 when induced at 64h AEL) and is reflected also by the percentage of twin clones that lose the trisomic clone, 33.33% and 27.14% for 77-79 and 77-80 trisomies respectively. Why the loss of the trisomic twin for the 77-79 region is not reflected in a decreased clone size it is not clear. It could be that the 77-79 trisomy is less deleterious than the 77-80 trisomy and that the trisomies that were able to survive for 72h (the ones whose size is quantified) could cope with whatever stress and decrease in fitness was caused by the trisomy. These results point to a potential non-autonomous role of trisomic clones in supporting growth of nearby monosomic cells. Whether this non-autonomous role of trisomic clones towards monosomic cells relies on stress-induced compensatory proliferation remains to be elucidated.

Similar results were obtained when analyzing the behavior of clones carrying segmental monosomies and trisomies in the genomic region 87-92 in the chromosome 3R, which comprises 1426 genes (Figure R23). Growth of clones of cells bearing segmental monosomies included within 87-89 and 89-92 was compromised (Figure R23C), which did not reflect on the % of twin clones losing the monosomic clones. This may be due to a slower elimination of the monosomic clone compared to what has been observed for Region 1 (Figure R18) so that at the time of the observation, 56h after clone induction, the majority of the monosomic clones are smaller but have not yet been eliminated. For the 87-89 region, the difference between the monosomy and the trisomy is not significant but there is a clear tendency (Figure R23C), which goes in accordance with the observation of pyknotic nuclei in the monosomic clone (Figure R23B) and with the gene eIF2γ in 88E6 being reported as haploinsufficient in a previous report (Ji et al., 2021).

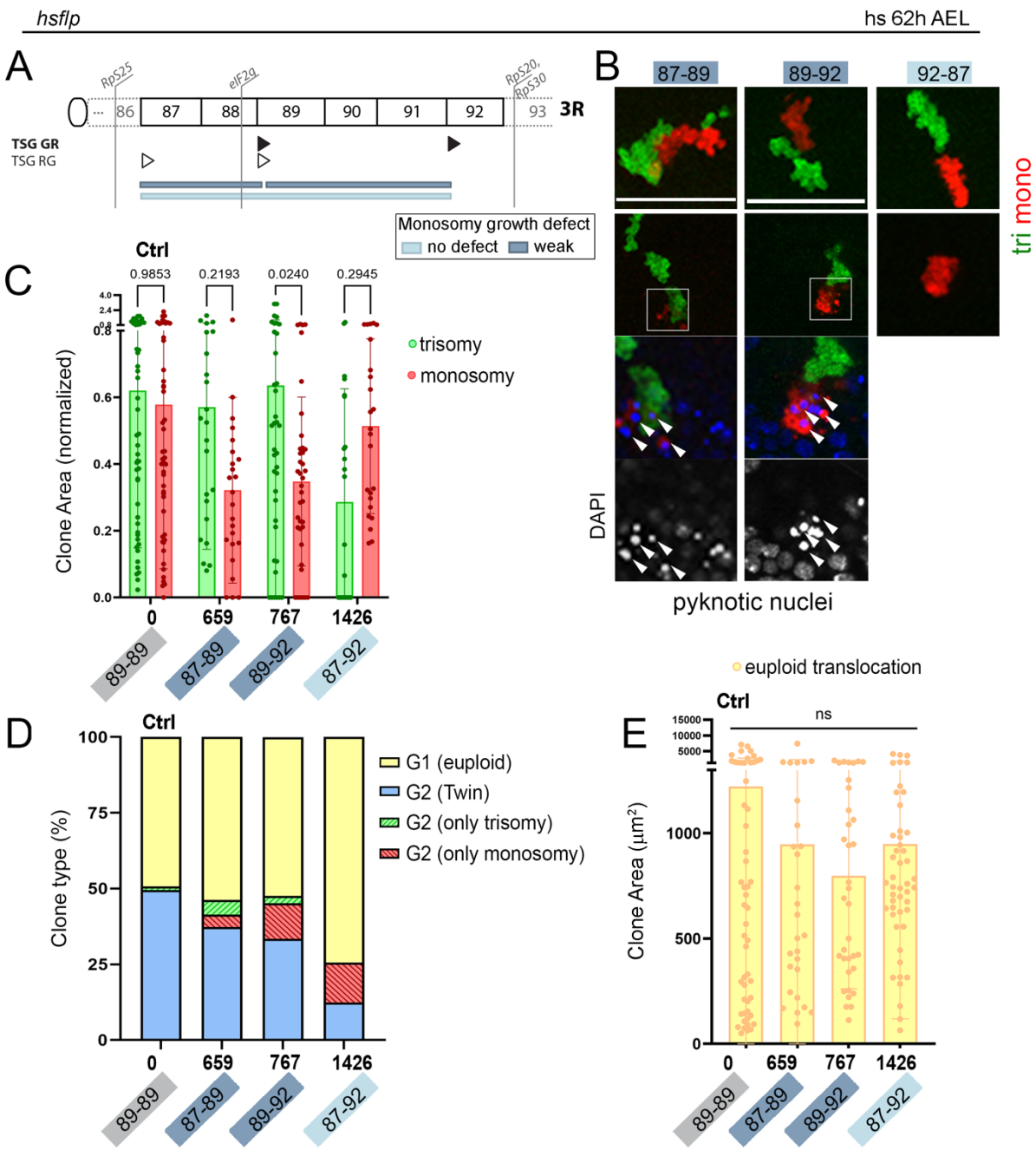

Figure R23. Triplosensitivity of a region in the 3R recues the growth of the monosomy of the same region. (**A**) Map of the trisomies and monosomies analyzed color coded according to the growth defect of the monosomy compared to the control. Light blue=no difference with control. Blue=weak growth defect. (**B**) Magnification of twin clones in the wing primordia. The cytological location of each FRT is indicated in the same color code used in **A**. Each image is 50x50 µm. Clones were induced at 64h AEL with a heat-shock at 38°C of 5-7 minutes for the control and of 1h for the other combinations. Plots representing clone area of monosomies and trisomies of the same region (**C**) normalized to the one of euploid cells (**E**) and clone type distribution (**D**) of clones induced at 64h AEL. Mean (**D**) and SD (**C,D**) are shown. 2way ANOVA with Šidák correction for multiple comparisons test was performed in **C** and **E**. ns, not significant (p>0.05); * $p \leq 0.05$; ** $p \leq 0.01$; *** $p \leq 0.001$; **** $p \leq 0.0001$.

Surprisingly, clones of cells bearing segmental monosomies of the whole region not only did not show a worse growth defect as could be expected due to cumulative haploinsufficiency, but did not show a growth defect at all. This was accompanied by a reduction in the size of trisomic clones (Figure R23C) as well as an increase of the percentage of twin clones that lost the trisomic clone (Figure R23D). This again points to a potential

non-autonomous role of trisomies in compensating growth defects of the monosomies (see more in Discussion).

3.10. *Rpl26* is a *Mn*-like gene that when present in three copies causes lethal cell competition of clones bearing one copy of *Rpl26*

Finally, we verified the negative impact of the haploinsufficient region including the *RpL26* gene on growth and survival.

When monosomies including the *Rpl26* gene were induced by RS-FRTs in a wild type context in the adult eye, they presented a strong growth defect (Figure R10). However, in this case, the presence of the trisomic clones turned this haploinsufficiency to cell lethality as almost no monosomic clone could be recovered when clones were induced at 64h AEL as can be seen both by the Area (Figure R24B,C) and the % of twin clones that lost the monosomy (Figure R24D). The percentage of clones in G1 ranges from a minimum of 48.2% for 75A-75F to 69.3% for 75A-79 and 68.6% for 70-79. These considerable deviations from the expected 50% can be attributed to the loss of both twin clones from the tissue. Overall, these results unravel a role of trisomic cells in enhancing the loser state into lethality. Interestingly, trisomic clones did not show any difference in size compared to controls (Figure R24C), even when they included the 72-73 region, responsible for a phenomenon of supercompetition (Figure R17B, 18B,C). For instance, we notice that the trisomies 72-77, 72-79, 70-77, 72-80, 70-79 do not overgrow compared to controls as did the trisomies 72-73, 72-75, 70-75, 69-75 (Figure R17B, see more in the Discussion).

This process of lethal competition was largely dependent of Xrp1, as Xrp1 depletion in the posterior (P) compartment of the wing disc through the *enGal4-UAS-Xrp1-i* construct rescued the size of monosomic clones (Figure R25 A,A') when clones were induced acutely with the *hsflp* construct and a heat-shock at 64h AEL. In order to see if Xrp1 depletion rescued bigger monosomies including *RpL26*, we used the chronic induction through the *en>flp* construct (Figure R13) and FRT pair 70-77. By inducing clones chronically, we cannot carefully analyze size since clones are induced at different developmental timings in the same tissue. However, this is not so relevant in this case for different reasons. First, since the monosomic clones of this region are eliminated from the tissue (Figure R24), it will be easy to qualitatively see an effect of Xrp1 depletion since we expect to rescue the presence of the clones, rather than to detect a difference in Area. Furthermore, this approach allowed us to increase system efficiency, enabling the observation of differences that would have been difficult to detect with acute induction, given the low frequency of clones when the FRTs are widely spaced and that we would have needed a considerable number of twin clones located posteriorly.

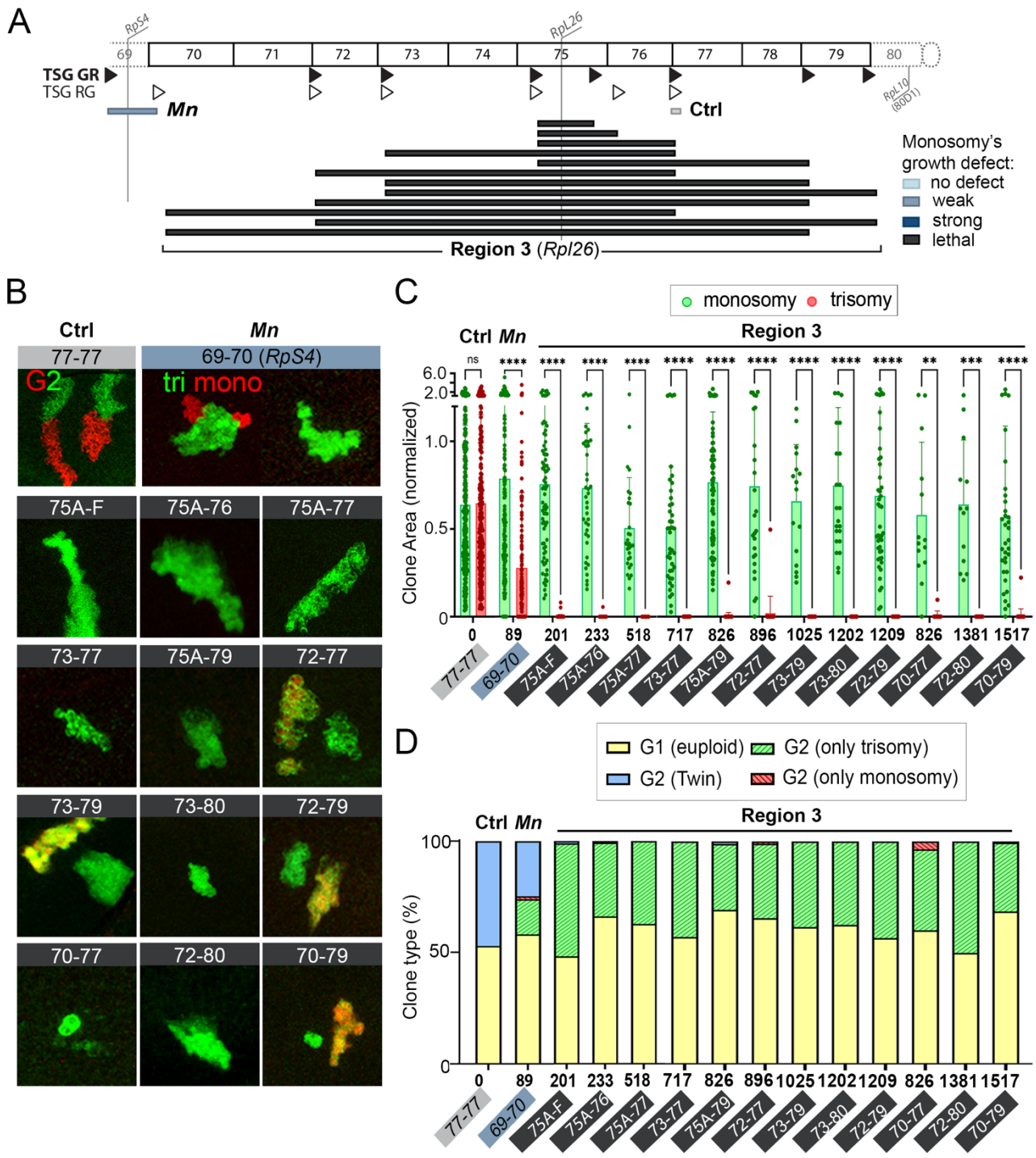

Figure R24. Monosomies including the region 75A-75F suffer lethal cell competition in presence of their complementary trisomy. (**A**) Map of the trisomies and monosomies analyzed color coded according to the growth defect of the monosomy compared to the control. Light blue=no difference with control. Blue=weak growth defect. Dark blue=strong growth defect. Dark grey=lethal. (**B**) Magnification of twin clones in the wing primordia. The cytological location of each FRT insertion is indicated in the same color code used in **A**. Each image is 50x50 µm. (**C, D**) Plots representing clone area of monosomies and trisomies of the same region (normalized to the one of euploid cells) (**C**) and clone type distribution (**D**). Average (**D**) and mean and SD (**C**) are shown. 2way ANOVA with Šidák correction for multiple comparisons test was performed in **C**. Clones were induced at 64h AEL with a heat-shock at 38°C of 5-7 minutes for the control and of 1h for the other combinations. ns, not significant (p>0.05); * $p \leq 0.05$; ** $p \leq 0.01$; *** $p \leq 0.001$; **** $p \leq 0.0001$.

We observe that with the *en>flp* induction system we are able to reproduce the loss of the monosomic clone for both the 75A-77 and the 70-77 combination, which is also rescued when Xrp1 is depleted (Figure R25B). The presence of the twin clones with both the monosomic and trisomic clones is rescued in the epithelium. Interestingly, when we tried to rescue the loss of the monosomic twin through overexpressing a miRNA against the proapoptotic genes *reaper, hid* and *grim* (*miRHG*) we did not obtain such a strong rescue. In fact, even if the presence of the monosomic twin is indeed recovered, the trisomic twin still seems to grow better and, in some cases, the monosomic cells are not attached to the main epithelium and have delaminated basally (Figure R25B). Certainly, the strongest mean to avoid this process of lethal cell competition is Xrp1 depletion (more in the Discussion).

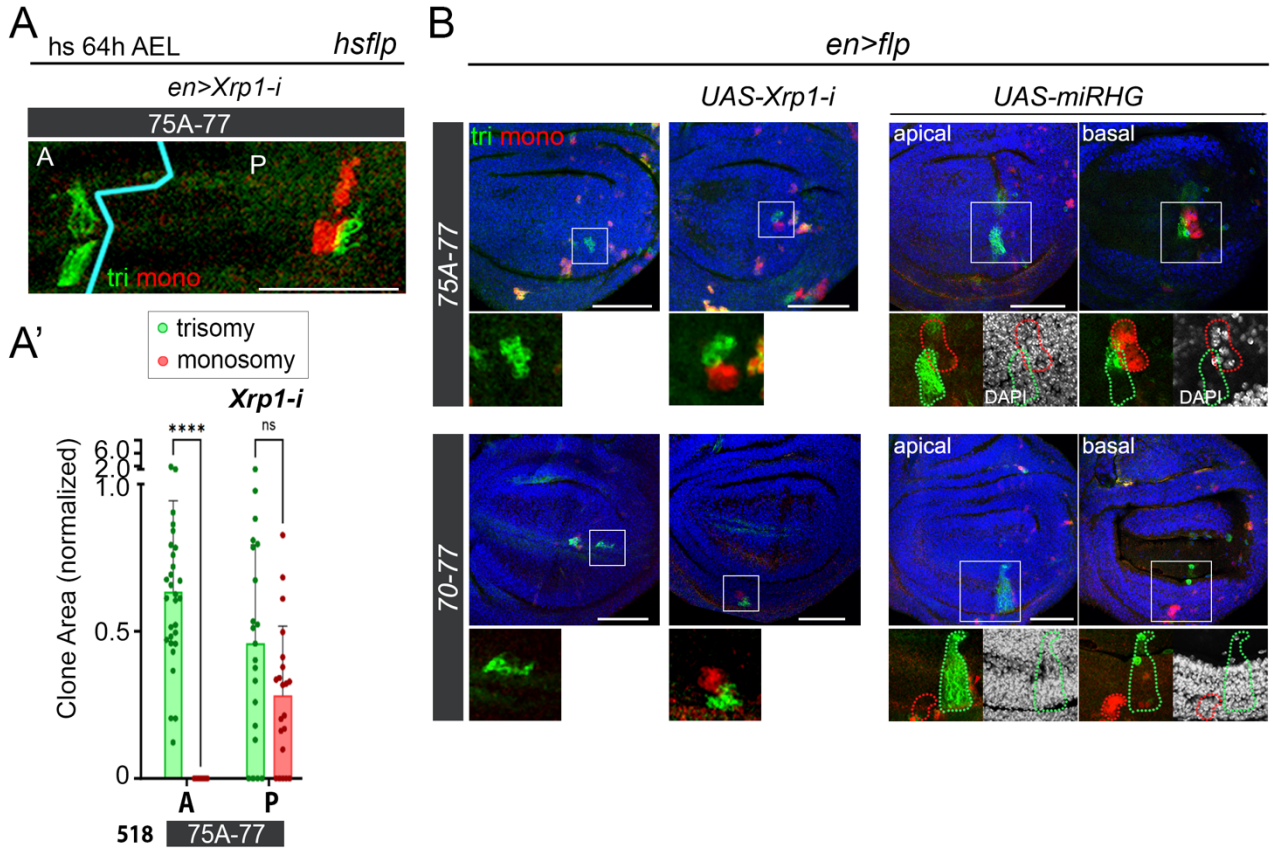

Figure R25. Lethal cell competition relies on Xrp1 induced cell death. (**A**) Magnification of clones in wing primordia in tissues that expressed an RNAi form of Xrp1 in the posterior (P) compartment. (**A'**) Plot representing clone area (normalized to the one of euploid cells) of monosomies and trisomies in absence (anterior compartment, A), or presence (posterior compartment, P) of *Xrp1-i*. Clones were induced at 64h AEL with a heat-shock at 38°C of 1h. (**B**) Wing primordia where clones were induced chronically through the *en>flp* construct in combination with an RNAi form of Xrp1 and a miRNA against proapoptotic genes. (**A,B**) Scale bars, 50 µm.

Finally, we wanted to prove that *Rpl26* is the gene responsible for haploinsufficiency and haplolethality of the region 75A-77. With this aim, we overexpressed the Rpl26 protein in the eye disc while chronically inducing clones in the same tissue through the *eye>flp* construct (Figure R26). We can observe how the monosomic clones, which are otherwise lost (Figure R26A), are recovered through overexpression of *Rpl26* (Figure R26B). This describes *Rpl26* for the first time as a haploinsufficient *Mn*-like gene which, when present in three copies alongside cells that present one copy, causes *Xrp1*-dependent lethal cell competition.

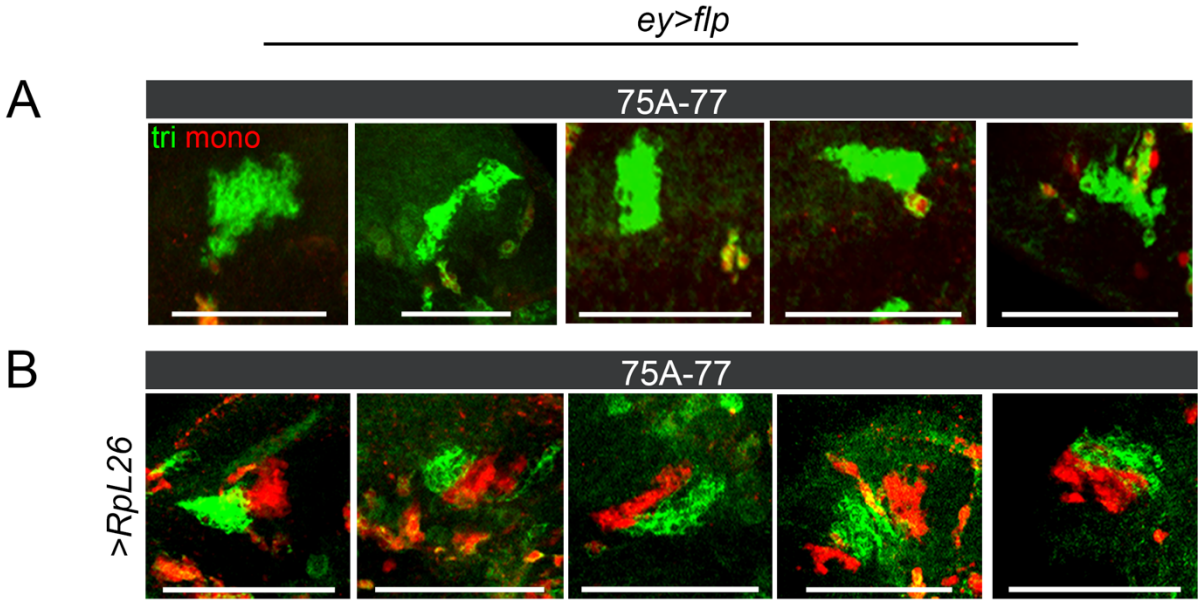

Figure R26. Rpl26 is responsible for haploinsufficiency of the region 75A-77. Magnification of clones in eye primordia in tissues that overexpressed the FLP under the control of the *eye-Gal4* construct (**A**) and the Rpl26 protein (**B**). Scale bars, 50 µm.

Discussion

In this work, we developed an innovative system leveraging the Flp-FRT sequence-specific recombination method to generate molecularly defined segmental aneuploidies in epithelial tissues of *Drosophila*. This system allows precise manipulation of chromosomal content, enabling us to model aneuploidy with high specificity. We assessed the efficiency of this approach and implemented two distinct methods for labeling aneuploid cells. In the first approach, segmental monosomies were marked with red pigment in the white wild type adult eye epithelium. In the second, complementary segmental monosomies and trisomies were simultaneously induced and labeled with red and green fluorescence, respectively, allowing visualization in the larval wing or eye primordium through confocal microscopy. Using these methods, we examined cellular behaviors, including clonal growth dynamics and cell death, resulting from segmental aneuploidies.

Our study focused on a collection of 21 segmental monosomies and 25 complementary pairs of segmental monosomies and trisomies within a wild-type tissue. We identified several mechanisms of haploinsufficiency and triplosensitivity in a genomic region devoid of previously described dosage-sensitive loci. Specifically, we characterized two distinct mechanisms driving the elimination of segmental monosomies: *Xrp1-mTor*-dependent *Mn*-induced cell competition and *Xrp1-mTor*-independent cumulative haploinsufficiency-induced cell competition. Additionally, we discovered that trisomies juxtaposed to their complementary monosomies can either exacerbate or mitigate their growth defects. Notably, we observed a phenomenon of supercompetition mediated by *fwe* and other unidentified genes, where cells with additional *fwe* copies overgrow while inducing the elimination of cells with fewer *fwe* copies. Moreover, we found that trisomic cells for a triplosensitive region can rescue the growth capacity of their complementary monosomic clones that would otherwise exhibit growth defects. Overall, our findings reveal that the genome contains numerous dosage-sensitive loci that interact through complex mechanisms and multiple molecular pathways to determine the fate of aneuploid cells.

This section will first examine the different types of cellular behaviors identified in aneuploid cells, that vary depending on the specific chromosome regions involved in the imbalances, and the type of cells interacting with each other, as well as open questions about molecular players underlying the observed behaviors. Then, we will discuss the strengths and weaknesses of our strategies for modeling aneuploidy, highlighting their potential to faithfully recapitulate key aspects of aneuploidy *in vivo* while acknowledging inherent limitations, and exploring possible improvements. Finally, we will address implications for future research.

1. The genome is full of cumulative dosage-sensitive genes

The data presented in this work reveals that the fly genome is populated of dosage sensitive regions either caused by single genes or a combination of genes that significantly influence the behavior of monosomies and trisomies.

1.1. Cumulative haploinsufficiency

Drosophila has perhaps the most comprehensive inventory of haploinsufficient genes affecting organismal and cellular growth and survival of any multicellular organism, thanks to the creation over the last fifty years of a large collection of fly strains with chromosomal deletions covering extensive genomic regions and breakpoint subdivisions (Cook et al., 2012; Lindsley et al., 1972; Marygold et al., 2007). Up to 66 loci in the fly genome, mostly genes encoding for ribosomal proteins (RPs) or translation initiation factors, have been reported to compromise organismal growth and survival when heterozygously deleted. Despite focusing on a region devoid of these genes, we have uncovered two haploinsufficient regions (Regions 1 and 2 in Figure R8) and one *Mn*-like haploinsufficient gene (*Rpl26* in Figure R10 and R24), suggesting that most if not all regions of the genome are dosage-sensitive. Whenever single loci did not impair growth, multiple loci depleted together showed to be haploinsufficient by cumulative haploinsufficiency, where the observed phenotype is not due to a single gene. We did not identify any haploinsufficient tumor suppressor genes, as none of the deletions led to overgrowth phenotypes (Figure R8 and R10). However, similar to observations with *scribble* mutants (Bilder et al., 2000), it is possible that haploinsufficient tumor suppressor genes may require mutations across the entire tissue to manifest overgrowth. In such cases, cells with these mutations could be outcompeted by wild-type cells as part of a tissue homeostasis maintenance mechanism.

Consistently with these data and the proposal that many regions across the genome are dosage-sensitive, many genes were reported to be haploinsufficient in different organisms. About 60% of 1,112 essential genes in yeast have been reported to be haploinsufficient under optimal growth conditions and an additional 16% showed a phenotype under sever growth conditions (Ohnuki & Ohya, 2018). An analysis on 90 mutant mice lines revealed that 42% of them presented haploinsufficient phenotypes (White et al., 2013). In humans, a study identified 300 haploinsufficient genes using a systematic search of PubMed and OMIM databases (Dang et al., 2008). These genes predominantly encode transcription factors and are involved in critical processes such as development, the cell cycle, and nucleic acid metabolism, reinforcing the idea that haploinsufficiency is widely spread across essential genes. A study that compared haplosufficient with haploinsufficient genes assessed that haploinsufficient genes exhibit higher levels of expression during early development and greater tissue specificity, as well as more interaction partners and greater network proximity to other known haploinsufficient genes (N. Huang et al., 2010). An analysis on epigenomic patterns at the level of haploinsufficient genes showed significantly broader H3K4me3 peaks at promoters, which are associated with reduced transcriptional noise and precise dosage control, broader peaks of the repressive marker H3K27me3 and enrichment of active marks like H3K9ac and H2A.Z, indicating a complex interplay between activation and repression. These genes also show an increased number of enhancer-promoter interactions, highlighting their regulatory complexity

and the need for spatiotemporal fine-tuning of expression (Han et al., 2018). Prediction models of haploinsufficiency estimate a much higher number of haploinsufficient genes than the ones described (N. Huang et al., 2010; Steinberg et al., 2015), up until 2,987 haploinsufficient genes predicted in a recent analysis (Collins et al., 2022). Accordingly, a recent study in embryonic stem cells identified over 650 essential haploinsufficiency genes in human embryonic stem cells (Sarel-Gallily et al., 2022). These genes are enriched in dosage-sensitive pathways, including WNT and TGF-β signaling, and are often associated with extracellular matrix and membrane components.

The widespread occurrence of haploinsufficiency across the genome aligns with the observation that RP genes are relatively few per chromosome in humans (Uechi et al., 2001). In *Drosophila*, it has been suggested that *Mn* genes, which are so prevalent that most segmental aneuploidies would deplete at least one, serve as guardians of ploidy status (Kiparaki et al., 2022). However, this mechanism would not be feasible in humans, at least for segmental monosomies. Consequently, it is logical that many other haploinsufficient genes may fulfill this role.

All these screens for haploinsufficient genes depend on selecting the appropriate complexity of phenotypic outputs, and because they often focus on mutations in single genes, they tend to underestimate the effects of cumulative haploinsufficiency. The *wupA* locus in *Drosophila* provides a compelling example of cumulative haploinsufficiency, where the additive effects of multiple Troponin I isoforms encoded by the gene are critical for organismal viability. This locus exhibits haplolethality, but overexpression of individual isoforms cannot rescue the haplolethal phenotype, highlighting the necessity of quantitative balance among all transcripts (Casas-Tintó & Ferrús, 2021).

In this work, we have provided multiple evidence that cumulative haploinsufficiency acts as a key element in the growth defects and elimination of monosomic cells. For instance, the segmental monosomies induced by the RS-FRTs in the adult eye covering Region 1 and Region 2 presented growth defects due to cumulative haploinsufficiency (Figure R8). Interestingly, despite presenting signs of outcompetition, they were not caused by the Xrp1-mTor axis that was instead responsible for *Mn*-induced cell competition (Figure R9). Supporting the idea that cumulative haploinsufficiency contributes to Xrp1-mTor-independent growth defects and outcompetition, larger monosomies including Rpl26 were less effectively rescued by Xrp1 depletion compared to smaller monosomies including Rpl26 (Figure R11B). This indicates that additional haploinsufficient genes contribute to the growth defects observed in larger monosomies independently of Xrp1. Interestingly, cumulative haploinsufficiency can act in an additive way to worsen the growth defect provoked by other mechanisms such as *Mn*-dependent cell competition and supercompetition (Figure R18). An elegant way to further show this by making use of the TSG technique would be to show until what point Xrp1-i would rescue growth of the 70-77 monosomy, that is compromised by Xrp1-dependent *Rpl26*-induced lethality, cumulative haploinsufficiency and supercompetition of the 72-73 region.

As highlighted in the introduction, cancer genomes often harbor deletions of regions enriched with multiple tumor suppressor genes, strongly suggesting that cumulative haploinsufficiency plays a critical role in cancer development (Solimini et al., 2012).

1.2. Cumulative triplosensitivity

The data presented in this study points to the existence of triplosensitive loci in the fly genome. In Region 2 of the chromosome 3L (Figure R22) trisomies are more frequently lost than monosomies. Surprisingly, this does not consistently correlate with a growth defect (compare Figure R22C,F with D,F), suggesting that this triplosensitive region induces elimination of trisomic cells from the tissue but if cells can survive, they do not present any growth defect. This differs significantly from what observed for haploinsufficient loci that show growth defects. It is to note that the frequency at which the trisomies disappear increases when they include bigger regions (76-80 and 77-80 in Figure R22), suggesting a cumulative effect rather than a single gene responsible for the triplosensitivity. In Region 3R, a phenomenon resembling cumulative triplosensitivity was also observed. Clones of cells with segmental monosomies restricted to subregions (87-89 and 89-92) displayed compromised growth, whereas clones of cells with segmental monosomies spanning the entire region showed normal growth. This normalization of growth was accompanied by a reduction in the size of trisomic clones. A previous study provided consistent findings, where monosomies spanning the region 87B8-93A2 showed normal growth, while those restricted to 87B8-89E5 exhibited impaired growth (Ji et al., 2021). Together, these observations suggest that two or more genes, which are haploinsufficient when deleted individually within the 87-89 and 89-92 regions, collectively rescue growth defects when deleted together. This, together with the growth defect observed in the 89-92 trisomy, suggests that this region contains a group of genes that act as growth suppressors. These genes impair cellular growth when present in three copies and mitigate the growth defects of individually haploinsufficient loci when deleted together. What genes these might be remains as an open question. These findings collectively underscore the complex interplay between haploinsufficient and triplosensitive genes in regulating growth.

In humans, only 15 triplosensitive loci have been described (Riggs et al., 2018). In *Drosophila* there is only one region that is reported to be triplosensitive, the triplo-lethal region (Tpl) located in chromosomal region 83D-E. Tpl is a unique locus that is lethal when present in either one or three copies (Denell, 1976). The locus is resistant to point mutations indicating that Tpl may operate differently from typical protein-coding genes, and its associated lethality cannot be attributed to a single structural gene but is likely linked to a broader regulatory function or structure (Keppy & Denell, 1979; Dorer et al., 1995). Cytogenetic evidence shows that the dose-sensitive behavior of the Tpl locus is independent of its genomic position, emphasizing the intrinsic importance of the locus itself. A later study identified within the Tpl locus a cluster of 20 genes known as the Osiris gene family, which is highly conserved across insect species but absent in non-insect species (Dorer et al., 2003). These genes exhibit unique dosage sensitivity, consistent with the triplo- and haplo-lethal characteristics of the Tpl locus. Osiris proteins are membrane-associated, containing signal peptides, transmembrane domains, conserved cysteine motifs, and intracellular tyrosine motifs, suggesting roles in redox sensing, signaling, or membrane protein interactions (Dorer et al., 2003). Lethality of the Tpl locus up to date was only rescued by mutation in a closely linked locus named Suppressor of Triplo-lethal (Su(Tpl)) within the cytological region 76B-76D (Dorer et al., 1995). Su(Tpl) mutations are recessive lethal and, in heterozygosis, they suppress the lethal effects of Tpl triplication but not of Tpl deletion (Dorer et al., 1995). Su(Tpl) was

identified as encoding the RNA polymerase II elongation factor dELL (76D3-D4), which enhances transcription elongation by RNA polymerase II by suppressing its transient pausing. It is particularly important for large gene transcription and, in triplolethal contexts, Su(Tpl) mutations suppress lethality, suggesting that reduced transcriptional elongation limits gene expression from the three copies of Tpl, bringing it closer to normal levels (Eissenberg et al., 2002).

Interestingly, Su(Tpl) is located within the Region 2 of chromosome 3R, that we have shown to be haploinsufficient when deleted in heterozygosis with RS FRTs (75F7-77C1 monosomy in Figure R8) and triplosensitive when trisomies are induced together with their complementary monosomies by the TSG (Figure R22). The non-autonomous effects on the monosomy will be discussed in the next chapter. Su(Tpl) was reported to be homozygous lethal but not haploinsufficient, at least at the organismal level (Dorer et al., 1995). Whether the phenotypes we observed for Region 2 are related to an undescribed role or a complex interaction between Su(Tpl) haploinsufficiency in a clonal context and triplosensitivity is an interesting scenario that remains to be assessed. Furthermore, whether the genes responsible for haploinsufficiency and triplosensitivity of Region 2 are the same, remains an open question. We do not have any experimental indication that this is the case, but a recent analysis on haploinsufficient and triplosensitive loci related to genomic disorders in humans present this at least as a compelling possibility (Collins et al., 2022). This study developed a prediction model where probability of haploinsufficiency and triplosensitivity were moderately correlated per gene (Pearson $R^2 = 0.30$; $p<10^{-100}$), and that bidirectionally dosage-sensitive genes were defined by their evolutionary conservation (Collins et al., 2022). Additionally, they identified distinct characteristics differentiating primarily haploinsufficient genes from primarily triplosensitive ones. Haploinsufficient genes were typically larger, located further from neighboring genes, and associated with a higher number of cis-regulatory enhancers, features indicative of precise regulation and developmental importance (Ovcharenko et al., 2005). This observation aligns with findings that most essential genes in mice and yeast exhibit haploinsufficiency. In contrast, triplosensitive genes were generally shorter, G/C-rich, and situated in gene-dense, highly active regions, consistent with the role of stoichiometric imbalances in driving trisomy-related defects.

Contrary to what has been reported in the literature for whole-chromosome trisomies (Williams et al., 2008; Torres et al., 2007; Stingele et al., 2012), none of the segmental trisomies on 3L analyzed in this study showed significant growth defects compared to controls, nor was there any tendency for larger trisomies to exhibit reduced growth potential (Figure R17). This may be attributed to gene-specific effects, suggesting that the 1,517 genes within this particular 3L subregion may not be sensitive to stoichiometric variations. To observe growth defects driven by proteostasis alterations, it may be necessary to generate whole-chromosome or more complex trisomies (Joy et al., 2021). The observation that these cells exhibit normal growth capacity does not necessarily indicate the absence of stress but rather suggests that they are capable of managing it effectively. While we have not directly assessed proteostasis in these trisomic cells, it is reasonable to assume that if their growth capacity is unaffected, these pathways are functioning correctly. However, it might be interesting to see if these trisomic cells respond worse than wild type cells to increasing the proteotoxic stress. This could

be done for instance by overexpression of the Htt25Q, a fusion protein consisting of human Huntingtin and a fluorescent protein that does not form aggregates on its own in wild type cells but, in presence of preformed protein aggregates in the cell, is polymerized in foci (Ramdzan et al., 2017). Another option that explains why we might not be able to see growth defects in the trisomic cells is that growth rate of these cells is influenced non-autonomously by the presence of the monosomy. Unfortunately, we are unable to induce only segmental trisomies in a wild type tissue and therefore we lack the means to further address this point experimentally. We will discuss this possibility in the next chapter.

2. How cell-to-cell interactions between complementary aneuploidies shape their behavior in the tissue

In this work, by disposing of two different methods of inducing segmental aneuploidies in a wild type tissue, one that generates segmental monosomies and one that generate segmental monosomies juxtaposed to their complementary trisomies, we could uncover non-autonomous effect between monosomies and their complementary trisomies which are summarized in Figure D1.

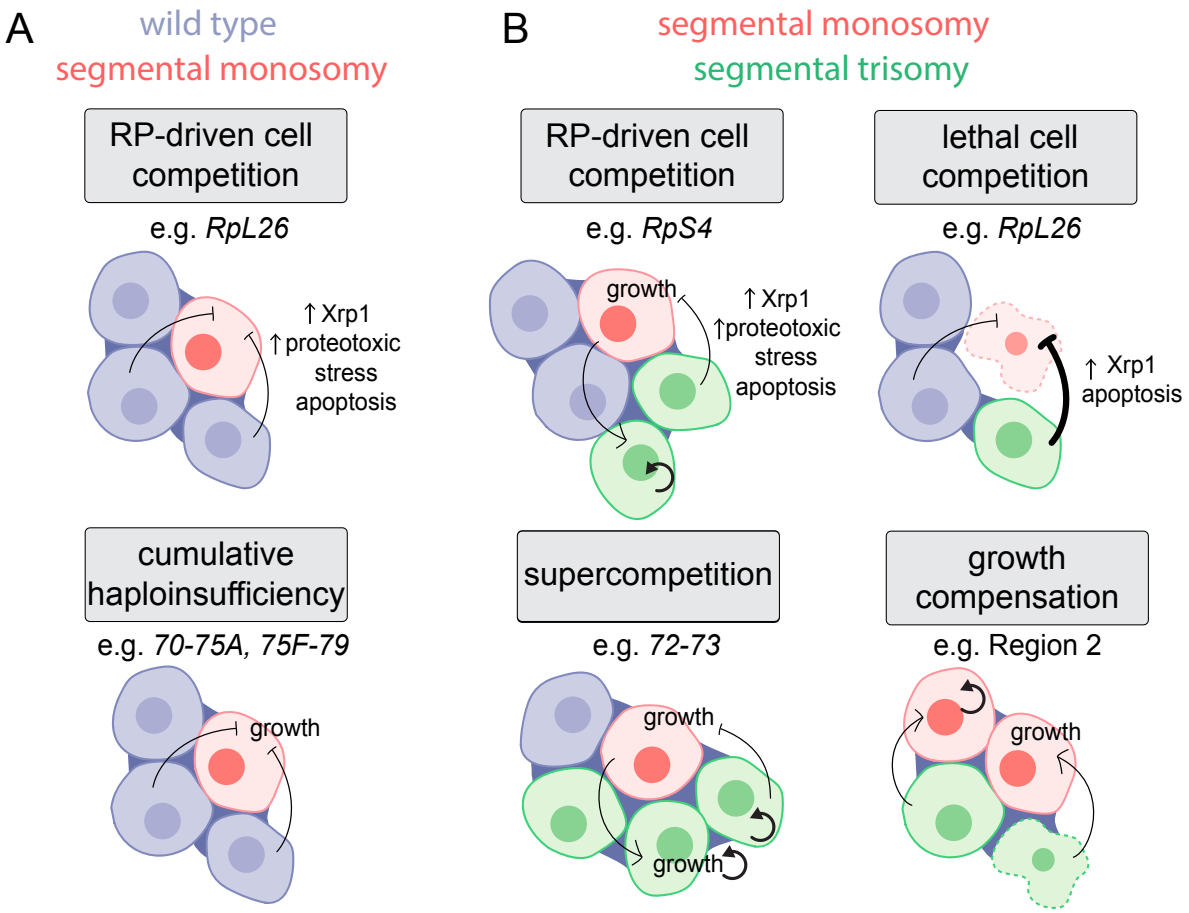

Figure D1. Model of the uncovered cell-to-cell interactions that influence the fate of aneuploid cells in *Drosophila epithelia*. (A) Xrp1-dependent and -independent processes of cell competition between segmental monosomies and wild type cells. **(B)** Cell interactions between complementary segmental monosomies and trisomies.

One example is the case of the supercompetition of the region 72-73. Monosomies for this region in fact are not outcompeted if generated alone in a wild type tissue (Figure R8), but are outcompeted in the presence of their complementary trisomy (Figure R18), which presents overgrowth respect to the control (Figure R17-18). This region includes Fwe, a protein involved in the elimination of wild type cells during *dMyc*-supercompetition (Rhiner et al., 2010). In particular, it was proposed that different *fwe* isoforms specifically marked cells expressing differential levels of dMyc as "winners" and "losers". Our data reveal that different doses of the *fwe* gene are enough to trigger a supercompetitive behavior between the clone that bears more copies of *fwe,* which overgrows, and the clone bearing less copies, which undergoes apoptosis (Figure R20). Furthermore, we couldn't detect differential expression of *fwe* isoforms between winner (trisomic) and loser (monosomic) cells in of region 72-73 (data not shown). While elimination of *fwe* mutant clones had already been described (Rhiner et al., 2010), overgrowth of clones with increased doses of *fwe* is a newly described phenotype. Interestingly, it seems that a precise difference in doses between the winner and the loser is able to trigger this type of supercompetition. In fact, a difference of two doses of *fwe* was present between winner and loser cells both in the case of clones bearing different copies of *fwe* alone (Figure R20, in which case winners had 2 copies and losers 0), and in clones bearing different doses of 179 genes including *fwe* (Figure R18, in which case winners had 3 copies of the region and losers 1). However, overexpression of *fwe* was not able to rescue the elimination of the loser clone, suggesting that other genes collaborate to the elimination of the monosomic clone. However, it is possible that overexpression of *fwe* is not the right tool to assess this, since it could further exacerbate competitive advantage of the winner against the loser. Consistently, we observed huge 72-73 trisomic clones when overexpressing *flower* that we did not observe in controls (Figure D2).

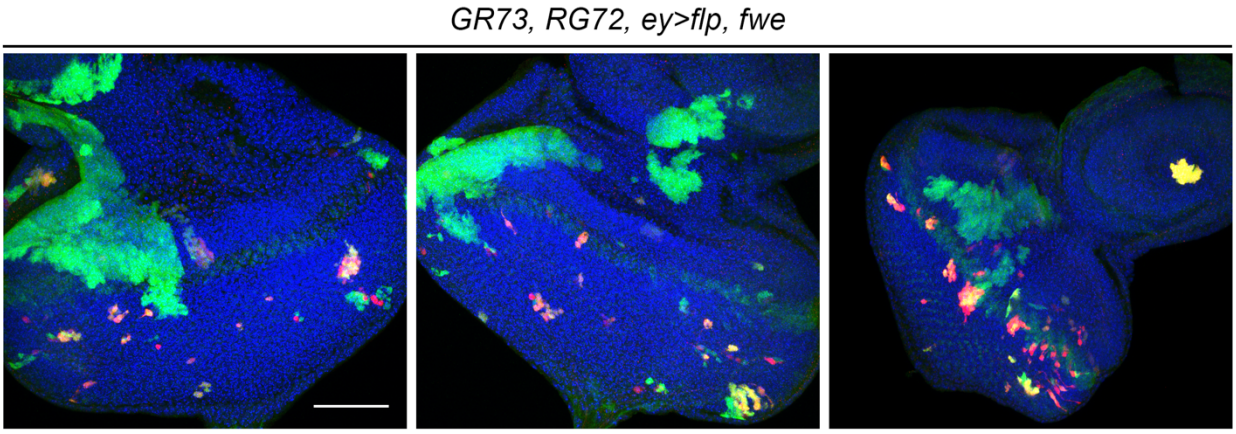

Figure D2. Overgrowth of 72-73 trisomic cells upon *fwe* overexpression. GFP marks trisomic cells for the 72-73 region. RFP the twin monosomy. Scale bar, 50 µm.

For genetic reasons, we were not able to perform overexpression of *fwe* while inducing clones acutely, which would allow for synchronization of all clones and thorough control of clonal growth. Since manipulation of *fwe* alone perfectly phenocopies the 72-73 supercompetition (Figure R20), we speculate that *fwe* is the main gene underlying the overgrowth of the trisomic clone. This would be answered by assessing whether overgrowth of the trisomic clone is rescued upon knockdown of *fwe* with acute clone induction. In the case of the 72-73 region-induced supercompetition (Figure R18), by making use of a transgene that tags with different

epitopes the different *fwe* isoforms, we did not observe differential expression of *fwe* isoforms in winners and losers (data not shown), indicating that in this case doses rather than isoforms trigger the competitive behavior. Interestingly, none of the segmental trisomies including *fwe* and *Rpl26* showed overgrowth (Figure R17,22). This could be to the fact that monosomies including *Rpl26* are haplolethal when produced together with their complementary trisomies. This suggests that the effect of overgrowth observed in the trisomies including the region 72-73 is not cell-autonomous, differently to *dMyc*-induced supercompetition, and instead relies on specific signaling between loser and winner cells. If loser cells were eliminated too fast, in this case due to *Rpl26*-induced haplolethality, the signaling from the loser to the winner would not have time to occur and therefore the winner would not overproliferate. Accordingly, when inducing clones bearing different copies of the *fwe* gene, clones bearing two copies of *fwe* do not induce cell death of cells bearing one copy of *fwe,* but only of cells bearing zero copies. This points to the fact that signaling between the loser and the winner cells depends on specific difference in the levels of *fwe*. It would be interesting to find a way to rescue the monosomic clone including the 72-73 region without altering the doses of genes included in this region, for example by inhibiting cell death. If the trisomic clone still overgrew, this would indicate that signaling between monosomic and trisomic cells is enough to trigger overgrowth of the trisomic. An analogous phenomenon has been described for Crumbs (Crb), also a transmembrane protein. When cells with different levels of Crb are juxtaposed, the relative levels influence cell survival, in this case the cells expressing higher levels of Crumbs being the losers (Hafezi et al., 2012). The paper proposes that Crb itself may function as a comparison factor to regulate cell survival non-autonomously. This is supported by the fact that Crb's extracellular domain (ECD) is necessary to establish non-autonomous effect on cell survival, indicating that it could mediate intercellular interactions that designate “winner” and “loser” cells at the boundaries (Hafezi et al., 2012).

Another non-autonomous effect that may influence the growth of the trisomic clone when the monosomic clone is eliminated is compensatory proliferation. Cell death in the proliferating wing disc and eye disc is known to trigger compensatory proliferation (Fan & Bergmann, 2008). This could explain the slight overgrowth observed in the 69-70 trisomy, which grows alongside the 69-70 monosomy that includes the *Mn* gene *RpS4*. Notably, the 69-72 trisomy does not exhibit overgrowth, despite growing adjacent to a monosomy that is being outcompeted. This could be because the 69-72 monosomy is eliminated more rapidly by the tissue, as suggested by the fewer twin clones recovered at the time of observation (Figure R18D). This faster elimination would generate compensatory proliferation signals for a shorter period, resulting in normal growth of the adjacent trisomic clone. In this sense, this overgrowth effect wouldn’t be different to the one induced by outcompeted *Mn* mutant cells in adjacent wild type cells. However, the inability to perform clonal analysis on adjacent wild type cells prevented this phenotype from being identified before. Coherently with the idea that this overgrowth effect is a result of compensatory proliferation induced by outcompeted cells, overgrowth is rescued when outcompetition is rescued by Xrp1-i (Figure R12G).

Interestingly, the 69-75 trisomy, despite its complementary monosomy being nearly haplolethal with only 6.3% of twin clones retaining the monosomy, still shows overgrowth. This suggests that the key driver of 69-75 trisomy overgrowth is not compensatory proliferation but rather specific signaling dependent on a gene within

the 72-73 region, likely *fwe*. This is further supported by the observation that overgrowth of trisomies including the 72-73 region is suppressed only when no twin clone with the monosomy is recovered (Figure R24D). This points to an intriguing scenario where even brief contact between trisomic and monosomic cells within the 72-73 region is enough to establish them as winners and losers, respectively, and to sustain the winner status of the trisomy, along with its proliferative capacity, over time, even after the monosomy, the source of the signaling, is eliminated.

Overall, these findings suggest that the duration of interaction between loser and winner cells is critical for non-autonomous effects to occur. Furthermore, they indicate that different non-autonomous effects require varying levels and durations of interaction. For example, compensatory proliferation may require more prolonged exposure, while signaling-driven effects can be triggered by briefer contacts. In order to further prove this point, it would be interesting to remove haplolethality of the 72-77 monosomy, for instance by overexpressing *Rpl26*, and see if the 70-77 trisomy presents overgrowth and the monosomy is still being outcompeted due to supercompetition of the 72-73 region.

Regarding the regions where the presence of the trisomy rescued the growth capacity of an otherwise haploinsufficient monosomy, this correlated with growth defects of the trisomic clone (Region 2, R22). Therefore, we speculate that rescue of the monosomic clone is induced by compensatory proliferation. Alternatively, an altered signaling between monosomies and trisomies could mark the monosomic cells as winners therefore rescuing their growth defect. The mechanism underlying rescue of otherwise haploinsufficient monosomies by their complementary trisomies remains as an open question.

Regarding the case of the 3R (Figure R23), the mechanism underlying the rescue of the bigger monosomy compared to the smaller ones seems to be a complex interaction between different genes involved in growth control more than non-autonomous interaction between the monosomy and the trisomy. In fact, a similar behavior was observed when only monosomies were induced (Ji et al., 2021). While compensatory proliferation effects could contribute to the phenotype observed, I interpret the fact that the trisomy presents a growth defect more as an indication of the types of genes included in the region.

Work in the *Drosophila* gut show that JNK and JNK-dependent JAK-STAT signaling are responsible for compensatory proliferation during competitive interactions either in *Mn*-induced cell competition (Kolahgar et al., 2015) or supercompetition of $APC^{-/-}$-induced intestinal adenomas (Suijkerbuijk et al., 2016). Furthermore, apoptosis in different contexts than cell competition was reported to induce compensatory proliferation through JNK (Ryoo et al., 2004) and JAK-STAT (Herz et al., 2006). Given these data, it would be interesting to address the role of JNK and JAK-STAT in the non-autonomous effects on growth and survival described in this work.

Cell autonomous and non-autonomous effects collaborate to determine the fate of aneuploid cells in epithelial tissues. We have presented several evidence that non-autonomous effects and especially cell competition mechanisms lead to the elimination of segmentally aneuploid cells. However, it is clear the cell autonomous effects also contribute to the deleterious effects of aneuploidy. In addition to the several evidence presented by *in vitro* models and thoroughly reviewed in the Introduction, interesting insights also come from a CIN-induced

aneuploidy model of tumorigenesis in *Drosophila* wing discs. In this model, aneuploid cells delaminate from the main epithelium and die through JNK-dependent apoptosis. When apoptosis is inhibited, aneuploid cells enter senescence and mediate tumorigenic effects through JNK-dependent SASP (Joy et al., 2021). Since CIN induces random events of missegregation, it is fair to say that upon CIN the tissue becomes a mosaic of euploid and aneuploid cells. In this context, aneuploid cells delamination and cell death could be mediated by cell competition.

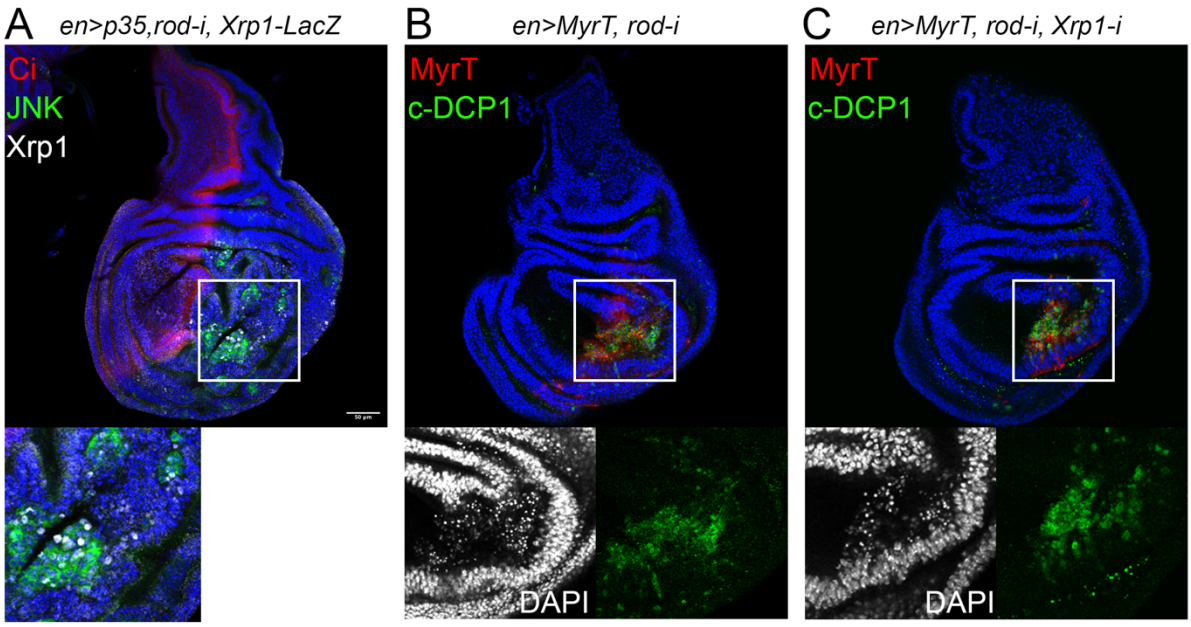

Figure D3. Xrp1 does not rescue CIN-induced cell death in wing discs epithelia. (A) Xrp1 activation shown with β-gal staining in CIN-induced tumors. **(B,C)** CIN-induced cell death showed by pyknosis with DAPI and c-DCP1 stainings without (A) and with (B) Xrp1 depletion. Scale bar, 50 µm.

However, despite Xrp1 being activated upon CIN-induced tumorigenesis (Figure D3A), Xrp1 depletion does not rescue CIN-induced cell death (Figure D3B,C). This indicates that CIN-induced aneuploidies, which have been reported to be mainly gains in this model (Dekanty et al., 2021), are eliminated through cell-autonomous Xrp1-independent processes. This is coherent with the reported cell-autonomous deleterious effects of trisomies that rely on stoichiometry alterations. Overall, these findings suggest that the mechanisms driving the elimination of aneuploid cells depend on the type and magnitude of the chromosomal imbalance. For example, CIN-induced aneuploidies, primarily characterized by large-scale gains, appear to trigger cell-autonomous elimination processes independent of Xrp1. This aligns with the notion that stoichiometric imbalances in gene expression, which are more pronounced in CIN-induced aneuploidies, drive cell-autonomous deleterious effects. Conversely, the segmental trisomies analyzed in this work did not exhibit growth defects linked to global stoichiometric disruptions. Instead, their growth defects were associated with triplosensitivity of specific loci. These observations suggest that cell-autonomous effects become predominant when aneuploidies involve drastic stoichiometric alterations, as seen with CIN-induced aneuploidies. In contrast, smaller dosage imbalances may reveal haploinsufficient or triplosensitive loci that may exert their effects through non-cell autonomous mechanisms.

3. *Rpl26* is a peculiar *Mn*-like gene

In this work, we uncovered a new *Mn*-like gene: *Rpl26.* Certain features of this gene make it similar to other *Mn* genes such as *RpS4*, which we analyzed in this work, but other emerge as peculiarities. In the context of monosomies including *Rpl26*, they suffer similar growth impairment as monosomies including other *Mn* genes (Figure R10). The underlying mechanisms behind this growth defects have been identified in the *Xrp1-mTor* axis. While monosomies including *Rpl26* and induced acutely by *hsflp* are clearly rescued by both Xrp1, mTor and apoptotic genes depletion, the monosomy including the other *Mn* genes is rescued only by Xrp1 depletion when induced with *hsflp.* This is probably a consequence of the fact that this monosomy includes not one but three *Mn* genes making it more difficult to alleviate growth defects. In fact, monosomies including only *RpS4* generated by TSG and induced acutely are rescued by mTor depletion (Figure D4A-C). Interestingly, we can again observe how rescuing the monosomic clone rescues the slight overgrow observed in the trisomic clone due to compensatory proliferation (Figure D4B).

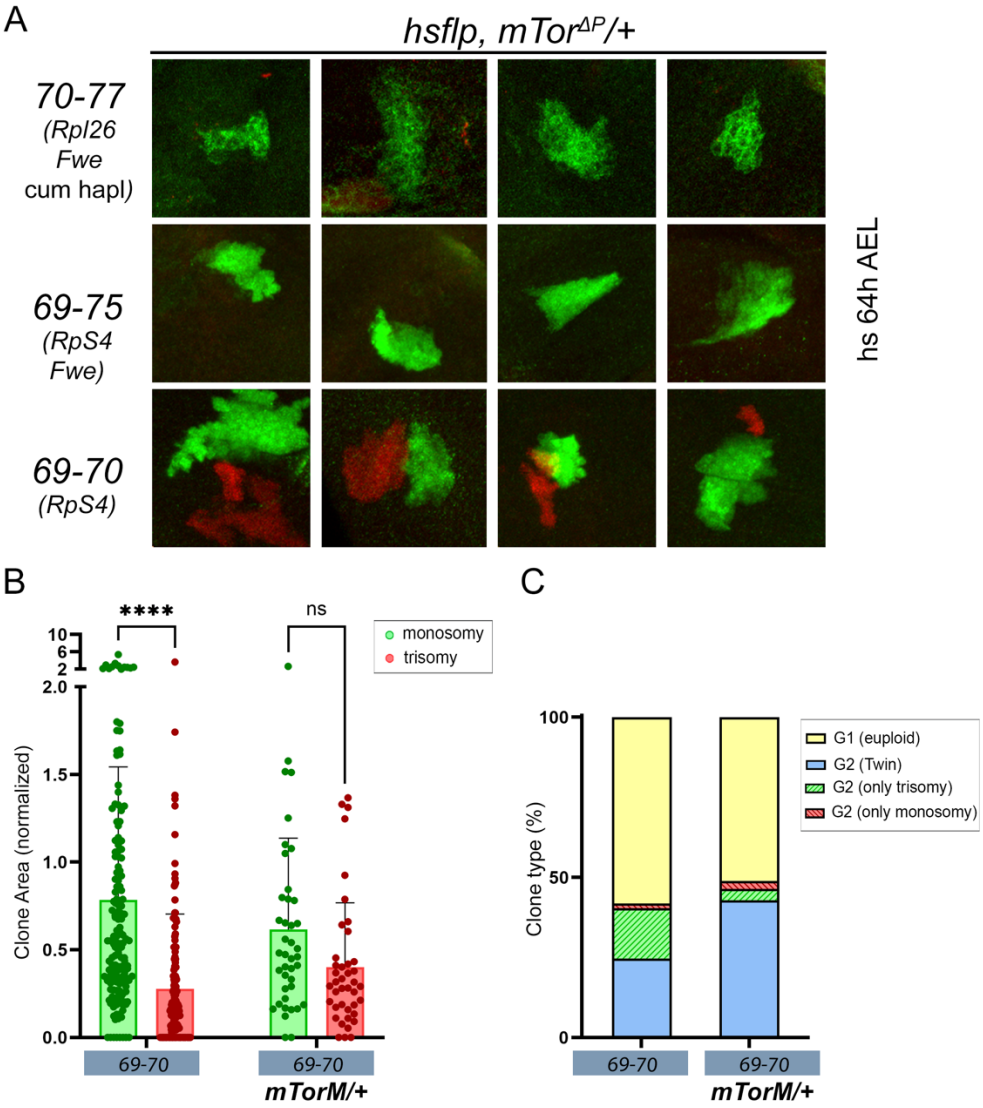

Figure D4. mTor depletion ameliorates *Mn*-induced cell competition but not *Rpl26*-dependent lethal cell competition, 72-73 supercompetition and cumulative haploinsufficiency. (**A**) Magnification of twin clones in the wing primordia. Each image is 50x50 µm. (**B**) Plots representing clone area of monosomies and trisomies of the same region (normalized to the one of euploid cells) and clone type distribution (**C**). Average (**C**) and mean and SD (**B**) are shown.

2way ANOVA with Šidák correction for multiple comparisons test was performed in **C**. Clones were induced at 64h AEL with a heat-shock at 38°C of 5-7 minutes for the control and of 1h for the other combinations. ns, not significant (p>0.05); * p ≤ 0.05; ** p ≤ 0.01; *** p≤ 0.001; **** p ≤ 0.0001.

When inducing monosomies including *Rpl26* through the TSG technique alongside their complementary trisomy, a process of Xrp1-dependent lethal cell competition emerges that does not emerge for monosomies and trisomies bearing different copies of *RpS4*. This process largely relies on *Rpl26* since specific overexpression of this gene rescues lethality of the monosomy (Figure R26). Interestingly and unlikely *RpS4*-induced cell competition, this process is not rescued by mTor depletion (Figure D4A). Interestingly, the 69-75 monosomy, where *RpS4* haploinsufficiency, supercompetition of the 72-73 region, and cumulative haploinsufficiency collaborate to induce a nearly lethal phenotype, is not rescued by *mTor* depletion, coherently with the observation that *Mn*-independent cumulative haploinsufficiency is mTor-independent (Figure R9). Overall, this suggests that mTor depletion has a role in alleviating growth defects of monosomies including haploinsufficient Rp-genes in wild type tissues, but that the observed process of lethal cell competition relies on the presence of clones bearing three copies of *Rpl26* that induce Xrp1-dependent elimination of clones bearing one *Rpl26* copy.

This is probably due to particular functions of Rpl26. In human cells, Rpl26 is the principal target of UFMylation by UFM1 (Walczak et al., 2019), a process that releases ribosome transcriptional stalling at the ER. Impaired UFMylation and in particular impaired Rpl26 UFMylation led to ER stress (Scavone et al., 2023; Walczak et al., 2019). The association of UFMylation genes with abnormal brain development in both humans (Muona et al., 2016) and *Drosophila* (Duan et al., 2016) suggests a role for UFMylation in tissue development. Accordingly, alteration in UFMylation in *Drosophila* (L. Wang et al., 2023), mice (Egunsola et al., 2017) and humans (Di Rocco et al., 2018) is associated with pathological conditions with impaired cell-cell and cell-matrix interactions. The role of Rpl26 in *Drosophila*'s processes of UFMylation and ER stress is largely unaddressed. Whether the process of lethal cell competition induced by extra copies of *Rpl26* is related to a possible role of Rpl26 in eliciting ER stress remains as an open question.

4. Cell competition and aneuploidy: autophagy or translation?

Several works support the idea that autophagy is an essential regulator of cell competition. Autophagy mediates elimination of aneuploid cells in embryo mosaics (Singla et al., 2020). Coherently, in Bmp defective and tetraploid-diploid embryo mosaics, p53-mediated mTor downregulation, which would upregulate autophagy, is responsible for loser cells elimination (Bowling et al., 2018). In a *Drosophila* model of the RNA helicase *Hel25E*- induced cell competition, winner cells activate autophagy in prospective loser cells (Nagata et al., 2019). Expression of lysosome markers has been observed in the loser cells (Lolo et al., 2012; Rhiner et al., 2010), supporting the view that autophagy happens within the loser cells. Autophagy-mediated cell competition may also drive tumor expansion as it happens in Ras^{V12}; $scrib^{-/-}$ eye disc tumors, where non-autonomous autophagy (NAA) was shown to depend on the JNK signaling in the tumor and the autocrine activation of JAK-STAT through the Upd cytokines (Katheder et al., 2017).

Autophagy has been shown to be upregulated upon mutations of Rp genes, in *Drosophila* (Kiparaki et al., 2022; Langton et al., 2021), *Zebrafish* (Boglev et al., 2013) and human cells (Heijnen et al., 2014). In humans, defects in ribosome biogenesis are associated with a group of diseases called ribosomopathies, of which Diamond-Blackfan anemia (DBA) is the most studied and is caused by one of several ribosomal proteins. Animal models reflect similar phenotypes, including developmental delays, hematopoietic defects, and structural abnormalities (Danilova et al., 2011; Keel et al., 2012; Marygold et al., 2007). Interestingly, a common feature among several ribosomopathies is p53 activation (Elghetany & Alter, 2002), as it is in Rp-induced cell competition in mammals. In the data presented in this study however, depletion of mTor, which should increase autophagy (J. Kim et al., 2011; Y. C. Kim & Guan, 2015), alleviates Rp-induced cell competition, both for *RpS4* and *Rpl26.* This is coherent with a report where *Mn*-induced cell competition is dampened by treatment with Rapamycin, which inhibits mTor activity (Recasens-Alvarez et al., 2021). Accordingly, increasing autophagy has been proposed as a therapeutic strategy for DBA (Doulatov et al., 2017). This might seem in disagreement with the observation that autophagy is increased in DBA patients and models. However, this observation might point to a defect in autophagy turnover that is ameliorated by increasing autophagic flux. Also, autophagy deficient ESC cells are eliminated by wild type cells by cell competition in a p53-dependent way (Sancho et al., 2013) highlighting that a defective autophagic flux or pathway is underlying defects in RP-mutant cells.

Furthermore, the interplay between autophagy and apoptosis is context-dependent and while in certain context a dysregulation of autophagy may enhance apoptosis, in other context it can exert pro-survival roles (Gump & Thorburn, 2011). For instance, in neurodegenerative disease, mTor inhibition leading to increased autophagy enhances the ability of cells to clear aggregated proteins improving the health and functioning of neurons (Ravikumar et al., 2004; Sarkar et al., 2007). Another example which is particularly intriguing is the interaction between caspase-8 and p62, a cargo receptor in autophagy. While p62 is crucial for the efficient activation of caspase-8 (Jin et al., 2009), caspase-8 has been shown recently to be degraded by autophagy (Hou et al., 2010). Until now, we have showed that aneuploid cells in embryo mosaics are eliminated through autophagy-mediated apoptosis (Singla et al., 2020). On the other hand, upon RP mutations, autophagy is upregulated and increasing autophagy ameliorates RP mutant phenotypes. We can explain this in terms of context-dependent role of autophagy in inducing or preventing apoptosis. Alternatively, we can propose that since aneuploid cells in the cited study are generated by CIN and cannot be monitored, and that the RP mutant phenotype would be relevant only in case of monosomies, autophagy has different roles in inducing aneuploid cells elimination depending on the type of aneuploidy.

Alternatively, it cannot be excluded that the role that we have observed from mTor in mediating *Mn*-induced cell competition could be mediated by its effect on translation (Ma & Blenis, 2009). Differences in translation levels between winner and loser cells is a key element in *Mn* induced cell competition (Kiparaki et al., 2022) and *dMyc*-induced super competition (de la Cova et al., 2004). Notably, RP genes downregulation has been identified as a signature for loser cells in natural cell competition occurring in the developing mouse skin (Ellis et al., 2019). Intuitively, winner cells with more proliferative capacity will need higher level of translation than

slowly proliferating loser cells. Whether the reduction in translation observed in *Mn*-induced cell competition is a consequence of defective ribosome assembly and proteotoxic stress or a consequence of specific transcriptional programs has been object of debate. On one side, defective ribosome assembly has been observed in $Mn^{+/-}$ cells, even if variable depending on the specific *Mn* gene (Kiparaki et al., 2022). Especially, it has been reported a differential change between small and large subunits of the ribosome, where small subunits are preferentially downregulated (Baumgartner et al., 2021; Langton et al., 2021; Recasens-Alvarez et al., 2021). Ribosome biogenesis defects might lead to the aggregation of orphan Rp and hence to proteotoxic stress that then contributes to cell competition (Tye et al., 2019). On the other side, it was shown that eIF2α is phosphorylated by Xrp1 and PERK to decrease translation in $Mn^{+/-}$ cells, but that this reduced translation is not the mechanism through which loser cells are outcompeted (Kiparaki et al., 2022). Similarly in mice, it is suggested that reduced translation in $RpS6^{+/-}$ cells depends on the transcription factor p53 (Tiu et al., 2021). Coherently, monosomic cells in humans, which would bear RPG heterozygous mutations, present impaired ribosome assembly and translation and are eliminated through p53-dependent apoptosis (Chunduri et al., 2021). However, the fact that monosomies bear RPG mutations, and that RPG mutations have been linked with increased proteotoxic stress and increased UPR genes expression, means that monosomies should also suffer from proteotoxic stress and increased autophagy. Nevertheless, monosomic human cells were not associated with UPR and proteotoxic stress. This could be for differences between *in vitro* and *in vivo* contexts or differences in the number of mutations. While mutation of single RPGs could be able to elicit proteotoxic stress, monosomy for an entire chromosome could trigger a different response. Coherently, depletion of mTor in our study did not rescue bigger monosomies such as 70-77 or 69-75 where multiple genes collaborate to impair the growth of the monosomy (Figure D4).

The role of mTor in controlling translation, and the evident role of translation in cell competition, raises the question if the effect we observed in mTorM on *Mn*-induced cell competition are due to effects on translation. Decreased levels of mTor have been shown both in mice (Bowling et al., 2018) and *Drosophila* (Sanaki et al., 2020) in loser cells during cell competition. One possibility is that by downregulating levels of Tor systemically using the mTor heterozygous mutant, we are decreasing translation levels of wild type cells therefore alleviating the difference in translation levels and growth capacity between aneuploid cells and wild type cells, similarly to when cell competition induced by a specific *Mn* gene in clones is rescued by making its environment as "loser" as the $Mn^{+/-}$ cells, using a heterozygous mutant background for another *Mn* gene (Ji et al., 2021). In order to unravel these interactions, it would be interesting to assess autophagy and proteotoxic stress contributions in the different types of cell competition described.

Interestingly, as for the so-called aneuploidy paradox (Vasudevan et al., 2021), in spite of the fact that in cellular models ribosomal insufficiency leads to a reduced proliferation rate, patients affected by ribosomopathies present a paradoxical increase in cancer incidence (D'Andrea et al., 2024; De Keersmaecker et al., 2015). While it seems unlikely that the oncogenic potential of ribosome loss is a cell-autonomous effect, modern views on cancer that have shifted the focus from the cancer cell to the tumor microenvironment may provide useful insights to this topic. Immune cells are particularly sensitive to the functionality of the

translational apparatus with levels of proteins crucial to both innate and adaptive immunity being regulated at the level of translation, with the strong contribution of the mTor kinase pathway (Piccirillo et al., 2014). In ribosomopathies, deficiency of the specific translation of some mRNAs impairs the immune response (Bohlen et al., 2023). This opens up the scenario in which increase of cancer in an organism with impaired ribosomal proteins is not necessarily due to the fact that abnormal ribosomes lead to cancer by altering the prospective cancer cell. It is possible that a reduction in the efficiency of the immune response, favors the emergence of weak, otherwise-depleted, ribosome-deficient cancer cells. An example is the Schwachman–Diamond Syndrome (SDS), a ribosomopathy characterized by mutation in the SBDS gene and increased risk for acute myeloid leukemia, among pancreatic insufficiency and growth deficits (Woloszynek et al., 2004). It has been shown that the ribosomopathy mutation in SDS is not oncogenic in a cell-autonomous fashion but rather tumor suppressive, therefore suggesting that alteration of the surrounding environment underlies increased cancer in SDS patients (Calamita et al., 2017). Another possibility is that hematopoietic stem cells carrying certain mutations are positively selected in the context of ribosomopathies. For instance, in SDS patients, it has been shown clonal expansion of cells bearing mutations in the translation initiation factor eIF6 in the myeloid lineage (Kennedy et al., 2021). Possibly, eIF6 mutated cells present improved translational efficiency. Consistently, the prognosis of patients with eIF6 mutations is generally favorable, indicating again that the loss of ribosomal components, if anything, decreases cancer malignancy (Kennedy et al., 2021). Other SDS patients present mutations of p53, in which case the prognosis is negative (Reilly & Shimamura, 2023). One explanation for these studies could be that SBDS-deficient cells are less prone to transformation in a cell-autonomous fashion, but the state of prolonged stress that they are suffering leads to either maladaptive or adaptive mutations, respectively, p53 and eIF6. Finally, cytoreductive chemotherapy for leukemia in SDS failed to prevent relapse and was unsuccessful due to high toxicity (Myers et al., 2020), suggesting that the therapeutic outcome of SDS patients does not correlate with reducing the malignancy of tumor cells but with the effect of ribosomal mutations in the host microenvironment.

These considerations overall highlight the importance of cell-to-cell interactions in the interplay between ribosome defective biogenesis, autophagy, cell competition and aneuploidy.

5. Strengths and limitations of the model

5.1. Types of aneuploidies simulated by the model

We have discussed in the Introduction the implications of using a *Drosophila* model to address key questions regarding the emergence of aneuploidy in mammals. Furthermore, it is important to consider that the system developed in this work specifically models segmental aneuploidies. As described in the Introduction, segmental aneuploidies typically arise from lagging chromosomes, DNA bridges, DNA damage, and improper repair, whereas whole-chromosome aneuploidies often result from events such as non-disjunction or defects in SAC genes. This distinction is critical, as cellular responses to segmental aneuploidies may differ from those triggered by whole-chromosome aneuploidies, requiring careful consideration of the specific phenomenon

being modeled. On one side, what happens in our system, where a DNA sequence is intentionally cut and recombined with a distal region on its homologous chromosome rather than being properly repaired, pretty much mirrors what happens *in vivo*, where DNA breaks are often improperly repaired, leading to deletions or amplifications. On the other side, experimental outcomes could be influenced by additional factors such as prolonged mitotic time or chromosomal distortions caused by recombination between distal FRTs. Whether these factors are relevant or not depends on the specific focus of the study, whether it is to investigate the effects of segmental aneuploidies, including potential DNA damage-related consequences, or solely the effects of chromosomal imbalances.

Using the *in trans* strategy, we didn't observe any increase in markers of DNA damage (data not shown), likely because observations were made at 120h AEL, 56 hours after aneuploid cell induction, by which time any initial DNA damage may have already been resolved. Nonetheless, characterizing the immediate impact of such recombination events could be valuable, as this is, to our knowledge, the first instance of recombining distant FRT sites *in trans*. Although we did not specifically analyze the effects on replication stress or DNA damage, the use of the Twin Spot Generator technique provided critical insights by allowing us to monitor growth rate as an indicator of fitness of euploid clones bearing translocations. Interestingly, these cells exhibited growth defects compared to controls in most cases after 56 hours of induction, indicating the presence of additional persistent stresses (Figure R15). We can find support to these data if we look at the clones induced *in trans* with RS FRTs, where both euploid rearrangements and duplications were marked in red in the adult eye of *Drosophila* (Figure R3). We can notice that Eye Coverage decreases at lower distances respect to Population Coverage, and this is particularly evident when looking at clones induced with *eyflp* (compare Figure R3B and C). On one side, this could be because, when efficiency decreases with increasing distance, we may observe less fused clones which would be reflected in a smaller Eye Coverage, but still the same Population Coverage. However, thanks to analysis of the clonal growth of euploid translocation induced through the TSG, we know that this could also be due to a decrease in fitness of the products of the recombination.

While such euploid rearranged cells may not be useful for studying aneuploidy directly, their characterization could provide significant insights both for technical reasons, to help refine the knowledge about this model, and to characterize additional cellular behaviors. In fact, studying the underlying mechanisms to the growth defect of cells bearing euploid translocations could help identify stress markers relevant to aneuploidy in real biological scenarios. Importantly, these markers may not originate from chromosomal imbalances themselves but rather from other etiological factors such as lagging chromosomes, DNA bridges, DNA breaks, improper repair and mitotic recombination. The smaller size of euploid translocation clones can likely be attributed to several factors. One possibility is a cell-autonomous effect of recombination-induced stress, which slows their proliferation compared to wild-type cells. Whether these slower-proliferating cells are actively eliminated by wild-type cells through a process similar to cell competition remains unclear. However, slower proliferation rates alone are insufficient to trigger cell competition (Potter et al., 2010). Another possibility is that cells unable to cope with recombination-induced stresses are removed from the tissue, while those that successfully

repair the damage continue to proliferate. The initial loss of stressed cells could explain the observed size difference compared to controls. This idea is supported by the percentage of clones in G1 observed across the different FRT pairs tested. The % of clones in G1 varies from a minimum of 48.2% for 75A-75F to 69.3% for 75A-79 and 68.6% for 70-79 (Figure R24D). Such considerable deviations from the expected 50% suggest that both twin clones are sometimes lost from the tissue. This aligns with the observation that a small fraction of clones consistently loses their twin, regardless of whether it is a monosomy or a trisomy (Figures R18D, 20D, 21D). Altogether, these data suggest that recombination itself induces damage and stress, which can stochastically lead to cell death if the damage is not adequately repaired. A key advantage of this system is that, by normalizing the size of monosomies and trisomies to that of the euploid rearrangements, we can distinguish the effects of recombination-induced stress from those caused by gene dosage imbalances.

This advantage is not present in the strategy of inducing segmental monosomies with RS FRTs. In this setup, the recombination event that creates the aneuploidy involves the excision of a large fragment of DNA, which means we cannot generate an internal control where the same recombination event occurs without causing a gene dosage imbalance. We are therefore limited to observe the growth capacity of a cell that not only is heterozygous for various genes, but also underwent a stressful recombination event where a large fragment of DNA was excised into a large circular DNA. Although studying the effects of circular DNA was not the goal of this project, it is worth noting that extrachromosomal circular DNA (ecDNA) is generated in chromosomally unstable cells through mechanisms closely linked to the emergence of segmental aneuploidies. For example, during breakage-fusion-bridge (BFB) cycles, chromosome ends without telomeres fuse to form dicentric chromosomes that break during segregation, creating segments that can eventually loop out to form ecDNA. (Toledo et al., 1993; Singer et al., 2000). Similarly, during chromothripsis, a catastrophic event where entire chromosomes are shuttered, some fragments can circularize into ecDNA (Stephens et al., 2011; C.-Z. Zhang et al., 2015). Another possibility is that during translocation events, segments near the translocation site are either amplified or deleted, leading to the formation of ecDNA (Röijer et al., 2002). Therefore, the fact that a segmental monosomy and ecDNA are generated together in this model closely reflects real biological contexts. Unfortunately, using RS FRTs *in cis*, we are unable to monitor the fate of the ecDNA while simultaneously marking the chromosome carrying the segmental monosomies, as the system relies on reconstructing a single marker, the *white* gene. As a result, the ecDNA remains "invisible", and we cannot determine whether it is retained in dividing cells, whether it is transcriptionally active, whether it contributes to the observed proliferation defects, or whether it leads to micronuclei formation or DNA damage. The literature suggests that ecDNA might be entrapped in micronuclei to reduce their deleterious effect as free cytoplasmic DNA (Von Hoff et al., 1992; Valent et al., 2001). Relevantly, micronuclei containing ecDNA have been shown to be transcriptionally active (Utani et al., 2007), although gene expression is reduced (Papathanasiou et al., 2023). This means that cells undergoing the excision event, if they retain the ecDNA, despite being marked in red, might not be fully monosomic at the transcriptional level for the excised genes. As a result, the effects of genome imbalance could be partially mitigated. This possibility introduces interesting scenarios. If the excision occurs in G1, a single micronucleated cell would give rise to the clone, requiring consideration of the various

possible fates of the micronuclei, including extrusion, reincorporation, degradation, persistence, chromothripsis, or elimination through apoptosis (reviewed in Hintzsche et al., 2017). If the excision occurs in G2 on only one chromatid, and the ecDNA is incorporated into a micronucleus, two daughter cells would result: one micronucleated with a deleted chromosome in the main nucleus and one carrying only the deletion. Consequently, half of the cells in the analyzed clone would experience the effects of the monosomy alone, while the other half would be impacted also by the presence of the micronucleus. Differences in the growth capacity between the micronucleated monosomic cell and the monosomic cell would not be distinguishable, as the growth effects are measured collectively for all red-labeled cells. Furthermore, while the mononucleated cells might be capable of dampening the deleterious effects of the dosage-imbalance, they will suffer from the consequences of having micronuclei. However, regardless of whether red clones originate from a single micronucleated cell or a pair comprising a monosomic and a micronucleated cell, it is unlikely that micronuclei are retained through all the mitotic events occurring in the eye primordium during the 72-hour period from clone induction to the end of tissue proliferation. Micronuclei are prone to rupture due to defects in the nuclear membrane, exposing the DNA to the cytoplasm. The catastrophic events that follow are likely to result in either a cessation of cell proliferation or cell death (Crasta et al., 2012; Hatch et al., 2013). This aligns with a model of centrosome inactivation and subsequent chromosome loss, where acentric fragments are gradually lost over successive rounds of cell division following their formation (Ly et al., 2017). Interestingly, we unintentionally generated a line with *in cis* FRTs at 75F and 79 where the *white* gene was reconstructed on the excised ecDNA (Figure D5A). To our surprise, we found a unique phenotype characterized by single red ommatidia scattered throughout the eye (Figure D5B). This observation aligns with the hypothesis that ecDNA is likely incorporated into micronuclei and remains transcriptionally active for a few rounds of cell division, leading to the formation of a limited number of red cells. However, cells harboring this transcriptionally active ecDNA are eventually lost, either due to stop in proliferation or cell death.

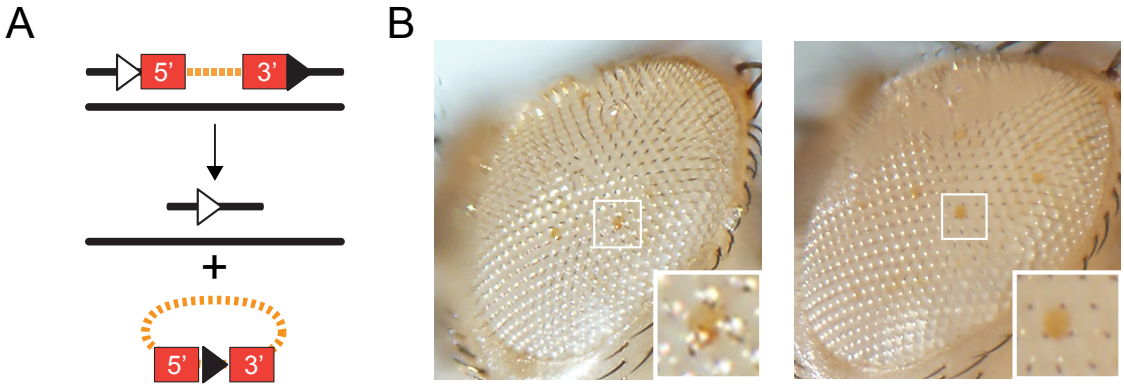

Figure D5. ecDNA is transcriptionally active for few rounds of cell divisions. Cartoon depicting how ecDNA is generated bearing the reconstructed *white* gene **(A)** and images of the eye epithelia with magnification of red cells bearing the ecDNA **(B)**.

Overall, these findings reinforce the idea that generating segmental aneuploidies through recombination effectively mimics the real biological processes underlying the emergence of segmental aneuploidies.

Furthermore, our model offers the technical capability to differentiate between stresses caused by recombination events and those resulting from gene-dosage imbalances. On one hand, we have demonstrated compelling evidence that ecDNA generated in monosomic cells via RS FRT excision in the eye is not significantly retained within the clone. On the other hand, the stress induced by recombination *in trans* between distal TSG FRTs can be systematically assessed by comparing aneuploid clones with control clones bearing euploid rearrangements.

To sum up, with the proposed systems we can either induce segmental monosomies in a wild type epithelium (*in cis*), or complementary segmental monosomies and trisomies in a wild type epithelium (*in trans*).

The *in trans* strategy using the TSG technique is particularly valuable for studying twins of monosomic and trisomic cells. Missegregation events in tissues, whether in embryos or adult somatic tissues, consistently result in twin daughter cells with complementary chromosomal losses and gains. This is especially true for whole-chromosome aneuploidies. Although our model generates segmental aneuploidies through recombination—which, as discussed previously, may involve different stresses compared to whole-chromosome aneuploidies—we can argue that this is still a valid strategy for modeling twin whole-chromosome aneuploidies with two key points. First, in CIN-induced models of whole-chromosome aneuploidies events such as micronuclei formation and ecDNA have been reported (Crasta et al., 2012; Bakhoum et al., 2018). However, this might be slightly different since in the case of segmental aneuploidies, aneuploidy arises as a result of chromosome breakage, whereas in whole-chromosome aneuploidies, chromosome breakage occurs as a consequence of aneuploidy and CIN. Second and most importantly, the TSG technique allows us to exclude recombination-induced effects specific to segmental aneuploidies by comparing aneuploid clones to euploid rearrangements. Therefore, we can reasonably conclude that any observed behavior resulting from a segmental aneuploidy in this model would likely be comparable to that of a whole-chromosome aneuploidy, provided the chromosome in question contains the same set of genes as the segmental aneuploidy. It is a safe comparison to make if we think that the segmental aneuploidies that we analyzed in *Drosophila* are comparable in size to whole-chromosome aneuploidies in mammals. We analyzed aneuploidies including from 89 to 1517 genes, with an average of 639 genes per aneuploidy. The shorter human chromosomes include 64, 235, 269 and 321 genes (the Y, 21, 18, 13, respectively), while the bigger 2056, 1472, 1320 and 1300 (the 1, 19, 11, 2, respectively) with an average of 849 genes per chromosome.

Furthermore, a report detected frequent segmental deletions and duplications that were reciprocal in sister blastomeres in embryo (Vanneste et al., 2009), indicating that events leading to segmental aneuploidies such as BFB-cycles and chromosome lagging can give rise to reciprocal twin clones. Given the high prevalence of segmental aneuploidies in mosaic embryos and in both healthy and unhealthy adult somatic tissues (Jacobs et al., 2014; Shao et al., 2019; Vanneste et al., 2009), it is highly relevant to dispose of models of segmental aneuploidies. While events leading to segmental aneuploidies might initially generate reciprocally aneuploid daughter cells, during further cell divisions one of the products might be lost. For instance, following chromosome bridges and BFB-cycles, some segments could undergo chromothripsis or DNA included in the micronuclei could be reincorporated in the nucleus. Therefore, only one of the segmentally aneuploid

daughters would remain in the tissue. The *in cis* model is able to reproduce a situation where a DNA segment has been excised leaving a segmentally monosomic cell in a wild type tissue. However, we lack the ability to model the complementary situation. In fact, we cannot induce by sequence-specific recombination methods a cell bearing a segmental trisomies in a wild type tissue. This has important limitations in the context of dissecting the consequences of gaining an extra copy of a chromosome segment. In fact, as we will further discuss later, the behavior of segmental trisomies is influenced by the presence of complementary monosomic cells. Disposing of a model where the same segmental trisomies could be induced in a wild type tissue with and without their monosomic twin, would allow us to distinguish the effects on trisomic cells that derive from the interaction with the monosomic cells and with the wild type cells.

5.2. Transferability of the strategy to mammalian models

Differently than previous models based on the induction of chromosomal instability, the emergence of aneuploid cells in our model is a consequence of sequence-specific mitotic recombination events. This is possible in *Drosophila* since somatic tissues in all Diptera experience homologous pairing. Homologous pairing in *Drosophila* is evident from the mitotic cycle 13 of embryogenesis, before cellularization, and is persistent from this point onwards (Csink & Henikoff, 1998; Hiraoka, 1993). In mammals, complete pairing of homologous chromosome is not reported outside of the germline in the context of meiotic pairing for homologous recombination. Normally, mammalian chromosomes are organized in specific territories where homologous are kept apart (Spector, 2003). However, homologous chromosome pairing can occur in somatic cells in specific chromosome segments in tightly regulated developmental contexts, to facilitate precise gene regulation and coordination during development. One example is during X chromosome inactivation in females, where transient pairing at the X inactivation center enables proper counting and choice of the inactive X chromosome (Augui et al., 2007; Bacher et al., 2006). Additionally, pairing occurs at certain loci like imprinted regions, where the copy from one parent has been silenced and therefore the region is monoallelic expressed. Pairing of imprinted regions seems necessary in order to silence one of the alleles (T. Li et al., 2008; Ling et al., 2006). The pairing seems crucial for proper development since its disruption is associated with developmental abnormalities (Lalande, 1996; Thatcher et al., 2005). In *Drosophila*, homologous pairing throughout the cell cycle facilitates similar gene regulation mechanisms such as transvection, that are not regulated through simple contact (Geyer et al., 1990). In budding yeast, *Saccharomyces cerevisiae*, evidence for homolog pairing in somatic cells is contradictory with some studies reporting some levels of pairing at several loci (Loidl et al., 1994) and others failing to detect significant pairing (Guacci et al., 1994). Fission yeast, *Schizosaccharomyces pombe*, seems to be, together with Diptera, an exception among eukaryotes, with consistent pairing in somatic cells (Scherthan et al., 1994).

If applicability of our strategy to other model organisms strictly relies on mitotic pairing of homologous chromosome, the fact that only fission yeast seems to display similar pairing level, looks like a great limitation of the model. Nevertheless, this might be overcome by the high conservation of relevant behaviors and

molecular mechanisms activated upon aneuploidy observed between *Drosophila* and other models. Leveraging the peculiarities of *Drosophila* genetics to obtain transferable information could be a winning approach.

However, let's consider the possibility of applying this strategy to mammalian models using the Cre/lox system, a similar sequence-specific recombination system widely used to generate conditional knock outs in mice and human cell lines, but also to induce chromosomal rearrangements. If homologous pairing is a requirement for recombination between distal lox sequences, implementing a recombination-based strategy to induce segmental aneuploidies would be possible mainly in meiotic cells, which experience homologous pairing. In this regard, an elegant *in vivo* system based on meiotic Cre recombination was developed: targeted meiotic recombination (TAMERE) (Hérault et al., 1998). This approach is based on the use of males expressing Cre in primary spermatocytes and engineered with two distant loxP sites in the same orientation on homologous chromosomes. In the germline of such trans-loxing males, Cre will catalyze recombination of *in trans* loxP sites, resulting in gametes carrying the reciprocal products of this rearrangement, the deletion and duplication of the chromosomal region comprehended between the loxP site breakpoints. By breeding this male to wild type females, paternal heterozygous progeny carrying the deletion and duplication allele can be recovered and used to establish the new mutant line. This strategy was used to generate reciprocal deletions and duplications at the HoxD locus (3-43 kb), which were recovered in 5-20% of the progeny (Hérault et al., 1998; Tarchini et al., 2005), and at a region of distal Chr 7 (~280 kb), which were recovered in approximately 17% of the progeny from trans-loxing males (Lefebvre et al., 2009). In the examples cited, laborious crosses are necessary to establish the lines carrying the mutant alleles. By implementing a system analogous to the TSG technique with split N- and C-termini of fluorescent markers at both sides of the lox loci, it would be possible to visualize recombinant embryos and follow their development. It is true that in the TAMERE examples reported the loxP loci were not placed at a great distance. However, given the fair efficiency of recombination in cells with homologous pairing for even large distances between FRTs that we have shown in this work, I speculate that increasing the distance between the loxP sites would still produce recombination product at a workable efficiency. Furthermore, implementing the system to fluorescently mark recombinant progeny, would avoid laborious mouse work and would allow to analyze the effect of organismal segmental aneuploidies, both monosomies and trisomies, in early development and, in case of embryo viability, in the health of the organism. To our knowledge, a systematic analysis on gene-dosage effects of segments of the genome on organismal viability and development in mice is still missing. Furthermore, it would be possible to obtain from these embryos individual blastomeres bearing specific segmental aneuploidies and reaggregate them into chimeras, similarly to what was done to generate chimeric embryos of euploid-aneuploid cells (Bolton et al., 2016). What we have shown in our studies is that juxtaposition of cells bearing certain segmental aneuploidies significantly impacts the fate of aneuploid cells in an epithelial tissue. The possibility described above to generate chimeric embryo bearing differentially marked segmental aneuploidies opens up interesting scenarios in which different combination of segmental trisomies and monosomies, either complementary or not, or in combination with euploid cells, could be studied in the developing embryo.

In the view of extending these strategies to induce aneuploidies to somatic cells, some works suggest that absence of homologous pairing would not preclude recombination between *loxP* insertions. If that was the case, a similar strategy to the FRT *in trans* that we have developed in this work could be implemented in mammalian somatic cells allowing for the study of aneuploid mosaics, whose relevance we have largely highlighted throughout this elaborate. In this direction, different studies showed that *lox*P sites inserted in the same chromosomal position in ES cells gave Cre-induced mitotic recombination products at a frequency of 4.2×10^{-5} to 7.0×10^{-3} despite absence of mitotic pairing (Liu et al., 2002). *In vivo* strategies, while less efficient and more challenging to implement, offer the advantage of utilizing widely available tissue-targeted Cre expression systems. In this regard, a technique called MADM (mosaic analysis with double marker), that similarly to the TSG relies on loxP sites flanked by N- or C- termini of GFP or RFP, was implemented in mice (Zong et al., 2005). In this work, interchromosomal recombination was induced efficiently in both mitotic and postmitotic cells for conditional knockouts and cell lineage analysis in neural cells (Zong et al., 2005). However, in this study, loxP sites were inserted at the same genomic location, leaving open the question of whether distant loxP sites would recombine *in vivo*. Interestingly, a similar strategy to Flp-FRT *in cis* recombination was tested with the Cre-lox system both in ES cells and in mice cardiac cells. In this work they first show an efficiency of approximately 10% both *in vitro* and *in vivo* in generating a deletion of a 2 cM (4 Mb) segment on chromosome 11 (Zheng et al., 2000). Then, they tested the efficiency of the system in generating larger chromosomal deletions in ES cells with *in cis* loxP sites in chromosome 11 at increasing distances and respectively at 2, 22, 24, 30, 60 cM. Coherently to what we showed in this work, recombination efficiency decreased with distance until a 0.01% for the largest segment tried and lethality was shown for bigger deletions (Zheng et al., 2000). Notably, they observed that while for closer loxP sites recombination *in cis* along the same chromosome was more efficient than *in trans* recombination, for loxP sites at larger distances recombination *in cis* and G2-recombination *in trans* between loxP sites located on sister chromatids were equally efficient and generated chromosomes with complementary deletions and duplications (Zheng et al., 2000). This indicates that distant loxP sites at least until 60 cM can recombine *in vivo* in mice. It is possible that the absence of mitotic pairing significantly impairs recombination between elements located at the same genomic location, but that for elements located at a greater distance, pairing is not a crucial factor.

Overall, the data presented suggest that implementing Cre-lox-based strategies to induce and fluorescently label specific aneuploidies both at the organismal level, in embryo mosaics and in somatic tissues *in vivo* is indeed possible and constitutes an appealing application of the method developed in this study.

5.3. Cellular behaviors and molecular pathways: beyond growth and cell death and epistatic interactions?

5.3.1. Extrusion of aneuploid cells

In the present work, we have focused on analyzing the impact of segmental aneuploidies on growth and cell death. A key advantage of our rationale was that we could differentiate the two parameters by separately

analyzing frequency and size of single cells-derived clones (details on quantification in Materials and Methods). While extremely relevant phenotypic outputs, indeed we could expand the characterization of specific-aneuploidies-induced cellular behavior.

One example of aneuploidy-induced cellular behavior that we didn't specifically address is extrusion from the epithelium. As mentioned multiple times during this elaborate, aneuploid cells are shown to be extruded from epithelial tissues in a variety of models. Indeed, we were also able to observe delamination of monosomic cells comprehending the gene *Rpl26* (Figure R25B) when blocking cell death though overexpression of the *miRHG* miRNA against proapoptotic genes. The presence of the monosomic clone was recovered but only basally, differently to what happens with Xrp1 knockdown (Figure R25B), indicating that cell delamination is an early event in the elimination of monosomic cells that depends on Xrp1 activation, and that cell death blockage is unable to retain monosomic cells in the epithelium. This is different to what is observed for monosomic cells including the *Rps4* gene which are rescued in the epithelium upon blockage of cell death (Figure R13B). This difference correlates with the strength of the phenotype of the two monosomies, where *Rpl26*-including monosomies are completely absent from the discs indicating rapid cell death while *RpS4*-including monosomies, though presenting a growth defect, can still be recovered. This opens up the interesting possibility that the capacity of rescuing delamination by blockage of cell death depends somehow on the levels and speed at which pathways responsible for initiating apoptosis are activated. Alternatively, the mechanisms controlling cell delamination could differ depending on the specific haploinsufficient genes involved and therefore suggesting different mechanisms of haploinsufficiency triggering cell elimination. This goes accordingly with the observation that the growth defect of the 66E1-70D1 monosomy including not one, but three *Mn* genes, and induced through RS-FRTs *in cis* was not rescued by blocking apoptosis (Figure R11A). Interestingly, growth appears to be partially rescued with the chronic induction with *eyflp* (Figure R11B). It is possible that heterozygosity for the proapoptotic rescues survival of certain monosomic cells allowing to observe a difference when they are produced chronically but that, similarly to what happens for *Rpl26* monosomic cells, they are not rescued in the main epithelia and therefore their growth potential is still compromised.

Notably, delaminated *Rpl26*-including monosomies have visibly enlarged nuclei (Figure R25B). This resembles what happens in CIN-induced aneuploidy in wing discs, where aneuploid cells delaminate before entering apoptosis (Dekanty et al., 2012). When apoptosis is blocked they remain in the tissue as delaminated senescent cells (one of whose prominent features is in fact enlarged nuclei) and cause malignant overgrowth of the tissue (Joy et al., 2021). Interestingly, a key feature of loser cells in cell competition is also extrusion from the tissue. In the context of cell competition and tumor, specific receptors that sense the polarity status between epithelial cells are responsible for elimination of potentially oncogenic cells. Both in a *Drosophila* model of polarity-loss-induced cell competition and in a pancreas model of oncogenic RAS mosaics, if this sensing is altered, potentially malignant cells are not properly extruded and eliminated leading to formation of tumors (Yamamoto et al., 2017; Hill et al., 2021). Overall, this evidence together suggests that extrusion of unhealthy cells is a fundamental process for maintaining tissue homeostasis and again establishes an interesting link between aneuploidy and cell competition.

In the context of both *Mn*-induced cell competition and *dMyc*-induced supercompetition in *Drosophila*, several works propose that extrusion of loser cells is fundamental for their elimination as it renders them accessible to immune cells clearance (Lolo et al., 2012; Casas-Tintó et al., 2015). These works challenge the previously proposed idea that engulfment of loser cells is performed by epithelial cells (W. Li & Baker, 2007). The fact that loser cells elimination depends on components of the innate immune system such as the Toll-related receptors (TRRs) and NFκB signaling pathways (Meyer et al., 2014) creates an interesting parallel with NFκB-dependent elimination of human aneuploid cells by natural killer cells *in vitro* (R. W. Wang et al., 2021). Interestingly, we observed cells that both for nuclear size and basal location in the wing disc resembled the hemocytes, the macrophages in *Drosophila*, marked in red in presence of an RFP-marked *Rpl26*-including monosomy (Figure D6).

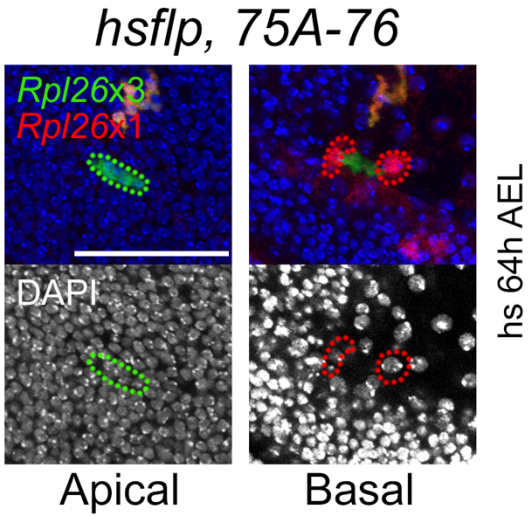

Figure D6. Hemocytes-like cells are RFP-positive in the presence of an eliminated RFP marked monosomy including *Rpl26*. Confocal images of apical and basal planes of wing discs where indicated aneuploidies were induced. Scale bar, 50 µm.

While we haven't check if these cells are in fact hemocytes, the fact that monosomic cells including *Rpl26* are consistently eliminated from the tissue (Figure R24) and the fact that there was not any additional mutation that could prevent monosomic cells' death, together with the fact that these nuclei are not pyknotic, present pretty convincing evidence that these are hemocytes that phagocyted the RFP-marked monosomic cells retaining their fluorescence.

Overall, these considerations present the technique developed in this study as a promising tool to investigate unaddressed issues such as the succession of events in aneuploidy-induced extrusion, the role of Xrp1 in the process of delamination, and the role of the immune system in clearance of aneuploid cells.

5.3.2. Application of molecular techniques

In the present study, we have focused on characterizing aneuploidy-induced behaviors by macroscopy and confocal microscopy and we have investigated molecular mechanisms underlying the observed growth and

survival phenotypes by epistatic interactions. In this section, I will discuss limitations of this approach and propose different application of the tools.

By using the RS FRTs to induce red segmental monosomies in the adult eye, the type of analysis that we could perform were limited by one main technical problem: almost all Gal4 and RNA-i transgenes in *Drosophila* bear a sequence of the *white* gene, as a way to positively select animals that successfully incorporated the transgene (Pirrotta, 1988). By using these tools, the entire eye would be red and therefore segmental aneuploid clones would not be visible. For this reason, to perform epistatic analysis, we have made use of mutants in a *white* mutant genetic background. Additionally, no anti-White antibody is available therefore not allowing for clonal analysis of aneuploid cells in larval tissue by confocal microscopy. A few laboratories had developed an anti-White antibody (Mackenzie et al., 2000; Borycz et al., 2008) but unfortunately had no remaining aliquots. Furthermore, the White protein is a trans-membrane transporter and highly sensitive antibody are hard to obtain. Producing anti-White antibody was beyond the scope of this work, but it would be a way to expand the analysis that we could make on segmental monosomies induced through RS-FRTs. Applying molecular techniques such as RNA extraction and sequencing to this set up would be extremely complicated since cells that underwent recombination and are therefore aneuploid cannot be specifically isolated.

The TSG technique *in trans* allows for more flexibility. In fact, isolation of fluorescently labeled cells from larval tissues by FACS is a widely diffused technique (Khan et al., 2016). Once isolated, qPCR or transcriptome analysis could be performed allowing to broaden candidates underlying the observed defects. However, to visualize the fluorescent markers in this work, we had to use anti-GFP and -RFP antibodies. It is possible that the fluorescence would be detected by the cell sorter, which has a much higher sensitivity, making this approach feasible. Otherwise, single-cell sequencing approaches should be implemented, and the GFP and RFP transcripts would serve as markers of the trisomic and monosomic populations in the UMAP plot (Everetts et al., 2021).

6. Future directions

In the future, the system developed in this study could be applied to studying segmental aneuploidies potentially across all fly genome and, as previously discussed, could be implemented in mice or human cells to assess haploinsufficiency, triplosensitivity, and their interaction for all chromosome segments.

In the present study, we focused on epithelial tissues. In the future, segmental aneuploidies in other tissues of *Drosophila* could be studied such as stem cells (neural stem cells, intestinal stem cells, germinal stem cells) or immune cells.

Alternatively, by engineering the system with inverted FRTs, we could generate dicentric chromosome for the study of chromosome bridges and micronuclei *in vivo*.

Conclusions

1. The Flp/FRT system can be efficiently used *in cis* to induce clones of cells carrying segmental monosomies of different sizes and ranges of overlap and characterize their impact on growth and survival

2.The Flp/FRT system can be efficiently used *in trans* to simultaneously induce clones of cells carrying complementary monosomies and trisomies of different sizes and ranges of overlap and characterize their impact on growth and survival, as well as unravel the role of cell interactions in shaping clonal behavior.

3. The genome is populated by dosage sensitive loci that act through different haploinsufficiency and triplosensitivity mechanisms to lead to the elimination of aneuploid cells.

3.1. Segmental monosomies in a wild type tissue are either eliminated through *Xrp1-mTor* dependent cell competition when they include *Mn* genes or through *Xrp1-mTor* independent cumulative haploinsufficiency-dependent mechanisms.

3.2. *Rpl26* is identified as a *Mn*-like haploinsufficient gene that when present in three copies induces Xrp1-dependent lethality in its monosomic twin.

3.3. In the region 72-73, *fwe* and other unidentified genes are responsible for the supercompetitive behavior of 72-73 trisomies that overgrow at the expense of their monosomic twin, which is outcompeted, in a Xrp1-independent process.

3.4. Cumulative haploinsufficiency acts in an additive manner to worsen other types of cell competition.

3.5. The region 76-80 of the 3L and the region 87-92 of the 3R are identified as triplosensitive loci.

4. Interactions between trisomic and monosomic cells as well as their interaction with wild type cells determines elimination or survival of aneuploid cells.

References

Abdel-Hafiz, H. A., Schafer, J. M., Chen, X., Xiao, T., Gauntner, T. D., Li, Z., & Theodorescu, D. (2023). Y chromosome loss in cancer drives growth by evasion of adaptive immunity. *Nature*, *619*(7970), 624–631. https://doi.org/10.1038/s41586-023-06234-x

Abyzov, A., Mariani, J., Palejev, D., Zhang, Y., Haney, M. S., Tomasini, L., Ferrandino, A. F., Rosenberg Belmaker, L. A., Szekely, A., Wilson, M., Kocabas, A., Calixto, N. E., Grigorenko, E. L., Huttner, A., Chawarska, K., Weissman, S., Urban, A. E., Gerstein, M., & Vaccarino, F. M. (2012). Somatic copy number mosaicism in human skin revealed by induced pluripotent stem cells. *Nature*, *492*(7429), 438–442. https://doi.org/10.1038/nature11629

Adikusuma, F., Williams, N., Grutzner, F., Hughes, J., & Thomas, P. (2017). Targeted Deletion of an Entire Chromosome Using CRISPR/Cas9. *Molecular Therapy: The Journal of the American Society of Gene Therapy*, *25*(8), 1736–1738. https://doi.org/10.1016/j.ymthe.2017.05.021

Agrawal, N., Kango, M., Mishra, A., & Sinha, P. (1995). Neoplastic Transformation and Aberrant Cell–Cell Interactions in Genetic Mosaics of*lethal(2)giant larvae (lgl),*a Tumor Suppressor Gene of*Drosophila*. *Developmental Biology*, *172*(1), 218–229. https://doi.org/10.1006/dbio.1995.0017

Akdemir, F., Christich, A., Sogame, N., Chapo, J., & Abrams, J. M. (2007). P53 directs focused genomic responses in Drosophila. *Oncogene*, *26*(36), 5184–5193. https://doi.org/10.1038/sj.onc.1210328

Alimonti, A., Nardella, C., Chen, Z., Clohessy, J. G., Carracedo, A., Trotman, L. C., Cheng, K., Varmeh, S., Kozma, S. C., Thomas, G., Rosivatz, E., Woscholski, R., Cognetti, F., Scher, H. I., & Pandolfi, P. P. (2010). A novel type of cellular senescence that can be enhanced in mouse models and human tumor xenografts to suppress prostate tumorigenesis. *The Journal of Clinical Investigation*, *120*(3), 681–693. https://doi.org/10.1172/JCI40535

Amor, D. J., Neo, W. T., Waters, E., Heussler, H., Pertile, M., & Halliday, J. (2006). Health and developmental outcome of children following prenatal diagnosis of confined placental mosaicism. *Prenatal Diagnosis*, *26*(5), 443–448. https://doi.org/10.1002/pd.1433

Andriani, G. A., Almeida, V. P., Faggioli, F., Mauro, M., Tsai, W. L., Santambrogio, L., Maslov, A., Gadina, M., Campisi, J., Vijg, J., & Montagna, C. (2016). Whole Chromosome Instability induces senescence and promotes SASP. *Scientific Reports*, *6*, 35218. https://doi.org/10.1038/srep35218

Andriani, G. A., Vijg, J., & Montagna, C. (2017). Mechanisms and consequences of aneuploidy and chromosome instability in the aging brain. *Mechanisms of Ageing and Development*, *161*(Pt A), 19–36. https://doi.org/10.1016/j.mad.2016.03.007

Antonarakis, S. E., Avramopoulos, D., Blouin, J. L., Talbot, C. C., & Schinzel, A. A. (1993). Mitotic errors in somatic cells cause trisomy 21 in about 4.5% of cases and are not associated with advanced maternal age. *Nature Genetics*, *3*(2), 146–150. https://doi.org/10.1038/ng0293-146

Antonarakis, S. E., Skotko, B. G., Rafii, M. S., Strydom, A., Pape, S. E., Bianchi, D. W., Sherman, S. L., & Reeves, R. H. (2020). Down syndrome. *Nature Reviews Disease Primers*, *6*(1), 1–20. https://doi.org/10.1038/s41572-019-0143-7

Augui, S., Filion, G. J., Huart, S., Nora, E., Guggiari, M., Maresca, M., Stewart, A. F., & Heard, E. (2007). Sensing X chromosome pairs before X inactivation via a novel X-pairing region of the Xic. *Science (New York, N.Y.)*, *318*(5856), 1632–1636. https://doi.org/10.1126/science.1149420

Babariya, D., Fragouli, E., Alfarawati, S., Spath, K., & Wells, D. (2017). The incidence and origin of segmental aneuploidy in human oocytes and preimplantation embryos. *Human Reproduction*, *32*(12), 2549–2560. https://doi.org/10.1093/humrep/dex324

Bacher, C. P., Guggiari, M., Brors, B., Augui, S., Clerc, P., Avner, P., Eils, R., & Heard, E. (2006). Transient colocalization of X-inactivation centres accompanies the initiation of X inactivation. *Nature Cell Biology*, *8*(3), 293–299. https://doi.org/10.1038/ncb1365

Baillon, L., Germani, F., Rockel, C., Hilchenbach, J., & Basler, K. (2018). Xrp1 is a transcription factor required for cell competition-driven elimination of loser cells. *Scientific Reports*, *8*(1), Article 1. https://doi.org/10.1038/s41598-018-36277-4

Baker, D. E. C., Harrison, N. J., Maltby, E., Smith, K., Moore, H. D., Shaw, P. J., Heath, P. R., Holden, H., & Andrews, P. W. (2007). Adaptation to culture of human embryonic stem cells and oncogenesis in vivo. *Nature Biotechnology*, *25*(2), 207–215. https://doi.org/10.1038/nbt1285

Baker, D., Hirst, A. J., Gokhale, P. J., Juarez, M. A., Williams, S., Wheeler, M., Bean, K., Allison, T. F., Moore, H. D., Andrews, P. W., & Barbaric, I. (2016). Detecting Genetic Mosaicism in Cultures of Human Pluripotent Stem Cells. *Stem Cell Reports*, *7*(5), 998–1012. https://doi.org/10.1016/j.stemcr.2016.10.003

Baker, D. J., Dawlaty, M. M., Wijshake, T., Jeganathan, K. B., Malureanu, L., van Ree, J. H., Crespo-Diaz, R., Reyes, S., Seaburg, L., Shapiro, V., Behfar, A., Terzic, A., van de Sluis, B., & van Deursen, J. M. (2013). Increased expression of BubR1 protects against aneuploidy and cancer and extends healthy lifespan. *Nature Cell Biology*, *15*(1), 96–102. https://doi.org/10.1038/ncb2643

Baker, D. J., Jeganathan, K. B., Cameron, J. D., Thompson, M., Juneja, S., Kopecka, A., Kumar, R., Jenkins, R. B., de Groen, P. C., Roche, P., & van Deursen, J. M. (2004). BubR1 insufficiency causes early onset of aging-associated phenotypes and infertility in mice. *Nature Genetics*, *36*(7), 744–749. https://doi.org/10.1038/ng1382

Baker, N. E. (2020). Emerging mechanisms of cell competition. *Nature Reviews Genetics*, *21*(11), 683–697. https://doi.org/10.1038/s41576-020-0262-8

Baker, N. E., Kiparaki, M., & Khan, C. (2019). A potential link between p53, cell competition and ribosomopathy in mammals and in *Drosophila*. *Developmental Biology*, *446*(1), 17–19. https://doi.org/10.1016/j.ydbio.2018.11.018

Bakhoum, S. F., Ngo, B., Laughney, A. M., Cavallo, J.-A., Murphy, C. J., Ly, P., Shah, P., Sriram, R. K., Watkins, T. B. K., Taunk, N. K., Duran, M., Pauli, C., Shaw, C., Chadalavada, K., Rajasekhar, V. K.,

Genovese, G., Venkatesan, S., Birkbak, N. J., McGranahan, N., … Cantley, L. C. (2018). Chromosomal instability drives metastasis through a cytosolic DNA response. *Nature*, *553*(7689), 467–472. https://doi.org/10.1038/nature25432

Balbeur, S., Grisart, B., Parmentier, B., Sartenaer, D., Leonard, P., Ullmann, U., Boulanger, S., Leroy, L., Ngendahayo, P., Lungu-Silviu, C., Lysy, P., & Maystadt, I. (2016). Trisomy rescue mechanism: The case of concomitant mosaic trisomy 14 and maternal uniparental disomy 14 in a 15-year-old girl. *Clinical Case Reports*, *4*(3), 265–271. https://doi.org/10.1002/ccr3.501

Ballesteros-Arias, L., Saavedra, V., & Morata, G. (2014). Cell competition may function either as tumour-suppressing or as tumour-stimulating factor in Drosophila. *Oncogene*, *33*(35), 4377–4384. https://doi.org/10.1038/onc.2013.407

Baumgartner, M. E., Dinan, M. P., Langton, P. F., Kucinski, I., & Piddini, E. (2021). Proteotoxic stress is a driver of the loser status and cell competition. *Nature Cell Biology*, *23*(2), 136–146. https://doi.org/10.1038/s41556-020-00627-0

Beach, R. R., Ricci-Tam, C., Brennan, C. M., Moomau, C. A., Hsu, P.-H., Hua, B., Silberman, R. E., Springer, M., & Amon, A. (2017). Aneuploidy Causes Non-genetic Individuality. *Cell*, *169*(2), 229-242.e21. https://doi.org/10.1016/j.cell.2017.03.021

Bellott, D. W., Hughes, J. F., Skaletsky, H., Brown, L. G., Pyntikova, T., Cho, T.-J., Koutseva, N., Zaghlul, S., Graves, T., Rock, S., Kremitzki, C., Fulton, R. S., Dugan, S., Ding, Y., Morton, D., Khan, Z., Lewis, L., Buhay, C., Wang, Q., … Page, D. C. (2014). Mammalian Y chromosomes retain widely expressed dosage-sensitive regulators. *Nature*, *508*(7497), 494–499. https://doi.org/10.1038/nature13206

Berger, A. H., & Pandolfi, P. P. (2011). Haplo-insufficiency: A driving force in cancer. *The Journal of Pathology*, *223*(2), 138–147. https://doi.org/10.1002/path.2800

Berglund, A., Stochholm, K., & Gravholt, C. H. (2020). The epidemiology of sex chromosome abnormalities. *American Journal of Medical Genetics Part C: Seminars in Medical Genetics*, *184*(2), 202–215. https://doi.org/10.1002/ajmg.c.31805

Beroukhim, R., Mermel, C. H., Porter, D., Wei, G., Raychaudhuri, S., Donovan, J., Barretina, J., Boehm, J. S., Dobson, J., Urashima, M., Mc Henry, K. T., Pinchback, R. M., Ligon, A. H., Cho, Y.-J., Haery, L., Greulich, H., Reich, M., Winckler, W., Lawrence, M. S., … Meyerson, M. (2010). The landscape of somatic copy-number alteration across human cancers. *Nature*, *463*(7283), 899–905. https://doi.org/10.1038/nature08822

Bilder, D., Li, M., & Perrimon, N. (2000). Cooperative regulation of cell polarity and growth by Drosophila tumor suppressors. *Science (New York, N.Y.)*, *289*(5476), 113–116. https://doi.org/10.1126/science.289.5476.113

Boglev, Y., Badrock, A. P., Trotter, A. J., Du, Q., Richardson, E. J., Parslow, A. C., Markmiller, S. J., Hall, N. E., Jong-Curtain, T. A. de, Ng, A. Y., Verkade, H., Ober, E. A., Field, H. A., Shin, D., Shin, C. H., Hannan, K. M., Hannan, R. D., Pearson, R. B., Kim, S.-H., … Heath, J. K. (2013). Autophagy

Induction Is a Tor- and Tp53-Independent Cell Survival Response in a Zebrafish Model of Disrupted Ribosome Biogenesis. *PLOS Genetics*, *9*(2), e1003279. https://doi.org/10.1371/journal.pgen.1003279

Bohlen, J., Zhou, Q., Philippot, Q., Ogishi, M., Rinchai, D., Nieminen, T., Seyedpour, S., Parvaneh, N., Rezaei, N., Yazdanpanah, N., Momenilandi, M., Conil, C., Neehus, A.-L., Schmidt, C., Arango-Franco, C. A., Voyer, T. L., Khan, T., Yang, R., Puchan, J., … Casanova, J.-L. (2023). Human MCTS1-dependent translation of JAK2 is essential for IFN-γ immunity to mycobacteria. *Cell*, *186*(23), 5114-5134.e27. https://doi.org/10.1016/j.cell.2023.09.024

Bojesen, A., Juul, S., & Gravholt, C. H. (2003). Prenatal and postnatal prevalence of Klinefelter syndrome: A national registry study. *The Journal of Clinical Endocrinology and Metabolism*, *88*(2), 622–626. https://doi.org/10.1210/jc.2002-021491

Bolton, H., Graham, S. J. L., Van der Aa, N., Kumar, P., Theunis, K., Fernandez Gallardo, E., Voet, T., & Zernicka-Goetz, M. (2016). Mouse model of chromosome mosaicism reveals lineage-specific depletion of aneuploid cells and normal developmental potential. *Nature Communications*, *7*(1), 11165. https://doi.org/10.1038/ncomms11165

Bondar, T., & Medzhitov, R. (2010). P53-Mediated Hematopoietic Stem and Progenitor Cell Competition. *Cell Stem Cell*, *6*(4), 309–322. https://doi.org/10.1016/j.stem.2010.03.002

Bonomi, M., Rochira, V., Pasquali, D., Balercia, G., Jannini, E. A., Ferlin, A., & Klinefelter ItaliaN Group (KING). (2017). Klinefelter syndrome (KS): Genetics, clinical phenotype and hypogonadism. *Journal of Endocrinological Investigation*, *40*(2), 123–134. https://doi.org/10.1007/s40618-016-0541-6

Borycz, J., Borycz, J. A., Kubów, A., Lloyd, V., & Meinertzhagen, I. A. (2008). Drosophila ABC transporter mutants white, brown and scarlet have altered contents and distribution of biogenic amines in the brain. *The Journal of Experimental Biology*, *211*(Pt 21), 3454–3466. https://doi.org/10.1242/jeb.021162

Bosco, N., Goldberg, A., Zhao, X., Mays, J. C., Cheng, P., Johnson, A. F., Bianchi, J. J., Toscani, C., Di Tommaso, E., Katsnelson, L., Annuar, D., Mei, S., Faitelson, R. E., Pesselev, I. Y., Mohamed, K. S., Mermerian, A., Camacho-Hernandez, E. M., Gionco, C. A., Manikas, J., … Davoli, T. (2023). KaryoCreate: A CRISPR-based technology to study chromosome-specific aneuploidy by targeting human centromeres. *Cell*, *186*(9), 1985-2001.e19. https://doi.org/10.1016/j.cell.2023.03.029

Bowling, S., Di Gregorio, A., Sancho, M., Pozzi, S., Aarts, M., Signore, M., D. Schneider, M., Martinez-Barbera, J. P., Gil, J., & Rodríguez, T. A. (2018). P53 and mTOR signalling determine fitness selection through cell competition during early mouse embryonic development. *Nature Communications*, *9*(1), 1763. https://doi.org/10.1038/s41467-018-04167-y

Brand, A. H., & Perrimon, N. (1993). Targeted gene expression as a means of altering cell fates and generating dominant phenotypes. *Development (Cambridge, England)*, *118*(2), 401–415.

Brennan, C. M., Vaites, L. P., Wells, J. N., Santaguida, S., Paulo, J. A., Storchova, Z., Harper, J. W., Marsh, J. A., & Amon, A. (2019). Protein aggregation mediates stoichiometry of protein complexes in aneuploid cells. *Genes & Development*, *33*(15–16), 1031–1047. https://doi.org/10.1101/gad.327494.119

Brezina, P., Barker, A., Benner, A., Ross, R., Nguyen, K.-H., Anchan, R., Richter, K., Cutting, G., & Kearns, W. (2011). Genetic Normalization of Differentiating Aneuploid Human Embryos. *Nature Precedings*, 1–1. https://doi.org/10.1038/npre.2011.6045.1

Bridges, C. B. (1921). Triploid Intersexes in Drosophila melanogaster. *Science*, *54*(1394), 252–254. https://doi.org/10.1126/science.54.1394.252

Bridges, C. B. (1925). Sex in Relation to Chromosomes and Genes. *The American Naturalist*, *59*(661), 127–137.

Brown, S., Pineda, C. M., Xin, T., Boucher, J., Suozzi, K. C., Park, S., Matte-Martone, C., Gonzalez, D. G., Rytlewski, J., Beronja, S., & Greco, V. (2017). Correction of aberrant growth preserves tissue homeostasis. *Nature*, *548*(7667), 334–337. https://doi.org/10.1038/nature23304

Bruder, C. E. G., Piotrowski, A., Gijsbers, A. A. C. J., Andersson, R., Erickson, S., Diaz de Ståhl, T., Menzel, U., Sandgren, J., von Tell, D., Poplawski, A., Crowley, M., Crasto, C., Partridge, E. C., Tiwari, H., Allison, D. B., Komorowski, J., van Ommen, G.-J. B., Boomsma, D. I., Pedersen, N. L., … Dumanski, J. P. (2008). Phenotypically Concordant and Discordant Monozygotic Twins Display Different DNA Copy-Number-Variation Profiles. *American Journal of Human Genetics*, *82*(3), 763–771. https://doi.org/10.1016/j.ajhg.2007.12.011

Brumby, A. M., & Richardson, H. E. (2003). Scribble mutants cooperate with oncogenic Ras or Notch to cause neoplastic overgrowth in Drosophila. *The EMBO Journal*, *22*(21), 5769–5779. https://doi.org/10.1093/emboj/cdg548

Buckley, C. E., & St Johnston, D. (2022). Apical-basal polarity and the control of epithelial form and function. *Nature Reviews. Molecular Cell Biology*, *23*(8), 559–577. https://doi.org/10.1038/s41580-022-00465-y

Bugge, M., Collins, A., Hertz, J. M., Eiberg, H., Lundsteen, C., Brandt, C. A., Bak, M., Hansen, C., deLozier, C. D., Lespinasse, J., Tranebjaerg, L., Hahnemann, J. M. D., Rasmussen, K., Bruun-Petersen, G., Duprez, L., Tommerup, N., & Petersen, M. B. (2007). Non-disjunction of chromosome 13. *Human Molecular Genetics*, *16*(16), 2004–2010. https://doi.org/10.1093/hmg/ddm148

Burgoyne, P. S., & Baker, T. G. (1981). Oocyte depletion in XO mice and their XX sibs from 12 to 200 days post partum. *Journal of Reproduction and Fertility*, *61*(1), 207–212. https://doi.org/10.1530/jrf.0.0610207

Burgoyne, P. S., Evans, E. P., & Holland, K. (1983). XO monosomy is associated with reduced birthweight and lowered weight gain in the mouse. *Journal of Reproduction and Fertility*, *68*(2), 381–385. https://doi.org/10.1530/jrf.0.0680381

Burrell, R. A., McClelland, S. E., Endesfelder, D., Groth, P., Weller, M.-C., Shaikh, N., Domingo, E., Kanu, N., Dewhurst, S. M., Gronroos, E., Chew, S. K., Rowan, A. J., Schenk, A., Sheffer, M., Howell, M., Kschischo, M., Behrens, A., Helleday, T., Bartek, J., … Swanton, C. (2013). Replication stress links structural and numerical cancer chromosomal instability. *Nature*, *494*(7438), 492–496. https://doi.org/10.1038/nature11935

Cahill, D. P., Lengauer, C., Yu, J., Riggins, G. J., Willson, J. K., Markowitz, S. D., Kinzler, K. W., & Vogelstein, B. (1998). Mutations of mitotic checkpoint genes in human cancers. *Nature*, *392*(6673), 300–303. https://doi.org/10.1038/32688

Calamita, P., Miluzio, A., Russo, A., Pesce, E., Ricciardi, S., Khanim, F., Cheroni, C., Alfieri, R., Mancino, M., Gorrini, C., Rossetti, G., Peluso, I., Pagani, M., Medina, D. L., Rommens, J., & Biffo, S. (2017). SBDS-Deficient Cells Have an Altered Homeostatic Equilibrium due to Translational Inefficiency Which Explains their Reduced Fitness and Provides a Logical Framework for Intervention. *PLOS Genetics*, *13*(1), e1006552. https://doi.org/10.1371/journal.pgen.1006552

Capalbo, A., Poli, M., Rienzi, L., Girardi, L., Patassini, C., Fabiani, M., Cimadomo, D., Benini, F., Farcomeni, A., Cuzzi, J., Rubio, C., Albani, E., Sacchi, L., Vaiarelli, A., Figliuzzi, M., Findikli, N., Coban, O., Boynukalin, F. K., Vogel, I., … Simón, C. (2021). Mosaic human preimplantation embryos and their developmental potential in a prospective, non-selection clinical trial. *The American Journal of Human Genetics*, *108*(12), 2238–2247. https://doi.org/10.1016/j.ajhg.2021.11.002

Carrel, L., & Willard, H. F. (2005). X-inactivation profile reveals extensive variability in X-linked gene expression in females. *Nature*, *434*(7031), 400–404. https://doi.org/10.1038/nature03479

Casas-Tintó, S., & Ferrús, A. (2021). The haplolethality paradox of the wupA gene in Drosophila. *PLoS Genetics*, *17*(3), e1009108. https://doi.org/10.1371/journal.pgen.1009108

Casas-Tintó, S., Lolo, F.-N., & Moreno, E. (2015). Active JNK-dependent secretion of Drosophila Tyrosyl-tRNA synthetase by loser cells recruits haemocytes during cell competition. *Nature Communications*, *6*, 10022. https://doi.org/10.1038/ncomms10022

Cereda, A., & Carey, J. C. (2012). The trisomy 18 syndrome. *Orphanet Journal of Rare Diseases*, *7*(1), Article 1. https://doi.org/10.1186/1750-1172-7-81

Chang, Y.-Y., & Neufeld, T. P. (2009). An Atg1/Atg13 Complex with Multiple Roles in TOR-mediated Autophagy Regulation. *Molecular Biology of the Cell*, *20*(7), 2004–2014. https://doi.org/10.1091/mbc.e08-12-1250

Chavli, E. A., Klaasen, S. J., Van Opstal, D., Laven, J. S., Kops, G. J., & Baart, E. B. (2024). Single-cell DNA sequencing reveals a high incidence of chromosomal abnormalities in human blastocysts. *The Journal of Clinical Investigation*, *134*(6), e174483. https://doi.org/10.1172/JCI174483

Chen, Z., Trotman, L. C., Shaffer, D., Lin, H.-K., Dotan, Z. A., Niki, M., Koutcher, J. A., Scher, H. I., Ludwig, T., Gerald, W., Cordon-Cardo, C., & Pandolfi, P. P. (2005). Crucial role of p53-dependent cellular senescence in suppression of Pten-deficient tumorigenesis. *Nature*, *436*(7051), 725–730. https://doi.org/10.1038/nature03918

Chiang, T., Duncan, F. E., Schindler, K., Schultz, R. M., & Lampson, M. A. (2010). Evidence that weakened centromere cohesion is a leading cause of age-related aneuploidy in oocytes. *Current Biology: CB*, *20*(17), 1522–1528. https://doi.org/10.1016/j.cub.2010.06.069

Chinta, S. J., Woods, G., Rane, A., Demaria, M., Campisi, J., & Andersen, J. K. (2015). Cellular senescence and the aging brain. *Experimental Gerontology*, *68*, 3–7. https://doi.org/10.1016/j.exger.2014.09.018

Chunduri, N. K., Menges, P., Zhang, X., Wieland, A., Gotsmann, V. L., Mardin, B. R., Buccitelli, C., Korbel, J. O., Willmund, F., Kschischo, M., Raeschle, M., & Storchova, Z. (2021). Systems approaches identify the consequences of monosomy in somatic human cells. *Nature Communications*, *12*, 5576. https://doi.org/10.1038/s41467-021-25288-x

Cimini, D., Howell, B., Maddox, P., Khodjakov, A., Degrassi, F., & Salmon, E. D. (2001). Merotelic Kinetochore Orientation Is a Major Mechanism of Aneuploidy in Mitotic Mammalian Tissue Cells. *The Journal of Cell Biology*, *153*(3), 517. https://doi.org/10.1083/jcb.153.3.517

Clavería, C., Giovinazzo, G., Sierra, R., & Torres, M. (2013). Myc-driven endogenous cell competition in the early mammalian embryo. *Nature*, *500*(7460), 39–44. https://doi.org/10.1038/nature12389

Clemente-Ruiz, M., Murillo-Maldonado, J. M., Benhra, N., Barrio, L., Pérez, L., Quiroga, G., Nebreda, A. R., & Milán, M. (2016). Gene Dosage Imbalance Contributes to Chromosomal Instability-Induced Tumorigenesis. *Developmental Cell*, *36*(3), 290–302. https://doi.org/10.1016/j.devcel.2016.01.008

Collins, R. L., Glessner, J. T., Porcu, E., Lepamets, M., Brandon, R., Lauricella, C., Han, L., Morley, T., Niestroj, L.-M., Ulirsch, J., Everett, S., Howrigan, D. P., Boone, P. M., Fu, J., Karczewski, K. J., Kellaris, G., Lowther, C., Lucente, D., Mohajeri, K., … Esko, T. (2022). A cross-disorder dosage sensitivity map of the human genome. *Cell*, *185*(16), 3041-3055.e25. https://doi.org/10.1016/j.cell.2022.06.036

Colom, B., Alcolea, M. P., Piedrafita, G., Hall, M. W. J., Wabik, A., Dentro, S. C., Fowler, J. C., Herms, A., King, C., Ong, S. H., Sood, R. K., Gerstung, M., Martincorena, I., Hall, B. A., & Jones, P. H. (2020). Spatial competition shapes the dynamic mutational landscape of normal esophageal epithelium. *Nature Genetics*, *52*(6), 604–614. https://doi.org/10.1038/s41588-020-0624-3

Colom, B., Herms, A., Hall, M. W. J., Dentro, S. C., King, C., Sood, R. K., Alcolea, M. P., Piedrafita, G., Fernandez-Antoran, D., Ong, S. H., Fowler, J. C., Mahbubani, K. T., Saeb-Parsy, K., Gerstung, M., Hall, B. A., & Jones, P. H. (2021). Mutant clones in normal epithelium outcompete and eliminate emerging tumours. *Nature*, *598*(7881), 510–514. https://doi.org/10.1038/s41586-021-03965-7

Conlin, L. K., Thiel, B. D., Bonnemann, C. G., Medne, L., Ernst, L. M., Zackai, E. H., Deardorff, M. A., Krantz, I. D., Hakonarson, H., & Spinner, N. B. (2010). Mechanisms of mosaicism, chimerism and uniparental disomy identified by single nucleotide polymorphism array analysis. *Human Molecular Genetics*, *19*(7), 1263–1275. https://doi.org/10.1093/hmg/ddq003

Cook, R. K., Christensen, S. J., Deal, J. A., Coburn, R. A., Deal, M. E., Gresens, J. M., Kaufman, T. C., & Cook, K. R. (2012). The generation of chromosomal deletions to provide extensive coverage and subdivision of the Drosophila melanogaster genome. *Genome Biology*, *13*(3), R21. https://doi.org/10.1186/gb-2012-13-3-r21

Coorens, T. H. H., Oliver, T. R. W., Sanghvi, R., Sovio, U., Cook, E., Vento-Tormo, R., Haniffa, M., Young, M. D., Rahbari, R., Sebire, N., Campbell, P. J., Charnock-Jones, D. S., Smith, G. C. S., & Behjati, S. (2021). Inherent mosaicism and extensive mutation of human placentas. *Nature*, *592*(7852), 80–85. https://doi.org/10.1038/s41586-021-03345-1

Crasta, K., Ganem, N. J., Dagher, R., Lantermann, A. B., Ivanova, E. V., Pan, Y., Nezi, L., Protopopov, A., Chowdhury, D., & Pellman, D. (2012). DNA breaks and chromosome pulverization from errors in mitosis. *Nature*, *482*(7383), 53–58. https://doi.org/10.1038/nature10802

Crowley, E. A., Hermance, N. M., Herlihy, C. P., & Manning, A. L. (2022). Suppression of Chromosome Instability Limits Acquired Drug Resistance. *Molecular Cancer Therapeutics*, *21*(10), 1583–1593. https://doi.org/10.1158/1535-7163.MCT-22-0263

Csink, A. K., & Henikoff, S. (1998). Large-scale Chromosomal Movements During Interphase Progression in *Drosophila*. *The Journal of Cell Biology*, *143*(1), 13–22. https://doi.org/10.1083/jcb.143.1.13

Currie, C. E., Ford, E., Benham Whyte, L., Taylor, D. M., Mihalas, B. P., Erent, M., Marston, A. L., Hartshorne, G. M., & McAinsh, A. D. (2022). The first mitotic division of human embryos is highly error prone. *Nature Communications*, *13*(1), 6755. https://doi.org/10.1038/s41467-022-34294-6

D'Andrea, G., Deroma, G., Miluzio, A., & Biffo, S. (2024). The Paradox of Ribosomal Insufficiency Coupled with Increased Cancer: Shifting the Perspective from the Cancer Cell to the Microenvironment. *Cancers*, *16*(13), Article 13. https://doi.org/10.3390/cancers16132392

Dang, V. T., Kassahn, K. S., Marcos, A. E., & Ragan, M. A. (2008). Identification of human haploinsufficient genes and their genomic proximity to segmental duplications. *European Journal of Human Genetics: EJHG*, *16*(11), 1350–1357. https://doi.org/10.1038/ejhg.2008.111

Danilova, N., Sakamoto, K. M., & Lin, S. (2011). Ribosomal protein L11 mutation in zebrafish leads to haematopoietic and metabolic defects. *British Journal of Haematology*, *152*(2), 217–228. https://doi.org/10.1111/j.1365-2141.2010.08396.x

Daughtry, B. L., Rosenkrantz, J. L., Lazar, N. H., Fei, S. S., Redmayne, N., Torkenczy, K. A., Adey, A., Yan, M., Gao, L., Park, B., Nevonen, K. A., Carbone, L., & Chavez, S. L. (2019). Single-cell sequencing of primate preimplantation embryos reveals chromosome elimination via cellular fragmentation and blastomere exclusion. *Genome Research*, *29*(3), 367–382. https://doi.org/10.1101/gr.239830.118

Davoli, T., Uno, H., Wooten, E. C., & Elledge, S. J. (2017). Tumor aneuploidy correlates with markers of immune evasion and with reduced response to immunotherapy. *Science (New York, N.Y.)*, *355*(6322), eaaf8399. https://doi.org/10.1126/science.aaf8399

Davoli, T., Xu, A. W., Mengwasser, K. E., Sack, L. M., Yoon, J. C., Park, P. J., & Elledge, S. J. (2013). Cumulative haploinsufficiency and triplosensitivity drive aneuploidy patterns and shape the cancer genome. *Cell*, *155*(4), 948–962. https://doi.org/10.1016/j.cell.2013.10.011

De Keersmaecker, K., Sulima, S. O., & Dinman, J. D. (2015). Ribosomopathies and the paradox of cellular hypo- to hyperproliferation. *Blood*, *125*(9), 1377–1382. https://doi.org/10.1182/blood-2014-10-569616

de la Cova, C., Abril, M., Bellosta, P., Gallant, P., & Johnston, L. A. (2004). Drosophila myc regulates organ size by inducing cell competition. *Cell*, *117*(1), 107–116. https://doi.org/10.1016/s0092-8674(04)00214-4

de la Cova, C., Senoo-Matsuda, N., Ziosi, M., Wu, D. C., Bellosta, P., Quinzii, C. M., & Johnston, L. A. (2014). Supercompetitor Status of *Drosophila* Myc Cells Requires p53 as a Fitness Sensor to Reprogram Metabolism and Promote Viability. *Cell Metabolism*, *19*(3), 470–483. https://doi.org/10.1016/j.cmet.2014.01.012

Degtyareva, N. P., Chen, L., Mieczkowski, P., Petes, T. D., & Doetsch, P. W. (2008). Chronic Oxidative DNA Damage Due to DNA Repair Defects Causes Chromosomal Instability in Saccharomyces cerevisiae. *Molecular and Cellular Biology*, *28*(17), 5432–5445. https://doi.org/10.1128/MCB.00307-08

Deisenroth, C., Franklin, D. A., & Zhang, Y. (2016). The Evolution of the Ribosomal Protein-MDM2-p53 Pathway. *Cold Spring Harbor Perspectives in Medicine*, *6*(12), a026138. https://doi.org/10.1101/cshperspect.a026138

Dekanty, A., Barrio, L., Muzzopappa, M., Auer, H., & Milán, M. (2012). Aneuploidy-induced delaminating cells drive tumorigenesis in Drosophila epithelia. *Proceedings of the National Academy of Sciences*, *109*(50), 20549–20554. https://doi.org/10.1073/pnas.1206675109

Denell, R. E. (1976). The genetic analysis of a uniquely dose-sensitive chromosomal region of Drosophila melanogaster. *Genetics*, *84*(2), 193–210. https://doi.org/10.1093/genetics/84.2.193

Deng, C., Ya, A., Compton, D. A., & Godek, K. M. (2023). A pluripotent developmental state confers a low fidelity of chromosome segregation. *Stem Cell Reports*, *18*(2), 475–488. https://doi.org/10.1016/j.stemcr.2022.12.008

Dephoure, N., Hwang, S., O'Sullivan, C., Dodgson, S. E., Gygi, S. P., Amon, A., & Torres, E. M. (2014). Quantitative proteomic analysis reveals posttranslational responses to aneuploidy in yeast. *eLife*, *3*, e03023. https://doi.org/10.7554/eLife.03023

Di Rocco, M., Rusmini, M., Caroli, F., Madeo, A., Bertamino, M., Marre-Brunenghi, G., & Ceccherini, I. (2018). Novel spondyloepimetaphyseal dysplasia due to UFSP2 gene mutation. *Clinical Genetics*, *93*(3), 671–674. https://doi.org/10.1111/cge.13134

Díaz-Díaz, C., Fernandez de Manuel, L., Jimenez-Carretero, D., Montoya, M. C., Clavería, C., & Torres, M. (2017). Pluripotency Surveillance by Myc-Driven Competitive Elimination of Differentiating Cells. *Developmental Cell*, *42*(6), 585-599.e4. https://doi.org/10.1016/j.devcel.2017.08.011

Díaz-Díaz, C., Manuel, L. F. de, Jimenez-Carretero, D., Montoya, M. C., Clavería, C., & Torres, M. (2017). Pluripotency Surveillance by Myc-Driven Competitive Elimination of Differentiating Cells. *Developmental Cell*, *42*(6), 585-599.e4. https://doi.org/10.1016/j.devcel.2017.08.011

Dierssen, M., Herault, Y., & Estivill, X. (2009). Aneuploidy: From a physiological mechanism of variance to Down syndrome. *Physiological Reviews*, *89*(3), 887–920. https://doi.org/10.1152/physrev.00032.2007

Ding, J., Yannam, G. R., Roy-Chowdhury, N., Hidvegi, T., Basma, H., Rennard, S. I., Wong, R. J., Avsar, Y., Guha, C., Perlmutter, D. H., Fox, I. J., & Roy-Chowdhury, J. (2011). Spontaneous hepatic repopulation in transgenic mice expressing mutant human α1-antitrypsin by wild-type donor hepatocytes. *The Journal of Clinical Investigation*, *121*(5), 1930–1934. https://doi.org/10.1172/JCI45260

Donnelly, N., Passerini, V., Dürrbaum, M., Stingele, S., & Storchová, Z. (2014). HSF1 deficiency and impaired HSP90-dependent protein folding are hallmarks of aneuploid human cells. *The EMBO Journal*, *33*(20), 2374–2387. https://doi.org/10.15252/embj.201488648

Dorer, D. R., Ezekiel, D. H., & Christensen, A. C. (1995). The Triplo-Lethal Locus of Drosophila: Reexamination of Mutants and Discovery of a Second-Site Suppressor. *Genetics*, *141*(3), 1037–1042.

Dorer, D. R., Rudnick, J. A., Moriyama, E. N., & Christensen, A. C. (2003). A family of genes clustered at the Triplo-lethal locus of Drosophila melanogaster has an unusual evolutionary history and significant synteny with Anopheles gambiae. *Genetics*, *165*(2), 613–621. https://doi.org/10.1093/genetics/165.2.613

Doulatov, S., Vo, L. T., Macari, E. R., Wahlster, L., Kinney, M. A., Taylor, A. M., Barragan, J., Gupta, M., McGrath, K., Lee, H.-Y., Humphries, J. M., DeVine, A., Narla, A., Alter, B. P., Beggs, A. H., Agarwal, S., Ebert, B. L., Gazda, H. T., Lodish, H. F., … Daley, G. Q. (2017). Drug discovery for Diamond-Blackfan anemia using reprogrammed hematopoietic progenitors. *Science Translational Medicine*, *9*(376), eaah5645. https://doi.org/10.1126/scitranslmed.aah5645

Draper, J. S., Smith, K., Gokhale, P., Moore, H. D., Maltby, E., Johnson, J., Meisner, L., Zwaka, T. P., Thomson, J. A., & Andrews, P. W. (2004). Recurrent gain of chromosomes 17q and 12 in cultured human embryonic stem cells. *Nature Biotechnology*, *22*(1), 53–54. https://doi.org/10.1038/nbt922

Duan, R., Shi, Y., Yu, L., Zhang, G., Li, J., Lin, Y., Guo, J., Wang, J., Shen, L., Jiang, H., Wang, G., & Tang, B. (2016). UBA5 Mutations Cause a New Form of Autosomal Recessive Cerebellar Ataxia. *PloS One*, *11*(2), e0149039. https://doi.org/10.1371/journal.pone.0149039

Duncan, A. W., Newell, A. E. H., Smith, L., Wilson, E. M., Olson, S. B., Thayer, M. J., Strom, S. C., & Grompe, M. (2012). Frequent Aneuploidy Among Normal Human Hepatocytes. *Gastroenterology*, *142*(1), 25–28. https://doi.org/10.1053/j.gastro.2011.10.029

Duncan, A. W., Taylor, M. H., Hickey, R. D., Hanlon Newell, A. E., Lenzi, M. L., Olson, S. B., Finegold, M. J., & Grompe, M. (2010). The ploidy conveyor of mature hepatocytes as a source of genetic variation. *Nature*, *467*(7316), 707–710. https://doi.org/10.1038/nature09414

Dürrbaum, M., Kuznetsova, A. Y., Passerini, V., Stingele, S., Stoehr, G., & Storchová, Z. (2014). Unique features of the transcriptional response to model aneuploidy in human cells. *BMC Genomics*, *15*, 139. https://doi.org/10.1186/1471-2164-15-139

Ebert, B. L. (2009). Deletion 5q in myelodysplastic syndrome: A paradigm for the study of hemizygous deletions in cancer. *Leukemia*, *23*(7), 1252–1256. https://doi.org/10.1038/leu.2009.53

Eggan, K., Rode, A., Jentsch, I., Samuel, C., Hennek, T., Tintrup, H., Zevnik, B., Erwin, J., Loring, J., Jackson-Grusby, L., Speicher, M. R., Kuehn, R., & Jaenisch, R. (2002). Male and female mice derived from the same embryonic stem cell clone by tetraploid embryo complementation. *Nature Biotechnology*, *20*(5), 455–459. https://doi.org/10.1038/nbt0502-455

Eggenhuizen, G. M., Go, A., Koster, M. P. H., Baart, E. B., & Galjaard, R. J. (2021). Confined placental mosaicism and the association with pregnancy outcome and fetal growth: A review of the literature. *Human Reproduction Update*, *27*(5), 885–903. https://doi.org/10.1093/humupd/dmab009

Egunsola, A. T., Bae, Y., Jiang, M.-M., Liu, D. S., Chen-Evenson, Y., Bertin, T., Chen, S., Lu, J. T., Nevarez, L., Magal, N., Raas-Rothschild, A., Swindell, E. C., Cohn, D. H., Gibbs, R. A., Campeau, P. M., Shohat, M., & Lee, B. H. (2017). Loss of DDRGK1 modulates SOX9 ubiquitination in spondyloepimetaphyseal dysplasia. *The Journal of Clinical Investigation*, *127*(4), 1475–1484. https://doi.org/10.1172/JCI90193

Eichenlaub, T., Cohen, S. M., & Herranz, H. (2016). Cell Competition Drives the Formation of Metastatic Tumors in a Drosophila Model of Epithelial Tumor Formation. *Current Biology*, *26*(4), 419–427. https://doi.org/10.1016/j.cub.2015.12.042

Eissenberg, J. C., Ma, J., Gerber, M. A., Christensen, A., Kennison, J. A., & Shilatifard, A. (2002). dELL is an essential RNA polymerase II elongation factor with a general role in development. *Proceedings of the National Academy of Sciences of the United States of America*, *99*(15), 9894–9899. https://doi.org/10.1073/pnas.152193699

Elghetany, M. T., & Alter, B. P. (2002). P53 Protein Overexpression in Bone Marrow Biopsies of Patients With Shwachman-Diamond Syndrome Has a Prevalence Similar to That of Patients With Refractory Anemia. *Archives of Pathology & Laboratory Medicine*, *126*(4), 452–455. https://doi.org/10.5858/2002-126-0452-PPOIBM

Ellis, S. J., Gomez, N. C., Levorse, J., Mertz, A. F., Ge, Y., & Fuchs, E. (2019). Distinct modes of cell competition shape mammalian tissue morphogenesis. *Nature*, *569*(7757), 497–502. https://doi.org/10.1038/s41586-019-1199-y

Essers, R., Lebedev, I. N., Kurg, A., Fonova, E. A., Stevens, S. J. C., Koeck, R. M., von Rango, U., Brandts, L., Deligiannis, S. P., Nikitina, T. V., Sazhenova, E. A., Tolmacheva, E. N., Kashevarova, A. A., Fedotov, D. A., Demeneva, V. V., Zhigalina, D. I., Drozdov, G. V., Al-Nasiry, S., Macville, M. V. E., … Zamani Esteki, M. (2023). Prevalence of chromosomal alterations in first-trimester spontaneous pregnancy loss. *Nature Medicine*, *29*(12), 3233–3242. https://doi.org/10.1038/s41591-023-02645-5

Everetts, N. J., Worley, M. I., Yasutomi, R., Yosef, N., & Hariharan, I. K. (2021). Single-cell transcriptomics of the Drosophila wing disc reveals instructive epithelium-to-myoblast interactions. *eLife*, *10*, e61276. https://doi.org/10.7554/eLife.61276

Evsikov, S., & Verlinsky, Y. (1998). Mosaicism in the inner cell mass of human blastocysts. *Human Reproduction*, *13*(11), 3151–3155. https://doi.org/10.1093/humrep/13.11.3151

Faggioli, F., Wang, T., Vijg, J., & Montagna, C. (2012). Chromosome-specific accumulation of aneuploidy in the aging mouse brain. *Human Molecular Genetics*, *21*(24), 5246–5253. https://doi.org/10.1093/hmg/dds375

Fan, Y., & Bergmann, A. (2008). Apoptosis-induced compensatory proliferation. The Cell is dead. Long live the Cell! *Trends in Cell Biology*, *18*(10), 467–473. https://doi.org/10.1016/j.tcb.2008.08.001

Fang, H., Disteche, C. M., & Berletch, J. B. (2019). X Inactivation and Escape: Epigenetic and Structural Features. *Frontiers in Cell and Developmental Biology*, *7*. https://doi.org/10.3389/fcell.2019.00219

Fero, M. L., Randel, E., Gurley, K. E., Roberts, J. M., & Kemp, C. J. (1998). The murine gene p27Kip1 is haplo-insufficient for tumour suppression. *Nature*, *396*(6707), 177–180. https://doi.org/10.1038/24179

Flowers, A. (2000). Brain tumors in the older person. *Cancer Control: Journal of the Moffitt Cancer Center*, *7*(6), 523–538. https://doi.org/10.1177/107327480000700604

Fournier, R. E., & Ruddle, F. H. (1977). Microcell-mediated transfer of murine chromosomes into mouse, Chinese hamster, and human somatic cells. *Proceedings of the National Academy of Sciences of the United States of America*, *74*(1), 319–323. https://doi.org/10.1073/pnas.74.1.319

Gallini, S., Annusver, K., Rahman, N.-T., Gonzalez, D. G., Yun, S., Matte-Martone, C., Xin, T., Lathrop, E., Suozzi, K. C., Kasper, M., & Greco, V. (2023). Injury prevents Ras mutant cell expansion in mosaic skin. *Nature*, *619*(7968), 167–175. https://doi.org/10.1038/s41586-023-06198-y

Ganem, N. J., Godinho, S. A., & Pellman, D. (2009). A mechanism linking extra centrosomes to chromosomal instability. *Nature*, *460*(7252), 278–282. https://doi.org/10.1038/nature08136

Gearhart, J. D., Davisson, M. T., & Oster-Granite, M. L. (1986). Autosomal aneuploidy in mice: Generation and developmental consequences. *Brain Research Bulletin*, *16*(6), 789–801. https://doi.org/10.1016/0361-9230(86)90075-4

Geigl, J. B., Langer, S., Barwisch, S., Pfleghaar, K., Lederer, G., & Speicher, M. R. (2004). Analysis of Gene Expression Patterns and Chromosomal Changes Associated with Aging. *Cancer Research*, *64*(23), 8550–8557. https://doi.org/10.1158/0008-5472.CAN-04-2151

Geyer, P. K., Green, M. M., & Corces, V. G. (1990). Tissue-specific transcriptional enhancers may act in trans on the gene located in the homologous chromosome: The molecular basis of transvection in Drosophila. *The EMBO Journal*, *9*(7), 2247–2256. https://doi.org/10.1002/j.1460-2075.1990.tb07395.x

Girish, V., Lakhani, A. A., Thompson, S. L., Scaduto, C. M., Brown, L. M., Hagenson, R. A., Sausville, E. L., Mendelson, B. E., Kandikuppa, P. K., Lukow, D. A., Yuan, M. L., Stevens, E. C., Lee, S. N., Schukken, K. M., Akalu, S. M., Vasudevan, A., Zou, C., Salovska, B., Li, W., … Sheltzer, J. M. (2023). Oncogene-like addiction to aneuploidy in human cancers. *Science (New York, N.Y.)*, *381*(6660), eadg4521. https://doi.org/10.1126/science.adg4521

Golic, K. G., & Golic, M. M. (1996). Engineering the Drosophila Genome: Chromosome Rearrangements by Design. *Genetics*, *144*(4), 1693–1711.

Golic, K. G., & Lindquist, S. (1989). The FLP recombinase of yeast catalyzes site-specific recombination in the drosophila genome. *Cell*, *59*(3), 499–509. https://doi.org/10.1016/0092-8674(89)90033-0

Graaf, G. de, Buckley, F., & Skotko, B. G. (2017). Estimation of the number of people with Down syndrome in the United States. *Genetics in Medicine*, *19*(4), 439–447. https://doi.org/10.1038/gim.2016.127

Grati, F. R., Ferreira, J., Benn, P., Izzi, C., Verdi, F., Vercellotti, E., Dalpiaz, C., D'Ajello, P., Filippi, E., Volpe, N., Malvestiti, F., Maggi, F., Simoni, G., Frusca, T., Cirelli, G., Bracalente, G., Re, A. L., Surico, D., Ghi, T., & Prefumo, F. (2020). Outcomes in pregnancies with a confined placental mosaicism and implications for prenatal screening using cell-free DNA. *Genetics in Medicine*, *22*(2), 309–316. https://doi.org/10.1038/s41436-019-0630-y

Greco, E., Minasi, M. G., & Fiorentino, F. (2015). Healthy Babies after Intrauterine Transfer of Mosaic Aneuploid Blastocysts. *New England Journal of Medicine*, *373*(21), 2089–2090. https://doi.org/10.1056/NEJMc1500421

Griffin, R., Binari, R., & Perrimon, N. (2014). Genetic odyssey to generate marked clones in *Drosophila* mosaics. *Proceedings of the National Academy of Sciences*, *111*(13), 4756–4763. https://doi.org/10.1073/pnas.1403218111

Griffin, R., Sustar, A., Bonvin, M., Binari, R., del Valle Rodriguez, A., Hohl, A. M., Bateman, J. R., Villalta, C., Heffern, E., Grunwald, D., Bakal, C., Desplan, C., Schubiger, G., Wu, C., & Perrimon, N. (2009). The twin spot generator for differential Drosophila lineage analysis. *Nature Methods*, *6*(8), 600–602. https://doi.org/10.1038/nmeth.1349

Gropp, A., Winking, H., Herbst, E. W., & Claussen, C. P. (1983). Murine trisomy: Developmental profiles of the embryo, and isolation of trisomic cellular systems. *Journal of Experimental Zoology*, *228*(2), 253–269. https://doi.org/10.1002/jez.1402280210

Guacci, V., Hogan, E., & Koshland, D. (1994). Chromosome condensation and sister chromatid pairing in budding yeast. *Journal of Cell Biology*, *125*(3), 517–530. https://doi.org/10.1083/jcb.125.3.517

Gump, J. M., & Thorburn, A. (2011). Autophagy and apoptosis: What is the connection? *Trends in Cell Biology*, *21*(7), 387–392. https://doi.org/10.1016/j.tcb.2011.03.007

Guttenbach, M., Schakowski, R., & Schmid, M. (1994). Aneuploidy and ageing: Sex chromosome exclusion into micronuclei. *Human Genetics*, *94*(3), 295–298. https://doi.org/10.1007/BF00208287

Hafezi, Y., Bosch, J. A., & Hariharan, I. K. (2012). Differences in levels of the transmembrane protein Crumbs can influence cell survival at clonal boundaries. *Developmental Biology*, *368*(2), 358–369. https://doi.org/10.1016/j.ydbio.2012.06.001

Hall, H. E., Surti, U., Hoffner, L., Shirley, S., Feingold, E., & Hassold, T. (2007). The origin of trisomy 22: Evidence for acrocentric chromosome-specific patterns of nondisjunction. *American Journal of Medical Genetics. Part A*, *143A*(19), 2249–2255. https://doi.org/10.1002/ajmg.a.31918

Han, X., Chen, S., Flynn, E., Wu, S., Wintner, D., & Shen, Y. (2018). Distinct epigenomic patterns are associated with haploinsufficiency and predict risk genes of developmental disorders. *Nature Communications*, *9*(1), 2138. https://doi.org/10.1038/s41467-018-04552-7

Hardy, K., Spanos, S., Becker, D., Iannelli, P., Winston, R. M. L., & Stark, J. (2001). From cell death to embryo arrest: Mathematical models of human preimplantation embryo development. *Proceedings of the National Academy of Sciences of the United States of America*, *98*(4), 1655–1660.

Harrison, R. H., Kuo, H. C., Scriven, P. N., Handyside, A. H., & Ogilvie, C. M. (2000). Lack of cell cycle checkpoints in human cleavage stage embryos revealed by a clonal pattern of chromosomal mosaicism analysed by sequential multicolour FISH. *Zygote (Cambridge, England)*, *8*(3), 217–224. https://doi.org/10.1017/s0967199400001015

Hashimoto, M., & Sasaki, H. (2019). Epiblast Formation by TEAD-YAP-Dependent Expression of Pluripotency Factors and Competitive Elimination of Unspecified Cells. *Developmental Cell*, *50*(2), 139-154.e5. https://doi.org/10.1016/j.devcel.2019.05.024

Hassold, T., & Hunt, P. (2001). To err (meiotically) is human: The genesis of human aneuploidy. *Nature Reviews Genetics*, *2*(4), 280–291. https://doi.org/10.1038/35066065

Hatch, E. M., Fischer, A. H., Deerinck, T. J., & Hetzer, M. W. (2013). Catastrophic nuclear envelope collapse in cancer cell micronuclei. *Cell*, *154*(1), 47–60. https://doi.org/10.1016/j.cell.2013.06.007

Heijnen, H. F., van Wijk, R., Pereboom, T. C., Goos, Y. J., Seinen, C. W., van Oirschot, B. A., van Dooren, R., Gastou, M., Giles, R. H., van Solinge, W., Kuijpers, T. W., Gazda, H. T., Bierings, M. B., Da Costa, L., & MacInnes, A. W. (2014). Ribosomal protein mutations induce autophagy through S6 kinase inhibition of the insulin pathway. *PLoS Genetics*, *10*(5), e1004371. https://doi.org/10.1371/journal.pgen.1004371

Hérault, Y., Duchon, A., Maréchal, D., Raveau, M., Pereira, P. L., Dalloneau, E., & Brault, V. (2010). Controlled somatic and germline copy number variation in the mouse model. *Current Genomics*, *11*(6), 470–480. https://doi.org/10.2174/138920210793176038

Hérault, Y., Rassoulzadegan, M., Cuzin, F., & Duboule, D. (1998). Engineering chromosomes in mice through targeted meiotic recombination (TAMERE). *Nature Genetics*, *20*(4), 381–384. https://doi.org/10.1038/3861

Hernandez-Segura, A., Nehme, J., & Demaria, M. (2018). Hallmarks of Cellular Senescence. *Trends in Cell Biology*, *28*(6), 436–453. https://doi.org/10.1016/j.tcb.2018.02.001

Herz, H.-M., Chen, Z., Scherr, H., Lackey, M., Bolduc, C., & Bergmann, A. (2006). Vps25 mosaics display non-autonomous cell survival and overgrowth, and autonomous apoptosis. *Development*, *133*(10), 1871–1880. https://doi.org/10.1242/dev.02356

Hill, W., Zaragkoulias, A., Salvador-Barbero, B., Parfitt, G. J., Alatsatianos, M., Padilha, A., Porazinski, S., Woolley, T. E., Morton, J. P., Sansom, O. J., & Hogan, C. (2021). EPHA2-dependent outcompetition of KRASG12D mutant cells by wild-type neighbors in the adult pancreas. *Current Biology*, *31*(12), 2550-2560.e5. https://doi.org/10.1016/j.cub.2021.03.094

Hintzen, D. C., Soto, M., Schubert, M., Bakker, B., Spierings, D. C. J., Szuhai, K., Lansdorp, P. M., Kluin, R. J. C., Foijer, F., Medema, R. H., & Raaijmakers, J. A. (2022). The impact of monosomies, trisomies and segmental aneuploidies on chromosomal stability. *PLOS ONE*, *17*(7), e0268579. https://doi.org/10.1371/journal.pone.0268579

Hintzsche, H., Hemmann, U., Poth, A., Utesch, D., Lott, J., & Stopper, H. (2017). Fate of micronuclei and micronucleated cells. *Mutation Research/Reviews in Mutation Research*, *771*, 85–98. https://doi.org/10.1016/j.mrrev.2017.02.002

Hiraoka, Y. (1993). The onset of homologous chromosome pairing during Drosophila melanogaster embryogenesis. *The Journal of Cell Biology*, *120*(3), 591–600. https://doi.org/10.1083/jcb.120.3.591

Holubcová, Z., Blayney, M., Elder, K., & Schuh, M. (2015). Human oocytes. Error-prone chromosome-mediated spindle assembly favors chromosome segregation defects in human oocytes. *Science (New York, N.Y.)*, *348*(6239), 1143–1147. https://doi.org/10.1126/science.aaa9529

Honda, H., Nagamachi, A., & Inaba, T. (2015). -7/7q- syndrome in myeloid-lineage hematopoietic malignancies: Attempts to understand this complex disease entity. *Oncogene*, *34*(19), 2413–2425. https://doi.org/10.1038/onc.2014.196

Hong, C., Schubert, M., Tijhuis, A. E., Requesens, M., Roorda, M., van den Brink, A., Ruiz, L. A., Bakker, P. L., van der Sluis, T., Pieters, W., Chen, M., Wardenaar, R., van der Vegt, B., Spierings, D. C. J., de Bruyn, M., van Vugt, M. A. T. M., & Foijer, F. (2022). cGAS–STING drives the IL-6-dependent survival of chromosomally instable cancers. *Nature*, *607*(7918), 366–373. https://doi.org/10.1038/s41586-022-04847-2

Hook, E. B., & Warburton, D. (1983). The distribution of chromosomal genotypes associated with Turner's syndrome: Livebirth prevalence rates and evidence for diminished fetal mortality and severity in genotypes associated with structural X abnormalities or mosaicism. *Human Genetics*, *64*(1), 24–27. https://doi.org/10.1007/BF00289473

Horii, T., Yamamoto, M., Morita, S., Kimura, M., Nagao, Y., & Hatada, I. (2015). P53 suppresses tetraploid development in mice. *Scientific Reports*, *5*, 8907. https://doi.org/10.1038/srep08907

Hou, W., Han, J., Lu, C., Goldstein, L. A., & Rabinowich, H. (2010). Autophagic degradation of active caspase-8: A crosstalk mechanism between autophagy and apoptosis. *Autophagy*, *6*(7), 891–900. https://doi.org/10.4161/auto.6.7.13038

Huang, A., Adusumalli, J., Patel, S., Liem, J., Williams, J., & Pisarska, M. D. (2009). Prevalence of chromosomal mosaicism in pregnancies from couples with infertility. *Fertility and Sterility*, *91*(6), 2355–2360. https://doi.org/10.1016/j.fertnstert.2008.03.044

Huang, N., Lee, I., Marcotte, E. M., & Hurles, M. E. (2010). Characterising and Predicting Haploinsufficiency in the Human Genome. *PLoS Genetics*, *6*(10), e1001154. https://doi.org/10.1371/journal.pgen.1001154

Hwang, S., Cavaliere, P., Li, R., Zhu, L. J., Dephoure, N., & Torres, E. M. (2021). Consequences of aneuploidy in human fibroblasts with trisomy 21. *Proceedings of the National Academy of Sciences of the United States of America*, *118*(6), e2014723118. https://doi.org/10.1073/pnas.2014723118

Igaki, T., Pagliarini, R. A., & Xu, T. (2006). Loss of cell polarity drives tumor growth and invasion through JNK activation in Drosophila. *Current Biology: CB*, *16*(11), 1139–1146. https://doi.org/10.1016/j.cub.2006.04.042

Igaki, T., Pastor-Pareja, J. C., Aonuma, H., Miura, M., & Xu, T. (2009). Intrinsic Tumor Suppression and Epithelial Maintenance by Endocytic Activation of Eiger/TNF Signaling in Drosophila. *Developmental Cell*, *16*(3), 458–465. https://doi.org/10.1016/j.devcel.2009.01.002

Inoue, K., & Fry, E. A. (2017). Haploinsufficient tumor suppressor genes. *Advances in Medicine and Biology*, *118*, 83–122.

Iourov, I. Y., Vorsanova, S. G., Liehr, T., & Yurov, Y. B. (2009). Aneuploidy in the normal, Alzheimer's disease and ataxia-telangiectasia brain: Differential expression and pathological meaning. *Neurobiology of Disease*, *34*(2), 212–220. https://doi.org/10.1016/j.nbd.2009.01.003

Iourov, I. Y., Vorsanova, S. G., & Yurov, Y. B. (2010). Somatic Genome Variations in Health and Disease. *Current Genomics*, *11*(6), 387–396. https://doi.org/10.2174/138920210793176065

Ippolito, M. R., Martis, V., Martin, S., Tijhuis, A. E., Hong, C., Wardenaar, R., Dumont, M., Zerbib, J., Spierings, D. C. J., Fachinetti, D., Ben-David, U., Foijer, F., & Santaguida, S. (2021). Gene copy-number changes and chromosomal instability induced by aneuploidy confer resistance to chemotherapy. *Developmental Cell*, *56*(17), 2440-2454.e6. https://doi.org/10.1016/j.devcel.2021.07.006

Jacobs, K. B., Yeager, M., Zhou, W., Wacholder, S., Wang, Z., Rodriguez-Santiago, B., Hutchinson, A., Deng, X., Liu, C., Horner, M.-J., Cullen, M., Epstein, C. G., Burdett, L., Dean, M. C., Chatterjee, N., Sampson, J., Chung, C. C., Kovaks, J., Gapstur, S. M., … Chanock, S. J. (2012). Detectable clonal mosaicism and its relationship to aging and cancer. *Nature Genetics*, *44*(6), 651–658. https://doi.org/10.1038/ng.2270

Jacobs, K., Mertzanidou, A., Geens, M., Thi Nguyen, H., Staessen, C., & Spits, C. (2014). Low-grade chromosomal mosaicism in human somatic and embryonic stem cell populations. *Nature Communications*, *5*(1), 4227. https://doi.org/10.1038/ncomms5227

Ji, L., Minna, J. D., & Roth, J. A. (2005). 3p21.3 tumor suppressor cluster: Prospects for translational applications. *Future Oncology (London, England)*, *1*(1), 79–92. https://doi.org/10.1517/14796694.1.1.79

Ji, Z., Chuen, J., Kiparaki, M., & Baker, N. (2021). Cell competition removes segmental aneuploid cells from Drosophila imaginal disc-derived tissues based on ribosomal protein gene dose. *eLife*, *10*, e61172. https://doi.org/10.7554/eLife.61172

Ji, Z., Kiparaki, M., Folgado, V., Kumar, A., Blanco, J., Rimesso, G., Chuen, J., Liu, Y., Zheng, D., & Baker, N. E. (2019). Drosophila RpS12 controls translation, growth, and cell competition through Xrp1. *PLoS Genetics*, *15*(12). https://doi.org/10.1371/journal.pgen.1008513

Jin, Z., Li, Y., Pitti, R., Lawrence, D., Pham, V. C., Lill, J. R., & Ashkenazi, A. (2009). Cullin3-based polyubiquitination and p62-dependent aggregation of caspase-8 mediate extrinsic apoptosis signaling. *Cell*, *137*(4), 721–735. https://doi.org/10.1016/j.cell.2009.03.015

Johansson, A.-M., Stenberg, P., Allgardsson, A., & Larsson, J. (2012). POF Regulates the Expression of Genes on the Fourth Chromosome in Drosophila melanogaster by Binding to Nascent RNA. *Molecular and Cellular Biology*, *32*(11), 2121. https://doi.org/10.1128/MCB.06622-11

Johansson, A.-M., Stenberg, P., Bernhardsson, C., & Larsson, J. (2007). Painting of fourth and chromosome-wide regulation of the 4th chromosome in Drosophila melanogaster. *The EMBO Journal*, *26*(9), 2307–2316. https://doi.org/10.1038/sj.emboj.7601604

Joy, J., Barrio, L., Santos-Tapia, C., Romão, D., Giakoumakis, N. N., Clemente-Ruiz, M., & Milán, M. (2021). Proteostasis failure and mitochondrial dysfunction leads to aneuploidy-induced senescence. *Developmental Cell*, *56*(14), 2043-2058.e7. https://doi.org/10.1016/j.devcel.2021.06.009

Joy, J., Fusari, E., & Milán, M. (2024). Aneuploidy-induced cellular behaviors: Insights from Drosophila. *Developmental Cell*, *59*(3), 295–307. https://doi.org/10.1016/j.devcel.2023.12.009

Kajita, M., & Fujita, Y. (2015). EDAC: Epithelial defence against cancer-cell competition between normal and transformed epithelial cells in mammals. *Journal of Biochemistry*, *158*(1), 15–23. https://doi.org/10.1093/jb/mvv050

Kale, A., Li, W., Lee, C.-H., & Baker, N. E. (2015). Apoptotic mechanisms during competition of ribosomal protein mutant cells: Roles of the initiator caspases Dronc and Dream/Strica. *Cell Death & Differentiation*, *22*(8), 1300–1312. https://doi.org/10.1038/cdd.2014.218

Kalousek, D. . K., & Dill, F. J. (1983). Chromosomal Mosaicism Confined to the Placenta in Human Conceptions. *Science*, *221*(4611), 665–667. https://doi.org/10.1126/science.6867735

Kamar, A., Turktekin, N., Ozyurt, R., Karakus, C., Saribal, D., & Hocaoglu-Emre, F. S. (2021). Cytogenetic analysis of early pregnancy loss after assisted reproduction treatment using intracytoplasmic sperm injection. *Ginekologia Polska*, *92*(7), Article 7. https://doi.org/10.5603/GP.a2020.0147

Katheder, N. S., Khezri, R., O'Farrell, F., Schultz, S. W., Jain, A., Rahman, M. M., Schink, K. O., Theodossiou, T. A., Johansen, T., Juhász, G., Bilder, D., Brech, A., Stenmark, H., & Rusten, T. E. (2017). Microenvironmental autophagy promotes tumour growth. *Nature*, *541*(7637), 417–420. https://doi.org/10.1038/nature20815

Katz-Jaffe, M. G., Trounson, A. O., & Cram, D. S. (2005). Chromosome 21 mosaic human preimplantation embryos predominantly arise from diploid conceptions. *Fertility and Sterility*, *84*(3), 634–643. https://doi.org/10.1016/j.fertnstert.2005.03.045

Kaushal, D., Contos, J. J. A., Treuner, K., Yang, A. H., Kingsbury, M. A., Rehen, S. K., McConnell, M. J., Okabe, M., Barlow, C., & Chun, J. (2003). Alteration of gene expression by chromosome loss in the postnatal mouse brain. *The Journal of Neuroscience: The Official Journal of the Society for Neuroscience*, *23*(13), 5599–5606. https://doi.org/10.1523/JNEUROSCI.23-13-05599.2003

Keel, S. B., Phelps, S., Sabo, K. M., O'Leary, M. N., Kirn-Safran, C. B., & Abkowitz, J. L. (2012). Establishing *Rps6* hemizygous mice as a model for studying how ribosomal protein haploinsufficiency impairs erythropoiesis. *Experimental Hematology*, *40*(4), 290–294. https://doi.org/10.1016/j.exphem.2011.12.003

Kennedy, A. L., Myers, K. C., Bowman, J., Gibson, C. J., Camarda, N. D., Furutani, E., Muscato, G. M., Klein, R. H., Ballotti, K., Liu, S., Harris, C. E., Galvin, A., Malsch, M., Dale, D., Gansner, J. M., Nakano, T. A., Bertuch, A., Vlachos, A., Lipton, J. M., … Lindsley, R. C. (2021). Distinct genetic pathways define pre-malignant versus compensatory clonal hematopoiesis in Shwachman-Diamond syndrome. *Nature Communications*, *12*(1), 1334. https://doi.org/10.1038/s41467-021-21588-4

Keppy, D. O., & Denell, R. E. (1979). A Mutational Analysis of the Triplo-Lethal Region of DROSOPHILA MELANOGASTER. *Genetics*, *91*(3), 421–441.

Khan, S. J., Abidi, S. N. F., Tian, Y., Skinner, A., & Smith-Bolton, R. K. (2016). A rapid, gentle and scalable method for dissociation and fluorescent sorting of imaginal disc cells for mRNA sequencing. *Fly*, *10*(2), 73–80. https://doi.org/10.1080/19336934.2016.1173296

Kiessling, A. A., Bletsa, R., Desmarais, B., Mara, C., Kallianidis, K., & Loutradis, D. (2010). Genome-wide microarray evidence that 8-cell human blastomeres over-express cell cycle drivers and under-express checkpoints. *Journal of Assisted Reproduction and Genetics*, *27*(6), 265–276. https://doi.org/10.1007/s10815-010-9407-6

Kim, J., Kundu, M., Viollet, B., & Guan, K.-L. (2011a). AMPK and mTOR regulate autophagy through direct phosphorylation of Ulk1. *Nature Cell Biology*, *13*(2), 132–141. https://doi.org/10.1038/ncb2152

Kim, J., Kundu, M., Viollet, B., & Guan, K.-L. (2011b). AMPK and mTOR regulate autophagy through direct phosphorylation of Ulk1. *Nature Cell Biology*, *13*(2), 132–141. https://doi.org/10.1038/ncb2152

Kim, Y. C., & Guan, K.-L. (2015). mTOR: A pharmacologic target for autophagy regulation. *The Journal of Clinical Investigation*, *125*(1), 25–32. https://doi.org/10.1172/JCI73939

Kingsbury, M. A., Friedman, B., McConnell, M. J., Rehen, S. K., Yang, A. H., Kaushal, D., & Chun, J. (2005). Aneuploid neurons are functionally active and integrated into brain circuitry. *Proceedings of the National Academy of Sciences*, *102*(17), 6143–6147. https://doi.org/10.1073/pnas.0408171102

Kiparaki, M., Khan, C., Folgado-Marco, V., Chuen, J., Moulos, P., & Baker, N. E. (2022). The transcription factor Xrp1 orchestrates both reduced translation and cell competition upon defective ribosome assembly or function. *eLife*, *11*, e71705. https://doi.org/10.7554/eLife.71705

Kitajima, T. S., Hauf, S., Ohsugi, M., Yamamoto, T., & Watanabe, Y. (2005). Human Bub1 defines the persistent cohesion site along the mitotic chromosome by affecting Shugoshin localization. *Current Biology: CB*, *15*(4), 353–359. https://doi.org/10.1016/j.cub.2004.12.044

Knouse, K. A., Wu, J., Whittaker, C. A., & Amon, A. (2014). Single cell sequencing reveals low levels of aneuploidy across mammalian tissues. *Proceedings of the National Academy of Sciences of the United States of America*, *111*(37), 13409–13414. https://doi.org/10.1073/pnas.1415287111

Knudson, A. G. (1971). Mutation and cancer: Statistical study of retinoblastoma. *Proceedings of the National Academy of Sciences of the United States of America*, *68*(4), 820–823. https://doi.org/10.1073/pnas.68.4.820

Kolahgar, G., Suijkerbuijk, S. J. E., Kucinski, I., Poirier, E. Z., Mansour, S., Simons, B. D., & Piddini, E. (2015). Cell Competition Modifies Adult Stem Cell and Tissue Population Dynamics in a JAK-STAT-

Dependent Manner. *Developmental Cell*, *34*(3), 297–309. https://doi.org/10.1016/j.devcel.2015.06.010

Konstantinidis, M., Milligan, K., Berkeley, A. S., Kennedy, J., Maxson, W., Racowsky, C., Wells, D., & Munne, S. (2016). Use of single nucleotide polymorphism (SNP) arrays and next generation sequencing (NGS) to study the incidence, type and origin of aneuploidy in the human preimplantation embryo. *Fertility and Sterility*, *106*(3), e22–e23. https://doi.org/10.1016/j.fertnstert.2016.07.076

Kort, D. H., Chia, G., Treff, N. R., Tanaka, A. J., Xing, T., Vensand, L. B., Micucci, S., Prosser, R., Lobo, R. A., Sauer, M. V., & Egli, D. (2016). Human embryos commonly form abnormal nuclei during development: A mechanism of DNA damage, embryonic aneuploidy, and developmental arrest. *Human Reproduction (Oxford, England)*, *31*(2), 312–323. https://doi.org/10.1093/humrep/dev281

Kubicek, D., Hornak, M., Horak, J., Navratil, R., Tauwinklova, G., Rubes, J., & Vesela, K. (2019). Incidence and origin of meiotic whole and segmental chromosomal aneuploidies detected by karyomapping. *Reproductive BioMedicine Online*, *38*(3), 330–339. https://doi.org/10.1016/j.rbmo.2018.11.023

Kucinski, I., Dinan, M., Kolahgar, G., & Piddini, E. (2017). Chronic activation of JNK JAK/STAT and oxidative stress signalling causes the loser cell status. *Nature Communications*, *8*(1), 136. https://doi.org/10.1038/s41467-017-00145-y

Kuijpers, T. W., van Leeuwen, E. M. M., Barendregt, B. H., Klarenbeek, P., aan de Kerk, D. J., Baars, P. A., Jansen, M. H., de Vries, N., van Lier, R. A. W., & van der Burg, M. (2013). A reversion of an IL2RG mutation in combined immunodeficiency providing competitive advantage to the majority of CD8+ T cells. *Haematologica*, *98*(7), 1030–1038. https://doi.org/10.3324/haematol.2012.077511

Kusumbe, A. P., & Bapat, S. A. (2009). Cancer Stem Cells and Aneuploid Populations within Developing Tumors Are the Major Determinants of Tumor Dormancy. *Cancer Research*, *69*(24), 9245–9253. https://doi.org/10.1158/0008-5472.CAN-09-2802

Lalande, M. (1996). Parental imprinting and human disease. *Annual Review of Genetics*, *30*, 173–195. https://doi.org/10.1146/annurev.genet.30.1.173

Langton, P. F., Baumgartner, M. E., Logeay, R., & Piddini, E. (2021). Xrp1 and Irbp18 trigger a feed-forward loop of proteotoxic stress to induce the loser status. *PLoS Genetics*, *17*(12), e1009946. https://doi.org/10.1371/journal.pgen.1009946

Larsson, J., Chen, J. D., Rasheva, V., Rasmuson-Lestander, Å., & Pirrotta, V. (2001). Painting of fourth, a chromosome-specific protein in Drosophila. *Proceedings of the National Academy of Sciences*, *98*(11), 6273–6278. https://doi.org/10.1073/pnas.111581298

Laughney, A. M., Elizalde, S., Genovese, G., & Bakhoum, S. F. (2015). Dynamics of Tumor Heterogeneity Derived from Clonal Karyotypic Evolution. *Cell Reports*, *12*(5), 809–820. https://doi.org/10.1016/j.celrep.2015.06.065

Laurie, C. C., Laurie, C. A., Rice, K., Doheny, K. F., Zelnick, L. R., McHugh, C. P., Ling, H., Hetrick, K. N., Pugh, E. W., Amos, C., Wei, Q., Wang, L., Lee, J. E., Barnes, K. C., Hansel, N. N., Mathias, R., Daley,

D., Beaty, T. H., Scott, A. F., … Weir, B. S. (2012). Detectable clonal mosaicism from birth to old age and its relationship to cancer. *Nature Genetics*, *44*(6), 642–650. https://doi.org/10.1038/ng.2271

Laverty, C., Lucci, J., & Akhtar, A. (2010). The MSL complex: X chromosome and beyond. *Current Opinion in Genetics & Development*, *20*(2), 171–178. https://doi.org/10.1016/j.gde.2010.01.007

Layalle, S., Arquier, N., & Léopold, P. (2008). The TOR Pathway Couples Nutrition and Developmental Timing in *Drosophila*. *Developmental Cell*, *15*(4), 568–577. https://doi.org/10.1016/j.devcel.2008.08.003

Leach, N. T., Rehder, C., Jensen, K., Holt, S., & Jackson-Cook, C. (2004). Human chromosomes with shorter telomeres and large heterochromatin regions have a higher frequency of acquired somatic cell aneuploidy. *Mechanisms of Ageing and Development*, *125*(8), 563–573. https://doi.org/10.1016/j.mad.2004.06.006

Lebedev, I. (2011). Mosaic Aneuploidy in Early Fetal Losses. *Cytogenetic and Genome Research*, *133*(2–4), 169–183. https://doi.org/10.1159/000324120

Lebedev, I. N., Ostroverkhova, N. V., Nikitina, T. V., Sukhanova, N. N., & Nazarenko, S. A. (2004). Features of chromosomal abnormalities in spontaneous abortion cell culture failures detected by interphase FISH analysis. *European Journal of Human Genetics*, *12*(7), 513–520. https://doi.org/10.1038/sj.ejhg.5201178

Lee, A., & Kiessling, A. A. (2017). Early human embryos are naturally aneuploid-can that be corrected? *Journal of Assisted Reproduction and Genetics*, *34*(1), 15–21. https://doi.org/10.1007/s10815-016-0845-7

Lee, C.-H., Kiparaki, M., Blanco, J., Folgado, V., Ji, Z., Kumar, A., Rimesso, G., & Baker, N. E. (2018). A Regulatory Response to Ribosomal Protein Mutations Controls Translation, Growth, and Cell Competition. *Developmental Cell*, *46*(4), 456-469.e4. https://doi.org/10.1016/j.devcel.2018.07.003

Lee, H., Cho, D.-Y., Whitworth, C., Eisman, R., Phelps, M., Roote, J., Kaufman, T., Cook, K., Russell, S., Przytycka, T., & Oliver, B. (2016). Effects of Gene Dose, Chromatin, and Network Topology on Expression in Drosophila melanogaster. *PLoS Genetics*, *12*(9), e1006295. https://doi.org/10.1371/journal.pgen.1006295

Lefebvre, L., Mar, L., Bogutz, A., Oh-McGinnis, R., Mandegar, M. A., Paderova, J., Gertsenstein, M., Squire, J. A., & Nagy, A. (2009). The interval between Ins2 and Ascl2 is dispensable for imprinting centre function in the murine Beckwith-Wiedemann region. *Human Molecular Genetics*, *18*(22), 4255–4267. https://doi.org/10.1093/hmg/ddp379

Leibowitz, M. L., Papathanasiou, S., Doerfler, P. A., Blaine, L. J., Sun, L., Yao, Y., Zhang, C.-Z., Weiss, M. J., & Pellman, D. (2021). Chromothripsis as an on-target consequence of CRISPR-Cas9 genome editing. *Nature Genetics*, *53*(6), 895–905. https://doi.org/10.1038/s41588-021-00838-7

Levayer, R., Dupont, C., & Moreno, E. (2016). Tissue Crowding Induces Caspase-Dependent Competition for Space. *Current Biology: CB*, *26*(5), 670–677. https://doi.org/10.1016/j.cub.2015.12.072

Li, M., Fang, X., Baker, D. J., Guo, L., Gao, X., Wei, Z., Han, S., van Deursen, J. M., & Zhang, P. (2010). The ATM-p53 pathway suppresses aneuploidy-induced tumorigenesis. *Proceedings of the National Academy of Sciences of the United States of America*, *107*(32), 14188–14193. https://doi.org/10.1073/pnas.1005960107

Li, T., Hu, J.-F., Qiu, X., Ling, J., Chen, H., Wang, S., Hou, A., Vu, T. H., & Hoffman, A. R. (2008). CTCF regulates allelic expression of Igf2 by orchestrating a promoter-polycomb repressive complex 2 intrachromosomal loop. *Molecular and Cellular Biology*, *28*(20), 6473–6482. https://doi.org/10.1128/MCB.00204-08

Li, W., & Baker, N. E. (2007). Engulfment is required for cell competition. *Cell*, *129*(6), 1215–1225. https://doi.org/10.1016/j.cell.2007.03.054

Lindsley, D. L., Sandler, L., Baker, B. S., Carpenter, A. T., Denell, R. E., Hall, J. C., Jacobs, P. A., Miklos, G. L., Davis, B. K., Gethmann, R. C., Hardy, R. W., Steven, A. H., Miller, M., Nozawa, H., Parry, D. M., Gould-Somero, M., & Gould-Somero, M. (1972). Segmental aneuploidy and the genetic gross structure of the Drosophila genome. *Genetics*, *71*(1), 157–184.

Ling, J. Q., Li, T., Hu, J. F., Vu, T. H., Chen, H. L., Qiu, X. W., Cherry, A. M., & Hoffman, A. R. (2006). CTCF mediates interchromosomal colocalization between Igf2/H19 and Wsb1/Nf1. *Science (New York, N.Y.)*, *312*(5771), 269–272. https://doi.org/10.1126/science.1123191

Liu, P., Jenkins, N. A., & Copeland, N. G. (2002). Efficient Cre-loxP-induced mitotic recombination in mouse embryonic stem cells. *Nature Genetics*, *30*(1), 66–72. https://doi.org/10.1038/ng788

Loidl, J., Klein, F., & Scherthan, H. (1994). Homologous pairing is reduced but not abolished in asynaptic mutants of yeast. *Journal of Cell Biology*, *125*(6), 1191–1200. https://doi.org/10.1083/jcb.125.6.1191

Lolo, F.-N., Casas-Tintó, S., & Moreno, E. (2012). Cell Competition Time Line: Winners Kill Losers, which Are Extruded and Engulfed by Hemocytes. *Cell Reports*, *2*(3), 526–539. https://doi.org/10.1016/j.celrep.2012.08.012

López-Otín, C., Blasco, M. A., Partridge, L., Serrano, M., & Kroemer, G. (2023). Hallmarks of aging: An expanding universe. *Cell*, *186*(2), 243–278. https://doi.org/10.1016/j.cell.2022.11.001

Lukow, D. A., Sausville, E. L., Suri, P., Chunduri, N. K., Wieland, A., Leu, J., Smith, J. C., Girish, V., Kumar, A. A., Kendall, J., Wang, Z., Storchova, Z., & Sheltzer, J. M. (2021). Chromosomal instability accelerates the evolution of resistance to anti-cancer therapies. *Developmental Cell*, *56*(17), 2427-2439.e4. https://doi.org/10.1016/j.devcel.2021.07.009

Lund, I. C. B., Becher, N., Christensen, R., Petersen, O. B., Steffensen, E. H., Vestergaard, E. M., & Vogel, I. (2020). Prevalence of mosaicism in uncultured chorionic villus samples after chromosomal microarray and clinical outcome in pregnancies affected by confined placental mosaicism. *Prenatal Diagnosis*, *40*(2), 244–259. https://doi.org/10.1002/pd.5584

Lupski, J. R. (1998). Genomic disorders: Structural features of the genome can lead to DNA rearrangements and human disease traits. *Trends in Genetics*, *14*(10), 417–422. https://doi.org/10.1016/S0168-9525(98)01555-8

Ly, P., Teitz, L. S., Kim, D. H., Shoshani, O., Skaletsky, H., Fachinetti, D., Page, D. C., & Cleveland, D. W. (2017). Selective Y centromere inactivation triggers chromosome shattering in micronuclei and repair by non-homologous end joining. *Nature Cell Biology*, *19*(1), 68–75. https://doi.org/10.1038/ncb3450

Lynch, C. J., & Milner, J. (2006). Loss of one p53 allele results in four-fold reduction of p53 mRNA and protein: A basis for p53 haplo-insufficiency. *Oncogene*, *25*(24), 3463–3470. https://doi.org/10.1038/sj.onc.1209387

Ma, X. M., & Blenis, J. (2009). Molecular mechanisms of mTOR-mediated translational control. *Nature Reviews Molecular Cell Biology*, *10*(5), 307–318. https://doi.org/10.1038/nrm2672

Macedo, J. C., Vaz, S., Bakker, B., Ribeiro, R., Bakker, P. L., Escandell, J. M., Ferreira, M. G., Medema, R., Foijer, F., & Logarinho, E. (2018). FoxM1 repression during human aging leads to mitotic decline and aneuploidy-driven full senescence. *Nature Communications*, *9*(1), 2834. https://doi.org/10.1038/s41467-018-05258-6

Maciejewska, Z., Polanski, Z., Kisiel, K., Kubiak, J. Z., & Ciemerych, M. A. (2009). Spindle assembly checkpoint-related failure perturbs early embryonic divisions and reduces reproductive performance of LT/Sv mice. *Reproduction (Cambridge, England)*, *137*(6), 931–942. https://doi.org/10.1530/REP-09-0011

Mackenzie, K. J., Carroll, P., Martin, C.-A., Murina, O., Fluteau, A., Simpson, D. J., Olova, N., Sutcliffe, H., Rainger, J. K., Leitch, A., Osborn, R. T., Wheeler, A. P., Nowotny, M., Gilbert, N., Chandra, T., Reijns, M. A. M., & Jackson, A. P. (2017). cGAS surveillance of micronuclei links genome instability to innate immunity. *Nature*, *548*(7668), 461–465. https://doi.org/10.1038/nature23449

Mackenzie, S. M., Howells, A. J., Cox, G. B., & Ewart, G. D. (2000). Sub-cellular localisation of the white/scarlet ABC transporter to pigment granule membranes within the compound eye of Drosophila melanogaster. *Genetica*, *108*(3), 239–252. https://doi.org/10.1023/a:1004115718597

Magli, M. C., Gianaroli, L., Ferraretti, A. P., Gordts, S., Fredericks, V., & Crippa, A. (2009). Paternal contribution to aneuploidy in preimplantation embryos. *Reproductive Biomedicine Online*, *18*(4), 536–542. https://doi.org/10.1016/s1472-6483(10)60131-9

Malumbres, M., & Villarroya-Beltri, C. (2024a). Mosaic variegated aneuploidy in development, ageing and cancer. *Nature Reviews Genetics*, *25*(12), 864–878. https://doi.org/10.1038/s41576-024-00762-6

Malumbres, M., & Villarroya-Beltri, C. (2024b). Mosaic variegated aneuploidy in development, ageing and cancer. *Nature Reviews Genetics*, *25*(12), 864–878. https://doi.org/10.1038/s41576-024-00762-6

Manieu, C., González, M., López-Fenner, J., Page, J., Ayarza, E., Fernández-Donoso, R., & Berríos, S. (2014). Aneuploidy in spermatids of Robertsonian (Rb) chromosome heterozygous mice. *Chromosome Research*, *22*(4), 545–557. https://doi.org/10.1007/s10577-014-9443-7

Mantikou, E., Wong, K. M., Repping, S., & Mastenbroek, S. (2012). Molecular origin of mitotic aneuploidies in preimplantation embryos. *Biochimica Et Biophysica Acta*, *1822*(12), 1921–1930. https://doi.org/10.1016/j.bbadis.2012.06.013

Martin, A., Mercader, A., Dominguez, F., Quiñonero, A., Perez, M., Gonzalez-Martin, R., Delgado, A., Mifsud, A., Pellicer, A., & De Los Santos, M. J. (2023). Mosaic results after preimplantation genetic testing for aneuploidy may be accompanied by changes in global gene expression. *Frontiers in Molecular Biosciences*, *10*. https://doi.org/10.3389/fmolb.2023.1180689

Martín, F. A., Herrera, S. C., & Morata, G. (2009). Cell competition, growth and size control in the Drosophila wing imaginal disc. *Development (Cambridge, England)*, *136*(22), 3747–3756. https://doi.org/10.1242/dev.038406

Martin, R. H. (2008). Meiotic errors in human oogenesis and spermatogenesis. *Reproductive BioMedicine Online*, *16*(4), 523–531. https://doi.org/10.1016/S1472-6483(10)60459-2

Martins, V. C., Busch, K., Juraeva, D., Blum, C., Ludwig, C., Rasche, V., Lasitschka, F., Mastitsky, S. E., Brors, B., Hielscher, T., Fehling, H. J., & Rodewald, H.-R. (2014). Cell competition is a tumour suppressor mechanism in the thymus. *Nature*, *509*(7501), 465–470. https://doi.org/10.1038/nature13317

Marusyk, A., Porter, C. C., Zaberezhnyy, V., & DeGregori, J. (2010). Irradiation selects for p53-deficient hematopoietic progenitors. *PLoS Biology*, *8*(3), e1000324. https://doi.org/10.1371/journal.pbio.1000324

Marygold, S. J., Roote, J., Reuter, G., Lambertsson, A., Ashburner, M., Millburn, G. H., Harrison, P. M., Yu, Z., Kenmochi, N., Kaufman, T. C., Leevers, S. J., & Cook, K. R. (2007). The ribosomal protein genes and Minute loci of Drosophila melanogaster. *Genome Biology*, *8*(10), R216. https://doi.org/10.1186/gb-2007-8-10-r216

Matsumura, H., Tada, M., Otsuji, T., Yasuchika, K., Nakatsuji, N., Surani, A., & Tada, T. (2007). Targeted chromosome elimination from ES-somatic hybrid cells. *Nature Methods*, *4*(1), 23–25. https://doi.org/10.1038/nmeth973

Matsuura, S., Matsumoto, Y., Morishima, K., Izumi, H., Matsumoto, H., Ito, E., Tsutsui, K., Kobayashi, J., Tauchi, H., Kajiwara, Y., Hama, S., Kurisu, K., Tahara, H., Oshimura, M., Komatsu, K., Ikeuchi, T., & Kajii, T. (2006). Monoallelic BUB1B mutations and defective mitotic-spindle checkpoint in seven families with premature chromatid separation (PCS) syndrome. *American Journal of Medical Genetics. Part A*, *140*(4), 358–367. https://doi.org/10.1002/ajmg.a.31069

McConnell, M. J., Lindberg, M. R., Brennand, K. J., Piper, J. C., Voet, T., Cowing-Zitron, C., Shumilina, S., Lasken, R. S., Vermeesch, J., Hall, I. M., & Gage, F. H. (2013). Mosaic Copy Number Variation in Human Neurons. *Science (New York, N.Y.)*, *342*(6158), 632–637. https://doi.org/10.1126/science.1243472

Menthena, A., Koehler, C. I., Sandhu, J. S., Yovchev, M. I., Hurston, E., Shafritz, D. A., & Oertel, M. (2011). Activin A, p15INK4b signaling, and cell competition promote stem/progenitor cell repopulation of livers in aging rats. *Gastroenterology*, *140*(3), 1009–1020. https://doi.org/10.1053/j.gastro.2010.12.003

Merino, M. M., Rhiner, C., Lopez-Gay, J. M., Buechel, D., Hauert, B., & Moreno, E. (2015). Elimination of unfit cells maintains tissue health and prolongs lifespan. *Cell*, *160*(3), 461–476. https://doi.org/10.1016/j.cell.2014.12.017

Metz, C. W. (1916). Chromosome studies on the Diptera. II. The paired association of chromosomes in the Diptera, and its significance. *Journal of Experimental Zoology*, *21*(2), 213–279. https://doi.org/10.1002/jez.1400210204

Meyer, S. N., Amoyel, M., Bergantiños, C., de la Cova, C., Schertel, C., Basler, K., & Johnston, L. A. (2014). An ancient defense system eliminates unfit cells from developing tissues during cell competition. *Science (New York, N.Y.)*, *346*(6214), 1258236. https://doi.org/10.1126/science.1258236

Mihalas, B. P., Marston, A. L., Wu, L. E., & Gilchrist, R. B. (2024). Reproductive Ageing: Metabolic contribution to age-related chromosome missegregation in mammalian oocytes. *Reproduction (Cambridge, England)*, *168*(2), e230510. https://doi.org/10.1530/REP-23-0510

Mihalas, B. P., Pieper, G. H., Aboelenain, M., Munro, L., Srsen, V., Currie, C. E., Kelly, D. A., Hartshorne, G. M., Telfer, E. E., McAinsh, A. D., Anderson, R. A., & Marston, A. L. (2024). Age-dependent loss of cohesion protection in human oocytes. *Current Biology: CB*, *34*(1), 117-131.e5. https://doi.org/10.1016/j.cub.2023.11.061

Minello, A., & Carreira, A. (2024). BRCA1/2 Haploinsufficiency: Exploring the Impact of Losing one Allele. *Journal of Molecular Biology*, *436*(1), 168277. https://doi.org/10.1016/j.jmb.2023.168277

Miron, M., & Sonenberg, N. (2001). Regulation of Translation via TOR Signaling: Insights from *Drosophila melanogaster*. *The Journal of Nutrition*, *131*(11), 2988S-2993S. https://doi.org/10.1093/jn/131.11.2988S

Mirzaa, G. M., Vitre, B., Carpenter, G., Abramowicz, I., Gleeson, J. G., Paciorkowski, A. R., Cleveland, D. W., Dobyns, W. B., & O'Driscoll, M. (2014). Mutations in CENPE define a novel kinetochore-centromeric mechanism for microcephalic primordial dwarfism. *Human Genetics*, *133*(8), 1023–1039. https://doi.org/10.1007/s00439-014-1443-3

Morata, G. (2021). Cell competition: A historical perspective. *Developmental Biology*, *476*, 33–40. https://doi.org/10.1016/j.ydbio.2021.02.012

Morata, G., & Ripoll, P. (1975). Minutes: Mutants of drosophila autonomously affecting cell division rate. *Developmental Biology*, *42*(2), 211–221. https://doi.org/10.1016/0012-1606(75)90330-9

Moreno, E., & Basler, K. (2004). dMyc transforms cells into super-competitors. *Cell*, *117*(1), 117–129. https://doi.org/10.1016/s0092-8674(04)00262-4

Moreno, E., Basler, K., & Morata, G. (2002). Cells compete for decapentaplegic survival factor to prevent apoptosis in Drosophila wing development. *Nature*, *416*(6882), 755–759. https://doi.org/10.1038/416755a

Mukamel, E. A., Liu, H., Behrens, M. M., & Ecker, J. R. (2023). Cell type-specific enrichment of somatic aneuploidy in the mammalian brain. *bioRxiv*, 2023.12.18.572285. https://doi.org/10.1101/2023.12.18.572285

Mukherjee, A. B., Alejandro, J., Payne, S., & Thomas, S. (1996). Age-related aneuploidy analysis of human blood cells in vivo by fluorescence in situ hybridization (FISH). *Mechanisms of Ageing and Development*, *90*(2), 145–156. https://doi.org/10.1016/0047-6374(96)01762-9

Mukherjee, A. B., & Thomas, S. (1997). A longitudinal study of human age-related chromosomal analysis in skin fibroblasts. *Experimental Cell Research*, *235*(1), 161–169. https://doi.org/10.1006/excr.1997.3673

Munné, S., Blazek, J., Large, M., Martinez-Ortiz, P. A., Nisson, H., Liu, E., Tarozzi, N., Borini, A., Becker, A., Zhang, J., Maxwell, S., Grifo, J., Babariya, D., Wells, D., & Fragouli, E. (2017). Detailed investigation into the cytogenetic constitution and pregnancy outcome of replacing mosaic blastocysts detected with the use of high-resolution next-generation sequencing. *Fertility and Sterility*, *108*(1), 62-71.e8. https://doi.org/10.1016/j.fertnstert.2017.05.002

Munné, S., Sultan, K. M., Weier, H. U., Grifo, J. A., Cohen, J., & Rosenwaks, Z. (1995). Assessment of numeric abnormalities of X, Y, 18, and 16 chromosomes in preimplantation human embryos before transfer. *American Journal of Obstetrics and Gynecology*, *172*(4 Pt 1), 1191–1199; discussion 1199-1201. https://doi.org/10.1016/0002-9378(95)91479-x

Muona, M., Ishimura, R., Laari, A., Ichimura, Y., Linnankivi, T., Keski-Filppula, R., Herva, R., Rantala, H., Paetau, A., Pöyhönen, M., Obata, M., Uemura, T., Karhu, T., Bizen, N., Takebayashi, H., McKee, S., Parker, M. J., Akawi, N., McRae, J., … Komatsu, M. (2016). Biallelic Variants in UBA5 Link Dysfunctional UFM1 Ubiquitin-like Modifier Pathway to Severe Infantile-Onset Encephalopathy. *American Journal of Human Genetics*, *99*(3), 683–694. https://doi.org/10.1016/j.ajhg.2016.06.020

Muotri, A. R., & Gage, F. H. (2006). Generation of neuronal variability and complexity. *Nature*, *441*(7097), 1087–1093. https://doi.org/10.1038/nature04959

Musio, A., Montagna, C., Zambroni, D., Indino, E., Barbieri, O., Citti, L., Villa, A., Ried, T., & Vezzoni, P. (2003). Inhibition of BUB1 results in genomic instability and anchorage-independent growth of normal human fibroblasts. *Cancer Research*, *63*(11), 2855–2863.

Myers, K. C., Furutani, E., Weller, E., Siegele, B., Galvin, A., Arsenault, V., Alter, B. P., Boulad, F., Bueso-Ramos, C., Burroughs, L., Castillo, P., Connelly, J., Davies, S. M., DiNardo, C. D., Hanif, I., Ho, R. H., Karras, N., Manalang, M., McReynolds, L. J., … Shimamura, A. (2020). Myelodysplastic syndrome and acute myeloid leukemia in patients with Shwachman Diamond syndrome: A multicentre, retrospective, cohort study. *The Lancet. Haematology*, *7*(3), e238–e246. https://doi.org/10.1016/S2352-3026(19)30206-6

Nagata, R., Nakamura, M., Sanaki, Y., & Igaki, T. (2019). Cell Competition Is Driven by Autophagy. *Developmental Cell*, *51*(1), 99-112.e4. https://doi.org/10.1016/j.devcel.2019.08.018

Neufeld, T. P., de la Cruz, A. F. A., Johnston, L. A., & Edgar, B. A. (1998). Coordination of Growth and Cell Division in the *Drosophila* Wing. *Cell*, *93*(7), 1183–1193. https://doi.org/10.1016/S0092-8674(00)81462-2

Norman, M., Wisniewska, K. A., Lawrenson, K., Garcia-Miranda, P., Tada, M., Kajita, M., Mano, H., Ishikawa, S., Ikegawa, M., Shimada, T., & Fujita, Y. (2012). Loss of Scribble causes cell competition in mammalian cells. *Journal of Cell Science*, *125*(Pt 1), 59–66. https://doi.org/10.1242/jcs.085803

Oertel, M., Menthena, A., Dabeva, M. D., & Shafritz, D. A. (2006). Cell competition leads to a high level of normal liver reconstitution by transplanted fetal liver stem/progenitor cells. *Gastroenterology*, *130*(2), 507–520; quiz 590. https://doi.org/10.1053/j.gastro.2005.10.049

Ohashi, A., Ohori, M., Iwai, K., Nakayama, Y., Nambu, T., Morishita, D., Kawamoto, T., Miyamoto, M., Hirayama, T., Okaniwa, M., Banno, H., Ishikawa, T., Kandori, H., & Iwata, K. (2015). Aneuploidy generates proteotoxic stress and DNA damage concurrently with p53-mediated post-mitotic apoptosis in SAC-impaired cells. *Nature Communications*, *6*, 7668. https://doi.org/10.1038/ncomms8668

Ohnuki, S., & Ohya, Y. (2018). High-dimensional single-cell phenotyping reveals extensive haploinsufficiency. *PLoS Biology*, *16*(5), e2005130. https://doi.org/10.1371/journal.pbio.2005130

Oldham, S., Montagne, J., Radimerski, T., Thomas, G., & Hafen, E. (2000). Genetic and biochemical characterization of dTOR, the Drosophila homolog of the target of rapamycin. *Genes & Development*, *14*(21), 2689–2694. https://doi.org/10.1101/gad.845700

Oliver, E. R., Saunders, T. L., Tarlé, S. A., & Glaser, T. (2004). Ribosomal protein L24 defect in belly spot and tail (Bst), a mouse Minute. *Development (Cambridge, England)*, *131*(16), 3907–3920. https://doi.org/10.1242/dev.01268

Oliver, T. R., Feingold, E., Yu, K., Cheung, V., Tinker, S., Yadav-Shah, M., Masse, N., & Sherman, S. L. (2008). New insights into human nondisjunction of chromosome 21 in oocytes. *PLoS Genetics*, *4*(3), e1000033. https://doi.org/10.1371/journal.pgen.1000033

Oromendia, A. B., Dodgson, S. E., & Amon, A. (2012). Aneuploidy causes proteotoxic stress in yeast. *Genes & Development*, *26*(24), 2696–2708. https://doi.org/10.1101/gad.207407.112

Orvieto, R., Shimon, C., Rienstein, S., Jonish-Grossman, A., Shani, H., & Aizer, A. (2020). Do human embryos have the ability of self-correction? *Reproductive Biology and Endocrinology : RB&E*, *18*, 98. https://doi.org/10.1186/s12958-020-00650-8

Otter, M., Schrander-Stumpel, C. T., & Curfs, L. M. (2010). Triple X syndrome: A review of the literature. *European Journal of Human Genetics*, *18*(3), 265–271. https://doi.org/10.1038/ejhg.2009.109

Ovcharenko, I., Loots, G. G., Nobrega, M. A., Hardison, R. C., Miller, W., & Stubbs, L. (2005). Evolution and functional classification of vertebrate gene deserts. *Genome Research*, *15*(1), 137–145. https://doi.org/10.1101/gr.3015505

Papathanasiou, S., Markoulaki, S., Blaine, L. J., Leibowitz, M. L., Zhang, C.-Z., Jaenisch, R., & Pellman, D. (2021). Whole chromosome loss and genomic instability in mouse embryos after CRISPR-Cas9 genome editing. *Nature Communications*, *12*(1), 5855. https://doi.org/10.1038/s41467-021-26097-y

Papathanasiou, S., Mynhier, N. A., Liu, S., Brunette, G., Stokasimov, E., Jacob, E., Li, L., Comenho, C., van Steensel, B., Buenrostro, J. D., Zhang, C.-Z., & Pellman, D. (2023). Heritable transcriptional defects

from aberrations of nuclear architecture. *Nature*, *619*(7968), 184–192. https://doi.org/10.1038/s41586-023-06157-7

Papp, I., Iglesias, V. A., Moscone, E. A., Michalowski, S., Spiker, S., Park, Y. D., Matzke, M. A., & Matzke, A. J. (1996). Structural instability of a transgene locus in tobacco is associated with aneuploidy. *The Plant Journal: For Cell and Molecular Biology*, *10*(3), 469–478. https://doi.org/10.1046/j.1365-313x.1996.10030469.x

Passerini, V., Ozeri-Galai, E., Pagter, M. S. de, Donnelly, N., Schmalbrock, S., Kloosterman, W. P., Kerem, B., & Storchová, Z. (2016). The presence of extra chromosomes leads to genomic instability. *Nature Communications*, *7*(1), 1–12. https://doi.org/10.1038/ncomms10754

Patel, J., Tan, S. L., Hartshorne, G. M., & McAinsh, A. D. (2015). Unique geometry of sister kinetochores in human oocytes during meiosis I may explain maternal age-associated increases in chromosomal abnormalities. *Biology Open*, *5*(2), 178–184. https://doi.org/10.1242/bio.016394

Patterson, J. T., Stone, W., & Bedichek, S. (1935). The Genetics of X-Hyperploid Females. *Genetics*, *20*(3), 259–279.

Pavelka, N., Rancati, G., Zhu, J., Bradford, W. D., Saraf, A., Florens, L., Sanderson, B. W., Hattem, G. L., & Li, R. (2010). Aneuploidy confers quantitative proteome changes and phenotypic variation in budding yeast. *Nature*, *468*(7321), 321–325. https://doi.org/10.1038/nature09529

Payer, B., & Lee, J. T. (2008). X chromosome dosage compensation: How mammals keep the balance. *Annual Review of Genetics*, *42*, 733–772. https://doi.org/10.1146/annurev.genet.42.110807.091711

Perera, D., Tilston, V., Hopwood, J. A., Barchi, M., Boot-Handford, R. P., & Taylor, S. S. (2007). Bub1 maintains centromeric cohesion by activation of the spindle checkpoint. *Developmental Cell*, *13*(4), 566–579. https://doi.org/10.1016/j.devcel.2007.08.008

Peri, S., Caretti, E., Tricarico, R., Devarajan, K., Cheung, M., Sementino, E., Menges, C. W., Nicolas, E., Vanderveer, L. A., Howard, S., Conrad, P., Crowell, J. A., Campbell, K. S., Ross, E. A., Godwin, A. K., Yeung, A. T., Clapper, M. L., Uzzo, R. G., Henske, E. P., … Knudson, A. G. (2016). Haploinsufficiency in tumor predisposition syndromes: Altered genomic transcription in morphologically normal cells heterozygous for VHL or TSC mutation. *Oncotarget*, *8*(11), 17628–17642. https://doi.org/10.18632/oncotarget.12192

Picchetta, L., Ottolini, C. S., O'Neill, H. C., & Capalbo, A. (2023). Investigating the significance of segmental aneuploidy findings in preimplantation embryos. *F&S Science*, *4*(2), 17–26. https://doi.org/10.1016/j.xfss.2023.03.004

Piccirillo, C. A., Bjur, E., Topisirovic, I., Sonenberg, N., & Larsson, O. (2014). Translational control of immune responses: From transcripts to translatomes. *Nature Immunology*, *15*(6), 503–511. https://doi.org/10.1038/ni.2891

Piotrowski, A., Bruder, C. E. G., Andersson, R., Diaz de Ståhl, T., Menzel, U., Sandgren, J., Poplawski, A., von Tell, D., Crasto, C., Bogdan, A., Bartoszewski, R., Bebok, Z., Krzyzanowski, M., Jankowski, Z., Partridge, E. C., Komorowski, J., & Dumanski, J. P. (2008). Somatic mosaicism for copy number

variation in differentiated human tissues. *Human Mutation*, *29*(9), 1118–1124. https://doi.org/10.1002/humu.20815

Pirrotta, V. (1988). Vectors for P-mediated transformation in Drosophila. *Biotechnology (Reading, Mass.)*, *10*, 437–456. https://doi.org/10.1016/b978-0-409-90042-2.50028-3

Pogribna, M., Melnyk, S., Pogribny, I., Chango, A., Yi, P., & James, S. J. (2001). Homocysteine metabolism in children with Down syndrome: In vitro modulation. *American Journal of Human Genetics*, *69*(1), 88–95. https://doi.org/10.1086/321262

Potter, C. J., Tasic, B., Russler, E. V., Liang, L., & Luo, L. (2010). The Q System: A Repressible Binary System for Transgene Expression, Lineage Tracing, and Mosaic Analysis. *Cell*, *141*(3), 536–548. https://doi.org/10.1016/j.cell.2010.02.025

Price, C. J., Stavish, D., Gokhale, P. J., Stevenson, B. A., Sargeant, S., Lacey, J., Rodriguez, T. A., & Barbaric, I. (2021). Genetically variant human pluripotent stem cells selectively eliminate wild-type counterparts through YAP-mediated cell competition. *Developmental Cell*, *56*(17), 2455-2470.e10. https://doi.org/10.1016/j.devcel.2021.07.019

Rabinowitz, M., Ryan, A., Gemelos, G., Hill, M., Baner, J., Cinnioglu, C., Banjevic, M., Potter, D., Petrov, D. A., & Demko, Z. (2012). Origins and rates of aneuploidy in human blastomeres. *Fertility and Sterility*, *97*(2), 395–401. https://doi.org/10.1016/j.fertnstert.2011.11.034

Rajendran, R. S., Zupanc, M. M., Lösche, A., Westra, J., Chun, J., & Zupanc, G. K. H. (2007). Numerical chromosome variation and mitotic segregation defects in the adult brain of teleost fish. *Developmental Neurobiology*, *67*(10), 1334–1347. https://doi.org/10.1002/dneu.20365

Ramdzan, Y. M., Trubetskov, M. M., Ormsby, A. R., Newcombe, E. A., Sui, X., Tobin, M. J., Bongiovanni, M. N., Gras, S. L., Dewson, G., Miller, J. M. L., Finkbeiner, S., Moily, N. S., Niclis, J., Parish, C. L., Purcell, A. W., Baker, M. J., Wilce, J. A., Waris, S., Stojanovski, D., … Hatters, D. M. (2017). Huntingtin Inclusions Trigger Cellular Quiescence, Deactivate Apoptosis, and Lead to Delayed Necrosis. *Cell Reports*, *19*(5), 919–927. https://doi.org/10.1016/j.celrep.2017.04.029

Rancati, G., Pavelka, N., Fleharty, B., Noll, A., Trimble, R., Walton, K., Perera, A., Staehling-Hampton, K., Seidel, C. W., & Li, R. (2008). Aneuploidy underlies rapid adaptive evolution of yeast cells deprived of a conserved cytokinesis motor. *Cell*, *135*(5), 879–893. https://doi.org/10.1016/j.cell.2008.09.039

Ravikumar, B., Vacher, C., Berger, Z., Davies, J. E., Luo, S., Oroz, L. G., Scaravilli, F., Easton, D. F., Duden, R., O'Kane, C. J., & Rubinsztein, D. C. (2004). Inhibition of mTOR induces autophagy and reduces toxicity of polyglutamine expansions in fly and mouse models of Huntington disease. *Nature Genetics*, *36*(6), 585–595. https://doi.org/10.1038/ng1362

Recasens-Alvarez, C., Alexandre, C., Kirkpatrick, J., Nojima, H., Huels, D. J., Snijders, A. P., & Vincent, J.-P. (2021). Ribosomopathy-associated mutations cause proteotoxic stress that is alleviated by TOR inhibition. *Nature Cell Biology*, *23*(2), 127–135. https://doi.org/10.1038/s41556-020-00626-1

Regan, L., Braude, P. R., & Trembath, P. L. (1989). Influence of past reproductive performance on risk of spontaneous abortion. *British Medical Journal*, *299*(6698), 541–545. https://doi.org/10.1136/bmj.299.6698.541

Regin, M., Lei, Y., Deckersberg, E. C. D., Janssens, C., Huyghebaert, A., Guns, Y., Verdyck, P., Verheyen, G., Velde, H. V. de, Sermon, K., & Spits, C. (2024). Complex aneuploidy triggers autophagy and p53-mediated apoptosis and impairs the second lineage segregation in human preimplantation embryos. *eLife*, *12*. https://doi.org/10.7554/eLife.88916.2

Rehen, S. K., McConnell, M. J., Kaushal, D., Kingsbury, M. A., Yang, A. H., & Chun, J. (2001). Chromosomal variation in neurons of the developing and adult mammalian nervous system. *Proceedings of the National Academy of Sciences*, *98*(23), 13361–13366. https://doi.org/10.1073/pnas.231487398

Rehen, S. K., Yung, Y. C., McCreight, M. P., Kaushal, D., Yang, A. H., Almeida, B. S. V., Kingsbury, M. A., Cabral, K. M. S., McConnell, M. J., Anliker, B., Fontanoz, M., & Chun, J. (2005). Constitutional Aneuploidy in the Normal Human Brain. *Journal of Neuroscience*, *25*(9), 2176–2180. https://doi.org/10.1523/JNEUROSCI.4560-04.2005

Reilly, C. R., & Shimamura, A. (2023). Predisposition to myeloid malignancies in Shwachman-Diamond syndrome: Biological insights and clinical advances. *Blood*, *141*(13), 1513–1523. https://doi.org/10.1182/blood.2022017739

Replogle, J. M., Zhou, W., Amaro, A. E., McFarland, J. M., Villalobos-Ortiz, M., Ryan, J., Letai, A., Yilmaz, O., Sheltzer, J., Lippard, S. J., Ben-David, U., & Amon, A. (2020). Aneuploidy increases resistance to chemotherapeutics by antagonizing cell division. *Proceedings of the National Academy of Sciences of the United States of America*, *117*(48), 30566–30576. https://doi.org/10.1073/pnas.2009506117

Revy, P., Kannengiesser, C., & Fischer, A. (2019). Somatic genetic rescue in Mendelian haematopoietic diseases. *Nature Reviews. Genetics*, *20*(10), 582–598. https://doi.org/10.1038/s41576-019-0139-x

Rhiner, C., López-Gay, J. M., Soldini, D., Casas-Tinto, S., Martín, F. A., Lombardía, L., & Moreno, E. (2010). Flower forms an extracellular code that reveals the fitness of a cell to its neighbors in Drosophila. *Developmental Cell*, *18*(6), 985–998. https://doi.org/10.1016/j.devcel.2010.05.010

Riggs, E. R., Nelson, T., Merz, A., Ackley, T., Bunke, B., Collins, C. D., Collinson, M. N., Fan, Y.-S., Goodenberger, M. L., Golden, D. M., Haglund-Hazy, L., Krgovic, D., Lamb, A. N., Lewis, Z., Li, G., Liu, Y., Meck, J., Neufeld-Kaiser, W., Runke, C. K., … Martin, C. L. (2018). Copy number variant discrepancy resolution using the ClinGen dosage sensitivity map results in updated clinical interpretations in ClinVar. *Human Mutation*, *39*(11), 1650–1659. https://doi.org/10.1002/humu.23610

Ripoll, P. (1980). Effect of Terminal Aneuploidy on Epidermal Cell Viability in DROSOPHILA MELANOGASTER. *Genetics*, *94*(1), 135–152.

Robertson, S. A., & Richards, R. I. (2024). Single-cell sequencing shows mosaic aneuploidy in most human embryos. *The Journal of Clinical Investigation*, *134*(6), e179134. https://doi.org/10.1172/JCI179134

Robinson, W. P., Barrett, I. J., Bernard, L., Telenius, A., Bernasconi, F., Wilson, R. D., Best, R. G., Howard-Peebles, P. N., Langlois, S., & Kalousek, D. K. (1997). Meiotic origin of trisomy in confined placental

mosaicism is correlated with presence of fetal uniparental disomy, high levels of trisomy in trophoblast, and increased risk of fetal intrauterine growth restriction. *American Journal of Human Genetics*, *60*(4), 917–927.

Rodríguez-Santiago, B., Malats, N., Rothman, N., Armengol, L., Garcia-Closas, M., Kogevinas, M., Villa, O., Hutchinson, A., Earl, J., Marenne, G., Jacobs, K., Rico, D., Tardón, A., Carrato, A., Thomas, G., Valencia, A., Silverman, D., Real, F. X., Chanock, S. J., & Pérez-Jurado, L. A. (2010). Mosaic uniparental disomies and aneuploidies as large structural variants of the human genome. *American Journal of Human Genetics*, *87*(1), 129–138. https://doi.org/10.1016/j.ajhg.2010.06.002

Röijer, E., Nordkvist, A., Ström, A.-K., Ryd, W., Behrendt, M., Bullerdiek, J., Mark, J., & Stenman, G. (2002). Translocation, Deletion/Amplification, and Expression of *HMGIC* and *MDM2* in a Carcinoma ex Pleomorphic Adenoma. *The American Journal of Pathology*, *160*(2), 433–440. https://doi.org/10.1016/S0002-9440(10)64862-6

Rosa, R. F. M., Zen, P. R. G., Ricachinevsky, C. P., Pilla, C. B., Pereira, V. L. B., Roman, T., Varella-Garcia, M., & Paskulin, G. A. (2009). 22q11.2 duplication and congenital heart defects. *Arquivos Brasileiros De Cardiologia*, *93*(4), e67-69, e55-57. https://doi.org/10.1590/s0066-782x2009001000025

Rutledge, S. D., Douglas, T. A., Nicholson, J. M., Vila-Casadesús, M., Kantzler, C. L., Wangsa, D., Barroso-Vilares, M., Kale, S. D., Logarinho, E., & Cimini, D. (2016). Selective advantage of trisomic human cells cultured in non-standard conditions. *Scientific Reports*, *6*, 22828. https://doi.org/10.1038/srep22828

Ryder, E., Ashburner, M., Bautista-Llacer, R., Drummond, J., Webster, J., Johnson, G., Morley, T., Chan, Y. S., Blows, F., Coulson, D., Reuter, G., Baisch, H., Apelt, C., Kauk, A., Rudolph, T., Kube, M., Klimm, M., Nickel, C., Szidonya, J., … Russell, S. (2007). The DrosDel Deletion Collection: A Drosophila Genomewide Chromosomal Deficiency Resource. *Genetics*, *177*(1), 615–629. https://doi.org/10.1534/genetics.107.076216

Ryder, E., Blows, F., Ashburner, M., Bautista-Llacer, R., Coulson, D., Drummond, J., Webster, J., Gubb, D., Gunton, N., Johnson, G., O'Kane, C. J., Huen, D., Sharma, P., Asztalos, Z., Baisch, H., Schulze, J., Kube, M., Kittlaus, K., Reuter, G., … Russell, S. (2004). The DrosDel Collection: A Set of *P* -Element Insertions for Generating Custom Chromosomal Aberrations in *Drosophila melanogaster*. *Genetics*, *167*(2), 797–813. https://doi.org/10.1534/genetics.104.026658

Ryoo, H. D., Gorenc, T., & Steller, H. (2004). Apoptotic cells can induce compensatory cell proliferation through the JNK and the Wingless signaling pathways. *Developmental Cell*, *7*(4), 491–501. https://doi.org/10.1016/j.devcel.2004.08.019

Sakaue-Sawano, A., Kurokawa, H., Morimura, T., Hanyu, A., Hama, H., Osawa, H., Kashiwagi, S., Fukami, K., Miyata, T., Miyoshi, H., Imamura, T., Ogawa, M., Masai, H., & Miyawaki, A. (2008). Visualizing Spatiotemporal Dynamics of Multicellular Cell-Cycle Progression. *Cell*, *132*(3), 487–498. https://doi.org/10.1016/j.cell.2007.12.033

Sanaki, Y., Nagata, R., Kizawa, D., Léopold, P., & Igaki, T. (2020). Hyperinsulinemia Drives Epithelial Tumorigenesis by Abrogating Cell Competition. *Developmental Cell*, *53*(4), 379-389.e5. https://doi.org/10.1016/j.devcel.2020.04.008

Sancho, M., Di-Gregorio, A., George, N., Pozzi, S., Sánchez, J. M., Pernaute, B., & Rodríguez, T. A. (2013). Competitive interactions eliminate unfit embryonic stem cells at the onset of differentiation. *Developmental Cell*, *26*(1), 19–30. https://doi.org/10.1016/j.devcel.2013.06.012

Santaguida, S., Richardson, A., Iyer, D. R., M'Saad, O., Zasadil, L., Knouse, K. A., Wong, Y. L., Rhind, N., Desai, A., & Amon, A. (2017). Chromosome Mis-segregation Generates Cell-Cycle-Arrested Cells with Complex Karyotypes that Are Eliminated by the Immune System. *Developmental Cell*, *41*(6), 638-651.e5. https://doi.org/10.1016/j.devcel.2017.05.022

Santaguida, S., Vasile, E., White, E., & Amon, A. (2015). Aneuploidy-induced cellular stresses limit autophagic degradation. *Genes & Development*, *29*(19), 2010–2021. https://doi.org/10.1101/gad.269118.115

Sarel-Gallily, R., Golan-Lev, T., Yilmaz, A., Sagi, I., & Benvenisty, N. (2022). Genome-wide analysis of haploinsufficiency in human embryonic stem cells. *Cell Reports*, *38*(13), 110573. https://doi.org/10.1016/j.celrep.2022.110573

Sarkar, S., Davies, J. E., Huang, Z., Tunnacliffe, A., & Rubinsztein, D. C. (2007). Trehalose, a novel mTOR-independent autophagy enhancer, accelerates the clearance of mutant huntingtin and alpha-synuclein. *The Journal of Biological Chemistry*, *282*(8), 5641–5652. https://doi.org/10.1074/jbc.M609532200

Scavone, F., Gumbin, S. C., Da Rosa, P. A., & Kopito, R. R. (2023). RPL26/uL24 UFMylation is essential for ribosome-associated quality control at the endoplasmic reticulum. *Proceedings of the National Academy of Sciences*, *120*(16), e2220340120. https://doi.org/10.1073/pnas.2220340120

Scherthan, H., Bähler, J., & Kohli, J. (1994). Dynamics of chromosome organization and pairing during meiotic prophase in fission yeast. *Journal of Cell Biology*, *127*(2), 273–285. https://doi.org/10.1083/jcb.127.2.273

Scott, R. T., Upham, K. M., Forman, E. J., Hong, K. H., Scott, K. L., Taylor, D., Tao, X., & Treff, N. R. (2013). Blastocyst biopsy with comprehensive chromosome screening and fresh embryo transfer significantly increases in vitro fertilization implantation and delivery rates: A randomized controlled trial. *Fertility and Sterility*, *100*(3), 697–703. https://doi.org/10.1016/j.fertnstert.2013.04.035

Scriven, P. N., Flinter, F. A., Braude, P. R., & Ogilvie, C. M. (2001). Robertsonian translocations—Reproductive risks and indications for preimplantation genetic diagnosis. *Human Reproduction*, *16*(11), 2267–2273. https://doi.org/10.1093/humrep/16.11.2267

Segal, D. J., & McCoy, E. E. (1974). Studies on Down's syndrome in tissue culture. I. Growth rates and protein contents of fibroblast cultures. *Journal of Cellular Physiology*, *83*(1), 85–90. https://doi.org/10.1002/jcp.1040830112

Shahbazi, M. N., Wang, T., Tao, X., Weatherbee, B. A. T., Sun, L., Zhan, Y., Keller, L., Smith, G. D., Pellicer, A., Scott, R. T., Seli, E., & Zernicka-Goetz, M. (2020). Developmental potential of aneuploid human

embryos cultured beyond implantation. *Nature Communications*, *11*(1), 3987. https://doi.org/10.1038/s41467-020-17764-7

Shao, X., Lv, N., Liao, J., Long, J., Xue, R., Ai, N., Xu, D., & Fan, X. (2019). Copy number variation is highly correlated with differential gene expression: A pan-cancer study. *BMC Medical Genetics*, *20*(1), 175. https://doi.org/10.1186/s12881-019-0909-5

Sheltzer, J. M., Blank, H. M., Pfau, S. J., Tange, Y., George, B. M., Humpton, T. J., Brito, I. L., Hiraoka, Y., Niwa, O., & Amon, A. (2011). Aneuploidy drives genomic instability in yeast. *Science (New York, N.Y.)*, *333*(6045), 1026–1030. https://doi.org/10.1126/science.1206412

Shiel, M. J., & Caplan, M. J. (1995). The generation of epithelial polarity in mammalian and *Drosophila* embryos. *Seminars in Developmental Biology*, *6*(1), 39–46. https://doi.org/10.1016/S1044-5781(06)80083-6

Shinohara, T., Tomizuka, K., Miyabara, S., Takehara, S., Kazuki, Y., Inoue, J., Katoh, M., Nakane, H., Iino, A., Ohguma, A., Ikegami, S., Inokuchi, K., Ishida, I., Reeves, R. H., & Oshimura, M. (2001). Mice containing a human chromosome 21 model behavioral impairment and cardiac anomalies of Down's syndrome. *Human Molecular Genetics*, *10*(11), 1163–1175. https://doi.org/10.1093/hmg/10.11.1163

Shoshani, O., Bakker, B., de Haan, L., Tijhuis, A. E., Wang, Y., Kim, D. H., Maldonado, M., Demarest, M. A., Artates, J., Zhengyu, O., Mark, A., Wardenaar, R., Sasik, R., Spierings, D. C. J., Vitre, B., Fisch, K., Foijer, F., & Cleveland, D. W. (2021). Transient genomic instability drives tumorigenesis through accelerated clonal evolution. *Genes & Development*, *35*(15–16), 1093–1108. https://doi.org/10.1101/gad.348319.121

Sifakis, S., Staboulidou, I., Maiz, N., Velissariou, V., & Nicolaides, K. H. (2010). Outcome of pregnancies with trisomy 2 cells in chorionic villi. *Prenatal Diagnosis*, *30*(4), 329–332. https://doi.org/10.1002/pd.2457

Singer, M. J., Mesner, L. D., Friedman, C. L., Trask, B. J., & Hamlin, J. L. (2000). Amplification of the human dihydrofolate reductase gene via double minutes is initiated by chromosome breaks. *Proceedings of the National Academy of Sciences of the United States of America*, *97*(14), 7921–7926. https://doi.org/10.1073/pnas.130194897

Singla, S., Iwamoto-Stohl, L. K., Zhu, M., & Zernicka-Goetz, M. (2020). Autophagy-mediated apoptosis eliminates aneuploid cells in a mouse model of chromosome mosaicism. *Nature Communications*, *11*(1), 2958. https://doi.org/10.1038/s41467-020-16796-3

Singleton, A. B., Farrer, M., Johnson, J., Singleton, A., Hague, S., Kachergus, J., Hulihan, M., Peuralinna, T., Dutra, A., Nussbaum, R., Lincoln, S., Crawley, A., Hanson, M., Maraganore, D., Adler, C., Cookson, M. R., Muenter, M., Baptista, M., Miller, D., … Gwinn-Hardy, K. (2003). Alpha-Synuclein locus triplication causes Parkinson's disease. *Science (New York, N.Y.)*, *302*(5646), 841. https://doi.org/10.1126/science.1090278

Soler, A., Morales, C., Mademont-Soler, I., Margarit, E., Borrell, A., Borobio, V., Muñoz, M., & Sánchez, A. (2017). Overview of Chromosome Abnormalities in First Trimester Miscarriages: A Series of 1,011

Consecutive Chorionic Villi Sample Karyotypes. *Cytogenetic and Genome Research*, *152*(2), 81–89. https://doi.org/10.1159/000477707

Solimini, N. L., Xu, Q., Mermel, C. H., Liang, A. C., Schlabach, M. R., Luo, J., Burrows, A. E., Anselmo, A. N., Bredemeyer, A. L., Li, M. Z., Beroukhim, R., Meyerson, M., & Elledge, S. J. (2012). Recurrent Hemizygous Deletions in Cancers May Optimize Proliferative Potential. *Science*, *337*(6090), 104–109. https://doi.org/10.1126/science.1219580

Soucek, T., Rosner, M., Miloloza, A., Kubista, M., Cheadle, J. P., Sampson, J. R., & Hengstschläger, M. (2001). Tuberous sclerosis causing mutants of the TSC2 gene product affect proliferation and p27 expression. *Oncogene*, *20*(35), 4904–4909. https://doi.org/10.1038/sj.onc.1204627

Spanos, S., Rice, S., Karagiannis, P., Taylor, D., Becker, D. L., Winston, R. M. L., & Hardy, K. (2002). Caspase activity and expression of cell death genes during development of human preimplantation embryos. *Reproduction (Cambridge, England)*, *124*(3), 353–363. https://doi.org/10.1530/rep.0.1240353

Spector, D. L. (2003). The dynamics of chromosome organization and gene regulation. *Annual Review of Biochemistry*, *72*, 573–608. https://doi.org/10.1146/annurev.biochem.72.121801.161724

Steinberg, J., Honti, F., Meader, S., & Webber, C. (2015). Haploinsufficiency predictions without study bias. *Nucleic Acids Research*, *43*(15), e101. https://doi.org/10.1093/nar/gkv474

Stenberg, P., Lundberg, L. E., Johansson, A.-M., Rydén, P., Svensson, M. J., & Larsson, J. (2009). Buffering of Segmental and Chromosomal Aneuploidies in Drosophila melanogaster. *PLOS Genetics*, *5*(5), e1000465. https://doi.org/10.1371/journal.pgen.1000465

Stephens, P. J., Greenman, C. D., Fu, B., Yang, F., Bignell, G. R., Mudie, L. J., Pleasance, E. D., Lau, K. W., Beare, D., Stebbings, L. A., McLaren, S., Lin, M.-L., McBride, D. J., Varela, I., Nik-Zainal, S., Leroy, C., Jia, M., Menzies, A., Butler, A. P., … Campbell, P. J. (2011). Massive Genomic Rearrangement Acquired in a Single Catastrophic Event during Cancer Development. *Cell*, *144*(1), 27–40. https://doi.org/10.1016/j.cell.2010.11.055

Stern, C. (1936). Somatic Crossing over and Segregation in Drosophila Melanogaster. *Genetics*, *21*(6), 625–730.

Stingele, S., Stoehr, G., Peplowska, K., Cox, J., Mann, M., & Storchova, Z. (2012). Global analysis of genome, transcriptome and proteome reveals the response to aneuploidy in human cells. *Molecular Systems Biology*, *8*, 608. https://doi.org/10.1038/msb.2012.40

Stone, J. F., & Sandberg, A. A. (1995). Sex chromosome aneuploidy and aging. *Mutation Research/DNAging*, *338*(1), 107–113. https://doi.org/10.1016/0921-8734(95)00016-Y

Suijkerbuijk, S. J. E., Kolahgar, G., Kucinski, I., & Piddini, E. (2016). Cell Competition Drives the Growth of Intestinal Adenomas in Drosophila. *Current Biology*, *26*(4), 428–438. https://doi.org/10.1016/j.cub.2015.12.043

Sun, Y., Ji, P., Chen, T., Zhou, X., Yang, D., Guo, Y., Liu, Y., Hu, L., Xia, D., Liu, Y., Multani, A. S., Shmulevich, I., Kucherlapati, R., Kopetz, S., Sood, A. K., Hamilton, S. R., Sun, B., & Zhang, W.

(2017). MIIP haploinsufficiency induces chromosomal instability and promotes tumour progression in colorectal cancer. *The Journal of Pathology*, *241*(1), 67–79. https://doi.org/10.1002/path.4823

Tamori, Y., Bialucha, C. U., Tian, A.-G., Kajita, M., Huang, Y.-C., Norman, M., Harrison, N., Poulton, J., Ivanovitch, K., Disch, L., Liu, T., Deng, W.-M., & Fujita, Y. (2010). Involvement of Lgl and Mahjong/VprBP in cell competition. *PLoS Biology*, *8*(7), e1000422. https://doi.org/10.1371/journal.pbio.1000422

Tang, Y.-C., Williams, B. R., Siegel, J. J., & Amon, A. (2011). Identification of aneuploidy-selective antiproliferation compounds. *Cell*, *144*(4), 499–512. https://doi.org/10.1016/j.cell.2011.01.017

Tarchini, B., Huynh, T. H. N., Cox, G. A., & Duboule, D. (2005). HoxD cluster scanning deletions identify multiple defects leading to paralysis in the mouse mutant Ironside. *Genes & Development*, *19*(23), 2862–2876. https://doi.org/10.1101/gad.351105

Taylor, A. M., Shih, J., Ha, G., Gao, G. F., Zhang, X., Berger, A. C., Schumacher, S. E., Wang, C., Hu, H., Liu, J., Lazar, A. J., Cancer Genome Atlas Research Network, Cherniack, A. D., Beroukhim, R., & Meyerson, M. (2018). Genomic and Functional Approaches to Understanding Cancer Aneuploidy. *Cancer Cell*, *33*(4), 676-689.e3. https://doi.org/10.1016/j.ccell.2018.03.007

Thatcher, K. N., Peddada, S., Yasui, D. H., & Lasalle, J. M. (2005). Homologous pairing of 15q11-13 imprinted domains in brain is developmentally regulated but deficient in Rett and autism samples. *Human Molecular Genetics*, *14*(6), 785–797. https://doi.org/10.1093/hmg/ddi073

Thomas, R., Marks, D. H., Chin, Y., & Benezra, R. (2018). Whole chromosome loss and associated breakage-fusion-bridge cycles transform mouse tetraploid cells. *The EMBO Journal*, *37*(2), 201–218. https://doi.org/10.15252/embj.201797630

Thompson, S. L., & Compton, D. A. (2008). Examining the link between chromosomal instability and aneuploidy in human cells. *The Journal of Cell Biology*, *180*(4), 665–672. https://doi.org/10.1083/jcb.200712029

Tiu, G. C., Kerr, C. H., Forester, C. M., Krishnarao, P. S., Rosenblatt, H. D., Raj, N., Lantz, T. C., Zhulyn, O., Bowen, M. E., Shokat, L., Attardi, L. D., Ruggero, D., & Barna, M. (2021). A p53-dependent translational program directs tissue-selective phenotypes in a model of ribosomopathies. *Developmental Cell*, *56*(14), 2089-2102.e11. https://doi.org/10.1016/j.devcel.2021.06.013

Toledo, F., Buttin, G., & Debatisse, M. (1993). The origin of chromosome rearrangements at early stages of AMPD2 gene amplification in Chinese hamster cells. *Current Biology: CB*, *3*(5), 255–264. https://doi.org/10.1016/0960-9822(93)90175-n

Torres, E. M., Dephoure, N., Panneerselvam, A., Tucker, C. M., Whittaker, C. A., Gygi, S. P., Dunham, M. J., & Amon, A. (2010). Identification of aneuploidy-tolerating mutations. *Cell*, *143*(1), 71–83. https://doi.org/10.1016/j.cell.2010.08.038

Torres, E. M., Sokolsky, T., Tucker, C. M., Chan, L. Y., Boselli, M., Dunham, M. J., & Amon, A. (2007). Effects of aneuploidy on cellular physiology and cell division in haploid yeast. *Science (New York, N.Y.)*, *317*(5840), 916–924. https://doi.org/10.1126/science.1142210

Tovini, L., Johnson, S. C., Guscott, M. A., Andersen, A. M., Spierings, D. C. J., Wardenaar, R., Foijer, F., & McClelland, S. E. (2023). Targeted assembly of ectopic kinetochores to induce chromosome-specific segmental aneuploidies. *The EMBO Journal*, *42*(10), e111587. https://doi.org/10.15252/embj.2022111587

Trakala, M., Aggarwal, M., Sniffen, C., Zasadil, L., Carroll, A., Ma, D., Su, X. A., Wangsa, D., Meyer, A., Sieben, C. J., Zhong, J., Hsu, P.-H., Paradis, G., Ried, T., Holland, A., Van Deursen, J., & Amon, A. (2021). Clonal selection of stable aneuploidies in progenitor cells drives high-prevalence tumorigenesis. *Genes & Development*, *35*(15–16), 1079–1092. https://doi.org/10.1101/gad.348341.121

Truong, M. A., Cané-Gasull, P., de Vries, S. G., Nijenhuis, W., Wardenaar, R., Kapitein, L. C., Foijer, F., & Lens, S. M. (2023). A kinesin-based approach for inducing chromosome-specific mis-segregation in human cells. *The EMBO Journal*, *42*(10), e111559. https://doi.org/10.15252/embj.2022111559

Truong, M. A., Cané-Gasull, P., & Lens, S. M. A. (2023). Modeling specific aneuploidies: From karyotype manipulations to biological insights. *Chromosome Research: An International Journal on the Molecular, Supramolecular and Evolutionary Aspects of Chromosome Biology*, *31*(3), 25. https://doi.org/10.1007/s10577-023-09735-7

Turner, D. J., Miretti, M., Rajan, D., Fiegler, H., Carter, N. P., Blayney, M. L., Beck, S., & Hurles, M. E. (2008). Germline rates of de novo meiotic deletions and duplications causing several genomic disorders. *Nature Genetics*, *40*(1), 90–95. https://doi.org/10.1038/ng.2007.40

Tye, B. W., Commins, N., Ryazanova, L. V., Wühr, M., Springer, M., Pincus, D., & Churchman, L. S. (2019). Proteotoxicity from aberrant ribosome biogenesis compromises cell fitness. *eLife*, *8*, e43002. https://doi.org/10.7554/eLife.43002

Tyler, D. M., Li, W., Zhuo, N., Pellock, B., & Baker, N. E. (2007). Genes Affecting Cell Competition in Drosophila. *Genetics*, *175*(2), 643–657. https://doi.org/10.1534/genetics.106.061929

Uechi, T., Tanaka, T., & Kenmochi, N. (2001). A Complete Map of the Human Ribosomal Protein Genes: Assignment of 80 Genes to the Cytogenetic Map and Implications for Human Disorders. *Genomics*, *72*(3), 223–230. https://doi.org/10.1006/geno.2000.6470

Utani, K., Kawamoto, J., & Shimizu, N. (2007). Micronuclei bearing acentric extrachromosomal chromatin are transcriptionally competent and may perturb the cancer cell phenotype. *Molecular Cancer Research: MCR*, *5*(7), 695–704. https://doi.org/10.1158/1541-7786.MCR-07-0031

Valent, A., Bénard, J., Clausse, B., Barrois, M., Valteau-Couanet, D., Terrier-Lacombe, M.-J., Spengler, B., & Bernheim, A. (2001). *In Vivo* Elimination of Acentric Double Minutes Containing Amplified *MYCN* from Neuroblastoma Tumor Cells Through the Formation of Micronuclei. *The American Journal of Pathology*, *158*(5), 1579–1584. https://doi.org/10.1016/S0002-9440(10)64112-0

Valenti, D., Manente, G. A., Moro, L., Marra, E., & Vacca, R. A. (2011). Deficit of complex I activity in human skin fibroblasts with chromosome 21 trisomy and overproduction of reactive oxygen species by

mitochondria: Involvement of the cAMP/PKA signalling pathway. *The Biochemical Journal*, *435*(3), 679–688. https://doi.org/10.1042/BJ20101908

van Echten-Arends, J., Mastenbroek, S., Sikkema-Raddatz, B., Korevaar, J. C., Heineman, M. J., van der Veen, F., & Repping, S. (2011). Chromosomal mosaicism in human preimplantation embryos: A systematic review. *Human Reproduction Update*, *17*(5), 620–627. https://doi.org/10.1093/humupd/dmr014

Vanneste, E., Voet, T., Le Caignec, C., Ampe, M., Konings, P., Melotte, C., Debrock, S., Amyere, M., Vikkula, M., Schuit, F., Fryns, J.-P., Verbeke, G., D'Hooghe, T., Moreau, Y., & Vermeesch, J. R. (2009). Chromosome instability is common in human cleavage-stage embryos. *Nature Medicine*, *15*(5), 577–583. https://doi.org/10.1038/nm.1924

Vasudevan, A., Schukken, K. M., Sausville, E. L., Girish, V., Adebambo, O. A., & Sheltzer, J. M. (2021). Aneuploidy as a promoter and suppressor of malignant growth. *Nature Reviews. Cancer*, *21*(2), 89–103. https://doi.org/10.1038/s41568-020-00321-1

Vázquez-Diez, C., & FitzHarris, G. (2018). *Causes and consequences of chromosome segregation error in preimplantation embryos*. https://doi.org/10.1530/REP-17-0569

Venkatachalam, S., Shi, Y. P., Jones, S. N., Vogel, H., Bradley, A., Pinkel, D., & Donehower, L. A. (1998). Retention of wild-type p53 in tumors from p53 heterozygous mice: Reduction of p53 dosage can promote cancer formation. *The EMBO Journal*, *17*(16), 4657–4667. https://doi.org/10.1093/emboj/17.16.4657

Vicoso, B., & Bachtrog, D. (2013). Reversal of an ancient sex chromosome to an autosome in Drosophila. *Nature*, *499*(7458), 332–335. https://doi.org/10.1038/nature12235

Villa del Campo, C., Clavería, C., Sierra, R., & Torres, M. (2014). Cell Competition Promotes Phenotypically Silent Cardiomyocyte Replacement in the Mammalian Heart. *Cell Reports*, *8*(6), 1741–1751. https://doi.org/10.1016/j.celrep.2014.08.005

Vincent, J.-P., Kolahgar, G., Gagliardi, M., & Piddini, E. (2011). Steep differences in wingless signaling trigger Myc-independent competitive cell interactions. *Developmental Cell*, *21*(2), 366–374. https://doi.org/10.1016/j.devcel.2011.06.021

Von Hoff, D. D., McGill, J. R., Forseth, B. J., Davidson, K. K., Bradley, T. P., Van Devanter, D. R., & Wahl, G. M. (1992). Elimination of extrachromosomally amplified MYC genes from human tumor cells reduces their tumorigenicity. *Proceedings of the National Academy of Sciences*, *89*(17), 8165–8169. https://doi.org/10.1073/pnas.89.17.8165

Vorsanova, S. G., Kolotii, A. D., Iourov, I. Y., Monakhov, V. V., Kirillova, E. A., Soloviev, I. V., & Yurov, Y. B. (2005). Evidence for high frequency of chromosomal mosaicism in spontaneous abortions revealed by interphase FISH analysis. *The Journal of Histochemistry and Cytochemistry: Official Journal of the Histochemistry Society*, *53*(3), 375–380. https://doi.org/10.1369/jhc.4A6424.2005

Wada, T., & Candotti, F. (2008). Somatic mosaicism in primary immune deficiencies. *Current Opinion in Allergy and Clinical Immunology*, *8*(6), 510–514. https://doi.org/10.1097/ACI.0b013e328314b651

Wagstaff, L., Goschorska, M., Kozyrska, K., Duclos, G., Kucinski, I., Chessel, A., Hampton-O'Neil, L., Bradshaw, C. R., Allen, G. E., Rawlins, E. L., Silberzan, P., Carazo Salas, R. E., & Piddini, E. (2016). Mechanical cell competition kills cells via induction of lethal p53 levels. *Nature Communications*, *7*, 11373. https://doi.org/10.1038/ncomms11373

Walczak, C. P., Leto, D. E., Zhang, L., Riepe, C., Muller, R. Y., DaRosa, P. A., Ingolia, N. T., Elias, J. E., & Kopito, R. R. (2019). Ribosomal protein RPL26 is the principal target of UFMylation. *Proceedings of the National Academy of Sciences*, *116*(4), 1299–1308. https://doi.org/10.1073/pnas.1816202116

Wang, L., Xu, Y., Yun, S., Yuan, Q., Satpute-Krishnan, P., & Ye, Y. (2023). SAYSD1 senses UFMylated ribosome to safeguard co-translational protein translocation at the endoplasmic reticulum. *Cell Reports*, *42*(1). https://doi.org/10.1016/j.celrep.2023.112028

Wang, R. W., Viganò, S., Ben-David, U., Amon, A., & Santaguida, S. (2021). Aneuploid senescent cells activate NF-κB to promote their immune clearance by NK cells. *EMBO Reports*, *22*(8), e52032. https://doi.org/10.15252/embr.202052032

Wang, X., Chen, C., Wang, L., Chen, D., Guang, W., & French, J. (2003). Conception, early pregnancy loss, and time to clinical pregnancy: A population-based prospective study. *Fertility and Sterility*, *79*(3), 577–584. https://doi.org/10.1016/S0015-0282(02)04694-0

Weaver, B. A., & Cleveland, D. W. (2006). Does aneuploidy cause cancer? *Current Opinion in Cell Biology*, *18*(6), 658–667. https://doi.org/10.1016/j.ceb.2006.10.002

Webb, A. E., & Brunet, A. (2014). FOXO transcription factors: Key regulators of cellular quality control. *Trends in Biochemical Sciences*, *39*(4), 159–169. https://doi.org/10.1016/j.tibs.2014.02.003

Weinberg, R. A. (1994). Oncogenes and tumor suppressor genes. *CA: A Cancer Journal for Clinicians*, *44*(3), 160–170. https://doi.org/10.3322/canjclin.44.3.160

Weise, A., Mrasek, K., Klein, E., Mulatinho, M., Llerena, J. C., Hardekopf, D., Pekova, S., Bhatt, S., Kosyakova, N., & Liehr, T. (2012). Microdeletion and Microduplication Syndromes. *Journal of Histochemistry and Cytochemistry*, *60*(5), 346–358. https://doi.org/10.1369/0022155412440001

Wellesley, D., Dolk, H., Boyd, P. A., Greenlees, R., Haeusler, M., Nelen, V., Garne, E., Khoshnood, B., Doray, B., Rissmann, A., Mullaney, C., Calzolari, E., Bakker, M., Salvador, J., Addor, M.-C., Draper, E., Rankin, J., & Tucker, D. (2012). Rare chromosome abnormalities, prevalence and prenatal diagnosis rates from population-based congenital anomaly registers in Europe. *European Journal of Human Genetics: EJHG*, *20*(5), 521–526. https://doi.org/10.1038/ejhg.2011.246

Wells, D., Bermudez, M. G., Steuerwald, N., Thornhill, A. R., Walker, D. L., Malter, H., Delhanty, J. D. A., & Cohen, J. (2005). Expression of genes regulating chromosome segregation, the cell cycle and apoptosis during human preimplantation development. *Human Reproduction (Oxford, England)*, *20*(5), 1339–1348. https://doi.org/10.1093/humrep/deh778

Wells, D., & Delhanty, J. D. (2000). Comprehensive chromosomal analysis of human preimplantation embryos using whole genome amplification and single cell comparative genomic hybridization. *Molecular Human Reproduction*, *6*(11), 1055–1062. https://doi.org/10.1093/molehr/6.11.1055

Westra, J. W., Peterson, S. E., Yung, Y. C., Mutoh, T., Barral, S., & Chun, J. (2008). Aneuploid mosaicism in the developing and adult cerebellar cortex. *Journal of Comparative Neurology*, *507*(6), 1944–1951. https://doi.org/10.1002/cne.21648

White, J. K., Gerdin, A.-K., Karp, N. A., Ryder, E., Buljan, M., Bussell, J. N., Salisbury, J., Clare, S., Ingham, N. J., Podrini, C., Houghton, R., Estabel, J., Bottomley, J. R., Melvin, D. G., Sunter, D., Adams, N. C., Sanger Institute Mouse Genetics Project, Tannahill, D., Logan, D. W., … Steel, K. P. (2013). Genome-wide generation and systematic phenotyping of knockout mice reveals new roles for many genes. *Cell*, *154*(2), 452–464. https://doi.org/10.1016/j.cell.2013.06.022

Wilcox, A. J., Weinberg, C. R., O'Connor, J. F., Baird, D. D., Schlatterer, J. P., Canfield, R. E., Armstrong, E. G., & Nisula, B. C. (1988). Incidence of Early Loss of Pregnancy. *New England Journal of Medicine*, *319*(4), 189–194. https://doi.org/10.1056/NEJM198807283190401

Williams, B. R., Prabhu, V. R., Hunter, K. E., Glazier, C. M., Whittaker, C. A., Housman, D. E., & Amon, A. (2008). Aneuploidy affects proliferation and spontaneous immortalization in mammalian cells. *Science (New York, N.Y.)*, *322*(5902), 703–709. https://doi.org/10.1126/science.1160058

Wistuba, I. I., Behrens, C., Virmani, A. K., Milchgrub, S., Syed, S., Lam, S., Mackay, B., Minna, J. D., & Gazdar, A. F. (1999). Allelic losses at chromosome 8p21-23 are early and frequent events in the pathogenesis of lung cancer. *Cancer Research*, *59*(8), 1973–1979.

Woloszynek, J. R., Rothbaum, R. J., Rawls, A. S., Minx, P. J., Wilson, R. K., Mason, P. J., Bessler, M., & Link, D. C. (2004). Mutations of the SBDS gene are present in most patients with Shwachman-Diamond syndrome. *Blood*, *104*(12), 3588–3590. https://doi.org/10.1182/blood-2004-04-1516

Wyllie, J. P., Wright, M. J., Burn, J., & Hunter, S. (1994). Natural history of trisomy 13. *Archives of Disease in Childhood*, *71*(4), 343. https://doi.org/10.1136/adc.71.4.343

Xian, S., Dosset, M., Almanza, G., Searles, S., Sahani, P., Waller, T. C., Jepsen, K., Carter, H., & Zanetti, M. (2021). The unfolded protein response links tumor aneuploidy to local immune dysregulation. *EMBO Reports*, *22*(12), e52509. https://doi.org/10.15252/embr.202152509

Xue, W., Kitzing, T., Roessler, S., Zuber, J., Krasnitz, A., Schultz, N., Revill, K., Weissmueller, S., Rappaport, A. R., Simon, J., Zhang, J., Luo, W., Hicks, J., Zender, L., Wang, X. W., Powers, S., Wigler, M., & Lowe, S. W. (2012). A cluster of cooperating tumor-suppressor gene candidates in chromosomal deletions. *Proceedings of the National Academy of Sciences of the United States of America*, *109*(21), 8212–8217. https://doi.org/10.1073/pnas.1206062109

Yamamoto, M., Ohsawa, S., Kunimasa, K., & Igaki, T. (2017). The ligand Sas and its receptor PTP10D drive tumour-suppressive cell competition. *Nature*, *542*(7640), 246–250. https://doi.org/10.1038/nature21033

Yamanaka, T., Horikoshi, Y., Sugiyama, Y., Ishiyama, C., Suzuki, A., Hirose, T., Iwamatsu, A., Shinohara, A., & Ohno, S. (2003). Mammalian Lgl Forms a Protein Complex with PAR-6 and aPKC Independently of PAR-3 to Regulate Epithelial Cell Polarity. *Current Biology*, *13*(9), 734–743. https://doi.org/10.1016/S0960-9822(03)00244-6

Yang, A. H., Kaushal, D., Rehen, S. K., Kriedt, K., Kingsbury, M. A., McConnell, M. J., & Chun, J. (2003). Chromosome segregation defects contribute to aneuploidy in normal neural progenitor cells. *The Journal of Neuroscience: The Official Journal of the Society for Neuroscience*, *23*(32), 10454–10462. https://doi.org/10.1523/JNEUROSCI.23-32-10454.2003

Yang, M., Rito, T., Metzger, J., Naftaly, J., Soman, R., Hu, J., Albertini, D. F., Barad, D. H., Brivanlou, A. H., & Gleicher, N. (2021). Depletion of aneuploid cells in human embryos and gastruloids. *Nature Cell Biology*, *23*(4), 314–321. https://doi.org/10.1038/s41556-021-00660-7

Yao, C.-K., Lin, Y. Q., Ly, C. V., Ohyama, T., Haueter, C. M., Moiseenkova-Bell, V. Y., Wensel, T. G., & Bellen, H. J. (2009). A synaptic vesicle-associated Ca2+ channel promotes endocytosis and couples exocytosis to endocytosis. *Cell*, *138*(5), 947–960. https://doi.org/10.1016/j.cell.2009.06.033

Yurov, Y. B., Iourov, I. Y., Monakhov, V. V., Soloviev, I. V., Vostrikov, V. M., & Vorsanova, S. G. (2005). The variation of aneuploidy frequency in the developing and adult human brain revealed by an interphase FISH study. *The Journal of Histochemistry and Cytochemistry: Official Journal of the Histochemistry Society*, *53*(3), 385–390. https://doi.org/10.1369/jhc.4A6430.2005

Yurov, Y. B., Iourov, I. Y., Vorsanova, S. G., Liehr, T., Kolotii, A. D., Kutsev, S. I., Pellestor, F., Beresheva, A. K., Demidova, I. A., Kravets, V. S., Monakhov, V. V., & Soloviev, I. V. (2007). Aneuploidy and confined chromosomal mosaicism in the developing human brain. *PloS One*, *2*(6), e558. https://doi.org/10.1371/journal.pone.0000558

Yurov, Y. B., Vorsanova, S. G., & Iourov, I. Y. (2009). GIN'n'CIN hypothesis of brain aging: Deciphering the role of somatic genetic instabilities and neural aneuploidy during ontogeny. *Molecular Cytogenetics*, *2*, 23. https://doi.org/10.1186/1755-8166-2-23

Yurov, Y. B., Vorsanova, S. G., & Iourov, I. Y. (2019). Chromosome Instability in the Neurodegenerating Brain. *Frontiers in Genetics*, *10*, 892. https://doi.org/10.3389/fgene.2019.00892

Zeitlin, J., Mohangoo, A., & Cuttini, M. (2009). The European Perinatal Health Report: Comparing the health and care of pregnant women and newborn babies in Europe. *Journal of Epidemiology & Community Health*, *63*(9), 681–682. https://doi.org/10.1136/jech.2009.087296

Zhang, C.-Z., Spektor, A., Cornils, H., Francis, J. M., Jackson, E. K., Liu, S., Meyerson, M., & Pellman, D. (2015). Chromothripsis from DNA damage in micronuclei. *Nature*, *522*(7555), 179–184. https://doi.org/10.1038/nature14493

Zhang, F.-L., Li, W.-D., Zhu, K.-X., Zhou, X., Li, L., Lee, T.-L., & Shen, W. (2023). Aging-related aneuploidy is associated with mitochondrial imbalance and failure of spindle assembly. *Cell Death Discovery*, *9*(1), 1–12. https://doi.org/10.1038/s41420-023-01539-2

Zhang, G., Xie, Y., Zhou, Y., Xiang, C., Chen, L., Zhang, C., Hou, X., Chen, J., Zong, H., & Liu, G. (2017). P53 pathway is involved in cell competition during mouse embryogenesis. *Proceedings of the National Academy of Sciences*, *114*(3), 498–503. https://doi.org/10.1073/pnas.1617414114

Zhang, Y., Malone, J. H., Powell, S. K., Periwal, V., Spana, E., MacAlpine, D. M., & Oliver, B. (2010). Expression in Aneuploid Drosophila S2 Cells. *PLoS Biology*, *8*(2), e1000320. https://doi.org/10.1371/journal.pbio.1000320

Zheng, B., Sage, M., Sheppeard, E. A., Jurecic, V., & Bradley, A. (2000). Engineering Mouse Chromosomes with Cre-loxP: Range, Efficiency, and Somatic Applications. *Molecular and Cellular Biology*, *20*(2), 648. https://doi.org/10.1128/mcb.20.2.648-655.2000

Zhu, J., Pavelka, N., Bradford, W. D., Rancati, G., & Li, R. (2012). Karyotypic determinants of chromosome instability in aneuploid budding yeast. *PLoS Genetics*, *8*(5), e1002719. https://doi.org/10.1371/journal.pgen.1002719

Zhu, J., Tsai, H.-J., Gordon, M. R., & Li, R. (2018). Cellular Stress Associated with Aneuploidy. *Developmental Cell*, *44*(4), 420–431. https://doi.org/10.1016/j.devcel.2018.02.002

Zhu, P. J., Khatiwada, S., Cui, Y., Reineke, L. C., Dooling, S. W., Kim, J. J., Li, W., Walter, P., & Costa-Mattioli, M. (2019). Activation of the ISR mediates the behavioral and neurophysiological abnormalities in Down syndrome. *Science (New York, N.Y.)*, *366*(6467), 843–849. https://doi.org/10.1126/science.aaw5185

Zhu, Y., Kim, Y.-M., Li, S., & Zhuang, Y. (2010). Generation and analysis of partially haploid cells with Cre-mediated chromosome deletion in the lymphoid system. *The Journal of Biological Chemistry*, *285*(34), 26005–26012. https://doi.org/10.1074/jbc.M110.139196

Zielinska, A. P., Holubcova, Z., Blayney, M., Elder, K., & Schuh, M. (2015). Sister kinetochore splitting and precocious disintegration of bivalents could explain the maternal age effect. *eLife*, *4*, e11389. https://doi.org/10.7554/eLife.11389

Zielke, N., Korzelius, J., van Straaten, M., Bender, K., Schuhknecht, G. F. P., Dutta, D., Xiang, J., & Edgar, B. A. (2014). Fly-FUCCI: A Versatile Tool for Studying Cell Proliferation in Complex Tissues. *Cell Reports*, *7*(2), 588–598. https://doi.org/10.1016/j.celrep.2014.03.020

Zong, H., Espinosa, J. S., Su, H. H., Muzumdar, M. D., & Luo, L. (2005). Mosaic Analysis with Double Markers in Mice. *Cell*, *121*(3), 479–492. https://doi.org/10.1016/j.cell.2005.02.012

Annex I

Region	Phenomenon trisomies+monosomies	RS FRTs		TSG FRTs		Gene stable ID	Transcript stable	Gene start (bp)	Gene end (bp)	Gene description	Karyotype band	Gene name
		RS3 (ID)	RS5 (ID)	GR	RG							
		123215						8820579			66E1	
						FBgn0263930	FBtr0076583	8827505	8891192	daily	66	division abnormally delayed
						FBgn0052026	FBtr0076584	8836462	8838843	CG33026	66	
						FBgn0262788	FBtr0305902	8888145	8888833	CG43169	66	
						FBgn0020633	FBtr0076585	8891596	8894310	Mcm7	66	Minichromosome maintenance 7
						FBgn0035934	FBtr0331827	8894404	8905200	TrpA1	66	Transient receptor potential cation channel A1
						FBgn0266757	FBtr0273287	8905918	8912671	misfire	66	misfire
						FBgn0035936	FBtr0076606	8912499	8932065	Tsp66E	66	Tetraspanin 66E
						FBgn0264305	FBtr0331519	8932235	8954272	CG43783	66	
						FBgn0264307	FBtr0331511	8937103	8954463	srs2	66	srs2
						FBgn0040321	FBtr0076510	8955021	8956551	GNBP3	66	Gram-negative bacteria binding protein 3
						FBgn0011787	FBtr0076511	8956791	8957584	mRpL12	66	mitochondrial ribosomal protein L12
						FBgn0035941	FBtr0076612	8958857	8960921	CG13313	66	
						FBgn0035942	FBtr0346542	8961274	8964769	VaRS-m	66	valyl-tRNA synthetase, mitochondrial
						FBgn0035943	FBtr0076559	8964912	8966374	CG5653	66	
						FBgn0035944	FBtr0076614	8966829	8968171	CG5021	66	
						FBgn0035945	FBtr0076516	8968528	8971752	CG5026	66	
						FBgn0036706	FBtr0076557	8972056	8974765	pix	66	pixie
						FBgn0035947	FBtr0076517	8975046	8977401	Srp68	66	Signal recognition particle 68
						FBgn0035948	FBtr0076556	8977395	8979880	CG5644	66	
						FBgn0035949	FBtr0303233	8981795	8983212	CG13314	66	
						FBgn0263199	FBtr0076555	8982212	8986931	Galk	66	Galactokinase
						FBgn0035951	FBtr0076519	8987710	8989135	CG5068	66	
						FBgn0035952	FBtr0076552	8989069	8990228	CG5280	66	
						FBgn0016070	FBtr0076550	8990317	8997989	smg	66	smaug
						FBgn0035953	FBtr0333008	8998184	9002598	CG5087	66	
						FBgn0035954	FBtr0076521	9005196	9007249	Doc3	66	Dorsocross3
						FBgn0035955	FBtr0076548	9008624	9009838	CG5194	66	
						FBgn0035956	FBtr0076547	9012686	9015246	Doc2	66	Dorsocross2
						FBgn0028789	FBtr0076522	9041375	9045042	Doc1	66	Dorsocross1
						FBgn0035957	FBtr0076523	9047439	9048724	Argink2	66	Arginine kinase 2
						FBgn0000116	FBtr0331550	9048781	9066927	Argink-1	66	Arginine kinase 1
						FBgn0035959	FBtr0345351	9067195	9072731	CG4911	66	
						FBgn0035960	FBtr0076524	9073105	9074467	CG4942	66	
						FBgn0023479	FBtr0076525	9074643	9092131	teq	66	Tequila
						FBgn0043806	FBtr0076529	9093053	9094856	CG30032	66	
						FBgn0040827	FBtr0076530	9096573	9097494	CG13315	66	
						FBgn0011206	FBtr0481740	9097629	9134425	bol	67	boule
						FBgn0035964	FBtr0076531	9134580	9135916	Dhpr	67	Dihydropteridine reductase
						FBgn0035965	FBtr0076537	9135709	9137181	Use1	67	Unconventional SNARE in the ER 1
						FBgn0263456	FBtr0344242	9137860	9145985	nwk	67	nervous wreck
						FBgn0004244	FBtr0076534	9145838	9182149	Rdl	67	Resistant to dieldrin
						FBgn0035968	FBtr0332126	9203065	9208853	Slc45-1	67	Solute carrier family 45 member 1
						FBgn0035969	FBtr0076429	9211880	9215256	CG4476	67	
						FBgn0035970	FBtr0076502	9235150	9236648	CG4483	67	
						FBgn0035971	FBtr0076430	9250225	9251338	CG4477	67	
						FBgn0264000	FBtr0346866	9251978	9268522	GluRIB	67	Glutamate receptor IB
						FBgn0035975	FBtr0076433	9334332	9338336	PGRP-LA	67	Peptidoglycan recognition protein LA
						FBgn0035976	FBtr0300291	9338810	9348336	PGRP-LC	67	Peptidoglycan recognition protein LC
						FBgn0035977	FBtr0076439	9349609	9351489	PGRP-LF	67	Peptidoglycan recognition protein LF
						FBgn0035978	FBtr0076500	9350867	9356935	UGP	67	UDP-glucose pyrophosphorylase
						FBgn0052040	FBtr0076440	9354033	9355457	CG32040	67	
						FBgn0052039	FBtr0076441	9356996	9359966	Svp	67	small VCP interacting protein
						FBgn0085484	FBtr0112761	9360316	9362042	Pdxk	67	Pyridoxal kinase
						FBgn0085485	FBtr0112762	9362108	9362734	CG34456	67	
						FBgn0004379	FBtr0346530	9362636	9367046	Kip67A	67	Kinesin-like protein at 67A
						FBgn0035980	FBtr0076444	9364350	9365240	mRRF1	67	mitochondrial ribosome recycling factor 1
						FBgn0035981	FBtr0333883	9367377	9370300	CG4452	67	
						FBgn0011769	FBtr0303475	9370195	9371238	Fdx1	67	Ferredoxin 1
						FBgn0001229	FBtr0076497	9371511	9372407	Hsp67Bc	67	Heat shock gene 67Bc
						FBgn0001228	FBtr0303473	9372722	9374694	CG4456	67	
						FBgn0001223	FBtr0100558	9372931	9374664	Hsp22	67	Heat shock protein 22
						FBgn0035982	FBtr0076452	9375430	9376203	CG4461	67	
						FBgn0001225	FBtr0076496	9376418	9377427	Hsp26	67	Heat shock protein 26
						FBgn0001227	FBtr0076495	9377932	9379534	Hsp67Ba	67	Heat shock gene 67Ba
						FBgn0001224	FBtr0300504	9381852	9382765	Hsp23	67	Heat shock protein 23
						FBgn0001226	FBtr0346541	9384063	9385694	Hsp27	67	Heat shock protein 27
						FBgn0035983	FBtr0300506	9386827	9389227	CG4080	67	
						FBgn0015218	FBtr0076487	9399618	9402468	eIF4E1	67	eukaryotic translation initiation factor 4E1
						FBgn0035985	FBtr0076455	9404797	9406174	Cpr67B	67	Cuticular protein 67B
						FBgn0035986	FBtr0300088	9406179	9410832	CG4022	67	
						FBgn0288470	FBtr0110863	9411038	9413835	Cpsf5	67	Cleavage and polyadenylation specific factor 5
						FBgn0035989	FBtr0331584	9413596	9426758	Atat	67	alpha-tubulin acetylase
						FBgn0035988	FBtr0076485	9415755	9417388	CG30682	67	
						FBgn0023129	FBtr0076457	9425253	9424761	aay	67	aaray
						FBgn0015266	FBtr0076458	9427010	9428671	Shc	67	SHC-adaptor protein
						FBgn0005533	FBtr0076479	9428795	9429921	RpS17	67	Ribosomal protein S17
						FBgn0040305	FBtr0076460	9430312	9439460	MTF-1	67	Metal response element-binding Transcription Factor-1
						FBgn0260431	FBtr0300855	9433686	9435399	CG42526	67	
						FBgn0260859	FBtr0088879	9438482	9442267	Bet3	67	Blocked early in transport 3
						FBgn0035993	FBtr0076504	9440056	9442267	NF-YA	67	Nuclear factor Y-box A
						FBgn0053926	FBtr0344978	9443232	9446388	CG33026	67	
						FBgn0035995	FBtr0331582	9448694	9450785	CG3529	67	
						FBgn0035996	FBtr0076476	9450545	9451572	CG3448	67	
						FBgn0266124	FBtr0076462	9451876	9452766	ghi	67	ghiberti
						FBgn0035997	FBtr0076475	9452803	9456281	phol	67	pleiohomeotic like
						FBgn0035999	FBtr0076463	9456318	9459370	CG3552	67	
						FBgn0035998	FBtr0301032	9456342	9457659	CG3437	67	
						FBgn0036000	FBtr0076473	9459369	9460799	CG3434	67	
						FBgn0266101	FBtr0343556	9461050	9475475	CG44838	67	
						FBgn0011327	FBtr0076472	9475493	9476965	Uch-L5	67	Ubiquitin carboxy-terminal hydrolase L5
						FBgn0036004	FBtr0076468	9477038	9486530	Jarid2	67	Jumonji, AT rich interactive domain 2
						FBgn0036005	FBtr0076471	9486488	9487790	pall	67	palbearer
						FBgn0052036	FBtr0114525	9488050	9489233	CG32036	67	
						FBgn0052037	FBtr0333866	9489502	9492215	CG32037	67	
						FBgn0036007	FBtr0076427	9494555	9505328	path	67	pathetic
						FBgn0036008	FBtr0076426	9506818	9509583	CG3408	67	
						FBgn0010408	FBtr0076423	9509793	9511531	RpS9	67	Ribosomal protein S9
						FBgn0053703	FBtr0091691	9512008	9512860	CG33703	67	
						FBgn0053702	FBtr0091690	9512797	9513409	CG33702	67	
						FBgn0053700	FBtr0301069	9514119	9525544	CG33700	67	
						FBgn0036009	FBtr0076375	9529397	9531386	Or67a	67	Odorant receptor 67a
						FBgn0036010	FBtr0330953	9542246	9543669	Ir67a	67	Ionotropic receptor 67a
						FBgn0261555	FBtr0302709	9547220	9596713	CG42673	67	
						FBgn0267796	FBtr0347573	9597764	9614001	Trmc	67	Transmembrane channel-like
						FBgn0036014	FBtr0076379	9598988	9600341	CG3222	67	
						FBgn0036015	FBtr0076421	9600490	9601325	CG3088	67	
						FBgn0036016	FBtr0076380	9601522	9602548	CG3306	67	
						FBgn0267348	FBtr0076382	9614914	9623985	LanB2	67	Laminin B2
						FBgn0036018	FBtr0076383	9624237	9627321	CG3335	67	
						FBgn0036019	FBtr0076420	9627316	9629193	Or67b	67	Odorant receptor 67b
						FBgn0036020	FBtr0076385	9628676	9631765	Cyp40	67	Cyclophilin 40
						FBgn0036021	FBtr0333859	9631834	9637033	fry	67	fairy
						FBgn0036022	FBtr0076387	9638112	9639021	CG8329	67	
						FBgn0036023	FBtr0076388	9639271	9640140	CG18179	67	
						FBgn0036024	FBtr0076389	9641013	9641913	CG16180	67	
						FBgn0053696	FBtr0091684	9644109	9655433	CNMaR	67	CNMamide Receptor
						FBgn0036028	FBtr0076392	9676201	9681060	CG16717	67	
						FBgn0087040	FBtr0076393	9681268	9683370	alphaTub67C	67	alpha-Tubulin at 67C
						FBgn0036030	FBtr0333857	9683579	9686705	Prps	67	Phosphoribosyl pyrophosphate synthetase

				FBgn0036029	FBtr0076394	9685171	9686252	CG16719		67	
				FBgn0015321	FBtr0076395	9698338	9700481	Uba4		67	Ubiquitin conjugating enzyme 4
				FBgn0036031	FBtr0076414	9700517	9703595	CG6761		67	
				FBgn0036032	FBtr0330098	9704331	9710329	CG16711		67	
				FBgn0040475	FBtr0076413	9710422	9713827	SH3PX1		67	SH3 and PX domain containing 1
				FBgn0045923	FBtr0076398	9714324	9717716	vsg		67	Visgun
				FBgn0036035	FBtr0076412	9717786	9719144	CG18178		67	
				FBgn0036036	FBtr0076402	9719328	9720464	CG14174		67	
				FBgn0261530	FBtr0306040	9720414	9723194	nbs		67	nbs
				FBgn0036038	FBtr0076403	9723423	9726706	defl		67	deflated
				FBgn0036039	FBtr0308410	9726955	9729955	Naa60		67	N(alpha)-acetyltransferase 60
				FBgn0015944	FBtr0076405	9729999	9731224	ATPsynB		67	ATP synthase, subunit B
				FBgn0036040	FBtr0076410	9731238	9733807	CG6749		67	
				FBgn0259163	FBtr0331540	9734012	9760395	CG42268		67	
				FBgn0036043	FBtr0076322	9763544	9786466	Ae2		67	Anion exchanger 2
				FBgn0044328	FBtr0332818	9787046	9808713	CG32052		67	
				FBgn0036044	FBtr0310929	9787933	9797887	Zasp67		67	Z band alternatively spliced PDZ-motif protein 67
				FBgn0044051	FBtr0076328	9798420	9799052	Ilp1		67	Insulin-like peptide 1
				FBgn0036046	FBtr0076329	9798698	9800440	Ilp2		67	Insulin-like peptide 2
				FBgn0044050	FBtr0076373	9801298	9802120	Ilp3		67	Insulin-like peptide 3
				FBgn0044049	FBtr0076372	9803399	9804263	Ilp4		67	Insulin-like peptide 4
				FBgn0264489	FBtr0332823	9813847	9834345	CG43897		67	
				FBgn0044048	FBtr0472845	9823349	9823897	Ilp5		67	Insulin-like peptide 5
				FBgn0028429	FBtr0076370	9834367	9836855	I-2		67	Inhibitor-2
				FBgn0015918	FBtr0076369	9837085	9838870	Cdk8		67	Cyclin-dependant kinase 8
				FBgn0004390	FBtr0330168	9839093	9855285	RasGAP1		67	Ras GTPase activating protein 1
				FBgn0036052	FBtr0076386	9857383	9859889	CG10809		67	
				FBgn0036053	FBtr0076365	9860217	9864349	iPLA2-VIA		67	calcium-independent phospholipase A2 VIA
				FBgn0027567	FBtr0076340	9864638	9870674	Clz1		67	Clz1 zinc finger protein
				FBgn0036411	FBtr0332887	9878685	9884403	CG34382		67	
				FBgn0011836	FBtr0332888	9884411	9888883	Taf2		67	TBP-associated factor 2
				FBgn0025866	FBtr0076343	9888762	9893319	CalpB		67	Calpain-B
				FBgn0036057	FBtr0076359	9893188	9894743	Hez		67	Hezron
				FBgn0036056	FBtr0076360	9893188	9894743	CG8709		67	
				FBgn0036058	FBtr0076357	9894807	9898575	CG6707		67	
				FBgn0286833	FBtr0474772	9898626	9899387	CG46387		67	
				FBgn0036059	FBtr0076344	9899241	9903931	nudE		67	nudE
				FBgn0085385	FBtr0479874	9908120	9967298	bmx		67	black match
				FBgn0036062	FBtr0331581	9966603	9968317	CG6685		67	
				FBgn0026404	FBtr0076347	9968479	9971002	Dronc		67	Death regulator Nedd2-like caspase
				FBgn0036063	FBtr0076354	9971151	9973354	CG6674		67	
				FBgn0259952	FBtr0330239	9972312	9974023	CG40455		67	
				FBgn0263251	FBtr0076351	9972312	9974023	vnc		67	variable nurse cells
				FBgn0040923	FBtr0332665	9974651	10133360	dpr6		67	defective proboscis extension response 6
				FBgn0036066	FBtr0076316	10086747	10089400	CG14160		67	
				FBgn0052053	FBtr0076315	10090170	10092346	CG32053		67	
				FBgn0052054	FBtr0076314	10092768	10094738	CG32054		67	
				FBgn0262007	FBtr0303833	10095754	10098115	CG42825		67	
				FBgn0262008	FBtr0303832	10099357	10100861	CG42826		67	
				FBgn0052057	FBtr0331552	10147454	10186108	dpr10		67	defective proboscis extension response 10
				FBgn0036070	FBtr0076295	10151827	10152984	CG8072		67	
				FBgn0036072	FBtr0076311	10165839	10167023	CG8628		67	
				FBgn0000451	FBtr0301385	10199276	10201837	ect		67	ectodermal
				FBgn0036075	FBtr0345693	10215665	10216980	CG8065		67	
				FBgn0052055	FBtr0076304	10218504	10220164	CG32055		67	
				FBgn0052056	FBtr0076303	10220493	10222240	scramb1		67	scramblase 1
				FBgn0036078	FBtr0076300	10243329	10244706	Or67c		67	Odorant receptor 67c
				FBgn0011569	FBtr0076299	10263909	10267111	can		67	cannonball
				FBgn0036080	FBtr0076297	10273204	10274624	Or67d		67	Odorant receptor 67d
				FBgn0036082	FBtr0076281	10412818	10414774	CG12962		67	
				FBgn0036083	FBtr0076294	10429689	10431983	Irk67b		67	Ionotropic receptor 67b
				FBgn0052058	FBtr0076293	10432384	10434105	Irk67c		67	Ionotropic receptor 67c
				FBgn0011802	FBtr0076292	10459081	10463101	Gem3		67	Gemin 3
				FBgn0052061	FBtr0076285	10463816	10464835	CG32061		67	
				FBgn0045770	FBtr0334099	10465187	10468974	S-Lap3		67	Sperm-Leucylaminopeptidase 3
				FBgn0286933	FBtr0475208	10478514	10479447	CG46430		67	
				FBgn0052062	FBtr0473371	10481412	10594012	Rbfox1		67	RNA-binding Fox protein 1
				FBgn0052064	FBtr0076288	10490861	10492934	S-Lap4		67	Sperm-Leucylaminopeptidase 4
				FBgn0036085	FBtr0344999	10557023	10559082	CG6527		67	
				FBgn0260396	FBtr0300668	10623066	10623576	CG42521		67	
				FBgn0262592	FBtr0305200	10624726	10625599	CG43127		67	
				FBgn0085367	FBtr0113432	10626499	10627439	CG34238		67	
				FBgn0036089	FBtr0076280	10627680	10628484	CG14151		67	
				FBgn0260644	FBtr0300949	10629083	10630069	CG42536		67	
				FBgn0260643	FBtr0300948	10630034	10630935	CG42535		67	
				FBgn0001179	FBtr0114599	10631079	10633969	hay		67	haywire
				FBgn0054001	FBtr0334086	10631079	10634612	CG34001		67	
				FBgn0000629	FBtr0273338	10634575	10638130	E(z)		67	Enhancer of zeste
				FBgn0036090	FBtr0076255	10638146	10639678	Cnep1r2		67	CTD nuclear envelope phosphatase 1 regulatory subunit 2
				FBgn0036091	FBtr0076256	10639740	10640138	CG18628		67	
				FBgn0052066	FBtr0076277	10640286	10661013	CG33066		67	
				FBgn0036093	FBtr0076257	10641889	10643009	CG14154		67	
				FBgn0036094	FBtr0076259	10643528	10644815	CG14153		67	
				FBgn0036096	FBtr0076260	10661475	10663157	CG8003		67	
				FBgn0052068	FBtr0113421	10663376	10664435	Ald1		67	Acireductone dioxygenase 1
				FBgn0010762	FBtr0331573	10664739	10690734	simj		67	simjang
				FBgn0036099	FBtr0076265	10691024	10692598	CG11811		67	
				FBgn0053463	FBtr0089606	10692533	10693167	CG34463		67	
				FBgn0047038	FBtr0076276	10693184	10694108	ND-13B		67	NADH dehydrogenase (ubiquinone) 13 kDa B subunit
				FBgn0038101	FBtr0085969	10694369	10696877	Nrg1A		67	Neuregulin A
				FBgn0262890	FBtr0306304	10771925	10773399	CG43245		67	
				FBgn0036102	FBtr0076266	10801190	10802350	CG12523		67	
				FBgn0262020	FBtr0303850	10814819	10816384	CG42831		67	
				FBgn0026160	FBtr0076268	10835526	10876496	tna		67	tonalli
				FBgn0036104	FBtr0076274	10876315	10879037	CG6418		67	
				FBgn0036105	FBtr0076269	10879085	10880188	Bloc4		67	Biogenesis of lysosome-related organelles complex 1, subunit 4
				FBgn0036106	FBtr0076273	10880699	10882386	CG6409		67	
				FBgn0036107	FBtr0076270	10882890	10883575	galla-2		67	galla-2
				FBgn0027615	FBtr0076272	10884261	10886471	OXA1L		67	OXA1L mitochondrial inner membrane protein
				FBgn0036108	FBtr0076191	10889990	10890700	Cpr67Fa1		67	Cuticular protein 67Fa1
				FBgn0036109	FBtr0076192	10891714	10892516	Cpr67Fa2		67	Cuticular protein 67Fa2
				FBgn0036110	FBtr0076193	10894173	10894693	Cpr67Fb		67	Cuticular protein 67Fb
				FBgn0036111	FBtr0076251	10894776	10899123	Apa		67	Apa pyrophosphatase
				FBgn0036112	FBtr0076194	10972648	10973476	CG14147		68	
				FBgn0013469	FBtr0333361	10981171	11009188	klu		68	klumpfuss
				FBgn0029172	FBtr0076196	11023535	11024846	Fad2		68	Fad2
				FBgn0052079	FBtr0300188	11025561	11027332	CG33079		68	
				FBgn0052081	FBtr0076198	11027579	11029444	CG33081		68	
				FBgn0263776	FBtr0310569	11036358	11051371	CG43693		68	
				FBgn0036116	FBtr0076199	11054035	11059659	CG7888		68	
				FBgn0036117	FBtr0076242	11059437	11061224	CG8321		68	Biogenesis of lysosome-related organelles complex 1, subunit 2
				FBgn0036118	FBtr0076202	11061571	11062215	Bloc2		68	
				FBgn0052069	FBtr0076241	11062131	11063614	CG33069		68	
				FBgn0052075	FBtr0305868	11062726	11064941	CG33075		68	
				FBgn0286540	FBtr0344636	11064991	11069025	CG45101		68	
				FBgn0025355	FBtr0076203	11064991	11069025	SuUR		68	Suppressor of Under-Replication
				FBgn0036121	FBtr0076239	11066043	11069064	CG8310		68	
				FBgn0263241	FBtr0076204	11070526	11073348	Moco1		68	Molybdenum cofactor synthesis 1
				FBgn0010741	FBtr0076238	11072592	11074388	Pbp2		68	Prefoldin 2
				FBgn0036124	FBtr0076207	11074769	11076736	CG7839		68	
				FBgn0020412	FBtr0076236	11076752	11093193	JIL-1		68	JIL-1 kinase

				FBgn0286979	FBtr0475273	11093371	11096245	CG46439	68	
				FBgn0286980	FBtr0475275	11093371	11096245	Ivd	68	Iodotyrosine deiodinase
				FBgn0083068	FBtr0347287	11096496	11096556	CG33947	68	
				FBgn0036126	FBtr0076234	11097446	11098188	Irbp18	68	Inverted repeat binding protein 18 kDa
				FBgn0281112	FBtr0076208	11098412	11100578	APP-BP1	68	beta-Amyloid precursor protein binding protein 1
				FBgn0036128	FBtr0113161	11100675	11101698	Eloßbeta	68	Elongase 68beta
				FBgn0052072	FBtr0076232	11101875	11103030	Eloßalpha	68	Elongase 68alpha
				FBgn0052071	FBtr0076231	11103421	11103873	CG32071	68	
				FBgn0052073	FBtr0345348	11107008	11107582	CG32073	68	
				FBgn0036131	FBtr0076209	11108235	11108732	CG12522	68	
				FBgn0054012	FBtr0100067	11108920	11109505	CG34012	68	
				FBgn0036133	FBtr0076210	11109690	11112117	emal	68	emal
				FBgn0003462	FBtr0076229	11112281	11113740	Sod1	68	Superoxide dismutase 1
				FBgn0036134	FBtr0301967	11114169	11120783	FoxK	68	Forkhead box K
				FBgn0036135	FBtr0076211	11120847	11122041	mRpL2	68	mitochondrial ribosomal protein L2
				FBgn0036136	FBtr0076223	11121998	11123216	Ufd1	68	Ubiquitin fusion-degradation 1-like
				FBgn0260795	FBtr0332705	11123348	11134863	NaPi-III	68	Na(+)-dependent inorganic phosphate cotransporter type III
				FBgn0014388	FBtr0076214	11130835	11131402	nol	68	no optic lobe
				FBgn0052074	FBtr0076222	11131883	11132322	CG32074	68	
				FBgn0036138	FBtr0302875	11134987	11135480	CG14143	68	
				FBgn0052082	FBtr0076216	11136049	11163984	IRSp53	68	Insulin receptor substrate 53 kDa
				FBgn0036139	FBtr0076221	11149578	11150785	CG6216	68	
				FBgn0052076	FBtr0076217	11164971	11166920	Alg10	68	ALG10 alpha-1,2-glucosyltransferase
				FBgn0036141	FBtr0076218	11166520	11169925	wfs	68	wolfless
				FBgn0036142	FBtr0331829	11169817	11172411	Adck5	68	esaF domain containing kinase 5
				FBgn0036143	FBtr0300347	11173514	11176892	CG14142	68	
				FBgn0036144	FBtr0306254	11176954	11197536	GlcAT-P	68	Glucuronyltransferase P
				FBgn0036147	FBtr0076187	11198166	11206016	Plod	68	procollagen lysyl hydroxylase
				FBgn0036145	FBtr0076163	11199620	11200957	CG7607	68	
				FBgn0036146	FBtr0076164	11201351	11202158	nkd	68	nektochor
				FBgn0261469	FBtr0076186	11204422	11210583	Ube3a	68	Ubiquitin protein ligase E3A
				FBgn0084766	FBtr0076165	11210786	11214097	CG7600	68	
				FBgn0261553	FBtr0345849	11214505	11230745	CG42671	68	
				FBgn0036150	FBtr0345037	11232972	11236218	Ir68a	68	Ionotropic receptor 68a
				FBgn0041094	FBtr0339008	11252307	11256172	acyl	68	acylia
				FBgn0036152	FBtr0076183	11287936	11295919	Dyro	68	Dyt-YFP repressor by overexpression
				FBgn0036153	FBtr0076171	11311747	11313397	CG7573	68	
				FBgn0036154	FBtr0345692	11319642	11321719	CG8168	68	
				FBgn0036155	FBtr0076181	11361986	11364885	CG6163	68	
				FBgn0036156	FBtr0076172	11394690	11395673	CG11726	68	
				FBgn0265469	FBtr0339928	11397542	11397865	CG44362	68	
				FBgn0036157	FBtr0076173	11425158	11426365	CG7560	68	
				FBgn0036158	FBtr0330274	11434695	11435476	CG8149	68	
				FBgn0036159	FBtr0076175	11445161	11446579	CG7557	68	
				FBgn0036160	FBtr0076178	11457076	11458476	CG12289	68	
				FBgn0036161	FBtr0076176	11458490	11459625	CG7551	68	
				FBgn0036162	FBtr0076177	11463576	11465864	Fum3	68	Fumarase 3
				FBgn0028667	FBtr0302359	11473291	11473972	Vha16-3	68	Vacuolar H[+] ATPase 16kD subunit 3
				FBgn0028668	FBtr0076091	11474958	11475552	Vha16-2	68	Vacuolar H[+] ATPase 16kD subunit 2
				FBgn0036165	FBtr0344910	11487550	11489055	chrb	68	charybde
				FBgn0053500	FBtr0076094	11506837	11506903	CG33500	68	
				FBgn0003378	FBtr0076160	11508987	11509394	Sgs8	68	Salivary gland secretion 8
				FBgn0003377	FBtr0076095	11509861	11510247	Sgs7	68	Salivary gland secretion 7
				FBgn0053272	FBtr0076159	11510323	11510589	CG33272	68	
				FBgn0003373	FBtr0076096	11512221	11513402	Sgs3	68	Salivary gland secretion 3
				FBgn0036168	FBtr0113163	11513705	11518904	CG7512	68	
				FBgn0036170	FBtr0339510	11518798	11522713	CG11714	68	
				FBgn0265868	FBtr0100588	11518798	11522713	Fuca	68	alpha-L-fucosidase
				FBgn0259481	FBtr0089332	11522757	11562233	Mob2	68	Mob2
				FBgn0036173	FBtr0333215	11561996	11564312	CG7394	68	
				FBgn0286893	FBtr0475070	11563587	11564072	CG46412	68	
				FBgn0053267	FBtr0335649	11564483	11572798	CG33267	68	
				FBgn0053460	FBtr0089526	11572797	11574463	CG33460	68	
				FBgn0053489	FBtr0089525	11574764	11577044	CG33489	68	
				FBgn0053271	FBtr0076150	11577006	11577495	CG33271	68	
				FBgn0053270	FBtr0076149	11578236	11578923	CG33270	68	
				FBgn0263247	FBtr0336059	11579743	11579950	CG43390	68	
				FBgn0263248	FBtr0336058	11580329	11581019	CG43391	68	
				FBgn0053269	FBtr0076148	11581415	11582197	CG33269	68	
				FBgn0052086	FBtr0305322	11582401	11584064	CG33086	68	
				FBgn0003292	FBtr0076146	11584122	11587770	rt	68	rotated abdomen
				FBgn0036176	FBtr0076100	11589695	11589979	CG7377	68	
				FBgn0036177	FBtr0076145	11590872	11591251	CG33268	68	
				FBgn0036179	FBtr0307115	11597202	11605374	CG7368	68	
				FBgn0036178	FBtr0076144	11599505	11600065	CG14137	68	
				FBgn0286872	FBtr0475047	11600370	11600901	CG46394	68	
				FBgn0036180	FBtr0273304	11605436	11609465	Duba	68	Deubiquitinating enzyme A
				FBgn0262021	FBtr0303851	11610135	11610386	CG42832	68	
				FBgn0036181	FBtr0076140	11610578	11620101	Muc68Ca	68	Mucin 68Ca
				FBgn0086254	FBtr0076139	11620535	11624381	Akr1B	68	Aldo-keto reductase 1B
				FBgn0036183	FBtr0076137	11624528	11626125	CG6083	68	
				FBgn0036184	FBtr0076102	11626441	11627715	PCID2	68	PCI domain-containing protein 2
				FBgn0042138	FBtr0331545	11628037	11630749	Apt1	68	Acyl-protein thioesterase 1
				FBgn0052091	FBtr0076106	11631392	11642902	CG32091	68	
				FBgn0036186	FBtr0076136	11642906	11646033	CG6071	68	
				FBgn0036187	FBtr0076135	11646234	11646474	RIOK1	68	RIO kinase 1
				FBgn0036188	FBtr0331530	11648756	11650469	Polr3H	68	RNA polymerase III subunit H
				FBgn0052085	FBtr0076133	11650517	11680344	CG32085	68	
				FBgn0015828	FBtr0076108	11682038	11683835	TfIIEalpha	68	Transcription factor IIEalpha
				FBgn0036191	FBtr0300100	11685986	11690155	Sugb	68	Sugar baby
				FBgn0036192	FBtr0300097	11689631	11691369	Pldn	68	Pallidin
				FBgn0036193	FBtr0332762	11691571	11692757	CG14135	68	
				FBgn0036194	FBtr0332766	11693879	11696963	Dph1	68	Diphthamide biosynthesis 1
				FBgn0036195	FBtr0301326	11697126	11699283	Dnai2	68	dynein, axonemal, intermediate chain 2
				FBgn0036196	FBtr0076126	11699496	11706853	CG11658	68	
				FBgn0261381	FBtr0302272	11708979	11710570	mtTFB1	68	Mitochondrial Transcription Factor B1
				FBgn0261353	FBtr0302271	11708979	11710570	Ccdc56	68	Coiled-coil domain containing 56
				FBgn0036198	FBtr0076123	11710557	11711386	crim	68	crimpled
				FBgn0040817	FBtr0113334	11712229	11715285	CG14132	68	
				FBgn0036199	FBtr0076115	11720934	11728118	Bmcp	68	Bmcp
				FBgn0052088	FBtr0332764	11728348	11732016	sunn	68	sisters unbound
				FBgn0052087	FBtr0076117	11732141	11733810	CG32087	68	
				FBgn0036202	FBtr0113164	11733589	11768182	lost	68	lost and found
				FBgn0041231	FBtr0076118	11751305	11752474	Gr68a	68	Gustatory receptor 68a
				FBgn0036203	FBtr0076119	11767299	11772157	Muc68D	68	Mucin 68D
				FBgn0036204	FBtr0076089	11774060	11774501	Tim13	68	Tim13
				FBgn0015278	FBtr0076087	11774650	11790013	PI3Kl68D	68	Phosphatidylinositol 3-kinase 68D
				FBgn0036205	FBtr0332128	11777073	11780485	CG14131	68	
				FBgn0036206	FBtr0076085	11790212	11793283	lwy	68	lwitchy
				FBgn0036207	FBtr0076029	11795514	11795418	CG10937	68	
				FBgn0004381	FBtr0076030	11795514	11798875	Klp68D	68	Kinesin-like protein at 68D
				FBgn0036208	FBtr0076084	11798948	11800861	Gcat	68	Glycine C-acetyltransferase
				FBgn0259140	FBtr0332131	11801951	11814755	Cubn2	68	Cubulin 2
				FBgn0036210	FBtr0076031	11815444	11816710	CG14130	68	
				FBgn0036211	FBtr0301135	11816695	11822275	CG5946	68	
				FBgn0036212	FBtr0110780	11820138	11822275	CG11597	68	
				FBgn0036213	FBtr0076032	11822851	11824211	RpL10Ab	68	Ribosomal protein L10Ab
				FBgn0052095	FBtr0076077	11824207	11825732	CG32095	68	
				FBgn0000404	FBtr0076075	11826719	11833578	CycA	68	Cyclin A
				FBgn0036214	FBtr0076035	11829039	11833944	CG7364	68	
				FBgn0262366	FBtr0334649	11834727	11836721	CG43064	68	
				FBgn0040816	FBtr0076074	11847383	11847803	CG12521	68	
				FBgn0266100	FBtr0343554	11850645	11938872	CG44837	68	

				FBgn0036217	FBtr0076071	11870457	11571335	CG5906	68		
				FBgn0036218	FBtr0300721	11879115	11881182	Spm	68	Spermitin	
				FBgn0036219	FBtr0076037	11881384	11883546	CCDC151	68	Coiled-coil domain containing protein 151	
				FBgn0036220	FBtr0473619	11887299	11889010	CG5807	68		
				FBgn0036221	FBtr0076038	11921513	11922599	CG11588	68		
				FBgn0036222	FBtr0076069	11922610	11924757	SdhAL	68	Succinate dehydrogenase, subunit A (flavoprotein)-like	
				FBgn0011723	FBtr0332071	11927693	11935919	byn	68	brachyenteron	
				FBgn0036224	FBtr0346545	11941912	11943485	Rpt4R	68	Regulatory particle triple-A ATPase 4-related	
				FBgn0036225	FBtr0076067	11943646	11944852	CG5983	68		
				FBgn0036226	FBtr0076041	11947675	11949248	CG7252	68		
				FBgn0036227	FBtr0076042	11949839	11952225	CG17626	68		
				FBgn0036228	FBtr0076066	11952301	11953317	obst-G	68	obstructor -G	
				FBgn0036229	FBtr0076043	11954083	11956780	CG7248	68		
				FBgn0036230	FBtr0473578	11956708	11957768	CG11570	68		
				FBgn0262986	FBtr0306824	11958283	11958908	CG43294	68		
				FBgn0028573	FBtr0076064	11958872	11966131	prc	68	pericardin	
				FBgn0053265	FBtr0076063	11967343	11972979	Muc68E	68	Mucin 68E	
				FBgn0259748	FBtr0300506	11973085	11973790	CG42097	68		
				FBgn0036232	FBtr0310535	11974905	11975816	CG14125	68		
				FBgn0264488	FBtr0345868	11976111	11982764	CG43896	68		
				FBgn0036235	FBtr0290131	11984906	11990505	CG6938	68		
				FBgn0036236	FBtr0076048	11990736	11992000	CG6931	68		
				FBgn0036237	FBtr0076062	11991853	11993179	viaf	68	viral IAP-associated factor	
				FBgn0026432	FBtr0076061	11993274	11998138	Grip163	68	Grip163	
				FBgn0036239	FBtr0076058	11998398	12002915	Pop2	68	Pop2	
				FBgn0036240	FBtr0076050	12003155	12008951	CG6928	68		
				FBgn0041096	FBtr0076054	12008225	12064859	rols	68	rolling pebbles	
				FBgn0284725	FBtr0334108	12032557	12032999	CG43993	68		
				FBgn0036242	FBtr0076051	12042387	12044217	CG6793	68		
				FBgn0263947	FBtr0310008	12044579	12045356	CG43638	68		
				FBgn0284221	FBtr0076052	12067511	12081833	Sema5c	68	Semaphorin 5c	
				FBgn0036246	FBtr0075990	12088626	12089225	CG17154	68		
				FBgn0011335	FBtr0075991	12116101	12118055	vers	68	versatilie	
				FBgn0036248	FBtr0075992	12118257	12119769	eep	68	eurepot	
				FBgn0036249	FBtr0347572	12120019	12121185	CG11560	68		
				FBgn0022959	FBtr0305992	12121274	12125150	ypsk	68	psilon schachtel	
				FBgn0036250	FBtr0076026	12125487	12127394	Irk88b	68	Ionotropic receptor 68b	
				FBgn0259825	FBtr0112435	12127979	12128461	CG34241	68		
				FBgn0002565	FBtr0345352	12129393	12131869	Lsp2	68	Larval serum protein 2	
				FBgn0046296	FBtr0075995	12132146	12133834	DEF8	68	differentially expressed in FDCP 8 homolog	
				FBgn0036254	FBtr0076024	12133771	12136708	CG5845	68		
				FBgn0036255	FBtr0330011	12136967	12137655	Atg12	68	Autophagy-related 12	
				FBgn0011455	FBtr0334094	12137496	12138584	ND-SGDH	68	NADH dehydrogenase (ubiquinone) SGDH subunit	
				FBgn0036257	FBtr0334092	12138868	12143380	RhoGAP68F	68	Rho GTPase activating protein at 68F	
				FBgn0036258	FBtr0076022	12143446	12146937	eIF3I	68	eukaryotic translation initiation factor 3 subunit I	
				FBgn0013997	FBtr0075998	12146519	12156996	Nrx-IV	68	Neurexin IV	
				FBgn0052099	FBtr0076000	12149273	12150329	CG32099	68		
				FBgn0036259	FBtr0273438	12157052	12163735	CG9760	68		
				FBgn0036260	FBtr0076020	12164205	12175462	Rhodopsin 7	68	Rh7	
				FBgn0027843	FBtr0076001	12177601	12183347	Carbonic anhydrase 2	68	CAH2	
				FBgn0036262	FBtr0290130	12184984	12187860		68	CG6910	
				FBti0063216	FBti0063216-RA	12187580	12187654		68		
				FBti0063191	FBti0063191-RA	12187930	12188243		68		
				FBgn0000592	FBtr0333983	12188818	12190705	Esterase 6	68	Est-6	
				FBgn0036263	FBtr0346911	12190696	12190888	thoc6	68	thoc6	
				FBgn0000594	FBtr0076004	12190733	12192528	Esterase P	68	Est-P	
				FBgn0267310	FBtr0346565	12195787	12196049	long non-coding RNA:CR45746	68	lncRNA:CR45746	
				FBgn0036264	FBtr0076005	12197791	12199030		68	CG11529	
				FBgn0022709	FBtr0076018	12200322	12204362	Adenylate kinase 1	68	Adk1	
				FBgn0036266	FBtr0076016	12204123	12206022	tRNA splicing endonuclease subunit 54	68	Tsen54	
				FBgn0260941	FBtr0301056	12206238	12206941	approximated	68	app	
				FBti0063217	FBti0063217-RA	12206657	12206926		68		
				FBgn0284723	FBtr0344637	12245510	12246049	long non-coding RNA:CR43991	68	lncRNA:CR43991	
				FBgn0052100	FBtr0076006	12267528	12269803		68	CG32100	
				FBgn0036271	FBtr0333357	12269452	12271345	Porphobilinogen synthase	68	Pbgs	
				FBgn0036272	FBtr0076010	12277656	12277251	Spermine synthase	68	Sms	
				FBgn0036273	FBtr0076007	12277655	12281476	Inositol polyphosphate 5-phosphatase E	68	INPP5E	
				FBgn0267961	FBtr0347537	12286342	12286983	long non-coding RNA:CR46241	68	lncRNA:CR46241	
				FBgn0267218	FBtr0346386	12289304	12290161	long non-coding RNA:CR45658	68	lncRNA:CR45658	
				FBgn0036274	FBtr0301071	12290056	12296123		68	CG4328	
				FBgn0265743	FBtr0340700	12300980	12301942	long non-coding RNA:CR44550	68	lncRNA:CR44550	
				FBgn0265744	FBtr0340701	12302162	12302551	long non-coding RNA:CR44551	68	lncRNA:CR44551	
				FBgn0265455	FBtr0339812	12310805	12311961		68	CG44355	
				FBgn0052105	FBtr0333837	12329232	12335901	LIM homeobox transcription factor 1 alpha	68	Lmx1a	
				FBgn0036277	FBtr0075954	12336676	12337236		68	CG10418	
				FBgn0266993	FBtr0345915	12337352	12337699	long non-coding RNA:CR45444	68	lncRNA:CR45444	
				FBgn0036278	FBtr0075989	12339118	12351544	Corazonin receptor	68	CrzR	
				FBgn0036279	FBtr0075987	12369846	12391444	sodium chloride cotransporter 69	68	Nccc69	
				FBgn0267474	FBtr0346846	12380252	12381476	long non-coding RNA:CR45824	68	lncRNA:CR45824	
				FBgn0052104	FBtr0075986	12393804	12396322		68	CG32104	
				FBgn0011279	FBtr0075955	12396171	12396957	Odorant-binding protein 69a	68	Obp69a	
				FBgn0036282	FBtr0075985	12399539	12401935	SET and MYND domain containing, class 4, member 2	68	Smyd4-2	
				FBgn0052103	FBtr0332090	12402295	12414842	Short Calcium-binding Mitochondrial Carrier	68	SCaMC	
				FBgn0023655	FBtr0332088	12415026	12417585	ADP-ribosylation factor GTPase activating protein 1	68	Arf1GAP1	
				FBgn0036285	FBtr0332087	12422510	12432868	twin of eyg	68	twe	
				FBgn0000625	FBtr0075979	12462537	12468021	eyegone	68	eyg	
				FBgn0052102	FBtr0075978	12469072	12469784		68	CG32102	
				FBgn0036286	FBtr0308896	12471728	12474428		68	CG10616	
				FBgn0036287	FBtr0113167	12474418	12485035		68	CG10663	
				FBgn0053725	FBtr0091723	12482609	12488446		68	CG33725	
				FBgn0036288	FBtr0332646	12488668	12490676		68	CG10680	
				FBgn0267241	FBtr0346431	12490294	12491196	long non-coding RNA:CR45681	68	lncRNA:CR45681	
				FBgn0036289	FBtr0075975	12491830	12497216		68	CG10657	
				FBgn0267242	FBtr0346432	12491840	12493605	antisense RNA:CR45682	68	asRNA:CR45682	
				FBgn0036290	FBtr0345350	12498194	12501311		68	CG10638	
				FBgn0284460	FBtr0332781	12498487	12500307	antisense RNA:CR43868	68	asRNA:CR43868	
				FBgn0036291	FBtr0332634	12501513	12502847		68	CG10681	
				FBgn0036292	FBtr0075972	12502467	12503894		68	CG10646	
				FBgn0284848	FBtr0075958	12504292	12505921	vihar	68	vih	
				FBgn0036294	FBtr0075971	12505374	12507940		68	CG10654	
				FBgn0002466	FBtr0075970	12507998	12514815	sticky	68	sti	
				FBgn0266678	FBtr0345043	12514605	12515009	long non-coding RNA:CR45168	68	lncRNA:CR45168	
				FBgn0041775	FBtr0332635	12515059	12520954	trailer hitch	68	tral	
				FBgn0020388	FBtr0075969	12521129	12524014	Gcn5 acetyltransferase	68	Gcn5	
				FBgn0262524	FBtr0075960	12522987	12522163	verrocchio	68	ver	
				FBgn0004926	FBtr0075968	12525093	12526751	eukaryotic translation initiation factor 2 subunit beta	68	eIF2beta	
				FBgn0036298	FBtr0075967	12527215	12531071	realtocker	68	rtal	
				FBgn0036299	FBtr0075966	12530436	12533724	Transferrin 2	68	Tsf2	
				FBgn0085271	FBtr0300028	12533996	12534403		68	CG34242	
				FBgn0036300	FBtr0075961	12534590	12535513	Phosphomannomutase type 2	68	Pmm2	
				FBgn0036301	FBtr0075965	12535426	12537315		68	CG4069	
				FBgn0036302	FBtr0300887	12537513	12572542	sosondowah	68	sowah	
				FBgn0263587	FBtr0309823	12541710	12542563	long non-coding RNA:CR43612	68	lncRNA:CR43612	
				FBgn0015904	FBtr0075908	12580672	12596018	araucan	68	ara	
				FBgn0015919	FBtr0075909	12609631	12621708	caupolican	68	uap	
				FBgn0052111	FBtr0344477	12627934	12648280	long non-coding RNA:CR32111	68	lncRNA:CR32111	
				FBgn0263379	FBtr0309061	12648907	12653006	long non-coding RNA:CR43431	68	lncRNA:CR43431	
				FBgn0265746	FBtr0340703	12659903	12660095	long non-coding RNA:CR44553	68	lncRNA:CR44553	
				FBgn0265745	FBtr0340702	12661826	12662247	long non-coding RNA:CR44552	68	lncRNA:CR44552	
				FBgn0014343	FBtr0075912	12693639	12710249	mirror	68	mirr	
				FBgn0261933	FBtr0075952	12733364	12734811	Small ribonucleoprotein particle protein SmD1	68	SmD1	
				FBgn0014007	FBtr0075914	12734945	12741568	Protein tyrosine phosphatase 69D	68	Ptp69D	
				FBgn0052112	FBtr0301047	12741718	12745154		68	CG32112	
				FBti0063219	FBti0063219-RA	12745176	12745243		68		
				FBgn0052109	FBtr0075918	12746344	12746775		68	CG32109	

				FBgn0010235	FBtr0331555	12746616	12750358	Kinesin light chain		69	Klc
				FBgn0036305	FBtr0075920	12750119	12753402			69	CG10984
				FBgn0036306	FBtr0100354	12753239	12754774			69	CG10973
				FBgn0052113	FBtr0273390	12755049	12768605	Vacuolar protein sorting 13D		69	Vps13D
				FBgn0036309	FBtr0075949	12768432	12773573	Huntingtin interacting protein 1		69	Hip1
				FBgn0052106	FBtr0307888	12773951	12778716			69	CG32106
				FBgn0036310	FBtr0075946	12779750	12781007			69	CG10989
				FBgn0036311	FBtr0075923	12781325	12784377			69	CG17666
				FBgn0260945	FBtr0075945	12784429	12805116	Autophagy-related 1		69	Atg1
				FBgn0261674	FBtr0332681	12790192	12796684			69	CG42709
				FBgn0262714	FBtr0114506	12805902	12813038	Sin3A-associated protein 130		69	Sap130
				FBgn0267984	FBtr0347581	12806657	12808545	antisense RNA:CR46251		69	lncRNA:CR46251
				FBgn0052110	FBtr0075931	12808721	12810096			69	CG32110
				FBgn0036314	FBtr0075944	12813028	12814019	Splicing factor 3a subunit 2		69	Sf3a2
				FBgn0260965	FBtr0304053	12814254	12824650			69	CG42588
				FBgn0036316	FBtr0075942	12824880	12843108			69	CG10980
				FBgn0036317	FBtr0273237	12844254	12852117			69	CG10948
				FBgn0036318	FBtr0332047	12850165	12853169	WW domain binding protein 2		69	Wbp2
				FBgn0036319	FBtr0345343	12853646	12857428	Equilibrative nucleoside transporter 3		69	Ent3
				FBgn0052107	FBtr0345345	12857282	12861305			69	CG32107
				FBgn0036320	FBtr0075936	12861717	12862920			69	CG10943
				FBgn0002097	FBtr0020097-RA	12875004	12877212			69	
				FBgn0036321	FBtr0075868	12885039	12889244			69	CG14120
				FBgn0267312	FBtr0346567	12889532	12889938	long non-coding RNA:CR45748		69	lncRNA:CR45748
				FBgn0264486	FBtr0332802	12889770	12892162			69	CG43894
				FBgn0036323	FBtr0075870	12892658	12894758			69	CG14118
		69				12898169			69F1	
				FBgn0036324	FBtr0343628	12901247	12902737			69	CG12520
				FBgn0052117	FBtr0075905	12902925	12903711			69	CG32117
				FBgn0267591	FBtr0479871	12907085	12907635			69	CR46461
				FBgn0052115	FBtr0075904	12912027	12913846			69	CG32115
				FBgn0022098	FBtr0020098-RA	12919336	12924506			69	
				FBgn0060757	FBtr0060757-RA	12929767	12929892			69	
				FBgn0036325	FBtr0075903	12952686	12954847			69	CG10752
				FBgn0060759	FBtr0060759-RA	12953753	12953811			69	
				FBgn0022099	FBtr0020099-RA	12957842	12962265			69	
				FBgn0041622	FBtr0075901	12964360	12967733	Odorant receptor 69a		69	Or69a
				FBgn0036327	FBtr0075900	12971214	12972359			69	CG10748
				FBgn0036328	FBtr0075871	12972474	12973650			69	CG10749
				FBgn0036329	FBtr0075872	12995135	12997418			69	CG11262
				FBgn0060776	FBtr0060776-RA	13006498	13006640			69	
				FBgn0036330	FBtr0075873	13008817	13007881			69	CG11263
				FBgn0036331	FBtr0479869	13008285	13009450			69	CR14117
				FBgn0036332	FBtr0075899	13009398	13011685	Cullin 6		69	Cul6
				FBgn0036333	FBtr0075898	13011976	13016332	MICAL-like		69	MICAL-like
				FBgn0036334	FBtr0075875	13016050	13016903			69	CG11267
				FBgn0036335	FBtr0075897	13017149	13017967	mitochondrial ribosomal protein L20		69	mRpL20
				FBgn0036336	FBtr0075876	13018266	13019987	isoprenylcysteine carboxylmethyltransferase		69	Ide14
				FBgn0266994	FBtr0345916	13018315	13019110	antisense RNA:CR45445		69	asRNA:CR45445
				FBgn0036337	FBtr0075896	13019715	13022688	Adenosine Kinase		69	AdenoK
				FBgn0286213	FBtr0075878	13023352	13024762	Ribosomal protein S12		69	RpS12
				FBgn0086078	FBtr0114354	13023580	13023652			69	snoRNA:Me28S-A774b
				FBgn0086079	FBtr0114355	13024226	13024298			69	snoRNA:Me28S-A774a
				FBgn0266709	FBtr0075894	13024763	13026437	Zinc finger MYND-type containing 10		69	Zmynd10
				FBgn0266682	FBtr0345049	13028551	13029328	long non-coding RNA:CR45172		69	lncRNA:CR45172
				FBgn0036978	FBtr0110982	13028992	13036504			69	CG17672
				FBgn0266650	FBtr0344652	13032386	13033070	long non-coding RNA:CR45157		69	lncRNA:CR45157
				FBgn0036340	FBtr0075883	13036921	13040976	Serine-arginine repetitive matrix 1		69	Srrm1
				FBgn0011284	FBtr0346390	13041756	13044234	Ribosomal protein S4		69	RpS4
				FBgn0052967	FBtr0113611	13042767	13042906	snoRNA:Psi28S-3327a		69	snoRNA:Psi28S-3327a
				FBgn0052966	FBtr0113612	13042944	13043083	snoRNA:Psi28S-3327b		69	snoRNA:Psi28S-3327b
				FBgn0086601	FBtr0091754	13043371	13043510	snoRNA:Psi28S-3327c		69	snoRNA:Psi28S-3327c
				FBgn0036341	FBtr0075886	13044434	13046894	Syntaxin 13		69	Syx13
				FBgn0036342	FBtr0075887	13046977	13048919			69	CG11279
				FBgn0036343	FBtr0075893	13060400	13061422			69	CG14115
				FBgn0085457	FBtr0473611	13061759	13062715			69	CG34428
				FBgn0085458	FBtr0112730	13063046	13063926			69	CG34429
				FBgn0263681	FBtr0310106	13081299	13082652	long non-coding RNA:CR43652		70	lncRNA:CR43652
				FBgn0036345	FBtr0075892	13086387	13087289			70	CG17300
				FBgn0267313	FBtr0346568	13087491	13088588	long non-coding RNA:CR45749		70	lncRNA:CR45749
				FBgn0036346	FBtr0075891	13088581	13089969			70	CG11251
				FBgn0265747	FBtr0340704	13101489	13101662	long non-coding RNA:CR44554		70	lncRNA:CR44554
				FBgn0010452	FBtr0330075	13114271	13118077	tartan		70	trn
				FBgn0053262	FBtr0302393	13136269	13137086			70	CG33262
				FBgn0086916	FBtr0334063	13174478	13176781	sneaky		70	ienky
				FBgn0063244	FBtr0063244-RA	13200636	13200701			70	
				FBgn0266535	FBtr0344628	13208542	13208658	long non-coding RNA:CR45096		70	lncRNA:CR45096
				FBgn0052129	FBtr0075828	13211214	13211285	transfer RNA:Proline-AGG 1-5		70	tRNA:Pro-AGG-1-5
				FBgn0052128	FBtr0075829	13211551	13211622	transfer RNA:Proline-AGG 1-6		70	tRNA:Pro-AGG-1-6
				FBgn0052126	FBtr0075830	13212365	13212436	transfer RNA:Proline-AGG 1-7		70	tRNA:Pro-AGG-1-7
				FBgn0052127	FBtr0075831	13214109	13214233	transfer RNA:Leucine-CAA 2-2		70	tRNA:Leu-CAA-2-2
				FBgn0266536	FBtr0344628	13216267	13216569	long non-coding RNA:CR45007		70	lncRNA:CR45007
				FBgn0264515	FBtr0344583	13216103	13217527	long non-coding RNA:CR43914		70	lncRNA:CR43914
				FBgn0266537	FBtr0344627	13218203	13218864	long non-coding RNA:CR45098		70	lncRNA:CR45098
				FBgn0023095	FBtr0075833	13226692	13279942	capricious		70	caps
				FBgn0052119	FBtr0075867	13246884	13248702			70	CG32119
				FBgn0011844	FBtr0075834	13249547	13249618	transfer RNA:Aspartic acid-GTC 1-10		70	tRNA:Asp-GTC-1-10
				FBgn0052123	FBtr0075835	13279776	13279826	transfer RNA:CR32123 pseudogene		70	tRNA:CR32123:Psi
				FBgn0262822	FBtr0344572	13282393	13283410	long non-coding RNA:CR43146		70	lncRNA:CR43146
				FBgn0264514	FBtr0333132	13283663	13284496	long non-coding RNA:CR43913		70	lncRNA:CR43913
				FBgn0267316	FBtr0346599	13285265	13285835	long non-coding RNA:CR45752		70	lncRNA:CR45752
				FBgn0267317	FBtr0346598	13286388	13287166	long non-coding RNA:CR45753		70	lncRNA:CR45753
				FBgn0264513	FBtr0346597	13287769	13291770	long non-coding RNA:CR43912		70	lncRNA:CR43912
				FBgn0259970	FBtr0300316	13296530	13296860	Seminal fluid protein 70A4		70	Sfp70A4
				FBgn0266788	FBtr0345413	13297004	13297570	long non-coding RNA:CR45253		70	lncRNA:CR45253
				FBgn0266790	FBtr0345415	13297649	13297944	long non-coding RNA:CR45255		70	lncRNA:CR45255
				FBgn0266789	FBtr0345414	13298211	13298719	long non-coding RNA:CR45254		70	lncRNA:CR45254
				FBgn0259971	FBtr0300315	13298797	13299023			70	CG42481
				FBgn0262823	FBtr0344808	13299841	13300152			70	CG43147
				FBgn0003034	FBtr0075836	13301635	13301922	Sex Peptide		70	SP
				FBgn0264512	FBtr0333128	13302408	13303210	long non-coding RNA:CR43911		70	lncRNA:CR43911
				FBgn0265750	FBtr0340712	13302741	13303151	long non-coding RNA:CR44557		70	lncRNA:CR44557
				FBgn0265748	FBtr0340711	13303371	13303946	long non-coding RNA:CR44555		70	lncRNA:CR44555
				FBgn0265751	FBtr0340713	13324274	13324559	long non-coding RNA:CR44558		70	lncRNA:CR44558
				FBgn0040814	FBtr0075837	13329135	13329999			70	CG14113
				FBgn0265752	FBtr0340714	13343593	13344259	long non-coding RNA:CR44559		70	lncRNA:CR44559
				FBgn0036348	FBtr0476025	13346039	13354940			70	CG17687
				FBgn0287423	FBtr0075839	13356376	13357223	Neuropeptide-like precursor 2		70	Nplp2
				FBgn0036350	FBtr0331787	13377957	13380380			70	CG14111
				FBgn0036349	FBtr0075840	13378583	13379190	Sox/Neuro Co-Factor		70	SNCF
				FBgn0267546	FBtr0346693	13379142	13379854	antisense RNA:CR45886		70	asRNA:CR45886
				FBgn0036351	FBtr0075866	13380359	13381346			70	CG14107
				FBgn0001256	FBtr0075843	13382765	13383999	Ecdysone-inducible gene L1		70	ImpL1
				FBgn0036352	FBtr0075844	13384789	13385925			70	CG14110
				FBgn0036353	FBtr0075864	13385946	13387907			70	CG10171
				FBgn0036354	FBtr0075863	13388299	13390006	Proteome of centrioles 1		70	Poc1
		70				13394379			70A8	
1				FBgn0002573	FBtr0075862	13396228	13401125	sensless		70	sens
1				FBgn0036356	FBtr0075861	13411122	13412453			70	CG10222
1				FBgn0260049	FBtr0075845	13412843	13416453	flare		70	flr
1				FBgn0052121	FBtr0113424	13416576	13422336			70	CG32121
1				FBgn0053263	FBtr0075859	13423320	13424168			70	CG33263
1				FBgn0260459	FBtr0075858	13424571	13425671			70	CG14106
1				FBgn0036359	FBtr0075857	13425891	13426973			70	CG14105
1				FBgn0060782	FBtr0060782-RA	13428350	13428467			70	
1				FBgn0036360	FBtr0075855	13428839	13435229			70	CG10713
1				FBgn0012010	FBtr0075847	13433048	13433125	transfer RNA:Valine-AAC 2-3		70	tRNA:Val-AAC-2-3
1				FBgn0012009	FBtr0075856	13433846	13433718	transfer RNA:Valine-AAC 2-4		70	tRNA:Val-AAC-2-4
1				FBgn0036361	FBtr0075854	13435680	13437136			70	CG10154
1				FBgn0036362	FBtr0089323	13437954	13439009			70	CG10725

1				FBgn0036363	FBtr0075853	13439317	13440470		70	CG16140
1				FBgn0036364	FBtr0331532	13440916	13442425		70	CG14109
1				FBgn0036365	FBtr0331533	13442594	13445245	combover	70	cmb
1				FBgn0036366	FBtr0075825	13449187	13450283	Jumonji domain containing 7	70	JMJD7
1				FBgn0036368	FBtr0304792	13450770	13465539		70	CG10738
1				FBgn0036367	FBtr0075824	13456208	13457238		70	CG16116
1				FBgn0036369	FBtr0075821	13465532	13474767		70	CG10089
1				FBgn0086708	FBtr0075806	13477541	13483515	starvin	70	siv
1				FBgn0036372	FBtr0075819	13485533	13486280	Actin binding protein 1	70	Abp1
1				FBgn0036373	FBtr0075811	13486797	13502492	Inhibitor	70	Tgi
1				FBgn0036374	FBtr0075812	13502797	13511541	Sp20	70	Sp20
1				FBgn0036785	FBtr0075818	13511646	13513112	Vacuolar protein sorting 36	70	Vps36
1				FBgn0036376	FBtr0075813	13513254	13516276	Liprin-beta	70	Liprin-beta
1				FBgn0036377	FBtr0075817	13516273	13519605		70	CG10710
1				FBgn0264001	FBtr0330346	13521907	13803400	bruno 3	70	bru3
1				FBtr0020100	FBtr0020100-RA	13525212	13533949		70	
1				FBgn0262475	FBtr0346847	13559374	13561828	long non-coding RNA:CR45825	70	lncRNA:CR45825
1				FBgn0266688	FBtr0345655	13557755	13558101	long non-coding RNA:CR45178	70	lncRNA:CR45178
1				FBtr0020101	FBtr0020101-RA	13574910	13580104		70	
1				FBgn0266695	FBtr0344818	13599230	13599883	long non-coding RNA:CR45120	70	lncRNA:CR45120
1				FBgn0262415	FBtr0304349	13620822	13620920	mir-289 stem loop	70	mir-289
1				FBtr0304350_dl_mrg	FBtr0304350	13620837	13620962		70	
1				FBtr0059714	FBtr0059714-RA	13804601	13814138		70	
1				FBtr0020103	FBtr0020103-RA	13811235	13813708		70	
1				FBtr0060842	FBtr0060842-RA	13832074	13832129		70	
1				FBgn0262813	FBtr0336058	13837756	13838060		70	CG43184
1				FBgn0036380	FBtr0336083	13840157	13842240		70	CG8757
1				FBgn0275434	FBtr0392915	13840611	13842198	antisense RNA:CR46266	70	asRNA:CR46266
1				FBgn0040812	FBtr0075802	13842377	13843017		70	CG8750
1				FBgn0043550	FBtr0333019	13843656	13845316	Tetraspanin 68C	70	Tsp68C
1				FBgn0029167	FBtr0075753	13846054	13860001	Hemolectin	70	Hml
1				FBgn0036381	FBtr0075801	13860027	13866905		70	CG8745
1				FBgn0264006	FBtr0333021	13867414	13903236	dyschronic	70	dysc
1				FBgn0036382	FBtr0075755	13878994	13883056		70	CG13737
1				FBtr0060843	FBtr0060843-RA	13896388	13896438		70	
1				FBgn0036376	FBtr0075793	13906893	13925335	stimulator-like	70	Rgl
1				FBgn0036386	FBtr0075792	13925882	13929000		70	CG8833
1				FBgn0001108	FBtr0075756	13929387	13934656	Dynactin 1, p150 subunit	70	DCTN1-p150
1	**124054**					**13932268**		**70C6**		
1				FBgn0052137	FBtr0075758	13939250	13962847		70	CG32137
1				FBgn0025874	FBtr0333030	13962658	13964702	Meiotic central spindle	70	Meics
1				FBgn0263232	FBtr0479645	13965203	13973067	Nuclear export factor 3	70	Nxf3
1				FBgn0036389	FBtr0346845	13965203	13973067	short spindle 2	70	ssp2
1				FBgn0036390	FBtr0075790	13973123	13973477		70	CG13738
1				FBgn0001216	FBtr0075761	13974061	13977761	Heat shock protein cognate 1	70	Hsc70-1
1				FBgn0036391	FBtr0333026	13977905	13993400		70	CG17364
1				FBgn0036393	FBtr0333024	13988635	13987184		70	CG17362
1				FBgn0036394	FBtr0075785	13987878	13988626		70	CG9040
1				FBgn0250848	FBtr0075766	13994231	13996571	26-29kD-proteinase	70	26-29-p
1				FBgn0036395	FBtr0075767	13997191	13998055		70	CG17361
1				FBgn0036396	FBtr0075787	13997900	13999251		70	CG17359
1				FBgn0036397	FBtr0333025	13999380	14001885	Nitrogen permease regulator-like 3	70	Nprl3
1				FBgn0036398	FBtr0333050	14002127	14020148	upSET	70	upSET
1				FBgn0052133	FBtr0075784	14020315	14020121	Interacting protein	70	Pfip
1				FBgn0061515	FBtr0304673	14029579	14031706	endosulfine	70	endos
1				FBgn0036402	FBtr0343100	14031459	14034909		70	CG6950
1				FBgn0265295	FBtr0304128	14034531	14036838	antisense RNA:CR42871	70	asRNA:CR42871
1				FBgn0036403	FBtr0075770	14034776	14036751		70	CG6861
1				FBgn0026418	FBtr0304035	14037019	14043886	Hsc70Cb	70	Hsc70Cb
1				FBgn0263503	FBtr0445388	14043694	14049892	ligase 4	70	Neurl4
1				FBgn0036405	FBtr0075774	14051206	14052469		70	CG6833
1				FBgn0036406	FBtr0075780	14052428	14053079		70	CG13484
1				FBgn0267736	FBtr0347296	14053103	14054304	antisense RNA:CR46067	70	asRNA:CR46067
1				FBgn0267795	FBtr0075775	14063215	14071583	Formin-like	70	Frl
1				FBgn0013563	FBtr0075777	14071892	14076123	Peroxin 1	70	Pex1
1				FBgn0265896	FBtr0100676	14075772	14083229	breathless	70	btl
1				FBgn0036410	FBtr0347505	14083615	14086421		70	CG8160
1				FBgn0000639	FBtr0335515	14094589	14098835	Fat body protein 1	70	Fbp1
1				FBgn0036411	FBtr0075748	14103481	14108118	Sox21a	70	Sox21a
1				FBgn0042830	FBtr0330116	14112405	14131324	Sox21b	70	Sox21b
1				FBgn0267547	FBtr0346932	14134722	14135102	long non-coding RNA:CR45887	70	lncRNA:CR45887
1				FBgn0000411	FBtr0333034	14175610	14178925	Dichaete	70	D
1				FBgn0036414	FBtr0336524	14182449	14189448	nanchung	70	nan
1				FBgn0013718	FBtr0100043	14190870	14233250	nuclear fallout	70	nuf
1				FBgn0052141	FBtr0075735	14203323	14204294	saturn	70	saturn
1				FBgn0036415	FBtr0075737	14218204	14218974		70	CG7768
1				FBgn0036416	FBtr0075740	14233469	14234609		70	CG7624
1				FBgn0085273	FBtr0112438	14235053	14235941		70	CG34244
1				FBgn0036417	FBtr0075741	14239635	14238272		70	CG7606
1				FBgn0266948	FBtr0345840	14239607	14239440	long non-coding RNA:CR45399	70	lncRNA:CR45399
1				FBgn0265754	FBtr0340716	14245005	14245691	long non-coding RNA:CR44561	70	lncRNA:CR44561
1				FBtr0061303	FBtr0061303-RA	14245616	14245658		70	
1				FBgn0265753	FBtr0340715	14246993	14247011	long non-coding RNA:CR44560	70	lncRNA:CR44560
1				FBtr0020105	FBtr0020105-RA	14267428	14271755		70	
1				FBtr0001085	FBtr0330102	14274343	14368839	frizzled	70	fz
1				FBtr0020106	FBtr0020106-RA	14296038	14296465		70	
1				FBtr0020107	FBtr0020107-RA	14312098	14316928		70	
1				FBgn0266383	FBtr0344868	14322552	14326251	long non-coding RNA:CR45025	70	lncRNA:CR45025
1				FBgn0036419	FBtr0075744	14329346	14329885		70	CG13482
1				FBgn0036421	FBtr0113170	14368925	14369707		70	CG13481
1				FBgn0262580	FBtr0304959	14381913	14383399		70	CG43120
1				FBgn0036422	FBtr0075729	14400769	14402725		70	CG3868
1				FBt0061307	FBt0061307-RA	14402159	14402222		70	
1				FBgn0003459	FBtr0075728	14402930	14409939	stonewall	70	stwl
1				FBtr0061320	FBtr0061320-RA	14403417	14403464		70	
1				FBtr0061310	FBtr0061310-RA	14408198	14408255		70	
1				FBgn0266768	FBtr0346393	14410117	14410898	long non-coding RNA:CR45233	70	lncRNA:CR45233
1				FBgn0036423	FBtr0333040	14410628	14412735		70	CG3919
1				FBgn0087007	FBtr0273422	14412828	14536276	big bang	70	bbg
1				FBgn0267696	FBtr0347206	14420602	14421294	long non-coding RNA:CR46032	70	lncRNA:CR46032
1				FBgn0267695	FBtr0347205	14424501	14425926	long non-coding RNA:CR46031	70	lncRNA:CR46031
1				FBtr0020108	FBtr0020108-RA	14468500	14473847		70	
1				FBt0061324	FBt0061324-RA	14504176	14504477		70	
1				FBgn0036426	FBtr0290282	14517825	14518475		70	CG0592
1				FBgn0036427	FBtr0333038	14519760	14521690		70	CG4613
1	**126198**					**14530694**		**70E1**		
1				FBtr0020109	FBtr0020109-RA	14524380	14529076		70	
1				FBgn0262891	FBtr0336305	14536634	14537272		70	CG43246
1				FBgn0264009	FBtr0075718	14537651	14540441	protein 2	70	Mpcp2
1				FBgn0036428	FBtr0333037	14540937	14550975	Glycogen binding subunit 70E	70	Gbs-70E
1				FBgn0054039	FBtr0301014	14560000	14562613		70	CG34039
1				FBgn0266117	FBtr0343631	14560000	14560953	antisense RNA:CR44843	70	asRNA:CR44843
1				FBgn0028418	FBtr0075722	14560139	14560764	Leucokinin	70	lk
1				FBt0061336	FBt0061336-RA	14563202	14563283		70	
1				FBgn0261816	FBtr0303303	14567440	14568133		70	CG42758
1				FBgn0040318	FBtr0075720	14583222	14599540	HGTX	70	HGTX
1				FBgn0003388	FBtr0304700	14614458	14622205	shade	70	shd
1				FBgn0036433	FBtr0301259	14622798	14628174		70	CG9828
1	**123520**					**14625700**		**70E5**		
1				FBgn0027375	FBtr0075715	14628160	14632077	RecQ5 helicase	70	RecQ5
1				FBt0061338	FBt0061338-RA	14630298	14630465		70	
1				FBgn0041604	FBtr0333032	14632601	14671609	daily-like	70	dlp
1				FBgn0267548	FBtr0346931	14661455	14661946	long non-coding RNA:CR45888	70	lncRNA:CR45888
1				FBgn0262581	FBtr0304960	14671935	14672437		70	CG43121
1				FBgn0259175	FBtr0299650	14672839	14747888	omega	70	ome
1				FBgn0011927	FBtr0075713	14673942	14674013	CAT 1-4	70	RNA:iMet-CAT-1-4
1				FBgn0011928	FBtr0075681	14674344	14674415	CAT 1-5	70	RNA:iMet-CAT-1-5
1				FBgn0036436	FBtr0075712	14674538	14678147		70	CG4914
1				FBgn0036437	FBtr0075684	14684768	14685842		70	CG5048
1				FBgn0036438	FBtr0075685	14691347	14691962	goddard	70	goddard
1				FBgn0036439	FBtr0075711	14696551	14697105		70	CG13474
1				FBgn0036440	FBtr0333018	14697313	14701678		70	CG17177
1				FBgn0036441	FBtr0075687	14705464	14706157		70	CG13476
1				FBtr0020110	FBtr0020110-RA	14721232	14723921		70	

1			FBgn0020111	FBtr0020111-RA	14725654	14726982			70	
1			FBgn0036442	FBtr0075699	14726760	14728343			70	CG13473
1			FBgn0036443	FBtr0075709	14732589	14733517			70	CG13471
1			FBgn0260233	FBtr0300642	14747929	14757962			70	CG42507
1			FBgn0013263	FBtr0075703	14747929	14761049	Trithorax-like		70	Trl
1			FBgn0053260	FBtr0332436	14760526	14761844	34		70	Tsen34
1			FBgn0036446	FBtr0333044	14762028	14767703			70	CG0384
1			FBgn0036447	FBtr0075701	14767703	14769283			70	CG17173
1			FBgn0036448	FBtr0075700	14769341	14776129	myopic		70	mop
1			FBgn0036449	FBtr0075699	14776496	14786412	brummer		70	bmm
1			FBgn0036450	FBtr0075691	14786791	14789865	Tudor domain containing 3		70	Tdrd3
1			FBgn0036451	FBtr0075693	14789935	14801089	Helicase with zinc finger		70	Helz
1			FBgn0029148	FBtr0333076	14801328	14802168	NHP2		70	NHP2
1			FBgn0001120	FBtr0075697	14802380	14803360	giant nuclei		70	grn
1			FBgn0036454	FBtr0110825	14805136	14882224			70	CG17839
1			FBgn0020112	FBtr0020112-RA	14825181	14832850			70	
1			FBgn0260913	FBtr0342827	14885341	14888183	long non-coding RNA:CR44702		71	lncRNA:CR44702
1			FBgn0266947	FBtr0345839	14890090	14890920	long non-coding RNA:CR45398		71	lncRNA:CR45398
1			FBgn0085274	FBtr0302580	14893734	14894416			71	CG34245
1			FBgn0259069	FBtr0299510	14903805	14942907	achinodarm-microtubule-associated		71	DCX-EMAP
1			FBgn0040809	FBtr0075674	14943730	14944331			71	CG13465
1			FBgn0040467	FBtr0075673	14945499	14946125	Brother of Bearded A		71	BobA
1			FBgn0267640	FBtr0347095	14946884	14950703	long non-coding RNA:CR45978		71	lncRNA:CR45978
1			FBgn0020113	FBtr0020113-RA	14951135	14951341			71	
1			FBgn0061376	FBtr0061376-RA	14951617	14951679			71	
1			FBgn0061361	FBtr0061361-RA	14951722	14951985			71	
1			FBgn0020114	FBtr0020114-RA	14954422	14956932			71	
1			FBgn0026320	FBtr0075620	14969344	14970306	Twin of m4		71	Tom
1			FBgn0020115	FBtr0020115-RA	14970820	14971064			71	
1			FBgn0000216	FBtr0075621	14972667	14973198	Bearded		71	Brd
1			FBgn0040296	FBtr0259779	14974848	14976040	Ocho		71	Ocho
1			FBgn0263380	FBtr0300696	14976526	14977631	long non-coding RNA:CR43432		71	lncRNA:CR43432
1			FBgn0036459	FBtr0300663	14979620	14982432			71	CG3349
1			FBgn0036460	FBtr0075624	14982835	14984486			71	CG5114
1			FBgn0032778	FBtr0075626	14985100	14991667	minidiscs		71	mnd
1			FBgn0036461	FBtr0347146	14992289	14997983	related protein 71B		71	Zip71B
1			FBgn0036462	FBtr0075672	14997981	14999660	mitochondrial ribosomal protein L39		71	mRpL39
1			FBgn0023174	FBtr0075629	14999951	15001319	Proteasome beta2 subunit		71	Prosbeta2
1			FBgn0036463	FBtr0075671	15001238	15014062	protein with kazal motifs		71	Reck
1	**123418**				**15007519**			**71B1**		
1			FBgn0261090	FBtr0299849	15014695	15064077	Synaptotagmin beta		71	Sytbeta
1			FBgn0047338	FBtr0075630	15022492	15024009			71	CG32148
1			FBgn0036465	FBtr0075669	15041631	15042570	related		71	Rpn12R
1			FBgn0025776	FBtr0333875	15042799	15043924	intermediate neuroblasts defective		71	ind
1			FBgn0263761	FBtr0310458	15049179	15049465			71	CG43678
1			FBgn0036466	FBtr0075666	15049593	15050209			71	CG18581
1			FBgn0036467	FBtr0075665	15050263	15050808			71	CG12310
1			FBgn0263762	FBtr0310456	15050956	15051425			71	CG43679
1			FBgn0036468	FBtr0075664	15051931	15052466			71	CG13461
1			FBgn0061362	FBtr0061362-RA	15052710	15052764			71	
1			FBgn0263763	FBtr0310455	15052998	15053351			71	CG43680
1			FBgn0036469	FBtr0333874	15053568	15054135			71	CG18649
1			FBgn0036470	FBtr0075631	15054777	15055965	Chameau		71	EAChm
1			FBgn0061417	FBtr0061417-RA	15056356	15056430			71	
1			FBgn0036471	FBtr0114510	15061029	15061705			71	CG13480
1			FBgn0263767	FBtr0310484	15062207	15062622	long non-coding RNA:CR43684		71	lncRNA:CR43684
1			FBgn0086690	FBtr0333946	15066081	15094724	Pericentrin-like protein		71	Plp
1			FBgn0036474	FBtr0075659	15076607	15078447	Odorant receptor 71a		71	Or71a
1			FBgn0020116	FBtr0020116-RA	15085107	15086212			71	
1			FBgn0036476	FBtr0075657	15090823	15094719	slepping stone		71	sstn
1			FBgn0027088	FBtr0333934	15095142	15097686	Glycyl-tRNA synthetase		71	GlyRS
1			FBgn0266452	FBtr0345691	15097914	15113003	CTP synthase		71	CTPsyn
1			FBgn0264704	FBtr0333938	15098534	15098932	long non-coding RNA:CR43973		71	lncRNA:CR43973
1			FBgn0264703	FBtr0333937	15100054	15102040			71	CR43972
1			FBgn0266441	FBtr0344433	15105882	15110730			71	CG45071
1			FBgn0264702	FBtr0333936	15108001	15108695	antisense RNA:CR43971		71	asRNA:CR43971
1			FBgn0036479	FBtr0075637	15113557	15116372			71	CG13458
1			FBgn0061389	FBtr0061389-RA	15114676	15114738			71	
1			FBgn0036480	FBtr0333853	15116737	15128029	Centrosomal protein 135kDa		71	Cep135
1			FBgn0036481	FBtr0075656	15119878	15125321			71	CG16959
1			FBgn0052847	FBtr0075639	15121572	15122301			71	CG32847
1			FBgn0036482	FBtr0075653	15127940	15131378			71	CG13457
1			FBgn0036483	FBtr0075651	15131508	15136694			71	CG12316
1			FBgn0060051	FBtr0091708	15134550	15134660	MeU5-U42		71	scaRNA:MeU5-U42
1			FBgn0266818	FBtr0346644	15137738	15142840	Protein disulfide isomerase		71	Pdi
1			FBgn0266945	FBtr0345844	15142131	15142800	antisense RNA:CR45396		71	asRNA:CR45396
1			FBgn0047178	FBtr0075647	15143063	15144058			71	CG32147
1			FBgn0266946	FBtr0345838	15143801	15144170	antisense RNA:CR45397		71	asRNA:CR45397
1			FBgn0036484	FBtr0331830	15144355	15146379	Peroxin 3		71	Pex3
1			FBgn0061391	FBtr0061391-RA	15146628	15146682			71	
1			FBgn0036485	FBtr0075641	15147137	15154365	alpha1,3-fucosyltransferase A		71	FucTA
1			FBgn0036486	FBtr0075646	15154233	15158920	MafkI		71	Mafk6
1			FBgn0036487	FBtr0075642	15159100	15161138	Pre-mRNA processing factor 31		71	Prp31
1			FBgn0036489	FBtr0075645	15160876	15163628			71	CG7011
1			FBgn0036488	FBtr0075643	15161817	15162470			71	CG6878
1			FBgn0061393	FBtr0061393-RA	15172529	15172731			71	
1			FBgn0266755	FBtr0342717	15190440	15190988	long non-coding RNA:CR44562		71	lncRNA:CR44562
1			FBgn0036490	FBtr0075644	15207844	15208586			71	CG6888
1			FBgn0029114	FBtr0075607	15235619	15242832	Tollo		71	Tollo
1			FBgn0020117	FBtr0020117-RA	15255823	15256608			71	
1			FBgn0036491	FBtr0113172	15269598	15300942	Bestrophin 4		71	Best4
1			FBgn0036492	FBtr0075618	15300115	15302765	Bestrophin 3		71	Best3
1			FBgn0036493	FBtr0110881	15304255	15311195			71	CG7255
1			FBgn0267933	FBtr0347508	15319923	15320356	long non-coding RNA:CR46213		71	lncRNA:CR46213
1			FBgn0262892	FBtr0344641	15332246	15332877	long non-coding RNA:CR43247		71	lncRNA:CR43247
1			FBgn0264724	FBtr0334106	15334782	15336171	long non-coding RNA:CR43692		71	lncRNA:CR43692
1			FBgn0036494	FBtr0075614	15336692	15340315	Toll-6		71	Toll-6
1			FBgn0036495	FBtr0075615	15407832	15408267			71	CG33259
1			FBgn0020118	FBtr0020118-RA	15423798	15426602			71	
1			FBgn0263616	FBtr0300981	15437201	15437713	long non-coding RNA:CR43625		71	lncRNA:CR43625
1			FBgn0266944	FBtr0345836	15457491	15457878	long non-coding RNA:CR45395		71	lncRNA:CR45395
1			FBgn0266943	FBtr0345837	15457653	15458308	long non-coding RNA:CR45394		71	lncRNA:CR45394
1			FBgn0036496	FBtr0332815	15472197	15474110	cocoon		71	cocoon
1			FBgn0036497	FBtr0075616	15484396	15485402	Ran-like		71	Ran-like
1			FBgn0040805	FBtr0113333	15492964	15495549			71	CG12355
1			FBgn0036498	FBtr0075544	15496574	15496955			71	CG13455
1			FBgn0036499	FBtr0075546	15498202	15498921			71	CG7276
1			FBgn0036500	FBtr0075547	15499959	15500561			71	CG7275
1			FBgn0036501	FBtr0075548	15500938	15503768			71	CG7272
1			FBgn0026738	FBtr0075605	15503600	15504894			71	CG7857
1			FBgn0036502	FBtr0334085	15505188	15508252			71	CG7841
1			FBgn0004052	FBtr0075549	15506061	15509513	Z600		71	Z600
1			FBgn0001099	FBtr0346516	15509445	15511047	gonadal		71	gdl
1			FBgn0028377	FBtr0091756	15509445	15510837	gdl-ORF39		71	gdl-ORF39
1			FBgn0000565	FBtr0330176	15511052	15513202	Methionine sulfoxide reductase A		71	MsrA
1			FBgn0036503	FBtr0075603	15516539	15517056			71	CG13454
1			FBgn0004228	FBtr0334084	15517424	15519592	midgut expression 1		71	mex1
1			FBgn0262689	FBtr0306511	15520319	15521564	antisense RNA:CR43159		71	asRNA:CR43159
1			FBgn0036504	FBtr0075556	15520620	15521653	yellow-k		71	yellow-k
1			FBgn0036505	FBtr0075600	15521711	15524137			71	CG7945
1			FBgn0053986	FBtr0305542	15524325	15525253			71	CG33986
1	**123026**				**15525670**			**71E1**		
1			FBgn0053985	FBtr0100030	15525891	15526812			71	CG33985
1			FBgn0261682	FBtr0303077	15526910	15527516			71	CG42729
1			FBgn0261681	FBtr0303076	15527620	15528198			71	CG42728
1			FBgn0053983	FBtr0100028	15528265	15529243	obstructor-H		71	obst-H
1			FBgn0262893	FBtr0306309	15530085	15531479			71	CG43248
1			FBgn0004396	FBtr0075558	15530398	15532214	binding protein A		71	CrebA
1			FBgn0061447	FBtr0061447-RA	15553487	15553631			71	
1			FBgn0061450	FBtr0061450-RA	15553632	15553950			71	
1			FBgn0087035	FBtr0075559	15554113	15561042	Argonaute 2		71	AGO2
1			FBgn0020119	FBtr0020119-RA	15554974	15556705			71	
1			FBgn0036509	FBtr0075566	15560728	15563935			71	CG7739
1			FBgn0036510	FBtr0306156	15563427	15565559	oncogene		71	BCCRO

1				FBgn0267390	FBtr0332091	15566013	15576313	drop out		71	lkp
1				FBgn0036512	FBtr0075563	15576375	15578674			71	CG16979
1				FBgn0281109	FBtr0075695	15578769	15580537	marionette		71	mrn
1				FBgn0036514	FBtr0075564	15580800	15583373			71	CG12301
1				FBgn0036515	FBtr0075566	15583638	15585347	protein 2		71	AIMP2
1				FBgn0036516	FBtr0301186	15585431	15588175			71	CG7656
1				FBgn0036518	FBtr0332093	15588860	15609125	71E		71	RhoGAP71E
1				FBgn0036519	FBtr0075591	15608707	15610386			71	CG7650
1				FBgn0036520	FBtr0075590	15610631	15612828			71	CG13449
1				FBgn0259236	FBtr0299850	15613184	15647762	comm3		71	comm3
1				FBgn0036522	FBtr0075570	15619901	15624133	Phaser		71	Pha
1				FBgn0267639	FBtr0347094	15620200	15629803	long non-coding RNA:CR45977		71	lncRNA:CR45977
1				FBgn0262529	FBtr0304969	15648571	15649125			71	CG43083
1				FBgn0004588	FBtr0075587	15649128	15649981	Ecdysone-induced gene 71Ea		71	Eig71Ea
1				FBgn0004589	FBtr0303460	15649936	15650541	Ecdysone-induced gene 71Eb		71	Eig71Eb
1				FBgn0262530	FBtr0304970	15650652	15651392			71	CG43084
1				FBgn0004590	FBtr0075586	15651479	15652254	Ecdysone-induced gene 71Ec		71	Eig71Ec
1				FBgn0004591	FBtr0075572	15652537	15653096	Ecdysone-induced gene 71Ed		71	Eig71Ed
1				FBgn0004592	FBtr0075585	15654472	15656010	Ecdysone-induced gene 71Ee		71	Eig71Ee
1				FBgn0004593	FBtr0075584	15656655	15657390	Ecdysone-induced gene 71Ef		71	Eig71Ef
1				FBgn0004594	FBtr0075573	15657628	15658149	Ecdysone-induced gene 71Eg		71	Eig71Eg
1				FBgn0014848	FBtr0332334	15658936	15659441	Eig71Eh		71	Eig71Eh
1				FBgn0014849	FBtr0332123	15659707	15660351	Eig71Ei		71	Eig71Ei
1				FBgn0014850	FBtr0075582	15660549	15661015	Eig71Ej		71	Eig71Ej
1				FBgn0014851	FBtr0075575	15661248	15661809	Eig71Ek		71	Eig71Ek
1				FBgn0262528	FBtr0304968	15661863	15662279			71	CG43082
1				FBgn0036527	FBtr0075577	15670720	15681470			71	CG7304
1				FBgn0036528	FBtr0075581	15681633	15683445			71	CG7579
1				FBgn0036529	FBtr0075578	15683872	15686598	Acetylgalactosaminyltransferase 8		71	Pgant8
1				FBgn0085481	FBtr0345809	15686352	15687002			71	CG34452
1				FBgn0085480	FBtr0479781	15686517	15692068			71	CG34451
1				FBgn0041160	FBtr0075580	15687594	15689853	comm2		71	comm2
1				FBgn0260777	FBtr0331799	15716453	15717746			71	CG42571
1				FBgn0260776	FBtr0332689	15717819	15720073			71	CG42570
1				FBgn0010105	FBtr0075579	15721511	15728430	commissureless		71	comm
1				FBgn0286775	FBtr0345400	15747403	15748888	long non-coding RNA:CR45240		71	lncRNA:CR45240
1				FBgn0267916	FBtr0347475	15749026	15755021	long non-coding RNA:CR46197		71	lncRNA:CR46197
1			**72**			**15799228**			**72A1**	
1	**Supercompetition**			FBgn0036531	FBtr0075502	15808322	15808883			72	CG6244
1	**Supercompetition**			FBgn0036532	FBtr0075503	15809485	15809977			72	CG13445
1	**Supercompetition**			FBgn0261722	FBtr0075541	15810081	15816410	flower		72	fwe
1	**Supercompetition**			FBgn0015025	FBtr0075504	15816979	15818921	CKII-alpha subunit interactor-1		72	CKIIalpha-i1
1	**Supercompetition**			FBgn0036534	FBtr0075538	15818734	15828423	Decapping protein 2		72	DCP2
1	**Supercompetition**			FBgn0040230	FBtr0332133	15828688	15832004	diablo		72	dbo
1	**Supercompetition**			FBgn0036536	FBtr0075506	15832464	15833947			72	CG12713
1	**Supercompetition**			FBgn0036537	FBtr0332134	15833795	15835388			72	CG18081
1	**Supercompetition**			FBgn0036538	FBtr0306854	15835693	15837482			72	CG15715
1	**Supercompetition**			FBgn0052150	FBtr0075535	15837773	15844362	meru		72	meru
1	**Supercompetition**			FBgn0262371	FBtr0304186	15843406	15843465	mir-263b stem loop		72	mir-263b
1	**Supercompetition**			FBtr0472738_df_mrg	FBtr0472738	15843420	15843441			72	
1	**Supercompetition**			FBtr0304187_df_mrg	FBtr0304187	15843469	15843480			72	
1	**Supercompetition**			FBgn0264908	FBtr0334075	15845578	15859329	pH-sensitive chloride channel 1		72	pHCl-1
1	**Supercompetition**			FBgn0284843	FBtr0334745	15876091	15876472	long non-coding RNA:CR44051		72	lncRNA:CR44051
1	**Supercompetition**			FBgn0284842	FBtr0334744	15884593	15885747	long non-coding RNA:CR44050		72	lncRNA:CR44050
1	**Supercompetition**			FBti0020120	FBti0020120-RA	15899285	15899784			72	
1	**Supercompetition**			FBgn0036544	FBtr0334071	15900158	15924861	sugar-free frosting		72	sff
1	**Supercompetition**			FBgn0000489	FBtr0075529	15925805	15954767	catalytic subunit 3		72	Pka-C3
1	**Supercompetition**			FBti0020121	FBti0020121-RA	15929252	15939340			72	
1	**Supercompetition**	**126092**				**15948261**			**72B2**	
1	**Supercompetition**			FBgn0036545	FBtr0333572	15955096	15956485	GXIVsPLA2		72	GXIVsPLA2
1	**Supercompetition**			FBgn0283649	FBtr0333573	15956550	15958433	early girl		72	elgi
1	**Supercompetition**			FBgn0036547	FBtr0075511	15958843	15960809			72	CG17032
1	**Supercompetition**			FBgn0283599	FBtr0075527	15960836	15967972	lethal (3) 72Ab		72	l(3)72Ab
1	**Supercompetition**			FBgn0036549	FBtr0075512	15968204	15969902			72	CG10516
1	**Supercompetition**			FBgn0000212	FBtr0333580	15970082	15982869	brahma		72	brm
1	**Supercompetition**			FBgn0036550	FBtr0075513	15975368	15976428			72	CG17026
1	**Supercompetition**			FBgn0036551	FBtr0333575	15976870	15978435			72	CG17029
1	**Supercompetition**			FBgn0036552	FBtr0075515	15978524	15980004			72	CG17028
1	**Supercompetition**			FBgn0036553	FBtr0333576	15981102	15981888			72	CG17027
1	**Supercompetition**			FBgn0000115	FBtr0075517	15983135	15984362	ADP ribosylation factor-like 1		72	Arl1
1	**Supercompetition**			FBgn0263600	FBtr0075522	15984322	15987815	DNA polymerase delta		72	DNApol-delta
1	**Supercompetition**			FBgn0286995	FBtr0345917	15987784	15988041	long non-coding RNA:CR45446		72	lncRNA:CR45446
1	**Supercompetition**			FBgn0259824	FBtr0330161	15988236	15992464	Huntingtin-interacting protein 14		72	Hip14
1	**Supercompetition**			FBgn0036556	FBtr0333579	15992669	16004758	herring		72	hrg
1	**Supercompetition**			FBgn0036557	FBtr0075519	16005193	16006599	mitochondrial ribosomal protein S31		72	mRpS31
1	**Supercompetition**			FBgn0263601	FBtr0333578	16006552	16011812	mind bomb 1		72	mib1
1	**Supercompetition**			FBgn0284601	FBtr0344585	16017165	16018317	long non-coding RNA:CR43950		72	lncRNA:CR43950
1	**Supercompetition**			FBgn0267660	FBtr0347119	16017537	16021582	long non-coding RNA:CR45998		72	lncRNA:CR45998
1	**Supercompetition**			FBgn0284600	FBtr0344584	16020409	16021926	long non-coding RNA:CR43949		72	lncRNA:CR43949
1	**Supercompetition**			FBgn0044028	FBtr0075435	16023480	16032752	Notum		72	Notum
1	**Supercompetition**			FBgn0263570	FBtr0300722	16031189	16031261	mir-4941 stem loop		72	mir-4941
1	**Supercompetition**			FBtr0309723_df_mrg	FBtr0309723	16031212	16031232			72	
1	**Supercompetition**			FBtr0309724_df_mrg	FBtr0309724	16031248	16031271			72	
1	**Supercompetition**			FBgn0261634	FBtr0332699	16032762	16033195			72	CG42717
1	**Supercompetition**			FBgn0261633	FBtr0332698	16033778	16034170			72	CG42716
1	**Supercompetition**			FBgn0260646	FBtr0301002	16034524	16034853			72	CG42538
1	**Supercompetition**			FBgn0036560	FBtr0075437	16035485	16037227			72	CG5895
1	**Supercompetition**			FBgn0260635	FBtr0075469	16038419	16051034	apoptosis 1		72	Diap1
1	**Supercompetition**			FBgn0267549	FBtr0346930	16042395	16042985	antisense RNA:CR45889		72	asRNA:CR45889
1	**Supercompetition**			FBgn0284602	FBtr0333615	16046235	16050303	long non-coding RNA:CR43951		72	lncRNA:CR43951
1	**Supercompetition**			FBgn0005536	FBtr0112850	16051959	16082026	Myosin binding subunit		72	Mbs
1	**Supercompetition**			FBgn0053258	FBtr0301030	16082551	16083638			72	CG33258
1	**Supercompetition**			FBgn0036563	FBtr0301031	16083993	16085264			72	CG13075
1	**Supercompetition**			FBgn0263602	FBtr0075498	16085221	16087525	Taspase 1		72	Taspr1
1	**Supercompetition**			FBgn0036565	FBtr0075497	16087627	16090362			72	CG5235
1	**Supercompetition**			FBgn0036566	FBtr0333598	16090454	16096151	Chloride channel-c		72	ClC-c
1	**Supercompetition**			FBgn0036567	FBtr0075496	16095768	16097493			72	CG13074
1	**Supercompetition**			FBgn0036568	FBtr0075446	16097834	16100088	ATP synthase, beta subunit-like		72	ATPsynbetaL
1	**Supercompetition**			FBgn0036569	FBtr0332328	16100280	16103482	mitochondrial		72	leuRS-m
1	**Supercompetition**			FBgn0036570	FBtr0075495	16103432	16105627	Integrator 9		72	Int9
1	**Supercompetition**			FBgn0262987	FBtr0306825	16105852	16106428			72	CG43295
1	**Supercompetition**			FBgn0263603	FBtr0310582	16106594	16112626	Zinc-finger protein at 72D		72	Zn72D
1	**Supercompetition**			FBgn0010280	FBtr0075451	16113212	16121651	TBP-associated factor 4		72	TaF4
1	**Supercompetition**			FBgn0036571	FBtr0301912	16122002	16126552	Strumpellin		72	Strump
1	**Supercompetition**			FBgn0003076	FBtr0075492	16126018	16128531	Phosphoglucose mutase 1		72	Pgm1
1	**Supercompetition**			FBgn0011016	FBtr0075453	16129617	16130983	Signal sequence receptor beta		72	SsRbeta
1	**Supercompetition**			FBgn0286724	FBtr0075491	16131001	16131632	TRAPP subunit 20		72	Trs20
1	**Supercompetition**			FBgn0036574	FBtr0307518	16132028	16136991	1		72	elg1
1	**Supercompetition**			FBgn0036575	FBtr0075490	16134487	16137976			72	CG5157
1	**Supercompetition**			FBgn0036576	FBtr0307519	16137802	16164701			72	CG5151
1	**Supercompetition**			FBgn0052152	FBtr0346507	16139501	16144236			72	CG32152
1	**Supercompetition**	**125972**				**16157381**			**72D9**	
1	**Supercompetition**			FBti0061502	FBti0061502-RA	16164961	16164998			72	
1	**Supercompetition**			FBgn0053796	FBtr0301800	16169455	16170108			72	CG33796
1	**Supercompetition**			FBti0061504	FBti0061504-RA	16170452	16170534			72	
1	**Supercompetition**			FBgn0053795	FBtr0346810	16170729	16171380			72	CG33795
1	**Supercompetition**			FBgn0267318	FBtr0346800	16176810	16177256	long non-coding RNA:CR45754		72	lncRNA:CR45754
1	**Supercompetition**			FBgn0267319	FBtr0346801	16177345	16177635	long non-coding RNA:CR45755		72	lncRNA:CR45755
1	**Supercompetition**			FBti0020122	FBti0020122-RA	16184180	16188908			72	
1	**Supercompetition**			FBgn0269986	FBtr0345860	16190552	16197216	long non-coding RNA:CR45437		72	lncRNA:CR45437
1	**Supercompetition**			FBti0061869	FBti0061869-RA	16197614	16197655			72	
1	**Supercompetition**			FBgn0053687	FBtr0345888	16197868	16198852			72	CG33687
1	**Supercompetition**			FBgn0053688	FBtr0091668	16199220	16199926			72	CG33688
1	**Supercompetition**			FBgn0053689	FBtr0346809	16200229	16200926			72	CG33689
1	**Supercompetition**			FBgn0053690	FBtr0479892	16201328	16202032			72	CG33690
1	**Supercompetition**			FBgn0036577	FBtr0075485	16213051	16217303			72	CG13073
1	**Supercompetition**			FBgn0284483	FBtr0344761	16213928	16214376	antisense RNA:CR43891		72	asRNA:CR43891
1	**Supercompetition**			FBgn0052153	FBtr0075456	16222031	16222103	transfer RNA:Methionine-CAT 1-3		72	tRNA:Met-CAT-1-3
1	**Supercompetition**			FBgn0263605	FBtr0075464	16226128	16228707	lethal (3) 72Dn		72	l(3)72Dn
1	**Supercompetition**			FBgn0036579	FBtr0075457	16229100	16231139			72	CG9027
1	**Supercompetition**			FBgn0036580	FBtr0075483	16231081	16232038	Programmed Cell Death 5		72	PDCD-5
1	**Supercompetition**			FBgn0036581	FBtr0301481	16232084	16232777	Mediator complex subunit 10		72	MED10
1	**Supercompetition**			FBgn0263606	FBtr0112440	16233127	16234165	Heat shock protein cognate 20		72	Hsc20

1	Supercompetition			FBgn0263607	FBtr0075459	16234140	16236988	lethal (3) 72Dp		72	l(3)72Dp
1	Supercompetition			FBs0261894	FBst0261894-RA	16237359	16237486			72	
1	Supercompetition			FBgn0263608	FBtr0075460	16237723	16239462	lethal (3) 72Dr		72	l(3)72Dr
1	Supercompetition			FBgn0036583	FBtr0333564	16240560	16252355			72	CG13055
1	Supercompetition			FBgn0036584	FBtr0075481	16255852	16257191			72	CG13054
1	Supercompetition			FBgn0042801	FBtr0333563	16259037	16259722			72	CG13053
1	Supercompetition			FBgn0085276	FBtr0112441	16261185	16261605			72	CG34047
1	Supercompetition			FBgn0036585	FBtr0303379	16262740	16263247			72	CG13071
1	Supercompetition			FBgn0036586	FBtr0303380	16263343	16264151			72	CG13070
1	Supercompetition			FBgn0040799	FBtr0112771	16264713	16265100			72	CG13051
1	Supercompetition			FBgn0040798	FBtr0075463	16265385	16265804			72	CG13069
1	Supercompetition			FBgn0036587	FBtr0290260	16265797	16268198			72	CG4650
1	Supercompetition			FBgn0036588	FBtr0075464	16269392	16269911			72	CG13068
1	Supercompetition			FBgn0085277	FBtr0112442	16270369	16270902			72	CG34048
1	Supercompetition			FBgn0036589	FBtr0075465	16271282	16271918			72	CG13067
1	Supercompetition			FBgn0040797	FBtr0332928	16272909	16273038			72	CG13066
1	Supercompetition			FBgn0036590	FBtr0075468	16277435	16278183			72	CG13065
1	Supercompetition			FBgn0036591	FBtr0075478	16279498	16279271			72	CG13050
1	Supercompetition			FBgn0040796	FBtr0289378	16280404	16280860			72	CG13064
1	Supercompetition			FBgn0036592	FBtr0075477	16281132	16281930			72	CG13049
1	Supercompetition			FBgn0036593	FBtr0075475	16282809	16283921			72	CG13048
1	Supercompetition			FBgn0036594	FBtr0289564	16284680	16285398			72	CG13047
1	Supercompetition			FBgn0036595	FBtr0289563	16287584	16288422			72	CG13046
1	Supercompetition			FBs0061887	FBst0061887-RA	16289412	16289531			72	
1	Supercompetition			FBgn0036596	FBtr0306796	16289712	16290950			72	CG13045
1	Supercompetition			FBgn0036597	FBtr0075471	16294711	16295547			72	CG4962
1	Supercompetition			FBgn0036598	FBtr0075469	16301453	16302027			72	CG4682
1	Supercompetition			FBgn0036599	FBtr0075470	16302490	16303178			72	CG13044
1	Supercompetition			FBgn0267550	FBtr0346929	16302544	16303531	antisense RNA:CR45890		72	asRNA:CR45890
1	Supercompetition			FBs0061889	FBst0061889-RA	16303722	16303788			72	
1	Supercompetition			FBgn0262894	FBtr0306310	16304282	16304862			72	CG43249
1	Supercompetition			FBgn0036600	FBtr0075434	16305225	16305978			72	CG13043
1	Supercompetition			FBgn0036601	FBtr0075366	16306600	16307305			72	CG13063
1	Supercompetition			FBgn0036602	FBtr0075433	16307846	16308485			72	CG13042
1	Supercompetition			FBgn0052160	FBtr0308930	16308940	16311318	long non-coding RNA:CR32160		72	lncRNA:CR32160
1	Supercompetition			FBgn0036603	FBtr0333000	16314285	16315149			72	CG13062
1	Supercompetition			FBgn0042301	FBtr0075369	16318524	16319868	Neuropeptide-like precursor 3		72	Nplp3
1	Supercompetition			FBgn0267223	FBtr0346365	16318941	16319083	antisense RNA:CR45863		72	asRNA:CR45863
1	Supercompetition			FBgn0036605	FBtr0075432	16318954	16319526			72	CG13041
1	Supercompetition			FBgn0267224	FBtr0346396	16319440	16319931	long non-coding RNA:CR45864		72	lncRNA:CR45864
1	Supercompetition			FBgn0036606	FBtr0075370	16319856	16320454			72	CG13060
1	Supercompetition			FBgn0261635	FBtr0303001	16320830	16321272			72	CG42718
1	Supercompetition			FBgn0036607	FBtr0075371	16322672	16324308			72	CG13059
1	Supercompetition			FBgn0036608	FBtr0310461	16325083	16326757			72	CG13040
1	Supercompetition			FBgn0036609	FBtr0075430	16326057	16326762			72	CG13039
1	Supercompetition			FBgn0040795	FBtr0075429	16327258	16327893			72	CG13038
1	Supercompetition			FBgn0036610	FBtr0075372	16328941	16329534			72	CG13058
1	Supercompetition			FBgn0053261	FBtr0113448	16329766	16331027			72	CG33061
1	Supercompetition			FBgn0053060	FBtr0305307	16331040	16331767			72	CG33060
1	Supercompetition			FBgn0040074	FBtr0075375	16331933	16332789	netrin		72	netrin
1	Supercompetition			FBgn0040794	FBtr0075376	16333313	16333782			72	CG13056
1	Supercompetition			FBgn0036612	FBtr0110866	16339003	16345241			72	CG4698
1	Supercompetition			FBgn0267553	FBtr0346928	16341188	16345241	long non-coding RNA:CR45893		72	lncRNA:CR45893
1	Supercompetition			FBgn0053257	FBtr0075378	16346323	16347620			72	mt:CR32257
1	Supercompetition			FBgn0285951	FBtr0075379	16348074	16348782	mitochondrial ribosomal protein S34		72	mRpS34
1	Supercompetition			FBgn0036614	FBtr0075428	16348747	16351951	Golgin 104		72	Golgin104
1	Supercompetition			FBgn0052357	FBtr0075380	16349917	16349988	transfer RNA:Methionine-CAT:1-4		72	tRNA:Met-CAT:1-4
1	Supercompetition			FBgn0263681	FBtr0075381	16351991	16353286	Tcs3		72	Tcs3
1	Supercompetition			FBgn0011693	FBtr0114536	16353233	16354297	Photoreceptor dehydrogenase		72	Pdh
1	Supercompetition			FBgn0267554	FBtr0346925	16353498	16353916	antisense RNA:CR45894		72	asRNA:CR45894
1	Supercompetition			FBgn0286417	FBtr0344398	16354746	16359428	ringmaker		72	ringer
1	Supercompetition			FBgn0036617	FBtr0075382	16362603	16363758	Cuticular protein 72Ea		72	Cpr72Ea
1	Supercompetition			FBgn0036618	FBtr0075383	16364884	16365707	Cuticular protein 72Eb		72	Cpr72Eb
1	Supercompetition			FBgn0036619	FBtr0075424	16365894	16367340	Cuticular protein 72Ec		72	Cpr72Ec
1	Supercompetition			FBgn0036620	FBtr0075384	16368389	16369518			72	CG4842
1	Supercompetition			FBgn0042137	FBtr0307504	16369626	16370945			72	CG16814
1	Supercompetition			FBgn0036621	FBtr0333385	16370938	16375999	roquin		72	req
1	Supercompetition			FBgn0036622	FBtr0331172	16378974	16381570	acyltransferase 4		72	Agpat4
1	Supercompetition			FBgn0036623	FBtr0075417	16381772	16385957	acyltransferase 3		72	Agpat3
1	Supercompetition			FBgn0036624	FBtr0333596	16386327	16390816	RING-associated factor 2		72	RAF2
1	Supercompetition			FBgn0286099	FBtr0343550	16390952	16400275			72	CG44836
1	Supercompetition			FBgn0036627	FBtr0343534	16394589	16398880	Gag-related		72	Gagr
1	Supercompetition			FBgn0014163	FBtr0100477	16402796	16411828	failed axon connections		72	fax
1	Supercompetition			FBgn0028399	FBtr0310552	16412722	16415386	TMS1		72	TMS1
1	Supercompetition			FBgn0036629	FBtr0075411	16415292	16417177	mitochondrial		72	SlvRS-m
1	Supercompetition			FBgn0027080	FBtr0075410	16417349	16419302	Tyrosyl-tRNA synthetase		72	TyrRS
1	Supercompetition			FBgn0053158	FBtr0075390	16419597	16496950			72	CG33158
1	Supercompetition			FBgn0261799	FBtr0075409	16422795	16451958	doublesex cognate 73A		73	dsx-c73A
1	Supercompetition			FBs0020123	FBst0020123-RA	16443902	16446186			72	
1	Supercompetition			FBgn0004569	FBtr0075408	16470388	16483650	argos		73	aos
1	Supercompetition			FBgn0263388	FBtr0300655	16491838	16496236			73	CG42514
1	Supercompetition			FBgn0263131	FBtr0307368	16491839	16543370			73	CG43373
1	Supercompetition			FBs0020124	FBst0020124-RA	16494049	16494489			73	
1	Supercompetition			FBgn0003515	FBtr0075391	16497651	16500466	scarlet		73	st
1	Supercompetition			FBs0020125	FBst0020125-RA	16523336	16528459			73	
1	Supercompetition			FBgn0036638	FBtr0075400	16544567	16545628			73	CG13033
			73				16549092		73A5		
1			73				16549092		73A5		
1				FBgn0036639	FBtr0075392	16556823	16557358			73	CG4229
1				FBgn0036361	FBtr0075398	16563446	16573334	phosphatase 1		73	Mpp1
1				FBgn0262842	FBtr0306084	16566750	16567300			73	CG43206
1				FBgn0262732	FBtr0330137	16574436	16576871	multiprotein bridging factor 1		73	mbf1
1				FBgn0036640	FBtr0331561	16576859	16580306	nuclear RNA export factor 2		73	nxf2
1				FBs0061962	FBst0061962-RA	16576994	16577893			73	
1				FBgn0036641	FBtr0075395	16580398	16581547	survival motor neuron		73	Smn
1				FBgn0263975	FBtr0347098	16581637	16582767			73	CR43727
1				FBgn0028693	FBtr0075308	16583028	16584022	Regulatory particle non-ATPase 12		73	Rpn12
1				FBgn0259814	FBtr0331557	16584124	16586111	core protein 2		73	IJQCR-C2
1				FBgn0036643	FBtr0075385	16586108	16587057	Syntaxin 8		73	Syx8
1				FBgn0267555	FBtr0346363	16587111	16587922	antisense RNA:CR45895		73	asRNA:CR45895
1				FBgn0052163	FBtr0344805	16587157	16588143			73	CG32163
1				FBgn0002283	FBtr0075311	16588475	16590132	lethal (3) 73Ah		73	l(3)73Ah
1				FBgn0003741	FBtr0100244	16590059	16591050	transformer		73	tra
1				FBgn0027500	FBtr0075363	16591207	16595014	spindle defective 2		73	spd-2
1				FBgn0042178	FBtr0075312	16595181	16602459	Apollo		73	Apl
1				FBgn0036646	FBtr0301925	16600448	16602723			73	CR18217
1				FBgn0042177	FBtr0331559	16603053	16608146	Artemis		73	Arts
1		125965				16605347			73B1		
1				FBgn0036648	FBtr0075361	16608138	16609347			73	CG4098
1				FBgn0002384	FBtr0075360	16609409	16610418	Proteasome beta5 subunit		73	Prosbeta5
1				FBgn0004465	FBtr0075359	16610662	16612199	Suppressor of net(2)P sterility		73	Su(P)
1				FBgn0025558	FBtr0075314	16612486	16612955			73	CG4101
1				FBgn0267525	FBtr0346913	16612500	16612827	antisense RNA:CR45865		73	asRNA:CR45865
1				FBgn0017572	FBtr0331560	16613218	16615472	Mo25		73	Mo25
1				FBgn0000017	FBtr0330132	16615988	16647862	Abl tyrosine kinase		73	Abl
1				FBs0020126	FBst0020126-RA	16616565	16621835			73	
1				FBgn0260960	FBtr0075356	16648442	16661615	Baldspot		73	Baldspot
1				FBgn0041721	FBtr0075315	16653769	16654006	small nuclear RNA U12		73	snRNA:U12
1				FBgn0010223	FBtr0075354	16662557	16667694	G protein alpha f subunit		73	Galphaf
1				FBgn0267697	FBtr0346207	16663928	16664013	antisense RNA:CR46033		73	asRNA:CR46033
1				FBgn0266776	FBtr0345401	16670355	16670741	long non-coding RNA:CR45241		73	lncRNA:CR45241
1				FBgn0040512	FBtr0075353	16671664	16673555	Coat Protein (coatomer) zeta		73	zetaCOP
1				FBgn0036652	FBtr0075316	16673964	16676264			73	CG13032
1				FBgn0083485	FBtr0306152	16676406	16711677	Lasp		73	Lasp
1				FBgn0284605	FBtr0333628	16676408	16711677			73	CG43954
1				FBs0020127	FBst0020127-RA	16684075	16685237			73	
1				FBgn0266689	FBtr0345057	16685268	16697897	long non-coding RNA:CR45179		73	lncRNA:CR45179
1				FBgn0267557	FBtr0346964	16700829	16701468	long non-coding RNA:CR45897		73	lncRNA:CR45897
1				FBgn0036654	FBtr0075317	16704973	16706428			73	CG9692
1				FBgn0000414	FBtr0330189	16721238	16724273	Disabled		73	Dab
1				FBgn0036656	FBtr0299542	16724678	16726169			73	CG13026
1				FBgn0036655	FBtr0075319	16724861	16725375			73	CG13031
1				FBgn0043577	FBtr0075320	16726541	16727288	SB2		73	PGRP-SB2

1				FBgn0043578	FBtr0075348	16727269	16727989	SB1	73	PGRP-SB1
1				FBgn0004556	FBtr0075347	16728496	16730818	Dead box protein 73D	73	Dbp73D
1				FBti0020128	FBtr0020128-RA	16730986	16731111		73	
1				FBgn0036859	FBtr0075331	16733546	16735364		73	CG9701
1				FBgn0262099	FBtr0304017	16755489	16755720		73	CG42852
1				FBgn0267904	FBtr0347509	16759393	16762883	long non-coding RNA:CR46214	73	lncRNA:CR46214
1				FBgn0004108	FBtr0304018	16766072	16777465	Neurotactin	73	Nrt
1				FBgn0036860	FBtr0075346	16776531	16779736		73	CG13935
1				FBgn0036861	FBtr0333607	16780100	16782419		73	CG9705
1				FBgn0036862	FBtr0075327	16783010	16785246		73	CG9706
1				FBgn0025582	FBtr0075345	16785242	16786941	3 subunit e	73	eIF3e
1				FBgn0036863	FBtr0333608	16787573	16807731		73	CG9674
1	123095					16800857			73D1	
1				FBgn0021768	FBtr0075328	16804994	16819332	nudC	73	nudC
1				FBgn0036865	FBtr0273320	16805658	16823074		73	CG13934
1				FBgn0036866	FBtr0075329	16842294	16844585	Tumor susceptibility gene 101	73	TSG101
1				FBgn0036867	FBtr0305272	16844568	16844991	kuduk	73	kud
1				FBgn0036868	FBtr0075330	16845386	16852350	Zinc finger CCHC-type containing 7	73	Zcchc7
1				FBgn0052161	FBtr0075331	16846227	16847000		73	CG32161
1				FBgn0003250	FBtr0075338	16852527	16852517	Rhodopsin 4	73	Rh4
1				FBgn0003410	FBtr0075332	16853751	16858712	seven in absentia	73	sina
1				FBgn0259794	FBtr0301683	16859080	16860526	sina homologue	73	sinah
1				FBgn0036870	FBtr0332702	16860622	16861838		73	CG13929
1				FBgn0036871	FBtr0075337	16863164	16864869		73	CG9951
1				FBgn0261565	FBtr0330704	16865295	16922467	Limpet	73	Lmpt
1				FBgn0052170	FBtr0075258	16877309	16879372		73	CG32170
1				FBgn0267558	FBtr0346966	16882191	16882539	long non-coding RNA:CR45898	73	lncRNA:CR45898
1				FBgn0036876	FBtr0075261	16922252	16923994		73	CG13928
1				FBgn0036877	FBtr0075267	16925914	16927434		73	CG13923
1				FBgn0036878	FBtr0113173	16928381	16935536		73	CG11905
1				FBgn0036879	FBtr0273313	16938330	16938952		73	CG13922
1				FBgn0036880	FBtr0347065	16939100	16957689	Cuticular protein 73D	73	Cpr73D
1				FBgn0036881	FBtr0113177	16944361	16954942	Odorant-binding protein 73a	73	Obp73a
1				FBti0020129	FBtr0020129-RA	16945783	16954877		73	
1				FBgn0010352	FBtr0075264	16954522	16968724	Neural conserved at 73EF	73	Nc73EF
1				FBgn0261547	FBtr0302651	16970013	16994388	Ephexin	73	Exn
1				FBgn0036884	FBtr0332122	16994717	17012565		73	CG3764
1				FBgn0262189	FBtr0304207	16998457	16998524	mir-2500 stem loop	73	mir-2500
1				FBtr0304209_df_rng	FBtr0304209	16998458	16998479		73	
1				FBtr0304208_df_rng	FBtr0304208	16998500	16998524		73	
1				FBti0061973	FBtr0061973-RA	16999637	16999862		73	
1				FBgn0036885	FBtr0075294	17012886	17016180		73	CG6864
1				FBgn0036886	FBtr0075274	17016536	17020270		73	CG7728
1				FBgn0036887	FBtr0075291	17020348	17022856		73	CG6852
1				FBgn0051293	FBtr0075290	17021125	17023741	antennal protein 10	73	a10
1				FBgn0036888	FBtr0075275	17024328	17027117	Fermitin 2	73	Fit2
1				FBgn0036889	FBtr0089584	17027515	17029814		73	CG7730
1				FBgn0036890	FBtr0290221	17029812	17033080	Insulin-like peptide 8	73	Ilp8
1				FBgn0267320	FBtr0346802	17032055	17033828	long non-coding RNA:CR45756	73	lncRNA:CR45756
1				FBgn0262895	FBtr0344440	17033119	17033676	long non-coding RNA:CR43250	73	lncRNA:CR43250
1				FBti0020130	FBtr0020130-RA	17034996	17035119		73	
1				FBgn0036891	FBtr0075278	17035668	17036865	bad egg	73	beg
1				FBgn0261872	FBtr0345067	17038859	17042574	SR-related CTD associated factor 6	73	scaf6
1	126291					17042518			73E5	
1				FBgn0036895	FBtr0075279	17042797	17044465	PAPS transporter 2	73	Papst2
1				FBgn0036896	FBtr0300718	17044401	17045038	POPS ribonuclease P/MRP subunit	73	Pop5
1				FBgn0010424	FBtr0089585	17046063	17048390	Troponin C at 73F	73	TpnC73F
1				FBgn0036897	FBtr0075282	17049512	17055454	rogdi	73	rogdi
1				FBgn0036898	FBtr0075284	17055613	17058533		73	CG7724
1				FBgn0260943	FBtr0113427	17058774	17238212	RNA-binding protein 6	74	Rbp6
1				FBti0020131	FBtr0020131-RA	17085060	17094152		73	
1				FBgn0263381	FBtr0300067	17166863	17167542	antisense RNA:CR43433	73	asRNA:CR43433
1				FBgn0036702	FBtr0075252	17238613	17242128		74	CG6512
1				FBti0062030	FBtr0062030-RA	17242604	17243176		74	
1				FBgn0036703	FBtr0075212	17244384	17244746		74	CG7707
1				FBti0062031	FBtr0062031-RA	17245042	17245738		74	
1				FBgn0264462	FBtr0332783	17245882	17264290	long non-coding RNA:CR43870	74	lncRNA:CR43870
1				FBti0062025	FBtr0062025-RA	17246300	17246402		74	
1				FBti0062032	FBtr0062032-RA	17247216	17247338		74	
1				FBgn0036704	FBtr0332785	17252377	17253937		74	CG6497
1				FBgn0264466	FBtr0332784	17259661	17260449	long non-coding RNA:CR43874	74	lncRNA:CR43874
1				FBgn0036705	FBtr0075213	17264416	17264986		74	CG13723
1				FBgn0266985	FBtr0345887	17275050	17275549	long non-coding RNA:CR45436	74	lncRNA:CR45436
1				FBgn0262376	FBtr0304210	17315006	17315105	mir-219 stem loop	74	mir-219
1				FBtr0304211_df_rng	FBtr0304211	17315024	17315044		74	
1				FBtr0472720_df_rng	FBtr0472720	17315064	17315085		74	
1				FBgn0036706	FBtr0075249	17319969	17320811	24 kDa subunit-like	74	ND-24L
1				FBgn0036707	FBtr0075214	17322841	17324463		74	CG13724
1				FBgn0036708	FBtr0075248	17324618	17325518		74	CG13725
1				FBgn0036709	FBtr0075247	17327733	17329169	Odorant receptor 74a	74	Or74a
1				FBgn0265756	FBtr0340718	17334006	17334469	long non-coding RNA:CR44563	74	lncRNA:CR44563
1				FBgn0265757	FBtr0340719	17335921	17337097	long non-coding RNA:CR44564	74	lncRNA:CR44564
1				FBgn0036710	FBtr0331847	17337172	17339262		74	CG6479
1				FBgn0052173	FBtr0075244	17339909	17339980	transfer RNA:Proline-CGG 2-2	74	tRNA:Pro-CGG-2-2
1				FBgn0036711	FBtr0075243	17340279	17341356		74	CG10727
1				FBgn0036712	FBtr0331846	17342050	17344666	brivido-2	74	biv2
1				FBgn0036713	FBtr0075241	17344947	17349988	Myoinhibiting peptide precursor	74	Mip
1				FBgn0036714	FBtr0344911	17351822	17358056		74	CG7692
1				FBgn0015550	FBtr0075216	17356982	17361811	target of Poxn	74	tap
1				FBgn0267248	FBtr0346435	17362775	17367365	long non-coding RNA:CR45988	74	lncRNA:CR45988
1				FBgn0036715	FBtr0075259	17367753	17379530	Cadherin 74A	74	Cad74A
1				FBgn0036716	FBtr0075238	17380026	17382728		74	CG13728
1				FBgn0036717	FBtr0300800	17383636	17388956		74	CG13731
1				FBgn0027660	FBtr0336898	17399031	17421514	bloated tubules	74	blot
1				FBgn0026197	FBtr0345670	17400272	17401348	long non-coding RNA:noe	74	lncRNA:noe
1				FBgn0266669	FBtr0075231	17421787	17425217	Secretory 3	74	Sec3
1				FBgn0040793	FBtr0075217	17425477	17426282		74	CG7630
1				FBgn0053051	FBtr0075230	17426286	17427130		74	CG33051
1				FBgn0053052	FBtr0075229	17427305	17428936	Golgin, RAB6 interacting	74	Gorab
1				FBgn0042941	FBtr0075228	17428938	17433160	Fringe connection	74	fnc
1				FBgn0052174	FBtr0075227	17428936	17433921	Coenzyme Q4	74	Coq4
1				FBgn0052176	FBtr0075218	17433868	17437971		74	CG32176
1				FBgn0036723	FBtr0075226	17434472	17436431		74	CG12229
1				FBgn0036725	FBtr0333689	17439401	17457461		74	CG16265
1				FBgn0265758	FBtr0340720	17460139	17460498	long non-coding RNA:CR44565	74	lncRNA:CR44565
1				FBgn0036726	FBtr0075220	17465945	17466768	QIL1	74	QIL1
1				FBgn0036727	FBtr0075221	17470127	17474517	Secretory chloride channel	74	SecCl
1				FBgn0036728	FBtr0302509	17474761	17476124	ubiquinone-binding protein	74	UQCR-Q
1				FBgn0085279	FBtr0346594	17476222	17477103		74	CG34250
1				FBgn0036729	FBtr0075225	17477796	17478926		74	CG10733
1				FBgn0036730	FBtr0075223	17479096	17480141	quijote	74	qjt
1				FBgn0036731	FBtr0302208	17480129	17486230		74	CG6333
1				FBgn0036732	FBtr0302041	17487118	17511693	polypeptide 74D	74	Dalp74D
1				FBgn0052185	FBtr0075174	17494880	17495300	elevated during infaction	74	edin
1				FBgn0036733	FBtr0075269	17511852	17513952	factor 60K	74	4-4-U6-60K
1				FBgn0036734	FBtr0344941	17514298	17524740		74	CG7564
1				FBti0020132	FBtr0020132-RA	17517035	17524535		74	
1				FBgn0036735	FBtr0075208	17525333	17529861	Enhancer of decapping 3	74	Edc3
1				FBgn0263478	FBtr0300777	17528700	17528840		74	snoRNA:Edc3-a
1				FBgn0268675	FBtr0345940	17528888	17530302	long non-coding RNA:CR45165	74	lncRNA:CR45165
1				FBgn0259174	FBtr0331844	17530081	17546660	Nedd4	74	Nedd4
1				FBgn0023197	FBtr0473621	17548077	17549127	Jonah 74E	74	Jon74E
1				FBgn0036738	FBtr0075181	17549826	17550980		74	CG7542
1				FBgn0025455	FBtr0075205	17551004	17557788	Cyclin T	74	CycT
1				FBgn0000567	FBtr0035796	17558672	17619325	Ecdysone-induced protein 74EF	74	Eip74EF
1				FBgn0086080	FBtr0114356	17566042	17566162		74	snoRNA:Mo28S-A576
1				FBgn0036740	FBtr0333123	17620123	17621625	Vacuolar protein sorting 60	74	Vps60
1				FBgn0036741	FBtr0333121	17621824	17630971	anchor	74	anchor
1				FBgn0261454	FBtr0330755	17628057	17628203	MeU4-A85	74	scaRNA:MeU4-A85
1				FBgn0265759	FBtr0340721	17631398	17633253	long non-coding RNA:CR44566	74	lncRNA:CR44566
1				FBgn0265760	FBtr0340722	17633040	17633317	long non-coding RNA:CR44567	74	lncRNA:CR44567
1				FBgn0036742	FBtr0345385	17633449	17638001		74	CG7497
1				FBgn0004401	FBtr0075198	17638103	17645036	Protein on ecdysone puffs	74	Pep
1				FBgn0262531	FBtr0333122	17645486	17646737		74	CG43085

1				FBgn0052177	FBtr0075210	17647442	17654285	Nedd4 family interacting protein		74	Ndfip
1				FBgn0052179	FBtr0075197	17649563	17654283	Keren		74	Krn
1				FBgn0036745	FBtr0075184	17654617	17655945			74	CG7484
1				FBgn0036746	FBtr0345384	17659818	17665234	coactivator		74	Crtc
1				FBgn0065088	FBtr0091663	17668588	17668730	small non-messenger RNA 641		74	smnRNA:641
1				FBgn0085280	FBtr0301012	17671622	17683581			74	CG34251
1				FBgn0052183	FBtr0075186	17680015	17748839	Ccn		74	Ccn
1				FBgn0267638	FBtr0347093	17696391	17696967	long non-coding RNA:CR45976		74	lncRNA:CR45976
1				FBgn0020133	FBtr0020133-RA	17698327	17698838			74	
1				FBgn0062044	FBtr0062044-RA	17700473	17700518			74	
1				FBgn0261294	FBtr0091928	17719193	17719854	Chemosensory protein B 74a		74	CheB74a
1				FBgn0036747	FBtr0076912	17723713	17723378			74	CG6552
1				FBgn0020134	FBtr0020134-RA	17730906	17731510			74	
1				FBgn0059671	FBtr0059671-RA	17730906	17738178			74	
1				FBgn0059672	FBtr0059672-RA	17731511	17737054			74	
1				FBgn0020136	FBtr0020136-RA	17737055	17738178			74	
1				FBgn0036749	FBtr0075187	17740546	17740540			74	CG7460
1				FBgn0036750	FBtr0075194	17745173	17746860			75	CG6034
1				FBgn0036751	FBtr0075193	17748833	17750588	growth factor B		75	Adgf-B
1				FBgn0036752	FBtr0075191	17751731	17764158	growth factor A		75	Adgf-A
1				FBgn0043025	FBtr0110846	17754936	17764158	growth factor A2		75	Adgf-A2
1				FBgn0052182	FBtr0075188	17759113	17759503			75	CG32182
1				FBgn0052181	FBtr0301018	17759697	17762904			75	CG32181
1			75A			17779154			75A1		
1			75A			17779154			75A1		
1				FBgn0265879	FBtr0342747	17784788	17785284	long non-coding RNA:CR44668		75	lncRNA:CR44668
1				FBgn0261997	FBtr0303827	17791079	17791498			75	CG42815
1				FBgn0261998	FBtr0303890	17792088	17793794			75	CG42816
1				FBgn0052190	FBtr0075171	17797739	17802279	NUCB1		75	NUCB1
1				FBgn0020137	FBtr0020137-RA	17799864	17801595			75	
1				FBgn0036754	FBtr0075170	17802490	17804715			75	CG5589
1				FBgn0052187	FBtr0075169	17804916	17806365			75	CG32187
1				FBgn0052191	FBtr0307509	17808451	17809148			75	CG32191
1				FBgn0036756	FBtr0333693	17809231	17814119	Cln3		75	Cln3
1				FBgn0036757	FBtr0273392	17815570	17817921	ionotropic receptor 75a		75	ir75a
1				FBgn0261402	FBtr0302293	17818073	17820193	ionotropic receptor 75b		75	ir75b
1				FBgn0261401	FBtr0302292	17820493	17823834	ionotropic receptor 75c		75	ir75c
1				FBgn0001134	FBtr0075139	17823333	17833767	Glycine receptor		75	Grd
1				FBgn0052188	FBtr0075164	17833277	17833625			75	CG32188
1				FBgn0062554	FBtr0062554-RA	17834612	17834730			75	
1				FBgn0052189	FBtr0075163	17834745	17835174			75	CG32189
1				FBgn0062556	FBtr0062556-RA	17835839	17836181			75	
1				FBgn0036759	FBtr0075162	17836650	17841427			75	CG5577
1				FBgn0036760	FBtr0075161	17841540	17843544			75	CG5567
1				FBgn0266885	FBtr0345052	17841671	17842599	antisense RNA:CR45175		75	asRNA:CR45175
1				FBgn0036761	FBtr0075160	17843725	17846501	Mediator complex subunit 19		75	MED19
1				FBgn0036762	FBtr0331810	17846916	17849601			75	CG7430
1				FBgn0036763	FBtr0331811	17849727	17852453	mitochondrial		75	TrpRS-m
1		124168				17859477			75A4		
1		126206				17859544			74A4		
3	Lethal cell competition			FBgn0036764	FBtr0273277	17852624	17856794			75	CG5535
3	Lethal cell competition			FBgn0054002	FBtr0302155	17859474	17860452			75	CG34002
3	Lethal cell competition			FBgn0062567	FBtr0062567-RA	17858895	17859394			75	
3	Lethal cell competition			FBgn0020138	FBtr0020138-RA	17860914	17861259			75	
3	Lethal cell competition			FBgn0062568	FBtr0062568-RA	17861289	17861333			75	
3	Lethal cell competition			FBgn0062600	FBtr0062600-RA	17861744	17861810			75	
3	Lethal cell competition			FBgn0020139	FBtr0020139-RA	17861829	17863485			75	
3	Lethal cell competition			FBgn0020140	FBtr0020140-RA	17863843	17866557			75	
3	Lethal cell competition			FBgn0262532	FBtr0304978	17868740	17870573			75	CR43086
3	Lethal cell competition			FBgn0062569	FBtr0062569-RA	17868141	17869603			75	
3	Lethal cell competition			FBgn0020143	FBtr0020143-RA	17871251	17874018			75	
3	Lethal cell competition			FBgn0020141	FBtr0020141-RA	17871336	17873086			75	
3	Lethal cell competition			FBgn0020142	FBtr0020142-RA	17872681	17873086			75	
3	Lethal cell competition			FBgn0262533	FBtr0304979	17874715	17876573			75	CR43087
3	Lethal cell competition			FBgn0062570	FBtr0062570-RA	17875116	17875615			75	
3	Lethal cell competition			FBgn0036765	FBtr0300281	17879096	17883653			75	CG7408
3	Lethal cell competition			FBgn0036766	FBtr0075157	17883649	17884376			75	CG5506
3	Lethal cell competition			FBgn0260721	FBtr0475316	17885254	17885528			75	CR42548
3	Lethal cell competition			FBgn0062572	FBtr0062572-RA	17885580	17885754			75	
3	Lethal cell competition			FBgn0036767	FBtr0290028	17885948	17886945			75	CG16775
3	Lethal cell competition			FBgn0036768	FBtr0075143	17887705	17891404			75	CG7402
3	Lethal cell competition			FBgn0036769	FBtr0075155	17891820	17895862	Tetraspanin 74F		75	Tsp74F
3	Lethal cell competition			FBgn0036770	FBtr0075153	17898889	17907812	Prestin		75	Prestin
3	Lethal cell competition			FBgn0036771	FBtr0075144	17908143	17909983	WD repeat domain 92		75	Wdr92
3	Lethal cell competition			FBgn0036772	FBtr0075152	17909483	17912955			75	CG5290
3	Lethal cell competition			FBgn0062625	FBtr0062625-RA	17916868	17916938			75	
3	Lethal cell competition			FBgn0020144	FBtr0020144-RA	17918427	17921174			75	
3	Lethal cell competition			FBgn0267794	FBtr0347291	17934032	17946114	long non-coding RNA:CR43174		75	lncRNA:CR43174
3	Lethal cell competition			FBgn0266942	FBtr0345835	17947192	17947700	long non-coding RNA:CR45393		75	lncRNA:CR45393
3	Lethal cell competition			FBgn0003568	FBtr0075149	17950953	18004668	Ecdysone-induced protein 75B		75	Eip75B
3	Lethal cell competition			FBgn0267581	FBtr0346907	17981321	17981841	long non-coding RNA:CR45921		75	lncRNA:CR45921
3	Lethal cell competition			FBgn0080081	FBtr0114357	18002978	18003078			75	snoRNA:Me28S-A30
3	Lethal cell competition			FBgn0267582	FBtr0346996	18037723	18038280	long non-coding RNA:CR45922		75	lncRNA:CR45922
3	Lethal cell competition			FBgn0052192	FBtr0300047	18040317	18041738			75	CG32192
3	Lethal cell competition			FBgn0259739	FBtr0300044	18042733	18044214			75	CG42593
3	Lethal cell competition			FBgn0020145	FBtr0020145-RA	18047763	18050761			75	
3	Lethal cell competition			FBgn0264748	FBtr0334132	18068728	18070150			75	CG44006
3	Lethal cell competition			FBgn0264747	FBtr0334130	18070300	18072123			75	CG44005
3	Lethal cell competition			FBgn0264746	FBtr0344997	18072362	18073863			75	CG44004
3	Lethal cell competition			FBgn0266940	FBtr0345834	18074504	18075084			75	CR45391
3	Lethal cell competition			FBgn0266941	FBtr0345833	18077581	18078103	long non-coding RNA:CR45392		75	lncRNA:CR45392
3	Lethal cell competition			FBgn0262898	FBtr0344581	18081121	18085310	long non-coding RNA:CR43253		75	lncRNA:CR43253
3	Lethal cell competition			FBgn0052194	FBtr0306733	18085305	18087058	long non-coding RNA:CR32194		75	lncRNA:CR32194
3	Lethal cell competition			FBgn0085282	FBtr0112447	18086674	18087320			75	CG34253
3	Lethal cell competition			FBgn0062626	FBtr0062626-RA	18087746	18088077			75	
3	Lethal cell competition			FBgn0036773	FBtr0333868	18088417	18106149			75	CG13698
3	Lethal cell competition			FBgn0036774	FBtr0075121	18100579	18107469	mitochondrial ribosomal protein S26		75	mRpS26
3	Lethal cell competition			FBgn0036775	FBtr0075136	18107846	18108574	RNA polymerase III subunit C53		75	RpIIIC53
3	Lethal cell competition			FBgn0002901	FBtr0075122	18108814	18112847	mutagen-sensitive 304		75	mus304
3	Lethal cell competition			FBgn0052195	FBtr0075125	18112959	18119150			75	CG32195
3	Lethal cell competition			FBgn0036777	FBtr0075124	18112959	18121003			75	CG7341
3	Lethal cell competition			FBgn0262100	FBtr0304019	18120932	18121989			75	CG42853
3	Lethal cell competition			FBgn0062643	FBtr0062643-RA	18122109	18122245			75	
3	Lethal cell competition			FBgn0036778	FBtr0075135	18128940	18132889	Cyp312a1		75	Cyp312a1
3	Lethal cell competition			FBgn0265880	FBtr0342748	18135786	18136231	long non-coding RNA:CR44669		75	lncRNA:CR44669
3	Lethal cell competition			FBgn0020300	FBtr0075126	18139402	18145418	geiko		75	geiko
3	Lethal cell competition			FBgn0036780	FBtr0332861	18148923	18153807			75	CG7330
3	Lethal cell competition			FBgn0036781	FBtr0075134	18154807	18163522			75	CG13699
3	Lethal cell competition			FBgn0003997	FBtr0075133	18167745	18185941	head involution defective		75	hid
3	Lethal cell competition			FBgn0020146	FBtr0020146-RA	18189644	18190189			75	
3	Lethal cell competition			FBgn0266769	FBtr0345394	18196172	18196932	long non-coding RNA:CR45234		75	lncRNA:CR45234
3	Lethal cell competition			FBgn0036782	FBtr0310156	18201494	18203637			75	CG7320
3	Lethal cell competition			FBgn0267597	FBtr0347042	18230329	18231056	long non-coding RNA:CR45935		75	lncRNA:CR45935
3	Lethal cell competition			FBgn0267599	FBtr0347044	18234246	18234760	long non-coding RNA:CR45937		75	lncRNA:CR45937
3	Lethal cell competition			FBgn0267598	FBtr0347043	18243700	18244239	long non-coding RNA:CR45936		75	lncRNA:CR45936
3	Lethal cell competition			FBgn0036783	FBtr0075129	18252088	18252846	Chemosensory protein A 75a		75	CheA75a
3	Lethal cell competition			FBgn0036784	FBtr0075132	18292125	18294262			75	CG5103
3	Lethal cell competition			FBgn0262898	FBtr0336840	18294604	18295800	long non-coding RNA:CR43306		75	lncRNA:CR43306
3	Lethal cell competition			FBgn0036785	FBtr0332865	18298742	18301260			75	CG13700
3	Lethal cell competition			FBgn0015946	FBtr0075130	18302719	18304417	grim		75	grim
3	Lethal cell competition			FBgn0267637	FBtr0347092	18303241	18303341	long non-coding RNA:CR45975		75	lncRNA:CR45975
3	Lethal cell competition			FBgn0267636	FBtr0347091	18303431	18304179	antisense RNA:CR45974		75	asRNA:CR45974
3	Lethal cell competition			FBgn0266033	FBtr0473373	18323584	18323985	long non-coding RNA:CR46353		75	lncRNA:CR46353
3	Lethal cell competition			FBgn0011706	FBtr0075120	18397535	18398435	reaper		75	rpr
3	Lethal cell competition			FBgn0267605	FBtr0347510	18428524	18429255	long non-coding RNA:CR46215		75	lncRNA:CR46215
3	Lethal cell competition			FBgn0036786	FBtr0075119	18438561	18439942	sickle		75	sid
3	Lethal cell competition			FBgn0262969	FBtr0336721	18440730	18441871	long non-coding RNA:CR43280		75	lncRNA:CR43280
3	Lethal cell competition			FBgn0265881	FBtr0342750	18456399	18458800	long non-coding RNA:CR44670		75	lncRNA:CR44670
3	Lethal cell competition			FBgn0265882	FBtr0342749	18457201	18457550	long non-coding RNA:CR44671		75	lncRNA:CR44671
3	Lethal cell competition			FBgn0052196	FBtr0332868	18459464	18461024			75	CG32196
3	Lethal cell competition			FBgn0036787	FBtr0075117	18461957	18463163			75	CG4306
3	Lethal cell competition			FBgn0062659	FBtr0062659-RA	18463700	18464102			75	
3	Lethal cell competition			FBgn0028415	FBtr0075116	18466378	18468618	Mal75Cb		75	Mal75Cb

3	Lethal cell competition			FBti0020147	FBtr0020147-RA	18469825	18471291			75	
3	Lethal cell competition			FBgn0028416	FBtr0075115	18472143	18472384	Mef75Ca		75	Mef75Ca
3	Lethal cell competition			FBgn0265883	FBtr0342751	18475296	18475979	long non-coding RNA:CR44672		75	lncRNA:CR44672
3	Lethal cell competition			FBti0062663	FBtr0362663-RA	18475837	18475939			75	
3	Lethal cell competition			FBgn0265884	FBtr0342752	18478822	18479223	long non-coding RNA:CR44673		75	lncRNA:CR44673
3	Lethal cell competition			FBgn0036789	FBtr0330088	18485137	18502557	Allatostatin C receptor 2		75	AstC-R2
3	Lethal cell competition			FBti0020148	FBtr0020148-RA	18506186	18509586			75	
3	Lethal cell competition			FBti0020149	FBtr0020149-RA	18514973	18520360			75	
3	Lethal cell competition			FBgn0052198	FBtr0075090	18526976	18527445			75	CG32198
3	Lethal cell competition			FBti0020150	FBtr0020150-RA	18528683	18537785			75	
3	Lethal cell competition			FBgn0036790	FBtr0089578	18560258	18576326	Allatostatin C receptor 1		75	AstC-R1
3	Lethal cell competition			FBti0062665	FBtr0362665-RA	18567881	18568037			75	
3	Lethal cell competition			FBgn0265884	FBtr0345886	18583437	18584235	long non-coding RNA:CR45435		75	lncRNA:CR45435
3	Lethal cell competition			FBgn0036791	FBtr0075101	18588759	18590165			75	CG7271
3	Lethal cell competition			FBti0020151	FBtr0020151-RA	18590703	18591377			75	
3	Lethal cell competition			FBgn0003683	FBtr0075112	18592303	18593771	terminus		75	term
3	Lethal cell competition			FBti0020152	FBtr0020152-RA	18594004	18595923			75	
3	Lethal cell competition			FBgn0265938	FBtr0345831	18598322	18598762	long non-coding RNA:CR45389		75	lncRNA:CR45389
3	Lethal cell competition			FBgn0265939	FBtr0345832	18597995	18598420	long non-coding RNA:CR45390		75	lncRNA:CR45390
3	Lethal cell competition			FBgn0036799	FBtr0100555	18600150	18617943			75	CG13380
3	Lethal cell competition			FBgn0036793	FBtr0344519	18600150	18617943			75	CG4174
3	Lethal cell competition			FBgn0265268	FBtr0300049	18603425	18605415			75	CG18234
3	Lethal cell competition			FBgn0036795	FBtr0304702	18605472	18607349			75	CG18233
3	Lethal cell competition			FBgn0036796	FBtr0300052	18607462	18608512			75	CG18231
3	Lethal cell competition			FBgn0052201	FBtr0300051	18609620	18611862			75	CG32201
3	Lethal cell competition			FBgn0052199	FBtr0331419	18611900	18614004			75	CG32199
3	Lethal cell competition			FBgn0013717	FBtr0346438	18618305	18622129	non-stop		75	not
3	Lethal cell competition			FBgn0052200	FBtr0075107	18618390	18618461	transfer RNA:Proline-CGG 2-3		75	tRNA:Pro-CGG-2-3
3	Lethal cell competition			FBgn0259791	FBtr0075108	18620692	18624751	aurora borealis		75	bora
3	Lethal cell competition			FBgn0036801	FBtr0331421	18625959	18667177	Myosin phosphatase targeting subunit 75D		75	MYPT-75D
3	Lethal cell competition			FBgn0260027	FBtr0300082	18667351	18668155			75	CG42465
3	Lethal cell competition			FBgn0042134	FBtr0345806	18668153	18673324	Caprin		75	Capr
3	Lethal cell competition			FBgn0040322	FBtr0075095	18673474	18675413	Gram-negative bacteria binding protein 2		75	GNBP2
3	Lethal cell competition			FBgn0040323	FBtr0075050	18675800	18677976	Gram-negative bacteria binding protein 1		75	GNBP1
3	Lethal cell competition			FBgn0286925	FBtr0475182	18677931	18679297			75	CR46422
3	Lethal cell competition			FBgn0085283	FBtr0475188	18679559	18680779			75	CR36254
3	Lethal cell competition			FBgn0036804	FBtr0113179	18681037	18681836	SAGA associated factor 11kDa		75	Saf11
3	Lethal cell competition			FBgn0052202	FBtr0075051	18682184	18682865			75	CG32202
3	Lethal cell competition			FBgn0036805	FBtr0075092	18682895	18684061	Charged multivesicular body protein 1		75	Chmp1
3	Lethal cell competition			FBgn0036806	FBtr0345812	18684259	18686319	Cyp12c1		75	Cyp12c1
3	Lethal cell competition			FBgn0284719	FBtr0334058	18693352	18693952	long non-coding RNA:CR43987		75	lncRNA:CR43987
3	Lethal cell competition			FBgn0036807	FBtr0114373	18694187	18695948			75	CG6893
3	Lethal cell competition			FBgn0036808	FBtr0334057	18696402	18698412	Dicarboxylate carrier 4		75	Dic4
3	Lethal cell competition			FBti0062687	FBtr0362687-RA	18702749	18702760			75	
3	Lethal cell competition			FBgn0265885	FBtr0345003	18707933	18708892	long non-coding RNA:CR44674		75	lncRNA:CR44674
3	Lethal cell competition			FBti0020153	FBtr0020153-RA	18710814	18716708			75	
3	Lethal cell competition			FBgn0036809	FBtr0075089	18721893	18723272			75	CG12477
3	Lethal cell competition			FBgn0284717	FBtr0334051	18723807	18724312	long non-coding RNA:CR43985		75	lncRNA:CR43985
3	Lethal cell competition			FBti0062689	FBtr0362689-RA	18724098	18743182			75	
3	Lethal cell competition			FBgn0036810	FBtr0075053	18744488	18745999			75	CG6885
3	Lethal cell competition			FBgn0036811	FBtr0075054	18745856	18746623	Mediator complex subunit 11		75	MED11
3	Lethal cell competition			FBgn0036812	FBtr0075088	18746611	18748367	Nufip		75	Nufip
3	Lethal cell competition			FBgn0036813	FBtr0075055	18748697	18750483	Autophagy-related 3		75	Atg3
3	Lethal cell competition			FBgn0001078	FBtr0075087	18750607	18801309	ftz transcription factor 1		75	ftz-f1
3	Lethal cell competition			FBgn0267600	FBtr0347046	18753797	18754085	long non-coding RNA:CR45938		75	lncRNA:CR45938
3	Lethal cell competition			FBgn0267601	FBtr0347047	18772086	18801312	long non-coding RNA:CR45939		75	lncRNA:CR45939
3	Lethal cell competition			FBti0020154	FBtr0020154-RA	18772464	18781086			75	
3	Lethal cell competition			FBgn0036814	FBtr0332801	18802265	18820975			75	CG14073
3	Lethal cell competition			FBgn0036815	FBtr0075057	18821171	18822353	HP1-HOAP-interacting protein		75	HipHop
3	Lethal cell competition			FBgn0000261	FBtr0075058	18822604	18828188	Catalase		75	Cat
3	Lethal cell competition			FBgn0036816	FBtr0075081	18829832	18846267	I'm not dead yet		75	Indy
3	Lethal cell competition			FBti0020155	FBtr0020155-RA	18833837	18834940			75	
3	Lethal cell competition			FBgn0052027	FBtr0307116	18841579	18842788	long non-coding RNA:CR32027		75	lncRNA:CR32027
3	Lethal cell competition			FBti0062690	FBtr0362690-RA	18847653	18847987			75	
3	Lethal cell competition			FBgn0266937	FBtr0346910	18852573	18861363	long non-coding RNA:CR45388		75	lncRNA:CR45388
3	Lethal cell competition			FBgn0266936	FBtr0345829	18854317	18854622	long non-coding RNA:CR45387		75	lncRNA:CR45387
3	Lethal cell competition			FBgn0267572	FBtr0479722	18858690	18866107	antisense RNA:CR45912		75	asRNA:CR45912
3	Lethal cell competition			FBgn0262461	FBtr0304506	18860971	18861054	mir-315 stem loop		75	mir-315
3	Lethal cell competition			FBtr0304507_df_mrg	FBtr0304507	18860982	18861003			75	
3	Lethal cell competition			FBtr0472757_df_mrg	FBtr0472757	18861024	18861045			75	
3	Lethal cell competition			FBgn0036817	FBtr0308811	18863647	18865514			75	CG6865
3	Lethal cell competition			FBgn0036818	FBtr0308812	18866225	18867431			75	CG14074
3	Lethal cell competition			FBgn0036819	FBtr0333708	18867771	18869219	Dystrobrevin		75	Dysb
3	Lethal cell competition			FBgn0036820	FBtr0075063	18869236	18870357	Glutaredoxin 1		75	Grx1
3	Lethal cell competition			FBgn0025807	FBtr0075080	18870045	18872553	Rad9		75	Rad9
3	Lethal cell competition			FBgn0085284	FBtr0112449	18870224	18870897	Biogenesis of lysosome-related organelles complex 1, subunit 3		75	Blos3
3	Lethal cell competition			FBgn0014075	FBtr0075064	18872747	18878245	UDP-glucose-glycoprotein glucosyltransferase		75	Uggt
3	Lethal cell competition			FBgn0036821	FBtr0075077	18876250	18880483			75	CG3961
3	Lethal cell competition			FBgn0036822	FBtr0075065	18892383	18892278	Ninjurin B		75	NinB
3	Lethal cell competition			FBgn0036824	FBtr0075076	18893120	18896200			75	CG3902
3	Lethal cell competition			FBgn0086661	FBtr0091666	18896189	18896456	snoRNA:Psi28S-2566		75	snoRNA:Psi28S-2566
3	Lethal cell competition			FBgn0036825	FBtr0347494	18898875	18900408	Ribosomal protein L26		75	RpL26
3	Lethal cell competition			FBgn0036826	FBtr0075075	18900595	18901554	asterix		75	ate
3	Lethal cell competition			FBgn0036827	FBtr0075067	18901594	18902952			75	CG6843
3	Lethal cell competition			FBgn0027057	FBtr0075074	18903057	18904680	COP9 signalosome subunit 1b		75	CSN1b
3	Lethal cell competition			FBgn0036828	FBtr0346816	18905372	18906874			75	CG6841
3	Lethal cell competition			FBgn0036829	FBtr0300798	18908260	18911152	Ionotropic receptor 75d		75	Ir75d
3	Lethal cell competition			FBgn0036830	FBtr0298521	18908260	18914153			75	CG14077
3	Lethal cell competition			FBgn0036831	FBtr0075069	18917581	18919258			75	CG6839
3	Lethal cell competition			FBgn0036832	FBtr0333711	18919224	18920319			75	CG16223
3	Lethal cell competition			FBgn0036833	FBtr0075048	18920430	18922108			75	CG3819
3	Lethal cell competition			FBgn0052204	FBtr0113429	18922419	18946038			75	CG32204
3	Lethal cell competition			FBgn0262351	FBtr0304635	18925390	18926108			75	CG43049
3	Lethal cell competition			FBgn0262746	FBtr0362746-RA	18933429	18933407			75	
3	Lethal cell competition			FBgn0036834	FBtr0075023	18950629	18955406			75	CG6836
3	Lethal cell competition			FBgn0267249	FBtr0346439	18979368	18979590	long non-coding RNA:CR45689		75	lncRNA:CR45689
3	Lethal cell competition			FBgn0036835	FBtr0075024	18984961	18985834			75	CG14075
3	Lethal cell competition			FBgn0036836	FBtr0075046	18985905	18988323			75	CG11619
3	Lethal cell competition			FBgn0085285	FBtr0332318	18988736	18988815			75	CG34256
3	Lethal cell competition			FBgn0036837	FBtr0075043	18990026	18996283			75	CG18135
3	Lethal cell competition			FBgn0036838	FBtr0075041	18997875	19000938			75	CG3808
3	Lethal cell competition			FBgn0036839	FBtr0075040	19000985	19003252	SET and MYND domain containing, member A1		75	SmydA-2
3	Lethal cell competition			FBgn0002945	FBtr0075039	19003741	19045449	naked cuticle		75	nkd
3	Lethal cell competition			FBti0020156	FBtr0020156-RA	19008900	19009168			75	
3	Lethal cell competition			FBgn0267602	FBtr0347048	19033317	19033900	long non-coding RNA:CR45940		75	lncRNA:CR45940
3	Lethal cell competition			FBgn0015986	FBtr0300791	19050757	19052026	Accessory gland protein 76A		75	Acp76A
3	Lethal cell competition			FBgn0265886	FBtr0342756	19052302	19052792	long non-coding RNA:CR44675		75	lncRNA:CR44675
3	Lethal cell competition			FBgn0263326	FBtr0342757	19052902	19053389			75	CG43407
3	Lethal cell competition			FBgn0036842	FBtr0075037	19059400	19062816	UDP-glycosyltransferase family 316 member A1		75	Ugt316A1
3	Lethal cell competition			FBgn0036843	FBtr0075025	19063165	19066151	Sideroflexin 2		75	Sfxn2
3	Lethal cell competition			FBgn0036844	FBtr0333220	19066155	19086425	Mitogen-activated protein kinase phosphatase 3		75	Mkp3
3	Lethal cell competition			FBgn0266935	FBtr0345828	19090583	19090975	long non-coding RNA:CR45386		75	lncRNA:CR45386
3	Lethal cell competition			FBgn0036846	FBtr0330090	19092670	19094760	Misexpression suppressor of ras 6		75	MESR6
3	Lethal cell competition	124049				19094051			75F7		
3	Lethal cell competition			FBgn0036847	FBtr0075034	19094890	19096217	Canopy b		75	CNPYb
3	Lethal cell competition			FBgn0036848	FBtr0075033	19096399	19097709	NAD(P)HX dehydratase		75	Nkxd
3	Lethal cell competition			FBgn0036849	FBtr0075027	19097898	19099094			75	CG14079
3	Lethal cell competition			FBgn0036850	FBtr0075032	19099123	19100363	Gemin 2		75	Gem2
3	Lethal cell competition			FBgn0036851	FBtr0330092	19105381	19113895			75	CG14082
3	Lethal cell competition			FBti0020157	FBtr0020157-RA	19115676	19115812			75	
3	Lethal cell competition			FBti0020158	FBtr0020158-RA	19117098	19124487			75	
3	Lethal cell competition			FBgn0052203	FBtr0110771	19124459	19129662	Serpin 75F		75	Spn75F
3	Lethal cell competition			FBgn0016797	FBtr0075029	19140975	19235373	frizzled 2		76	fz2
3	Lethal cell competition			FBgn0267603	FBtr0347049	19183998	19184726	long non-coding RNA:CR45941		76	lncRNA:CR45941
3	Lethal cell competition			FBti0020159	FBtr0020159-RA	19208114	19209429			76	
3	Lethal cell competition			FBgn0284485	FBtr0332794	19229061	19230102	long non-coding RNA:CR43893		76	lncRNA:CR43893
3	Lethal cell competition			FBgn0033947	FBtr0091624	19236368	19237627			76	CG33947
3	Lethal cell competition			FBgn0284484	FBtr0332795	19239864	19240139	long non-coding RNA:CR43892		76	lncRNA:CR43892

2			76			19243468		76A3	
2				FBgn0267506	FBtr0479691	19243755	19251653	long non-coding RNA:CR46216	76	lncRNA:CR46216
2				FBgn0036853	FBtr0075022	19253290	19255061	mitochondrial ribosomal protein L21	76	mRpL21
2				FBgn0040075	FBtr0074988	19255340	19257111	raptin	76	Rapt
2				FBgn0026690	FBtr0075021	19257282	19260079	reaper	76	hes
2				FBgn0266737	FBtr0345237	19260040	19262895	antisense RNA:CR45210	76	asRNA:CR45210
2				FBgn0260857	FBtr0074990	19261394	19262437	Blocked early in transport 1	76	Bet1
2				FBgn0017578	FBtr0310276	19262232	19264184	Max	76	Max
2				FBgn0036856	FBtr0074991	19263766	19266838		76	CG9966
2				FBgn0259720	FBtr0344455	19263766	19266838		76	CG42374
2				FBgn0062775	FBtb0062775-RA	19265613	19266735		76	
2				FBgn0266456	FBtr0344456	19266061	19266838		76	CG45081
2				FBgn0036857	FBtr0075017	19266473	19268913	Aldehyde dehydrogenase 7 family member A1	76	Aldh7A1
2				FBgn0036859	FBtr0074992	19269351	19274168		76	CG14085
2				FBgn0036858	FBtr0300116	19269772	19270842		76	CG14088
2				FBgn0036860	FBtr0344806	19275791	19279916		76	CG14086
2				FBgn0036861	FBtr0075015	19280120	19280800		76	CG14089
2				FBgn0036862	FBtr0075014	19281364	19282768	Glycogen binding subunit 76A	76	Gbs-76A
2				FBtb0062776	FBtb0062776-RA	19293983	19294253		76	
2				FBgn0028380	FBtr0347258	19294564	19298830	fallen	76	fal
2				FBgn0267715	FBtr0347254	19294727	19295198	antisense RNA:CR46048	76	asRNA:CR46048
2				FBgn0003089	FBtr0075009	19298623	19337608	pipe	76	pip
2				FBgn0052206	FBtr0331192	19340321	19412912		76	CG32206
2				FBgn0036868	FBtr0330281	19387580	19390033	male-sterile (3) 76Ba	76	ms(3)76Ba
2				FBtb0063220	FBtb0063220-RA	19390125	19390167		76	
2				FBtb0020160	FBtb0020160-RA	19399952	19403653		76	
2				FBgn0284897	FBtr0333868	19405539	19406013	long non-coding RNA:CR43966	76	lncRNA:CR43966
2				FBgn0052205	FBtr0472918	19420350	19424183	hairpin RNA:CR32205	76	hpRNA:CR32205
2				FBtb0063225	FBtb0063225-RA	19422362	19422580		76	
2				FBgn0053255	FBtr0347036	19423758	19424146		76	CR33255
2				FBgn0262027	FBtr0303863	19424702	19424926		76	CR42838
2				FBtb0063227	FBtb0063227-RA	19425115	19425162		76	
2				FBgn0267296	FBtr0346561	19439027	19441165	long non-coding RNA:CR45732	76	lncRNA:CR45732
2				FBgn0053062	FBtr0332887	19441719	19446444		76	CG33062
2				FBgn0023395	FBtr0074998	19447173	19450238	Chd3	76	Chd3
2				FBgn0266983	FBtr0345885	19454760	19455672	long non-coding RNA:CR45434	76	lncRNA:CR45434
2				FBtb0063223	FBtb0063223-RA	19457458	19457508		76	
2				FBgn0036870	FBtr0074987	19460466	19464759		76	CG14095
2				FBgn0036871	FBtr0074986	19466567	19467079		76	CG14096
2				FBgn0052214	FBtr0333843	19467346	19468160		76	CG32214
2				FBtb0063230	FBtb0063230-RA	19468212	19468810		76	
2				FBtb0020161	FBtb0020161-RA	19469083	19471158		76	
2				FBtb0063233	FBtb0063233-RA	19471433	19471468		76	
2				FBtb0063236	FBtb0063236-RA	19471470	19471546		76	
2				FBgn0052208	FBtr0273406	19471656	19472228	825-Oak	76	825-Oak
2				FBgn0036872	FBtr0074990	19472491	19473345		76	CG12519
2				FBgn0267714	FBtr0347229	19474731	19475942	antisense RNA:CR46047	76	asRNA:CR46047
2				FBgn0036873	FBtr0074984	19475017	19475576		76	CG16294
2				FBgn0052213	FBtr0273409	19475839	19476423		76	CG32213
2				FBtb0063245	FBtb0063245-RA	19476516	19476555		76	
2				FBtb0063246	FBtb0063246-RA	19476556	19476579		76	
2				FBtb0063248	FBtb0063248-RA	19476580	19476884		76	
2				FBtb0063249	FBtb0063249-RA	19477121	19477317		76	
2				FBgn0052207	FBtr0472920	19477329	19478720	hairpin RNA:CR32207	76	hpRNA:CR32207
2				FBgn0262031	FBtr0303926	19478284	19478670		76	CR42842
2				FBgn0036874	FBtr0074982	19483826	19486498	brivido-1	76	Brv1
2				FBgn0262928	FBtr0472921	19486745	19488438	hairpin RNA:CR33940	76	hpRNA:CR33940
2				FBtb0020162	FBtb0020162-RA	19487226	19487657		76	
2				FBgn0052212	FBtr0074932	19487560	19488348		76	CG32212
2				FBtb0063251	FBtb0063251-RA	19488843	19488983		76	
2				FBtb0063253	FBtb0063253-RA	19490973	19491031		76	
2				FBgn0036875	FBtr0333846	19492053	19497723		76	CG9449
2				FBgn0036876	FBtr0074979	19498197	19500798		76	CG9451
2				FBgn0036877	FBtr0074978	19501010	19503870		76	CG9452
2				FBgn0267295	FBtr0346550	19504986	19505295	long non-coding RNA:CR45731	76	lncRNA:CR45731
2				FBgn0036878	FBtr0074977	19517552	19518332	Cuticular protein 76Ba	76	Cpr76Ba
2				FBgn0036879	FBtr0074933	19519646	19520419	Cuticular protein 76Bb	76	Cpr76Bb
2				FBgn0036880	FBtr0332754	19520945	19527272	Cuticular protein 76Bc	76	Cpr76Bc
2				FBgn0036881	FBtr0332756	19532743	19538289	Cuticular protein 76Bd	76	Cpr76Bd
2				FBgn0036882	FBtr0074976	19538425	19544205		76	CG9279
2				FBgn0286940	FBtr0475224	19538425	19544205		76	CG48434
2				FBgn0284477	FBtr0332757	19543106	19543602	antisense RNA:CR43885	76	asRNA:CR43885
2				FBgn0262517	FBtr0074974	19544345	19552200	Listerin E3 ubiquitin protein ligase 1	76	Ant1
2				FBgn0260461	FBtr0074937	19545110	19547293	Reduction in Cmn dots 7	76	Rcd7
2				FBgn0286941	FBtr0475226	19545110	19547293		76	CG48435
2				FBgn0036886	FBtr0074938	19552420	19554767		76	CG9300
2				FBgn0265888	FBtr0342759	19555533	19557202	long non-coding RNA:CR44677	76	lncRNA:CR44677
2				FBgn0265887	FBtr0342758	19559023	19561190	long non-coding RNA:CR44676	76	lncRNA:CR44676
2				FBgn0267576	FBtr0346990	19562636	19566533	long non-coding RNA:CR45916	76	lncRNA:CR45916
2				FBgn0262373	FBtr0304196	19565131	19565208	mir-9a stem loop	76	mir-9a
2				FBtr0304197_df_mrg	FBtr0304197	19565140	19565162		76	
2				FBtr0472710_df_mrg	FBtr0472710	19565179	19565208		76	
2				FBgn0005564	FBtr0333273	19566851	19584568	Shaker cognate l	76	Shal
2				FBgn0036887	FBtr0074972	19585093	19586003		76	CG9231
2				FBgn0036888	FBtr0074940	19586253	19589111		76	CG9330
2				FBgn0036889	FBtr0074971	19589072	19590524		76	CG14100
2				FBgn0035386	FBtr0306010	19590773	19598755	absent, small, or homeotic discs 1	76	ash1
2				FBgn0010417	FBtr0074941	19590086	19601362	TBP-associated factor 6	76	Taf8
2				FBgn0036890	FBtr0074944	19601633	19604120		76	CG9368
2				FBgn0020277	FBtr0301489	19604398	19606090	lush	76	lush
2				FBgn0036891	FBtr0074945	19606208	19606368		76	CG9372
2				FBgn0036892	FBtr0273410	19607857	19612169	Lon protease	76	Lon
2				FBgn0036893	FBtr0074946	19612455	19613489	Phosphatidylinositol glycan anchor biosynthesis class F	76	PIG-F
2				FBgn0260655	FBtr0074966	19613427	19618521	lethal (3) 76BDm	76	l(3)76BDm
2				FBgn0020694	FBtr0074947	19618594	19623368	anti-silencing factor 1	76	asf1
2				FBgn0036895	FBtr0074948	19620502	19624309	male-sterile (3) 76Cc	76	ms(3)76Cc
2				FBgn0036896	FBtr0074964	19624406	19635783	wallenda	76	wnd
2				FBtb0063274	FBtb0063274-RA	19628542	19629120		76	
2				FBgn0036897	FBtr0300116	19637207	19642816	Ring finger protein 146	76	Rnf146
2				FBgn0022774	FBtr0074961	19647280	19649851	Ornithine aminotransferase precursor	76	Oat
2				FBgn0036899	FBtr0331860	19650506	19664104	teyrha-meyrha	76	tey
2				FBgn0265889	FBtr0342760	19678921	19680121	long non-coding RNA:CR44678	76	lncRNA:CR44678
2				FBgn0036900	FBtr0305597	19683941	19687353		76	CG8765
2				FBtb0063275	FBtb0063275-RA	19684180	19684885		76	
2				FBgn0004623	FBtr0074949	19687637	19689992	G protein beta-subunit 76C	76	Gbeta76C
2				FBgn0261341	FBtr0345145	19690033	19695260	vermiform	76	verm
2				FBgn0260653	FBtr0333862	19700977	19708015	serpentine	76	serp
2				FBtb0020163	FBtb0020163-RA	19708521	19713241		76	
2				FBgn0262516	FBtr0074952	19744418	19749851	Transient receptor potential cation channel, mucolipin precursor	76	Trpml
2				FBgn0261360	FBtr0332277	19749527	19760569		76	CG42637
2				FBgn0260434	FBtr0300858	19728994	19730402		76	CG42529
2				FBgn0261361	FBtr0332283	19745834	19749744		76	CG42638
2				FBgn0286136	FBtr0333879	19750943	19793589	Guanylyl cyclase at 76C	76	Gyc76C
2				FBgn0036905	FBtr0074950	19760409	19761817	male-sterile (3) 76Ca	76	ms(3)76Ca
2				FBtb0063277	FBtb0063277-RA	19761958	19762013		76	
2				FBtb0020164	FBtb0020164-RA	19771346	19776973		76	
2				FBgn0261283	FBtr0074875	19793935	19799979	Sterol regulatory element binding protein	76	SREBP
2				FBgn0262393	FBtr0304279	19797961	19798059	mir-33 stem loop	76	mir-33
2				FBtr0304280_df_mrg	FBtr0304280	19797986	19798006		76	
2				FBtr0472725_df_mrg	FBtr0472725	19798025	19798046		76	
2				FBgn0036906	FBtr0074928	19798975	19801291		76	CG14102
2				FBgn0265874	FBtr0301806	19799278	19803427	Ionotropic receptor 76a	76	IR76a
2				FBgn0036908	FBtr0333878	19803738	19805280	Torsin interacting protein	76	TORIP
2				FBgn0036909	FBtr0074880	19805181	19806932	Coiled-coil domain-containing 58	76	Ccdc58
2				FBgn0083952	FBtr0110816	19805241	19806936		76	CG34116
2				FBgn0040786	FBtr0299563	19808811	19807199		76	CG14104
2				FBgn0024889	FBtr0074881	19807232	19810368	karyopherin alpha1	76	Kap-alpha1
2				FBgn0036910	FBtr0074925	19810403	19813339	Cyp305a1	76	Cyp305a1
2				FBgn0023094	FBtr0074924	19813770	19815938	cycle	76	cyc
2				FBgn0036911	FBtr0479622	19816085	19817967	Fitrp	76	Fitrp

2			FBgn0013799	FBtr0100666	19818174	19830886	Deformed epidermal autoregulatory factor-1		76	Deaf1
2			FBgn0020165	FBtr0020165-RA	19820341	19827846			76	
2			FBgn0003744	FBtr0332154	19830864	19834304	tricornered		76	trc
2			FBgn0052221	FBtr0301008	19834676	19836413			76	CG32221
2			FBgn0001324	FBtr0074884	19836514	19844644	kohtalo		76	kto
2			FBgn0020389	FBtr0074886	19845293	19860925	PAPS synthetase		76	Papss
2			FBgn0020166	FBtr0020166-RA	19848557	19857686			76	
2			FBgn0063333	FBtr0063333-RA	19861289	19861405			76	
2			FBgn0264982	FBtr0345884	19861458	19861869	long non-coding RNA:CR45433		76	lncRNA:CR45433
2			FBgn0020167	FBtr0020167-RA	19861875	19863607			76	
2			FBgn0020168	FBtr0020168-RA	19864201	19867041			76	
2			FBgn0262518	FBtr0074921	19867488	19871078	Rab8		76	Rab8
2			FBgn0036913	FBtr0476917	19871139	19881763	Ubiquitin specific protease 32		76	Usp32
2			FBgn0262519	FBtr0330046	19882051	19910215	Mi-2		76	Mi-2
2			FBgn0014037	FBtr0344257	19889120	19909410	Su(Tpl)		76	Su(Tpl)
2			FBgn0052218	FBtr0304110	19895216	19896391	long non-coding RNA:CR32218		76	lncRNA:CR32218
2			FBgn0264481	FBtr0332770	19900365	19910203	antisense RNA:CR43889		76	asRNA:CR43889
2			FBgn0036915	FBtr0074892	19910300	19912504	Precursor RNA processing 3		76	Prp3
2			FBgn0036916	FBtr0074918	19912405	19913715	Mtr3		76	Mtr3
2			FBgn0028695	FBtr0074893	19915051	19918165	Regulatory particle non-ATPase 1		76	Rpn1
2			FBgn0020887	FBtr0074916	19918242	19923462	Su(z)12		76	Su(z)12
2			FBgn0036918	FBtr0330181	19923671	19924688	Prefoldin 6		76	Pfdn6
2			FBgn0036919	FBtr0074895	19924943	19927175	Graspb5		76	Graspb5
2			FBgn0036920	FBtr0074915	19927194	19929508			76	CG8004
2			FBgn0036921	FBtr0331800	19928743	19932693	RhoGDI		76	RhoGDI
2			FBgn0287592	FBtr0479921	19931691	19932331			76	CG46462
2			FBgn0267238	FBtr0346408	19933720	19934201	long non-coding RNA:CR45678		76	lncRNA:CR45678
2			FBgn0004852	FBtr0304746	19939287	19977960	Adenylyl cyclase 76E		76	Ac76E
2			FBgn0052219	FBtr0074914	19950029	19951135			76	CG32219
2			FBgn0085287	FBtr0112452	19951235	19951988			76	CG34258
2			FBgn0053710	FBtr0091698	19951954	19952796			76	CG33710
2			FBgn0261507	FBtr0307886	19952971	19953712			76	CG42655
2			FBgn0261506	FBtr0335392	19953794	19954526			76	CG42654
2			FBgn0259148	FBtr0330430	19954547	19955768			76	CG42263
2			FBgn0063298	FBtr0063298-RA	19968718	19968765			76	
2			FBgn0036922	FBtr0074913	19978713	19979812			76	CG14182
2			FBgn0036923	FBtr0303781	19981685	19984191			76	CG17732
2			FBgn0036924	FBtr0074912	19984426	19985868	hale-bopp		76	hale
2			FBgn0036925	FBtr0074899	19986093	19988372	schumacher-levy		76	lechuy
2			FBgn0052220	FBtr0475016	19988027	19988991	CMP-sialic acid synthase		76	Csas
2			FBgn0005633	FBtr0332723	19988551	19991220	flightin		76	ffn
2			FBgn0264654	FBtr0344059	19989706	19990739	antisense RNA:CR45161		76	asRNA:CR45161
2			FBgn0013303	FBtr0074902	19991887	19997588	Neurocalcin		76	Nca
2			FBgn0036926	FBtr0344084	19991887	19996368			76	CG7646
2			FBgn0036927	FBtr0074908	19997714	20000689	gamma-aminobutyric acid transaminase		76	Gabat
2			FBgn0036928	FBtr0332719	20000644	20003446	Translocase of outer membrane 20		76	Tom20
2			FBgn0036929	FBtr0332720	20002736	20004834	CMP-sialic acid synthase		76	CG7668
2			FBgn0261574	FBtr0332722	20005301	20024607	kugelei		76	kug
2			FBgn0036931	FBtr0074907	20024687	20027835			76	CG14183
2			FBgn0036932	FBtr0074872	20027819	20029020			76	CG14184
2			FBgn0063339	FBtr0063339-RA	20034051	20034172			76	
2			FBgn0020169	FBtr0020169-RA	20040572	20040908			76	
2			FBgn0063342	FBtr0063342-RA	20055567	20055634			76	
2			FBgn0036934	FBtr0332667	20058511	20089007	short neuropeptide F receptor		76	sNPF-R
2			FBgn0036935	FBtr0074870	20089084	20103827			76	CG14186
2			FBgn0265890	FBtr0342761	20104503	20105544	long non-coding RNA:CR44679		76	lncRNA:CR44679
2			FBgn0036936	FBtr0074818	20108094	20107527			76	CG14185
2			FBgn0063344	FBtr0063344-RA	20107698	20108216			76	
2			FBgn0036937	FBtr0074869	20108484	20111534	ionotropic receptor 76b		76	ir76b
2			FBgn0036938	FBtr0332701	20112265	20112847			76	CG14187
2			FBgn0020170	FBtr0020170-RA	20113713	20122911			76	
2			FBgn0036939	FBtr0332750	20124298	20127381			76	CG7365
2			FBgn0005198	FBtr0332690	20129181	20139010	gigas		76	gig
2			FBgn0036940	FBtr0074866	20130451	20131743	obstructor-J		76	obst-J
2			FBgn0036941	FBtr0074865	20132032	20133088			76	CG7335
2			FBgn0036942	FBtr0074864	20139210	20140607			76	CG7328
2			FBgn0261556	FBtr0332698	20146914	20168377			77	CG42674
2			FBgn0267604	FBtr0347050	20159990	20160486	long non-coding RNA:CR45942		76	lncRNA:CR45942
2			FBgn0036945	FBtr0074821	20188522	20189779	Snakeskin		77	Sak
2			FBgn0262022	FBtr0303852	20200093	20200487			77	CG42833
2			FBgn0036947	FBtr0074860	20200443	20201638	obstructor-F		77	obst-F
2			FBgn0036948	FBtr0074859	20202070	20203687			77	CG7298
2			FBgn0036949	FBtr0074858	20204309	20206046			77	CG7290
2			FBgn0036950	FBtr0332691	20207534	20209600			77	CG6996
2			FBgn0052224	FBtr0347178	20207866	20208801	antisense RNA:CR32224		77	asRNA:CR32224
2			FBgn0036951	FBtr0332685	20210292	20212122			77	CG7017
2			FBgn0020171	FBtr0020171-RA	20212665	20218176			77	
2			FBgn0036952	FBtr0332694	20218500	20220425			77	CG6933
2			FBgn0036953	FBtr0332692	20221814	20223197			77	CG17145
2			FBgn0260393	FBtr0310467	20229932	20235304			77	CG17147
2			FBgn0063358	FBtr0063358-RA	20235409	20235462			77	
2			FBgn0260397	FBtr0332693	20236381	20239255	Suppressor of variegation 3-3		77	Su(var)3-3
2			FBgn0036956	FBtr0074827	20231669	20233255			77	CG13813
2			FBgn0036958	FBtr0392113	20233173	20241903			77	CG17233
2			FBgn0024814	FBtr0074830	20241053	20243735	Clathrin light chain		77	Clc
2			FBgn0036959	FBtr0074829	20241267	20245312			77	CG6951
2			FBgn0265959	FBtr0342946	20246085	20265554	retinal degeneration C		77	rdgC
2			FBgn0020172	FBtr0020172-RA	20257385	20258451			77	
2			FBgn0063359	FBtr0063359-RA	20259544	20259622			77	
2			FBgn0264468	FBtr0344956	20265596	20266200	antisense RNA:CR43876		77	asRNA:CR43876
2			FBgn0052228	FBtr0074836	20268514	20268800			77	CG32228
2			FBgn0052227	FBtr0074848	20268955	20269133	golden goal		77	gogo
2			FBgn0036962	FBtr0074849	20273389	20275335			77	CG17122
2			FBgn0063361	FBtr0063361-RA	20283884	20283942			77	
2			FBgn0264482	FBtr0344582	20290702	20291152	long non-coding RNA:CR43890		77	lncRNA:CR43890
2			FBgn0036964	FBtr0074847	20295832	20296971	FSHD region gene 1		77	FRG1
2			FBgn0052226	FBtr0074846	20297129	20302141	Pecoon 23		77	Pec23
2			FBgn0036967	FBtr0074837	20299410	20300511	Squamous cell carcinoma-related oncogene 4		77	SCCRO4
2			FBgn0264464	FBtr0332774	20299419	20302266	antisense RNA:CR43872		77	asRNA:CR43872
2			FBgn0052225	FBtr0074845	20304310	20306283			77	CG32225
2			FBgn0003124	FBtr0100318	20309654	20313468	polo		77	polo
2			FBgn0250791	FBtr0074840	20313632	20316577	alpha Soluble NSF attachment protein		77	alphaSnap
2			FBgn0264467	FBtr0332776	20315134	20317283	antisense RNA:CR43875		77	asRNA:CR43875
2			FBgn0262057	FBtr0074841	20317190	20320116	Serpin 77Ba		77	Spn77Ba
2			FBgn0036969	FBtr0074843	20320952	20322358	Serpin 77Bb		77	Spn77Bb
2			FBgn0036972	FBtr0347193	20322377	20323208			77	CR6434
2			FBgn0020173	FBtr0020173-RA	20322295	20324650			77	
2			FBgn0062048	FBtr0062048-RA	20324793	20343244			77	
2			FBgn0020174	FBtr0020174-RA	20327779	20334796			77	
2			FBgn0059763	FBtr0059763-RA	20334833	20341683			77	
2			FBgn0020176	FBtr0020176-RA	20336937	20337212			77	
2			FBgn0036970	FBtr0378172	20342634	20344318	Serpin 77Bc		77	Spn77Bc
2			FBgn0063381	FBtr0063381-RA	20344619	20344687			77	
2			FBgn0266934	FBtr0475131	20345323	20346934			77	CR45385
2			FBgn0036973	FBtr0078242	20345736	20347942	Retinoblastoma binding protein 5		77	Rbbp5
2			FBgn0036974	FBtr0331818	20348355	20353875	eukaryotic translation release factor 1		77	eRF1
2			FBgn0036975	FBtr0078179	20353449	20356632			77	CG5618
2			FBgn0024887	FBtr0078181	20358807	20358331	kirr17		77	kirr17
2			FBgn0036977	FBtr0336855	20358512	20359820			77	CG5865
2			FBgn0259676	FBtr0078241	20359833	20361585	DNA polymerase alpha 60kD subunit		77	DNApol-alpha60
2			FBgn0036978	FBtr0078240	20361843	20366724	Toll-9		77	Toll-9
2			FBgn0001259	FBtr0078193	20367196	20370259	inturned		77	in
2			FBgn0036979	FBtr0473581	20370313	20371746			77	CG13247
2			FBgn0001247	FBtr0273273	20371672	20375896	Insulin degrading metalloproteinase		77	Ide
2			FBgn0036980	FBtr0330157	20376242	20382398	Rho-related BTB domain containing		77	RhoBTB
2			FBgn0027585	FBtr0078238	20382405	20384169			77	CG5498
2			FBgn0011205	FBtr0307360	20384429	20391913	flumble		77	fbl
2			FBgn0264572	FBtr0333481	20386853	20391357	antisense RNA:CR43944		77	asRNA:CR43944
2			FBgn0053969	FBtr0100010	20391685	20393553			77	CG33969
2		**125973**			**20394712**			**77C1**		

2			FBgn0267237	FBtr0346407	20395394	20395851	long non-coding RNA:CR45677		77	lncRNA:CR45677
2			FBgn0028678	FBtr0078235	20399288	20401609	Inhibkas		77	Inhl
2			FBgn0267635	FBtr0347090	20404270	20407558	long non-coding RNA:CR45973		77	lncRNA:CR45973
2			FBgn0036984	FBtr0078234	20407103	20410598			77	CG13248
2			FBgn0036985	FBtr0078191	20413604	20424309	zye		77	zye
2			FBgn0036986	FBtr0078233	20424424	20426371			77	CG5282
2			FBgn0036987	FBtr0078231	20426199	20427666			77	CG5274
2			FBgn0036988	FBtr0310615	20427962	20430475			77	CG5262
2			FBgn0029158	FBtr0290266	20430605	20432361	Lipoic acid synthase		77	Las
2			FBgn0284421	FBtr0114517	20432468	20435156	Presenilin		77	Pen
2			FBgn0036990	FBtr0078227	20435110	20436209	mitochondrial ribosomal protein L15		77	mRpL15
2			FBgn0036991	FBtr0078194	20436250	20438370	CTBP-interacting protein		77	CtIP
2			FBgn0036992	FBtr0078225	20438166	20439872	4-hydroxyphenylpyruvate dioxygenase		77	Hpd
2			FBgn0266686	FBtr0345053	20439600	20439921	long non-coding RNA:CR45176		77	lncRNA:CR45176
2			FBgn0284571	FBtr0333480	20439954	20440593	long non-coding RNA:CR43943		77	lncRNA:CR43943
2			FBgn0036993	FBtr0078195	20442419	20450393			77	CG9510
2			FBgn0036994	FBtr0078224	20450532	20452864			77	CG5199
2			FBgn0083120	FBtr0300233	20453293	20454731	U snoRNA host gene 8		77	UhgB
2			FBgn0086082	FBtr0114358	20453733	20453821			77	snoRNA:Or-CD11
2			FBgn0082949	FBtr0113613	20454007	20454085	snoRNA:Me18S-U1356a		77	snoRNA:Me18S-U1356a
2			FBgn0082948	FBtr0113614	20454246	20454324	snoRNA:Me18S-U1356b		77	snoRNA:Me18S-U1356b
2			FBgn0082947	FBtr0113615	20454498	20454574	snoRNA:Me18S-U1356c		77	snoRNA:Me18S-U1356c
2			FBgn0036995	FBtr0331570	20454690	20464862	artichoke		77	atk
2			FBgn0036996	FBtr0078196	20460683	20462274	magro		77	mag
2			FBgn0261832	FBtr0331568	20464714	20466041			77	CG42764
2			FBgn0036997	FBtr0078197	20466944	20469592			77	CG5955
2		77			**20470000**			77C4		
2		**77**			**20470000**			**77C4**		
2			FBgn0052428	FBtr0300452	20469674	20473723			77	CG32428
2			FBgn0036998	FBtr0078198	20473783	20474791			77	CG5969
2			FBgn0036999	FBtr0078200	20474468	20477003	iso Glutaminyl cyclase		77	isoQC
2			FBti0020178	FBti0020178-RA	20476808	20484350			77	
2			FBgn0037000	FBtr0078220	20484293	20484921	Zinc transporter 77C		77	ZnT77C
2			FBti0063433	FBti0063433-RA	20487727	20487887			77	
2			FBgn0037001	FBtr0331564	20492082	20497084	NADH dehydrogenase (ubiquinone) 39 kDa subunit		77	ND-39
2			FBgn0052425	FBtr0078205	20497323	20514107			77	CG32425
2			FBti0063435	FBti0063435-RA	20499231	20499285			77	
2			FBgn0037003	FBtr0078206	20499836	20501500			77	CG16281
2			FBti0063437	FBti0063437-RA	20501558	20502154			77	
2			FBti0063438	FBti0063438-RA	20502491	20502893			77	
2			FBti0063439	FBti0063439-RA	20503177	20503452			77	
2			FBgn0037004	FBtr0078207	20504186	20505700			77	CG17637
2			FBgn0037005	FBtr0078208	20506032	20507375			77	CG5078
2			FBgn0037007	FBtr0078216	20514598	20519393			77	CG5059
2			FBgn0037008	FBtr0078215	20519590	20520772	mitochondrial transcription termination factor 3		77	mTerf3
2			FBgn0037009	FBtr0078209	20521009	20523434			77	CG5104
2			FBgn0267585	FBtr0078214	20522440	20526174	lethal (3) 77CDf		77	l(3)77CDf
2			FBgn0037011	FBtr0078210	20526576	20527910			77	CG4658
2			FBgn0037012	FBtr0078213	20527972	20540417	Reduction in Cnn dots 2		77	Rcd2
2			FBgn0037013	FBtr0078211	20533709	20535335			77	CG13250
2			FBti0063440	FBti0063440-RA	20535876	20536132			77	
2			FBgn0284411	FBtr0452191	20557219	20557810	long noncoding RNA: testis-specific 3		77	lncRNA:TS3
2			FBgn0284412	FBtr0452190	20558197	20558520	long non-coding RNA:CR46326		77	lncRNA:CR46326
2			FBti0063441	FBti0063441-RA	20564708	20564758			77	
2			FBti0020179	FBti0020179-RA	20590119	20590600			77	
2			FBgn0001323	FBtr0078212	20597141	20626659	knirps-like		77	knrl
2			FBgn0265895	FBtr0342782	20623851	20624491	long non-coding RNA:CR44684		77	lncRNA:CR44684
2			FBgn0265894	FBtr0342780	20626580	20626488	long non-coding RNA:CR44683		77	lncRNA:CR44683
2			FBgn0265891	FBtr0342776	20626601	20627624	long non-coding RNA:CR44680		77	lncRNA:CR44680
2			FBgn0265892	FBtr0342777	20633020	20633484	long non-coding RNA:CR44681		77	lncRNA:CR44681
2			FBgn0265893	FBtr0342778	20634172	20634465	long non-coding RNA:CR44682		77	lncRNA:CR44682
2			FBgn0037014	FBtr0078243	20637199	20640910			77	CG13251
2			FBti0063902	FBti0063902-RA	20641114	20641208			77	
2			FBgn0265896	FBtr0342779	20652906	20654128	long non-coding RNA:CR44685		77	lncRNA:CR44685
2			FBti0063903	FBti0063903-RA	20659518	20659809			77	
2			FBgn0001320	FBtr0078283	20662339	20665378	knirps		77	kni
2			FBti0063922	FBti0063922-RA	20711832	20711937			77	
2			FBti0063907	FBti0063907-RA	20712048	20712105			77	
2			FBti0063924	FBti0063924-RA	20712137	20712539			77	
2			FBti0063909	FBti0063909-RA	20712598	20712743			77	
2			FBgn0037015	FBtr0305579	20712838	20716200	crimpy		77	crmpy
2			FBgn0085289	FBtr0333482	20714100	20715158			77	CG34260
2	**124213**				**20723348**			**77E4**		
2			FBgn0284573	FBtr0333483	20729274	20729656	long non-coding RNA:CR43945		77	lncRNA:CR43945
2			FBgn0037016	FBtr0078245	20730591	20744508			77	CG13252
2			FBgn0045474	FBtr0078281	20737569	20739435	Gustatory receptor 77a		77	Gr77a
2			FBgn0052912	FBtr0091916	20754076	20755885			77	CG33912
2			FBti0063911	FBti0063911-RA	20756359	20756390			77	
2			FBgn0262896	FBtr0306312	20758883	20759192			77	CG43251
2			FBgn0037017	FBtr0476914	20768207	20769500			77	CG4074
2			FBgn0040634	FBtr0078246	20769586	20770138			77	CG4186
2			FBgn0037018	FBtr0078279	20770143	20771927			77	CG4042
2			FBgn0016896	FBtr0304935	20771528	20776931	Pitslre		77	Pitslre
2			FBgn0037019	FBtr0078278	20776766	20778264	Peroxin 16		77	Pex16
2			FBgn0037020	FBtr0078251	20778799	20780378	Peroxin 14		77	Pex14
2			FBgn0037021	FBtr0078277	20780350	20786197			77	CG113399
2			FBgn0267615	FBtr0476975	20785216	20788424	antisense RNA:CR46484		77	asRNA:CR46484
2			FBgn0037022	FBtr0078276	20786340	20788137			77	CG113396
2			FBgn0027364	FBtr0078275	20788886	20792777	Six4		77	Six4
2			FBgn0263844	FBtr0321301	20795019	20795678	long non-coding RNA:CR43705		77	lncRNA:CR43705
2			FBgn0263845	FBtr0321300	20795916	20796502	long non-coding RNA:CR43706		77	lncRNA:CR43706
2			FBgn0037023	FBtr0078273	20797241	20798375			77	CG36938
2			FBgn0037024	FBtr0078253	20798545	20800081	tanzing norgay		77	tzn
2			FBgn0037025	FBtr0078255	20800410	20806853	Spc105-related		77	Spc105R
2			FBgn0037026	FBtr0331529	20808868	20809272			77	CG36634
2			FBgn0037027	FBtr0331525	20809669	20813332	HP1 and insulator partner protein 1		77	HIPIP1
2			FBgn0037028	FBtr0302947	20813353	20816975			77	CG36118
2			FBgn0259243	FBtr0300533	20816118	20819048	Protein kinase, cAMP-dependent, regulatory subunit type 1		77	Pka-R1
2			FBgn0086915	FBtr0076270	20816901	20819027	Male-specific transcript 77F		77	msl77F
2			FBti0063931	FBti0063931-RA	20818229	20818368			77	
2			FBti0059736	FBti0059736-RA	20821333	20824739			77	
2			FBti0020181	FBti0020181-RA	20823034	20823992			77	
2			FBti0063932	FBti0063932-RA	20830334	20830385			77	
2			FBgn0266693	FBtr0345827	20836113	20837135	antisense RNA:CR45384		77	asRNA:CR45384
2			FBgn0037030	FBtr0345826	20836182	20837153			77	CG3288
2			FBgn0040636	FBtr0078263	20837488	20838839			77	CG13255
2			FBgn0267605	FBtr0347051	20838313	20838700	antisense RNA:CR45943		77	asRNA:CR45943
2			FBgn0027055	FBtr0078269	20839096	20841576	COP9 signalosome subunit 3		77	CSN3
2			FBgn0037031	FBtr0333371	20841957	20844340			77	CG11458
2			FBgn0052432	FBtr0078268	20844332	20865188			77	CG32432
2			FBgn0265897	FBtr0342762	20887006	20888002	long non-coding RNA:CR44686		77	lncRNA:CR44686
2			FBti0020183	FBti0020183-RA	20895297	20895582			77	
2			FBti0063933	FBti0063933-RA	20895769	20895886			77	
2			FBgn0259972	FBtr0300317	20896268	20897417	Seminal fluid protein 77F		77	Sfp77F
2			FBgn0264552	FBtr0333280	20897557	20898501			77	CG43931
2			FBgn0266932	FBtr0345825	20901854	20902524	long non-coding RNA:CR45383		77	lncRNA:CR45383
2			FBti0063934	FBti0063934-RA	20905093	20905361			77	
2			FBgn0040637	FBtr0078265	20905756	20906331			77	CG11456
2			FBgn0267297	FBtr0346552	20912888	20913169	long non-coding RNA:CR45733		77	lncRNA:CR45733
2			FBgn0264551	FBtr0333282	20913158	20913705	long non-coding RNA:CR43930		77	lncRNA:CR43930
2			FBgn0267298	FBtr0346553	20920802	20921073	long non-coding RNA:CR45734		78	lncRNA:CR45734
2			FBgn0264550	FBtr0333281	20921182	20921749	long non-coding RNA:CR43929		78	lncRNA:CR43929
2			FBgn0011591	FBtr0078267	20925891	20949512	fringe		78	fng
2			FBgn0037035	FBtr0078266	20927828	20929190			78	CG10589
2			FBgn0266778	FBtr0345403	20950359	20950783	long non-coding RNA:CR45243		78	lncRNA:CR45243
2			FBgn0037036	FBtr0078335	20955755	20956750	Seminase		78	Sems
2			FBgn0037037	FBtr0346528	20959934	20960980			78	CG10588
2			FBgn0037038	FBtr0078334	20960398	20961386			78	CG11037
2			FBgn0037039	FBtr0339891	20961537	20962555			78	CG10587
2			FBgn0037040	FBtr0114618	20962655	20966762			78	CG12983

2				FBgn0053287	FBtr0290073	20966766	20970863			79	CR33287
2				FBgn0053286	FBtr0113469	20970812	20974700			79	CR33286
2				FBgn0053283	FBtr0302444	20978765	20979650			79	CR33283
2				FBgn0037042	FBtr0344990	20991673	20992930			79	CG12984
2				FBgn0063948	FBtr0063948-RA	20992311	20992506			79	
2				FBgn0003415	FBtr0112830	20992814	21027434	skuld		79	skd
2				FBgn0267606	FBtr0347052	21003707	21004201	antisense RNA:CR45944		79	asRNA:CR45944
2				FBgn0263486	FBtr0309785	21006379	21006520	small Cajal body-specific RNA : PsiU6-40		79	scaRNA:PsiU6-40
2				FBtr0302184	FBtr0302184-RA	21014969	21023393			79	
2				FBgn0037044	FBtr0345136	21027915	21030141	Decaprenyl diphosphate synthase subunit 2		79	Pdss2
2				FBgn0267451	FBtr0346822	21028959	21029701	antisense RNA:CR45801		79	asRNA:CR45801
2				FBgn0037045	FBtr0078327	21030280	21031360			79	CG10584
2				FBgn0028402	FBtr0304820	21031825	21033561	Sex-lethal interactor		79	Sin
2				FBgn0037046	FBtr0078326	21033554	21034203			79	CG10581
2				FBgn0026179	FBtr0111038	21034535	21075444	schizo		79	siz
2				FBtr0063950	FBtr0063950-RA	21061412	21061465			79	
2				FBgn0262462	FBtr0304521	21065852	21066228			79	CG43072
2				FBgn0030294	FBtr0333449	21075581	21131159	knockout		79	ko
2				FBgn0053285	FBtr0078325	21088223	21088989			79	CG33285
2				FBgn0267607	FBtr0347053	21119413	21119801	long non-coding RNA:CR45945		79	lncRNA:CR45945
2				FBgn0284566	FBtr0333448	21121653	21123415			79	CG43938
2				FBgn0053284	FBtr0078291	21123753	21124884			79	CG33284
2				FBgn0037050	FBtr0078292	21131446	21133310	islet cell autoantigen 69 kDa		79	ICA69
2				FBgn0037051	FBtr0305502	21133250	21136353			79	CG10585
2				FBgn0024150	FBtr0330066	21136447	21171930	Adenylyl cyclase 78C		79	Ac78C
2				FBtr0063952	FBtr0063952-RA	21143392	21143429			79	
2				FBtr0063954	FBtr0063954-RA	21145340	21145574			79	
2				FBtr0020185	FBtr0020185-RA	21151919	21156945			79	
2				FBtr0063960	FBtr0063960-RA	21157189	21157255			79	
2				FBgn0021760	FBtr0089461	21172853	21183278	chromosome bows		79	mbs
2				FBgn0270926	FBtr0089463	21173118	21174973	Asparagine synthetase		79	AsnS
2				FBgn0259229	FBtr0305981	21183313	21193303			79	CG42337
2				FBgn0267613	FBtr0347054	21194617	21196136	antisense RNA:CR45951		79	asRNA:CR45951
2				FBgn0041100	FBtr0078318	21194754	21196853	parkin		79	park
2				FBgn0085290	FBtr0112456	21196831	21197738			79	CG34261
2				FBgn0053054	FBtr0078317	21197411	21202882			79	CG33054
2				FBgn0053056	FBtr0078311	21198261	21203232			79	CG33056
2				FBgn0037057	FBtr0078299	21202920	21206002			79	CG10512
2				FBtr0063976	FBtr0063976-RA	21206665	21206771			79	
2				FBgn0037059	FBtr0078310	21208148	21210084			79	CG10510
2				FBgn0037060	FBtr0307385	21210215	21216351			79	CG10508
2				FBgn0037061	FBtr0078309	21216995	21218838			79	CG12975
2				FBgn0028427	FBtr0307160	21216901	21219240	Integrin linked kinase		79	ilk
2				FBgn0262855	FBtr0306161	21220400	21223118			79	CG43219
2				FBgn0004865	FBtr0306158	21226609	21266503	Ecdysone-induced protein 78C		79	Eip78C
2				FBtr0063978	FBtr0063978-RA	21237902	21238138			79	
2				FBtr0020186	FBtr0020186-RA	21243600	21251305			79	
2				FBtr0020033	FBtr0020033-RA	21243865	21251304			79	
2				FBgn0262854	FBtr0306159	21258020	21258758			79	CG43218
2				FBgn0037063	FBtr0305708	21266680	21268335			79	CG10391
2				FBgn0037064	FBtr0078415	21268392	21270985			79	CG10389
2				FBgn0266855	FBtr0344981	21268601	21283142	antisense RNA:CR45162		79	asRNA:CR45162
2				FBgn0012034	FBtr0078414	21270722	21280243	Acetyl Coenzyme A synthase		79	AcCoAS
2				FBgn0027945	FBtr0078412	21280491	21281506	pumpless		79	ppl
2				FBgn0037065	FBtr0332860	21281752	21285962			79	CG12974
2				FBgn0259785	FBtr0078336	21286099	21290310	putzig		79	pzg
2				FBgn0037067	FBtr0078409	21291860	21292800	Cuticular protein 78Ca		79	Cpr78Ca
2				FBgn0037068	FBtr0078337	21294492	21296998	Cuticular protein 78Cb		79	Cpr78Cb
2				FBgn0000551	FBtr0344634	21296763	21297803	Ecdysone-dependent gene 78E		79	Edg78E
2				FBgn0263841	FBtr0321302	21298675	21299063			79	CG43702
2				FBgn0037069	FBtr0078338	21300580	21301171	Cuticular protein 78Cc		79	Cpr78Cc
2				FBgn0266981	FBtr0345862	21301477	21302159	long non-coding RNA:CR45432		79	lncRNA:CR45432
2				FBgn0037070	FBtr0078406	21301785	21304658			79	CG11309
2				FBgn0267614	FBtr0347571	21302421	21304135	antisense RNA:CR45952		79	asRNA:CR45952
2				FBgn0037071	FBtr0321281	21304697	21306197			79	CG7632
2				FBgn0003042	FBtr0078405	21306138	21318926	Polycomb		79	Pc
2				FBtr0020187	FBtr0020187-RA	21306205	21313031			79	
2				FBgn0267234	FBtr0346405	21318223	21318650	long non-coding RNA:CR45674		79	lncRNA:CR45674
2				FBgn0086913	FBtr0301529	21318774	21335027	Rab26		79	Rab26
2				FBgn0267737	FBtr0347297	21333010	21333511	antisense RNA:CR46068		79	asRNA:CR46068
2				FBgn0037073	FBtr0078342	21335215	21338252	Tsr1 ribosome assembly factor		79	Tsr1
2				FBgn0037074	FBtr0078404	21337681	21340716			79	CG7324
2				FBgn0052436	FBtr0078343	21344033	21355049			79	CG32436
2				FBgn0037076	FBtr0305306	21344768	21349288	earthbound 2		79	ebd2
2				FBgn0037078	FBtr0331796	21355100	21356495			79	CG12971
2				FBtr0064022	FBtr0064022-RA	21357269	21357341			79	
2				FBgn0052437	FBtr0078344	21357685	21358907			79	CG32437
2				FBgn0052440	FBtr0078345	21360179	21361229			79	CG32440
2				FBtr0020188	FBtr0020188-RA	21361775	21362678			79	
2				FBtr0062049	FBtr0062049-RA	21363113	21363437			79	
2				FBtr0020189	FBtr0020189-RA	21365893	21371264			79	
2				FBtr0064024	FBtr0064024-RA	21371401	21371432			79	
2				FBtr0020190	FBtr0020190-RA	21372776	21379225			79	
2				FBgn0261258	FBtr0333386	21382501	21424416	regeneration		79	rgn
2				FBgn0267615	FBtr0347056	21398317	21398941	long non-coding RNA:CR45953		79	lncRNA:CR45953
2				FBgn0002942	FBtr0078401	21405425	21406738	spermatocyte arrest		79	aa
2				FBtr0064025	FBtr0064025-RA	21408126	21408224			79	
2				FBgn0267616	FBtr0347057	21413303	21413843	long non-coding RNA:CR45954		79	lncRNA:CR45954
2				FBgn0037081	FBtr0078400	21420388	21433134	barricade		79	barc
2				FBtr0064026	FBtr0064026-RA	21426786	21426855			79	
2				FBgn0053288	FBtr0301013	21427790	21433088			79	CG33288
2				FBgn0005694	FBtr0078349	21433422	21438839	Adult enhancer factor 1		79	Aef1
2				FBgn0037082	FBtr0078397	21438628	21441363			79	CG5664
2				FBtr0020191	FBtr0020191-RA	21441565	21442116			79	
2				FBgn0283479	FBtr0078396	21442227	21444819	Alkaline phosphatase 1		79	Alp1
2				FBgn0267949	FBtr0078352	21445634	21448128	Syntaxin 7		79	Syx7
2				FBgn0014143	FBtr0078395	21474133	21476476	crocodile		79	croc
2				FBtr0064027	FBtr0064027-RA	21482810	21482906			79	
2				FBtr0060089	FBtr0060089-RA	21484279	21484456			79	
2				FBgn0037085	FBtr0332718	21484891	21490586	Neuroectoderm-expressed 2		79	Nee2
2				FBtr0020192	FBtr0020192-RA	21485202	21488805			79	
2				FBgn0037086	FBtr0078393	21491398	21492773			79	CG7202
2				FBgn0037087	FBtr0332711	21493083	21493907			79	CG7519
2				FBgn0015239	FBtr0078392	21494019	21497494	Hormone-receptor-like in 78		79	hr78
2				FBgn0284554	FBtr0344642	21496393	21498830	antisense RNA:CR43933		79	asRNA:CR43933
2				FBgn0284561	FBtr0078388	21497549	21507538	Golgi complex-localized glycoprotein 1		79	Glg1
2				FBtr0059779	FBtr0059779-RA	21498892	21501246			79	
2				FBtr0060090	FBtr0060090-RA	21501046	21501165			79	
2				FBgn0037090	FBtr0078354	21501421	21503959	Esterase Q		79	Est-Q
2				FBgn0037092	FBtr0078356	21507852	21512749	M6		79	M6
2				FBgn0026371	FBtr0078387	21512141	21515887	Sak kinase		79	SAK
2				FBgn0037093	FBtr0078357	21516306	21522884	Cyclin-dependent kinase 12		79	Cdk12
2				FBgn0037094	FBtr0301198	21523186	21528163			79	CG7611
2		**125886**				**21526836**			**78D5**		
2				FBgn0052442	FBtr0089797	21528218	21529333	ACAT-related protein required for viability 1		79	Arv1
2				FBgn0284469	FBtr0332793	21528546	21529115	antisense RNA:CR43877		79	asRNA:CR43877
2				FBgn0029152	FBtr0305331	21529599	21533713	Makorin 1		79	Mkrn1
2				FBgn0053289	FBtr0078328	21534968	21538981	pickpocket 5		79	ppk5
2				FBgn0015283	FBtr0333453	21537000	21538582	Regulatory particle non-ATPase 10		79	Rpn10
2				FBgn0263911	FBtr0078382	21538859	21539447	Cytochrome c oxidase subunit 8		79	COX8
2				FBgn0028663	FBtr0333454	21539862	21541215	Vacuolar H(+) ATPase M9.7 subunit b		79	VhaM9.7-b
2				FBgn0053290	FBtr0078370	21542359	21543012			79	CG33290
2				FBgn0037098	FBtr0346818	21543850	21554928	Wnk kinase		79	Wnk
2				FBgn0037099	FBtr0078360	21555373	21558228			79	CG7173
2				FBgn0037100	FBtr0333458	21558974	21562181	Capability receptor		79	CapaR
2				FBtr0060119	FBtr0060119-RA	21562387	21562534			79	
2				FBgn0037101	FBtr0078371	21565426	21567785			79	CG7634
2				FBtr0060122	FBtr0060122-RA	21567875	21567903			79	
2				FBgn0037102	FBtr0078377	21568859	21568898	CR6-interacting factor		79	CRIF
2				FBgn0052438	FBtr0333455	21569178	21573523	Structural maintenance of chromosomes 5		79	SMC5

2			FBgn0262330	FBtr0304508	21574014	21574121	mir-193 stem loop	79	mir-193
2			FBgn0472765_df_mrg	FBtr0472765	21574032	21574053		79	
2			FBgn0304509_df_mrg	FBtr0304509	21574086	21574107		79	
2			FBgn0052441	FBtr0300058	21574131	21575974	ER membrane protein complex subunit 10	79	EMC10
2			FBgn0264567	FBtr0333457	21576033	21577216	long non-coding RNA:CR43939	79	lncRNA:CR43939
2			FBgn0285994	FBtr0472835	21576460	21576661	hairpin RNA:CR46340	79	hpRNA:CR46340
2			FBgn0261953	FBtr0078418	21588628	21613349	Transcription factor AP-2	79	TFAP-2
2			FBgn0264968	FBtr0333469	21594597	21595460	long non-coding RNA:CR43940	79	lncRNA:CR43940
2			FBgn0037105	FBtr0078466	21613797	21617376	S1P	79	S1P
2			FBgn0037106	FBtr0333391	21617623	21619873		79	CG11307
2			FBgn0037107	FBtr0301161	21620000	21625947		79	CG7166
2			FBgn0037108	FBtr0078422	21625806	21628571	ALG11, alpha-1,2-mannosyltransferase	79	Alg11
2			FBgn0037109	FBtr0333972	21628325	21634446	Mediator complex subunit 1	79	MED1
2			FBgn0037110	FBtr0078423	21635305	21636251	Orosomucoid 1-like	79	ORMDL
2			FBgn0267617	FBtr0347058	21636643	21637314	antisense RNA:CR45955	79	asRNA:CR45955
2			FBgn0043783	FBtr0078424	21636947	21639363		79	CG32444
2			FBgn0020195	FBtr0020195-RA	21637447	21637915		79	
2			FBgn0052445	FBtr0078425	21639359	21640710		79	CG32445
2			FBgn0052446	FBtr0330117	21640995	21642586	Antioxidant 1 copper chaperone	79	Atox1
2			FBgn0267618	FBtr0347059	21642654	21644202	long non-coding RNA:CR45956	79	lncRNA:CR45956
2			FBgn0264711	FBtr0333973	21644958	21686306		79	CG43980
2			FBgn0260124	FBtr0060124-RA	21649023	21649559		79	
2			FBgn0037114	FBtr0078463	21666452	21686980	Cuticular protein 78E	79	Cpr78E
2			FBgn0264708	FBtr0333965	21667424	21668957	long non-coding RNA:CR43977	79	lncRNA:CR43977
2			FBgn0267580	FBtr0346995	21668035	21670043	long non-coding RNA:CR45920	79	lncRNA:CR45920
2			FBgn0262417	FBtr0304355	21668714	21688802	mir-316 stem loop	79	mir-316
2			FBgn0472758_df_mrg	FBtr0472758	21668728	21668749		79	
2			FBgn0304356_df_mrg	FBtr0304356	21668766	21668787		79	
2			FBgn0037115	FBtr0078429	21672139	21674518		79	CG11249
2			FBgn0037116	FBtr0078462	21674394	21679755	Amyotrophic lateral sclerosis 2	79	Als2
2			FBgn0264710	FBtr0333966	21678002	21679713	antisense RNA:CR43979	79	asRNA:CR43979
2			FBgn0037117	FBtr0333967	21680056	21683231		79	CG11248
2			FBgn0261059	FBtr0301939	21683098	21684042	Seminal fluid protein 78E	79	Sfp78E
2			FBgn0264709	FBtr0333968	21684000	21684951	long non-coding RNA:CR43978	79	lncRNA:CR43978
2			FBgn0052447	FBtr0333970	21690612	21706365		79	CG32447
2			FBgn0037120	FBtr0332769	21724326	21728808		79	CG11247
2			FBgn0037121	FBtr0078432	21726932	21729964	Rpb8	79	Rpb8
2			FBgn0037122	FBtr0078457	21729675	21730454		79	CG14570
2			FBgn0037123	FBtr0078456	21730725	21731550		79	CG14569
2			FBgn0060145	FBtr0060145-RA	21730835	21730870		79	
2			FBgn0060127	FBtr0060127-RA	21732134	21732582		79	
2			FBgn0037124	FBtr0078455	21732806	21733457		79	CG14568
2			FBgn0037125	FBtr0078433	21734069	21734788		79	CG14573
2			FBgn0264480	FBtr0332767	21735866	21736201	long non-coding RNA:CR43888	79	lncRNA:CR43888
2			FBgn0060152	FBtr0060152-RA	21736946	21737348		79	
2			FBgn0037126	FBtr0078454	21737706	21738435		79	CG14567
2			FBgn0037127	FBtr0332768	21739479	21740306		79	CG14566
2			FBgn0037128	FBtr0078434	21741534	21742441		79	CG14572
2			FBgn0037129	FBtr0078452	21743248	21744269		79	CG14565
2			FBgn0037130	FBtr0333893	21745359	21770534	Syntrophin-like 1	79	Syn1
2			FBgn0020197	FBtr0020197-RA	21749384	21754470		79	
2			FBgn0020196	FBtr0020196-RA	21749443	21754164		79	
2			FBgn0037131	FBtr0078435	21757157	21758046		79	CG14564
2			FBgn0267619	FBtr0347070	21767229	21767915	long non-coding RNA:CR45957	79	lncRNA:CR45957
2			FBgn0060187	FBtr0060187-RA	21768742	21768852		79	
2			FBgn0037133	FBtr0078436	21768815	21771321		79	CG7370
2			FBgn0267620	FBtr0347071	21776709	21777165	long non-coding RNA:CR45958	79	lncRNA:CR45958
2			FBgn0060165	FBtr0060165-RA	21780710	21787076		79	
2			FBgn0000560	FBtr0332810	21808703	21817600	eagle	79	eg
2			FBgn0264487	FBtr0332814	21813005	21813698		79	CG43895
2			FBgn0060166	FBtr0060166-RA	21813634	21814131		79	
125695					**21815696**			**79F3**	
2			FBgn0060190	FBtr0060190-RA	21820841	21820871		79	
2			FBgn0022936	FBtr0078439	21821997	21823309	Cyclin H	79	CycH
2			FBgn0037134	FBtr0078440	21823461	21824571		79	CG7407
2			FBgn0037135	FBtr0333247	21824740	21827856		79	CG7414
2			FBgn0052448	FBtr0333248	21827774	21828480		79	CG32448
2			FBgn0263001	FBtr0479863	21829541	21833218		79	CR43309
2			FBgn0046301	FBtr0078448	21830544	21832253		79	CG7148
2			FBgn0037137	FBtr0332812	21832774	21836885	Nopp140	79	Nopp140
2			FBgn0037138	FBtr0078447	21839665	21841356	delta-1-Pyrroline-5-carboxylate dehydrogenase 1	79	P5CDh1
2			FBgn0037139	FBtr0078444	21841808	21842386		79	CG14563
2			FBgn0262737	FBtr0304984	21844788	21932702	mushroom-body expressed	79	mub
2			FBgn0052449	FBtr0078490	21854094	21854165	transfer RNA:Cysteine-GCA-4-1	79	tRNA:Cys-GCA-4-1
2			FBgn0060167	FBtr0060167-RA	21857182	21857355		79	
2			FBgn0060168	FBtr0060168-RA	21859413	21859667		79	
2			FBgn0060169	FBtr0060169-RA	21877689	21877919		79	
2			FBgn0020198	FBtr0020198-RA	21881187	21881457		79	
2			FBgn0264470	FBtr0332737	21884511	21887039	long non-coding RNA:CR43878	79	lncRNA:CR43878
2			FBgn0267621	FBtr0347072	21904173	21904462	long non-coding RNA:CR45959	79	lncRNA:CR45959
2	**79**				**21932936**			**79A4**	
2			FBgn0037140	FBtr0078471	21934704	21938836	SLC22A family member	79	SLC22A
126261					**21935345**			**79A4**	
2			FBtr0060209	FBtr0060209-RA	21935901	21936032		79	
2			FBtr0060238	FBtr0060238-RA	21936102	21936139		79	
2			FBgn0037141	FBtr0078489	21939634	21941812	DNA polymerase eta	79	DNApol-eta
2			FBgn0037142	FBtr0334088	21942221	21946866		79	CG14562
2			FBtr0060211	FBtr0060211-RA	21946256	21946377		79	
2			FBgn0037143	FBtr0347604	21949825	21951550		79	CR7448
2			FBgn0267453	FBtr0346824	21950101	21951548	long non-coding RNA:CR45803	79	lncRNA:CR45803
2			FBtr0060239	FBtr0060239-RA	21952548	21953007		79	
2			FBtr0060213	FBtr0060213-RA	21954523	21954886		79	
2			FBgn0037144	FBtr0078475	21955110	21958941		79	CG7458
2			FBtr0060215	FBtr0060215-RA	21958450	21958748		79	
2			FBtr0059643	FBtr0059643-RA	21958769	21959136		79	
2			FBgn0085291	FBtr0112457	21959254	21960503		79	CR34262
2			FBtr0059641	FBtr0059641-RA	21960912	21961210		79	
2			FBtr0059644	FBtr0059644-RA	21961231	21961598		79	
2			FBgn0267321	FBtr0346603	21961871	21962196	long non-coding RNA:CR45757	79	lncRNA:CR45757
2			FBgn0039091	FBtr0334089	21962401	21969964	Chitin synthase 2	79	Chs2
2			FBgn0037146	FBtr0300869	21972002	21984608		79	CG7470
2			FBgn0000045	FBtr0334090	21982210	21987190	Actin 79B	79	Act79B
2			FBtr0060216	FBtr0060216-RA	22007365	22007454		79	
2			FBtr0060222	FBtr0060222-RA	22013705	22013821		79	
2			FBtr0060224	FBtr0060224-RA	22016682	22016745		79	
2			FBtr0060225	FBtr0060225-RA	22017109	22017403		79	
2			FBtr0060226	FBtr0060226-RA	22021152	22021280		79	
2			FBgn0037147	FBtr0114546	22026230	22028325		79	CG7140
2			FBtr0060227	FBtr0060227-RA	22028710	22028763		79	
2			FBgn0263249	FBtr0308060	22029453	22029770		79	CG43992
2			FBgn0265898	FBtr0342763	22029969	22030941	long non-coding RNA:CR44887	79	lncRNA:CR44887
2			FBgn0004514	FBtr0301930	22035003	22065276	Octopamine-Tyramine receptor	79	Oct-TyrR
2			FBtr0060228	FBtr0060228-RA	22036821	22037752		79	
2			FBtr0060230	FBtr0060230-RA	22063188	22063510		79	
2			FBgn0037149	FBtr0078480	22065907	22067216		79	CG14561
2			FBgn0027532	FBtr0078486	22067270	22071948		79	CG7139
2			FBtr0060231	FBtr0060231-RA	22072219	22072306		79	
2			FBgn0264727	FBtr0334112	22072369	22072620	long non-coding RNA:CR43995	79	lncRNA:CR43995
2			FBtr0060241	FBtr0060241-RA	22072925	22073024		79	
2			FBgn0037150	FBtr0078485	22073968	22074523		79	CG7133
2			FBgn0037151	FBtr0078484	22075056	22075758		79	CG7130
2			FBgn0000100	FBtr0078481	22075867	22077487	Ribosomal protein LP0	79	RpLP0
2			FBgn0259973	FBtr0300318	22080322	22080554	Seminal fluid protein 79	79	Sfp79B
2			FBgn0004414	FBtr0334114	22082720	22083367	male-specific opa containing gene	79	msopa
2			FBtr0060232	FBtr0060232-RA	22083478	22083532		79	
2			FBtr0020200	FBtr0020200-RA	22086072	22086318		79	
2			FBtr0060234	FBtr0060234-RA	22086275	22086413		79	
2			FBtr0020201	FBtr0020201-RA	22099731	22105858		79	
2			FBgn0266771	FBtr0445724	22121932	22122746	long non-coding RNA:CR45236	79	lncRNA:CR45236
2			FBgn0037153	FBtr0301492	22136090	22247702	dif413	79	dif413
2			FBgn0267633	FBtr0347088	22176423	22177568	long non-coding RNA:CR45971	79	lncRNA:CR45971
2			FBgn0267634	FBtr0347087	22197783	22198241	long non-coding RNA:CR45972	79	lncRNA:CR45972

2				FBgn0286395	FBtr0344307	22225528	22225878	long non-coding RNA:CR45035		79	lncRNA:CR45035
2				FBgn0028500	FBtr0078512	22257749	22262021	RIC1 homolog		79	Rich
2				FBgn0015075	FBtr0078492	22263369	22266017	Dead-box-1		79	Ddx1
2				FBgn0037156	FBtr0078511	22265806	22266679			79	CG11523
2				FBtr0060255	FBtb0060255-RA	22267141	22267311			79	
2				FBgn0034179	FBtr0078495	22267382	22273745	Cysteine string protein		79	Csp
2				FBgn0286037	FBtr0473386	22269932	22270220	stabla intronic sequence RNA 3		79	asRNA:3
2				FBgn0025702	FBtr0306596	22273985	22284335	Serine-arginine protein kinase at 79D		79	Srpk79D
2				FBgn0267622	FBtr0347073	22274083	22275776	antisense RNA:CR45960		79	asRNA:CR45960
2				FBtr0060249	FBtb0060249-RA	22282340	22282395			79	
2				FBgn0011771	FBtr0078510	22284354	22288195	HEM-protein		79	Hem
2				FBgn0027086	FBtr0078498	22289665	22292810	Isoleucyl-tRNA synthetase		79	IleRS
2				FBgn0034449	FBtr0078509	22293044	22407863	Tenascin major		79	Ten-m
2				FBgn0052460	FBtr0078501	22329779	22339657			79	CG32460
2				FBgn0267625	FBtr0347075	22345383	22346236	long non-coding RNA:CR45963		79	lncRNA:CR45963
2				FBgn0267624	FBtr0347077	22348168	22407547	long non-coding RNA:CR45962		79	lncRNA:CR45962
2				FBgn0267626	FBtr0347076	22350701	22351500	long non-coding RNA:CR45964		79	lncRNA:CR45964
2				FBgn0267627	FBtr0347078	22359458	22360868	long non-coding RNA:CR45965		79	lncRNA:CR45965
2				FBgn0286772	FBtr0345397	22409855	22421200	long non-coding RNA:CR45237		79	lncRNA:CR45237
2				FBgn0267628	FBtr0347079	22424489	22424609	long non-coding RNA:CR45966		79	lncRNA:CR45966
2				FBgn0037162	FBtr0078503	22454373	22455989			79	CG11449
2				FBgn0037163	FBtr0078508	22458816	22461131	lazaro		79	laza
2				FBgn0037164	FBtr0345586	22465619	22468076			79	CG11438
2				FBgn0037165	FBtr0078505	22468852	22469853			79	CG11437
2				FBgn0037166	FBtr0078506	22470556	22473509			79	CG11426
2				FBgn0286931	FBtr0345824	22473952	22474431	long non-coding RNA:CR45382		79	lncRNA:CR45382
2				FBgn0037167	FBtr0078507	22474795	22475762			79	CG11425
2				FBgn0286979	FBtr0345881	22496342	22497114	long non-coding RNA:CR45430		79	lncRNA:CR45430
2				FBgn0286980	FBtr0345880	22498319	22498838	long non-coding RNA:CR45431		79	lncRNA:CR45431
2				FBgn0263004	FBtr0306848	22501600	22502417			79	CG43312
2				FBgn0263036	FBtr0306916	22502978	22503830			79	CG43331
2				FBgn0263035	FBtr0306915	22503869	22504423			79	CG43330
2				FBgn0263034	FBtr0306914	22504487	22505218			79	CG43329
2				FBtr0060264	FBtb0060264-RA	22507357	22507452			79	
2				FBtr0060266	FBtb0060266-RA	22507993	22508158			79	
2				FBgn0286978	FBtr0345879	22510266	22511067	long non-coding RNA:CR45429		79	lncRNA:CR45429
2				FBtr0060268	FBtb0060268-RA	22511861	22512300			79	
2				FBgn0262182	FBtr0304192	22518196	22518291	mir-957 stem loop		79	mir-957
2				FBtr0304193_df_mrg	FBtr0304193	22518219	22518231			79	
2				FBtr0472767_df_mrg	FBtr0472767	22518255	22518277			79	
2				FBtr0060269	FBtb0060269-RA	22519073	22519112			79	
2				FBtr0020202	FBtb0020202-RA	22532307	22533849			79	
2				FBtr0060270	FBtb0060270-RA	22547967	22548312			79	
2				FBgn0037169	FBtr0078513	22548437	22549342			79	CG11404
2				FBgn0037170	FBtr0078514	22550226	22552019	thioredoxin reductase 2		79	Trxr-2
2				FBtr0020203	FBtb0020203-RA	22555825	22563237			79	
2				FBgn0286028	FBtr0473374	22570364	22572033	long non-coding RNA:CR46348		79	lncRNA:CR46348
2				FBgn0037171	FBtr0474121	22573114	22637916			79	CG14459
2				FBtr0020204	FBtb0020204-RA	22577677	22582365			79	
2				FBgn0037172	FBtr0078515	22606369	22607126	NADH dehydrogenase (ubiquinone) B14.5 A subunit-like		79	ND-B14.5AL
2				FBgn0267629	FBtr0347080	22607748	22608370	long non-coding RNA:CR45967		79	lncRNA:CR45967
2				FBtr0060609	FBtb0060609-RA	22609700	22609777			79	
2				FBtr0020205	FBtb0020205-RA	22617245	22624639			79	
2				FBtr0060610	FBtb0060610-RA	22639980	22639081			79	
2				FBtr0060611	FBtb0060611-RA	22639153	22639594			79	
2				FBtr0060612	FBtb0060612-RA	22640425	22640738			79	
2				FBtr0060262	FBtb0060262-RA	22640762	22641123			79	
2				FBtr0020206	FBtb0020206-RA	22641245	22641856			79	
2				FBgn0286930	FBtr0345823	22643881	22644470	long non-coding RNA:CR45381		79	lncRNA:CR45381
2				FBgn0053766	FBtr0091767	22645627	22646236			79	CG33766
2				FBgn0053767	FBtr0091768	22646307	22646958			79	CG33767
2				FBgn0053768	FBtr0473608	22647163	22647748			79	CG33768
2				FBgn0053769	FBtr0091770	22647927	22648519			79	CG33769
2				FBgn0053770	FBtr0290125	22648672	22649287			79	CG33770
2				FBgn0053771	FBtr0303713	22649396	22649988			79	CG33771
2				FBgn0053772	FBtr0303714	22651855	22652525			79	CG33772
2				FBgn0262951	FBtr0306851	22665300	22665828	long non-coding RNA:CR43270		79	lncRNA:CR43270
2				FBgn0262249	FBtr0304337	22669289	22669380	mir-958 stem loop		79	mir-958
2				FBtr0304338_df_mrg	FBtr0304338	22669302	22669323			79	
2				FBtr0472768_df_mrg	FBtr0472768	22669343	22669365			79	
2				FBgn0037174	FBtr0100869	22685958	22680034			79	CG14457
2				FBgn0037175	FBtr0331777	22686365	22687087			79	CG14455
2				FBgn0037176	FBtr0289975	22687222	22688288			79	CG14456
2				FBgn0037177	FBtr0078542	22691674	22692528			79	CG14454
2				FBtr0060650	FBtb0060650-RA	22693107	22693185			79	
2				FBgn0037178	FBtr0078541	22693324	22693812			79	CG12546
2				FBgn0037179	FBtr0078519	22694065	22694448			79	CG14453
2				FBtr0060649	FBtb0060649-RA	22694907	22695243			79	
2				FBtr0060651	FBtb0060651-RA	22695362	22696652			79	
2				FBgn0037180	FBtr0078520	22695953	22696435			79	CG14452
2				FBgn0052453	FBtr0078521	22697230	22697970			79	CG32453
2				FBtr0060652	FBtb0060652-RA	22698076	22698332			79	
2				FBgn0286591	FBtr0344814	22699433	22699870			79	CG45116
2				FBgn0267947	FBtr0347522	22709936	22705918	long non-coding RNA:CR46227		79	lncRNA:CR46227
2				FBgn0037181	FBtr0330172	22712155	22713660			79	CG11370
2				FBgn0037182	FBtr0331775	22714313	22717577	ADP-ribosylation factor GTPase activating protein 3		79	ArfGAP3
2				FBgn0052452	FBtr0345591	22717728	22719943			79	CG32452
2				FBtr0060654	FBtb0060654-RA	22720019	22720507			80	
2				FBtr0020207	FBtb0020207-RA	22720519	22721088			80	
2				FBgn0016034	FBtr0089633	22721203	22726234	maelstrom		80	mael
2				FBgn0037183	FBtr0078538	22721230	22722091			80	CG14451
2				FBtr0060734	FBtb0060734-RA	22722246	22722421			80	
2				FBtr0060655	FBtb0060655-RA	22722902	22723982			80	
2				FBtr0060717	FBtb0060717-RA	22723159	22723571			80	
2				FBgn0037184	FBtr0310503	22726234	22727788			80	CG14450
2				FBgn0037185	FBtr0078528	22728111	22733446			80	CG11367
2				FBgn0260481	FBtr0078529	22729766	22731600			80	CG32454
2				FBgn0037186	FBtr0113188	22730313	22738420			80	CG11241
2				FBtr0060656	FBtb0060656-RA	22737449	22737462			80	
2				FBgn0010830	FBtr0078535	22739602	22741388	lethal (3) 04053		80	l(3)04053
2				FBgn0286656	FBtr0344965	22738708	22739434	antisense RNA:CR45163		80	asRNA:CR45163
2				FBgn0037188	FBtr0078530	22741793	22748614			80	CG7369
2				FBtr0060657	FBtb0060657-RA	22742955	22743071			80	
2				FBtr0059665	FBtb0059665-RA	22743571	22751725			80	
2				FBtr0060659	FBtb0060659-RA	22744915	22744979			80	
2				FBgn0052451	FBtr0306600	22748444	22757631	Secretory Pathway Calcium atpase		80	SPoCk
2				FBtr0060673	FBtb0060673-RA	22759216	22756255			80	
2				FBgn0267623	FBtr0347074	22756766	22757328	long non-coding RNA:CR45961		80	lncRNA:CR45961
2				FBtr0060674	FBtb0060674-RA	22759024	22759146			80	
2				FBtr0060675	FBtb0060675-RA	22760879	22761314			80	
2				FBtr0020209	FBtb0020209-RA	22761446	22766814			80	
2				FBtr0060676	FBtb0060676-RA	22780109	22780938			80	
2			**80**			**22849957**			**80B1**		
				FBtr0060678	FBtb0060678-RA	22786396	22786593			80	
				FBtr0060680	FBtb0060680-RA	22788074	22788105			80	
				FBgn0037191	FBtr0078534	22788439	22789247			80	CG14448
				FBgn0027339	FBtr0100184	22789233	22835194	jim		80	jim
				FBtr0020210	FBtb0020210-RA	22803767	22811374			80	
				FBtr0060721	FBtb0060721-RA	22811916	22812230			80	
				FBtr0020211	FBtb0020211-RA	22812270	22819038			80	
				FBtr0060683	FBtb0060683-RA	22819753	22820076			80	
				FBgn0286977	FBtr0345874	22836555	22837070			80	CG45428
				FBgn0037195	FBtr0078546	22837068	22838170			80	CG11226
				FBgn0267219	FBtr0346387	22840293	22841302	long non-coding RNA:CR45859		80	lncRNA:CR45859
				FBgn0286585	FBtr0345647	22843264	22843348	transfer RNA:Leucine-CAG 1-8		80	tRNA:Leu-CAG-1-8
				FBtr0060685	FBtb0060685-RA	22844778	22845214			80	
				FBgn0052460	FBtr0078580	22847725	22847796	transfer RNA:Glutamic acid-CTC 2-3		80	tRNA:Glu-CTC-2-3
				FBtr0060687	FBtb0060687-RA	22848616	22848646			80	
				FBgn0263345	FBtr0306779	22850111	22854434	antisense RNA:CR43426		80	asRNA:CR43426
				FBgn0052462	FBtr0078579	22852270	22853512			80	CG32462
				FBtr0060699	FBtb0060699-RA	22854191	22854369			80	

				FBgn0052459	FBtr0078578	22854583	22856259			80	CG32459
				FBgn0037197	FBtr0078548	22860767	22861400			80	CG13239
				FBti0060701	FBti0060701-RA	22861391	22861453			80	
				FBgn0053169	FBtr0078549	22863864	22864496			80	CG33169
				FBgn0053170	FBtr0089836	22864600	22867535			80	CG33170
				FBti0020212	FBti0020212-RA	22866039	22867112			80	
				FBgn0037199	FBtr0078577	22867175	22868243	ER membrane protein complex subunit 4		80	EMC4
				FBgn0010348	FBtr0078574	22868380	22872231	ADP ribosylation factor at 79F		80	Arf79F
				FBgn0026518	FBtr0078576	22869546	22869622			80	snoRNA:Mu28S:-G764
				FBgn0267631	FBtr0347084	22871813	22872107	antisense RNA:CR45969		80	asRNA:CR45969
				FBgn0037200	FBtr0078552	22872200	22873702			80	CG11109
				FBgn0267630	FBtr0347085	22872380	22873723	antisense RNA:CR45968		80	asRNA:CR45968
				FBgn0044324	FBtr0078569	22873702	22878984	Chromator		80	Chro
				FBti0060702	FBti0060702-RA	22874625	22875968			80	
				FBgn0037202	FBtr0332051	22879089	22880983	Suppressor of stem-loop mutation		80	Sal1
				FBgn0267632	FBtr0347086	22879259	22880399	antisense RNA:CR45970		80	asRNA:CR45970
				FBgn0037203	FBtr0078557	22881045	22883821	slimfast		80	slif
				FBti0060755	FBti0060755-RA	22883443	22883529			80	
				FBti0060756	FBti0060756-RA	22894585	22894738			80	
				FBti0060758	FBti0060758-RA	22894800	22895018			80	
				FBti0060761	FBti0060761-RA	22890587	22890811			80	
				FBgn0265869	FBtr0342774	22896127	22896619	long non-coding RNA:CR44688		80	lncRNA:CR44688
				FBgn0265900	FBtr0342775	22898191	22898580	long non-coding RNA:CR44689		80	lncRNA:CR44689
				FBgn0037204	FBtr0332052	22898744	22900362			80	CG11131
				FBgn0037205	FBtr0078559	22901912	22905470	Brother of Yb		80	BoYb
				FBti0060762	FBti0060762-RA	22905485	22905684			80	
				FBti0061337	FBti0061337-RA	22905974	22906368			80	
				FBti0060771	FBti0060771-RA	22906551	22908614			80	
				FBgn0267221	FBtr0346394	22908318	22909807	long non-coding RNA:CR45961		80	lncRNA:CR45961
				FBgn0037206	FBtr0331397	22910491	22923532			80	CG12768
				FBti0060773	FBti0060773-RA	22912345	22912684			80	
				FBti0060775	FBti0060775-RA	22915802	22916099			80	
				FBti0060778	FBti0060778-RA	22922576	22923759			80	
				FBti0060780	FBti0060780-RA	22932794	22933268			80	
				FBti0060781	FBti0060781-RA	22938400	22938922			80	
				FBti0020213	FBti0020213-RA	22939923	22939836			80	
				FBti0060783	FBti0060783-RA	22940078	22940168			80	
				FBti0060785	FBti0060785-RA	22942021	22942250			80	
				FBti0060786	FBti0060786-RA	22942775	22943962			80	
				FBti0061313	FBti0061313-RA	22943032	22943106			80	
				FBti0060787	FBti0060787-RA	22944079	22944318			80	
				FBti0062062	FBti0062062-RA	22944373	22944653			80	
				FBti0060807	FBti0060807-RA	22944658	22944718			80	
				FBgn0283658	FBtr0445495	22945116	22945207	mir-9388 stem loop		80	mir-9388
				FBtr0445496_df_mrg	FBtr0445496	22945131	22945153			80	
				FBtr0445497_df_mrg	FBtr0445497	22945171	22945192			80	
				FBgn0037207	FBtr0078561	22945657	22952248	Mesoderm-expressed 2		80	Mes2
				FBti0060809	FBti0060809-RA	22953840	22954040			80	
				FBgn0052461	FBtr0078567	22954421	22955302			80	CG32461
				FBti0060811	FBti0060811-RA	22955686	22955755			80	
				FBti0060813	FBti0060813-RA	22957601	22957889			80	
				FBgn0267322	FBtr0346604	22960930	22961668	long non-coding RNA:CR45758		80	lncRNA:CR45758
				FBti0060816	FBti0060816-RA	22963064	22963200			80	
				FBti0060818	FBti0060818-RA	22965782	22966265			80	
				FBti0060819	FBti0060819-RA	22968033	22968160			80	
				FBti0060820	FBti0060820-RA	22968745	22968952			80	
				FBti0060821	FBti0060821-RA	22971397	22971483			80	
				FBti0060823	FBti0060823-RA	22972516	22972576			80	
				FBti0061220	FBti0061220-RA	22972667	22972728			80	
				FBti0061221	FBti0061221-RA	22973487	22973593			80	
				FBti0061222	FBti0061222-RA	22973653	22973781			80	
				FBti0061223	FBti0061223-RA	22973964	22974096			80	
				FBti0061224	FBti0061224-RA	22976134	22976266			80	
				FBti0020214	FBti0020214-RA	22976532	22976944			80	
				FBti0020215	FBti0020215-RA	22976953	22977127			80	
				FBti0061226	FBti0061226-RA	22977179	22977414			80	
				FBti0061228	FBti0061228-RA	22980719	22980756			80	
				FBti0020216	FBti0020216-RA	22980924	22981708			80	
				FBti0061230	FBti0061230-RA	22982507	22983836			80	
				FBti0061232	FBti0061232-RA	22983079	22983128			80	
				FBti0061235	FBti0061235-RA	22983229	22983561			80	
				FBti0061246	FBti0061246-RA	22984202	22984285			80	
				FBti0061247	FBti0061247-RA	22988322	22988415			80	
				FBti0020217	FBti0020217-RA	22988429	22989043			80	
				FBti0061248	FBti0061248-RA	22988815	22989879			80	
				FBgn0052457	FBtr0300620	22987642	22988262			80	CG32457
				FBti0061359	FBti0061359-RA	22988421	22988498			80	
				FBti0060751	FBti0060751-RA	22988530	22988605			80	
				FBti0020218	FBti0020218-RA	22989017	22989833			80	
		123975				**22991401**			**80C 2**		